Smart Metering and Its Use for Distribution Network Control

Alasdair H. Burchill

School of Engineering

Cardiff University

Thesis submitted in partial fulfilment of the requirements
for the degree of Doctor of Philosophy

2018

This page intentionally left blank

Dedicated to the memory of my dear friend Jess

This page intentionally left blank

Abstract

Global energy demand is increasing, with the adoption of electric vehicles, in particular, representing a significant prospective demand on electricity distribution networks. The exploitation of renewable generation sources, driven by increased economic viability, technological maturity, and the need for environmental sustainability, is expected to play an increasingly important role in meeting this demand. However, the adoption of such low-carbon technologies necessitates a significant change in the way that distribution networks are monitored and controlled. This work examines the state of the art in the impact of low-carbon technologies on distribution networks, the technical strategies available to mitigate these impacts and their relative merits, and the architecture of the control systems used to effect such strategies. Smart metering and advanced metering infrastructure (AMI) are a fundamental component of these smart grid systems, providing widespread visibility of conditions at the very periphery of distribution networks which has not previously been feasible, but where the impact of low-carbon technologies is significant. This work describes the development of a hardware-in-the-loop test rig incorporating multiple, custom-built, hardware smart meter test beds, and the use of this test rig to demonstrate the implementation of real-time voltage control within a simulated low voltage (LV) distribution network. However, the adoption of smart metering and AMI inevitably incurs cyber security vulnerabilities which did not exist in the case of meters with no facility for remote communication. This work examines cyber security issues pertinent to smart grids and AMI in particular, and describes the analysis of the cyber security vulnerabilities of a commercially deployed smart electricity meter. The exploitation of these vulnerabilities in a manner which permits unauthorised electronic access to the device is also described. Finally, recommendations are made of revisions to the hardware, firmware and communications protocols used by the compromised meter which may mitigate the vulnerabilities identified.

This page intentionally left blank

Contents

Acknowledgements

I am indebted to Prof Nick Jenkins for his unfaltering encouragement, patience, and meticulous review of my work.

Thanks are also due to Dr Jianzhong Wu, Dr Janaka Ekanayake, Dr Carlos Uglade-Loo and Dr Lee Thomas, for their academic wisdom and support, to Denley Slade, Paul Farrugia, Richard Rogers and Bill Whitehouse, for their technical support and good humour, and to Aderyn Reid, Jeanette Whyte, Chris Lee and Chiara Singh-Fisher, for their administrative support and free sandwiches.

I am of the opinion that the refectory and the public house are at least as fertile venues for inspiration as the office and the laboratory, so I thank my colleagues and friends for their companionship and intellectual discussion, in particular George O'Malley, Dr Luke Livermore, Dr Marc Rees, Dr Jonathan Stevens, Dr Ben Whitby, Dr Ian Moore, Dr Dave Clark, Dr Tracy Sweet and Catherine Roderick.

Finally, I would like to thank close friends for their patience and support over the journey which this thesis represents, in particular Jon Dickerson, Fabian Moore, Sarah Tatum, Julie Crowley, Tracey Plowman, Dr Davina Darmanin and Dr Edd Lewis. I would like to thank my mother, for instilling in me a sense of self-belief and confidence which has served me well, and my partner Claire, for her immense patience and care.

This page intentionally left blank

Abbreviations

2G	Second-Generation cellular technology
AC	Alternating Current
ACCM	Asynchronous Control Character Map
ADC	Analogue to Digital Converter
AES	Advanced Encryption Standard
AMI	Advanced metering infrastructure
AMR	Automatic Meter Reading
ANSI	American National Standards Institute
AT	Attention
AVC	Automatic Voltage Control
AVR	Automatic Voltage Regulator
AVRS	Automatic Voltage Reference Setting
BEV	Battery Electric Vehicle
BPL	Broadband over Power Line
CCDF	Complementary Cumulative Distribution Function
CCITT	Consultative Committee for International Telephony and Telegraphy
CESG	Communications-Electronics Security Group
CHAP	Challenge Handshake Authentication Protocol
CHP	Combined Heat and Power
CIA	Confidentiality, Integrity and Availability
CNE	Combined Neutral and Earth
COSEM	Companion Specification for Energy Metering
CPA	Commercial Product Assurance
CPU	Central Processing Unit
CRC	Cyclic Redundancy Check
CSC	Constant Set-Point Control
CTS	Clear To Send
DAC	Digital to Analogue Converter
DECC	Department of Energy & Climate Change
DG	Distributed Generation
DH	Diffie-Hellman
DLMS	Device Language Message Specification
DNO	Distribution Network Operator
DNP3	Distributed Network Protocol
DoS	Denial of Service
DSA	Digital Signature Algorithm
DSM	Demand-Side Management

DSTATCOM	Distribution Static Compensator
DTI	Department of Trade and Industry
EEPROM	Electrically Erasable Programmable Read-Only Memory
EHP	Electric Heat Pump
ENWL	Electricity North West Limited
ETX	End of Text
EU	European Union
EV	Electric Vehicle
FIPS	Federal Information Processing Standard
FLAG	Ferranti and Landis+Gyr
FP7	7th Framework Programme
GNU	GNU's Not Unix
GPC	Giga Processor Card
GPRS	General Packet Radio Service
GSM	Global System for Mobile communications
GTAO	Giga Transceiver Analogue Output
GTNET	Giga Transceiver Network interface
GTWIF	Giga Transceiver Workstation Interface
HAN	Home Area Network
HDLC	High-level Data Link Control
HMI	Human Machine Interface
HV	High Voltage (36–300 kV)
IDE4L	Ideal Grid for All
IEC	International Electrotechnical Commission
IEEE	Institute of Electrical and Electronics Engineers
IP	Internet Protocol
IPCP	Internet Protocol Control Protocol
IPsec	Internet Protocol security
IRA	Irish Republican Army
IRQ	Interrupt Request
ISO	International Organization for Standardization
JTAG	Joint Test Action Group
LAN	Local Area Network
LCD	Liquid Crystal Display
LCNF	Low Carbon Networks Fund
LCP	Link Control Protocol
LCT	Low-Carbon Technology
LDC	Line Drop Compensation
LED	Light Emitting Diode
LOVIA	Low Voltage Integrated Automation
LV	Low Voltage (<1 kV)

MCU	Metrology and Communications Unit
MDC	Meter Data Concentrator
MITM	Man-In-The-Middle
MOSI	Master Out Slave In
MPAN	Meter Point Administration Number
MRU	Maximum Receive Unit
MV	Medium Voltage (1–36 kV)
NAT	Network Address Translation
NCSC	National Cyber Security Centre
OECD	Organisation for Economic Co-operation and Development
OLTC	On-Load Tap Changer
OPC	Open Platform Communications
OPERA	Open PLC European Research Alliance
PAP	Password Authentication Protocol
PCB	Printed Circuit Board
PDP	Packet Data Protocol
PGA	Programmable-Gain Amplifier
PHEV	Plug-in Hybrid Electric Vehicle
PLC	Power Line Carrier
PMIC	Programmable Multilevel Interrupt Controller
PPM	Parts Per Million
PPP	Point-to-Point Protocol
PQ	Power Quality
PV	Photovoltaic
QoS	Quality of Service
R&D	Research and Development
RAM	Random Access Memory
RF	Radio frequency
RMC	Remote Monitoring-Based Control
RMS	Root Mean Square
RPC	Remote Procedure Call
RS-232	Recommended Standard 232
RTC	Real-Time Clock
RTDS	Real Time Digital Simulator
RTP	Room Temperature and Pressure
RTS	Ready to Send
RTT	Round-Trip Time
RTU	Remote Terminal Unit
RX	Receive
SAU	Substation Automation Unit
SCADA	Supervisory Control And Data Acquisition

SCK	Serial Clock
SDRAM	Synchronous Dynamic Random-Access Memory
SHA	Secure Hash Algorithm
SIM	Subscriber Identity Module
SM	Smart Meter
SMETS	Smart Metering Equipment Technical Specifications
SPI	Serial Peripheral Interface
SRAM	Static Random-Access Memory
SSL	Secure Sockets Layer
STX	Start of Text
TBC	Time-Based Control
TC	Timer/Counter
TCP	Transmission Control Protocol
TIA	Telecommunications Industry Association
TLS	Transport Layer Security
TX	Transmit
UART	Universal Asynchronous Receiver Transmitter
UDP	User Datagram Protocol
UK	United Kingdom
UKERC	UK Energy Research Centre
USART	Universal Synchronous/Asynchronous Receiver Transmitter
USB	Universal Serial Bus
V2G	Vehicle-to-Grid
VUF	Voltage Unbalance Factor
WAN	Wide Area Network

Symbols

$I_{K,gen}$	Fault current from distributed generation source (p.u.)
$I_{K,grid}$	Fault current from grid (p.u.)
P	Real power (p.u.)
P_{LINE}	Active power in line (p.u.)
P_{LOAD}	Active power to load (p.u.)
P_{PV}	Active power from photovoltaic generation source (p.u.)
Q	Reactive power (p.u.)
Q_{LINE}	Reactive power in line (p.u.)
Q_{LOAD}	Reactive power to load (p.u.)
Q_{PV}	Reactive power from photovoltaic generation source (p.u)
REF	Substation bus reference voltage (p.u.)
R_L	Feeder resistance (p.u.)
R_{SET}	Resistive set-point (p.u.)
S	Apparent power (p.u.)
U_0	Busbar voltage (p.u.)
U_{LC}	Feeder-end load centre voltage (p.u.)
U_{SET}	Voltage set-point (p.u.)
V_1	DG connection point feeder voltage (V)
V_2	DG voltage source voltage (V)
V_{DG}	Voltage at DG source (p.u.)
V_L	Voltage at load (p.u.)
V_{MAX}	Maximum voltage measured (p.u.)
V_{MIN}	Minimum voltage measured (p.u.)
$V_{pre\text{-}set}$	Default reference voltage (p.u.)
V_{ref}	Current reference voltage (p.u.)
V_s	Sending-end voltage (p.u.)
X	DG source series reactance (Ω)
X_L	Feeder reactance (p.u.)
X_{SET}	Reactive set-point (p.u.)
δ_1	DG connection point feeder phase angle (rad)
δ_2	DG voltage source phase angle (rad)
φ	Phase angle of DG source (rad)
$I_{K,gen}$	Fault current from distributed generation source (p.u.)
$I_{K,grid}$	Fault current from grid (p.u.)
P	Real power (p.u.)
P_{LINE}	Active power in line (p.u.)

Symbols

P_{LOAD}	Active power to load (p.u.)
P_{PV}	Active power from photovoltaic generation source (p.u.)

1 - Introduction

1.1 - Background

Worldwide, electricity systems are undergoing rapid change. As energy demand increases, renewable generation sources are becoming widely adopted. Smart meters are a fundamental element of the smart grids needed to accommodate such developments, and are the subject of this research.

1.1.1 - Energy demand and renewable generation

Global energy consumption in 2050 is predicted to be more than 50 % greater than in 2018. More than half of this increase is expected to be driven by economic development and growing populations in non-OECD countries, such as India and China [1]. This is shown in Figure 1.1 [1].

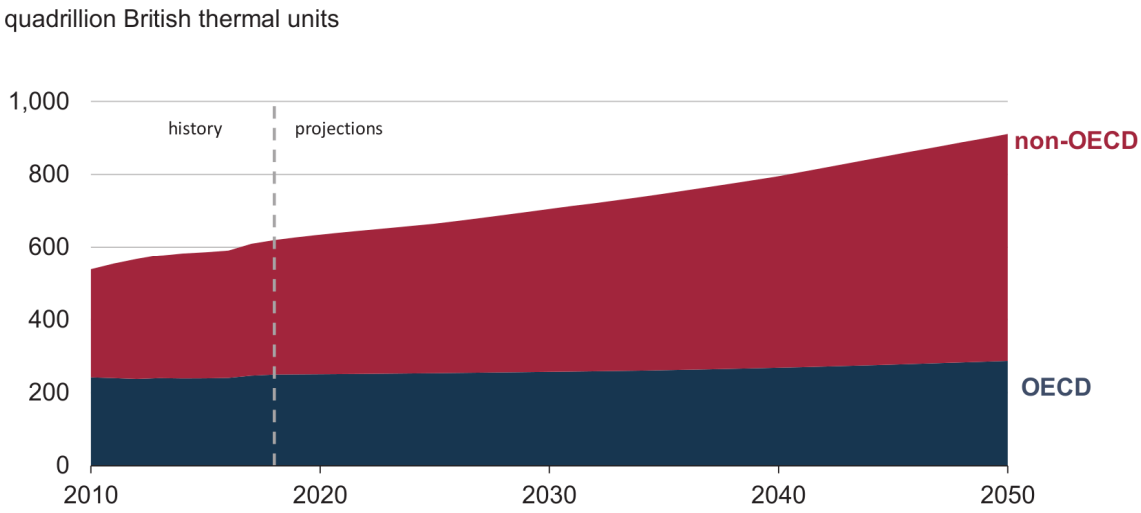

Figure 1.1: World energy consumption [1]

Renewable energy is predicted to be the fastest-growing electricity generation source, with increased economic viability, technological maturity, and the need for environmental sustainability expected to result in renewable sources contributing almost 50 % of world electricity generation in 2050. Of these renewable sources, the greatest increase is predicted to be in wind and solar generation [1]. This is shown in Figure 1.2 [1].

The European Union (EU) has committed to reduce greenhouse gas emissions to 80–95 % below the levels in 1990, by 2050. In order to achieve this, a greater proportion of electricity in total energy consumption is proposed, up to 39 % by 2050, of which up to 97 % is to be generated by renewable sources [2].

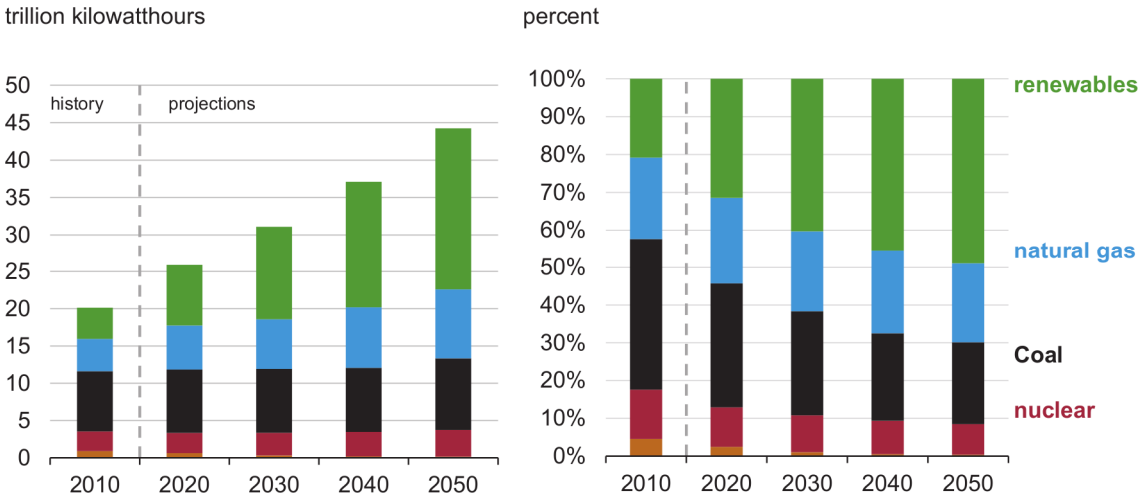

Figure 1.2: Global electricity generation [1]

More immediately, the 2009 Renewable Energy Directive [3], a component of the EU's *2020 climate & energy package*, requires member countries to increase the proportion of renewable energy in their national consumption, with an overall European target of 20 % by 2020. This represents more than double the 2010 proportion of 9.8 %.

Under the Renewable Energy Directive [3], targets for renewable production were based on member countries' current capacity, and anticipated scope for growth. In the case of the UK, the target is 15 %. In response to this, the Government's 2010 *National Renewable Energy Action Plan for the United Kingdom* [4] proposed a target of 30 % renewable electricity generation by 2020. In 2019, renewables constituted 36.9 % of total UK electricity generation, with an installed capacity of 47.4 GW at the end of 2019 [5]. This is shown in Figure 1.3 [6].

At the end of May 2020, solar photovoltaic (PV) generation capacity in the UK was approximately 13 436 MW across 1 036 077 installations, or 28 % of total renewable generation capacity. Small-scale installations of up to 4 kW represent approximately 20 % of solar PV generation capacity in the UK [7], encouraged by feed-in tariffs introduced under the *Energy Act 2008* [8], and available from 2010.

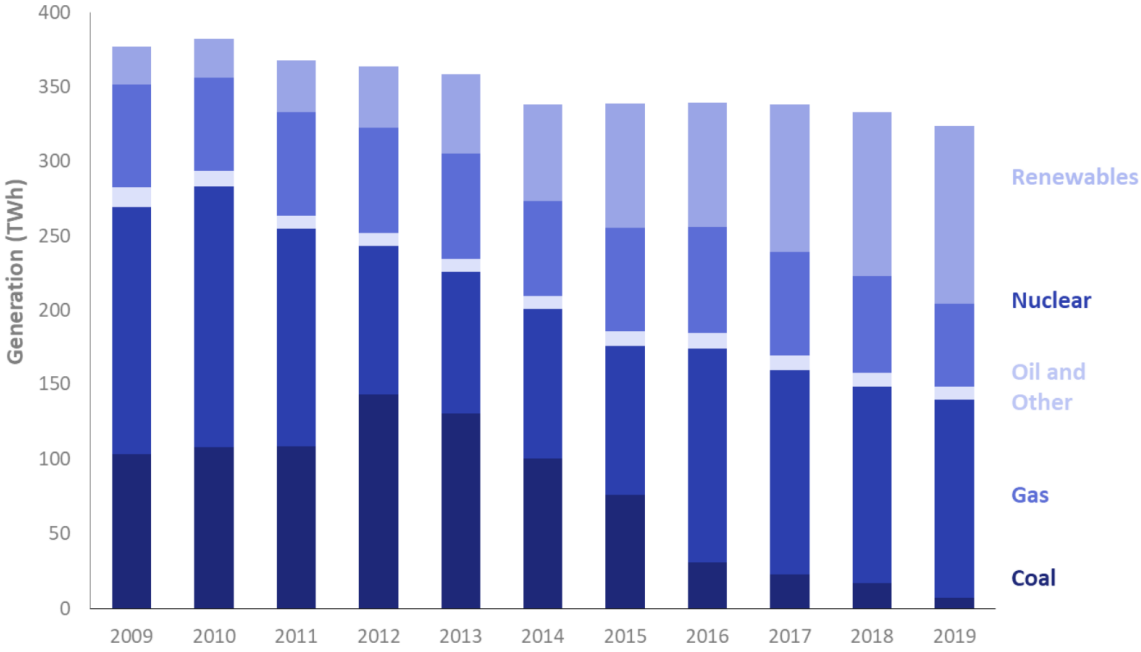

Figure 1.3: UK electricity generation by fuel type [6]

1.1.2 - Electric vehicles

The global electric car stock, including both purely electric, battery electric vehicles (BEVs), and plug-in hybrid electric vehicles (PHEVs), reached 7.2 million vehicles in 2019. The stock of electric buses also increased to approximately 500 000 vehicles, and the stock of two-wheeled electric vehicles reached 350 million. By 2030, the global stock of electric cars and commercial vehicles is predicted to be as high as 245 million [9]. The evolution of the global electric car stock from 2013 to 2017, and now dominated by China, is shown in Figure 1.4 [9].

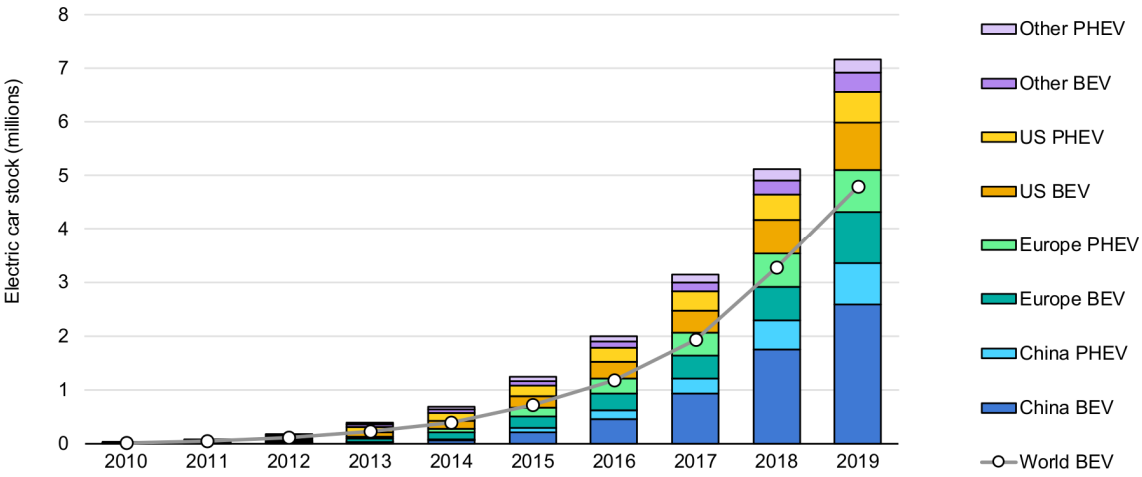

Figure 1.4: Evolution of the global electric car stock, 2013–2017 [9]

A mandate of the EU's 2009 Renewable Energy Directive [3] was that at least 10 % of energy used for transportation in member countries should be from renewable sources by 2020. In the UK, plug-in car grants, introduced in 2011 and facilitated by the *Energy Act 2008* [8], have contributed to a total of over 244 000 licensed plug-in electric cars on the road, as of the end of December 2019 [10]. The Society of Motor Manufacturers and Traders expects plug-in vehicles to constitute approximately 10 % of new car registrations in 2020 [11]

Electric vehicle charging, ranging from connections to domestic outlets to commercial charging stations, represents a significant prospective demand on distribution networks. For example, the Supercharger charger, manufactured by Tesla, is capable of charging a single vehicle at 120 kW, with 16 585 such chargers installed worldwide as of the end of May 2020 [12].

1.1.3 - Smart grids

The adoption of low-carbon technologies, such as renewable generation, energy storage, and electric vehicles, imposes a significant change in the demands on electricity distribution networks, and necessitates a change in the way that they are monitored and controlled. The adoption of renewable energy sources, in particular, is leading to a departure from the historical approach of centralised generation by a comparatively small number of large-scale, typically thermal plants. Instead, generation is increasingly decentralised and geographically distributed, existing at the very periphery of distribution networks in the case of, for example, domestic solar PV installations. A smart grid may be broadly defined as one which accommodates such low-carbon technologies, with monitoring and control achieved by means of additional technology installed on distribution networks, and associated telecommunications infrastructure [13], [14]. An overview of the topology and components typical of prospective smart grids is illustrated in Figure 1.5 [15].

The *American Recovery and Reinvestment Act of 2009* [16] provided $4.5 billion of funding for power system modernisation, including smart grid development. China's State Grid Corporation presented plans for a pilot smart grid programme in 2010, with $96 billion expected to have been invested by 2020 [17].

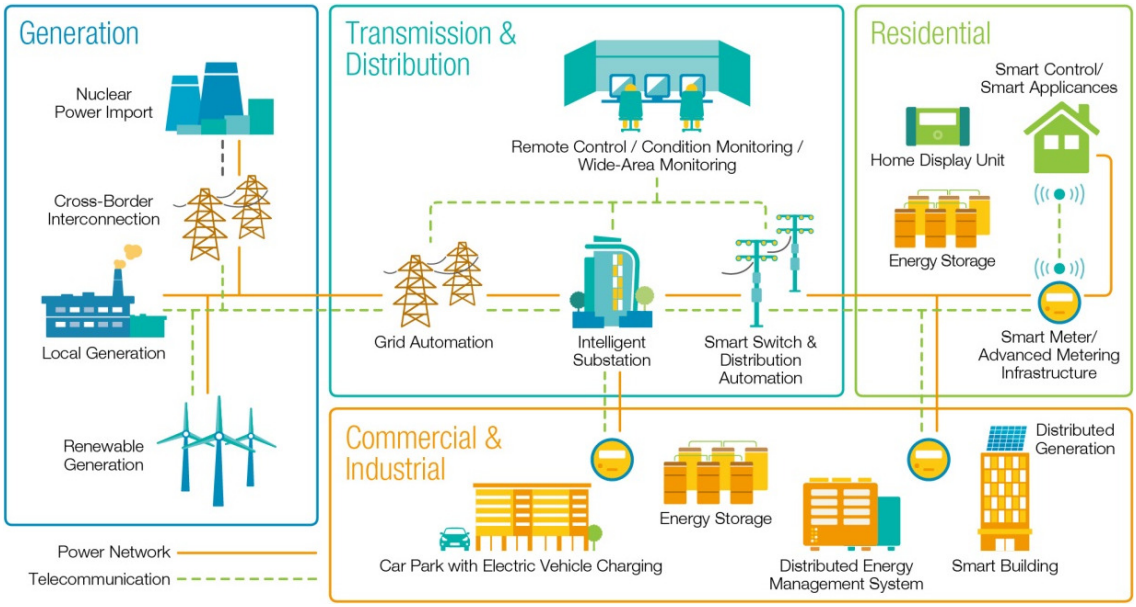

Figure 1.5: Smart grid topology and components [15]

In Europe, at least 950 projects have been, or are being, undertaken, across the 28 EU member countries plus Norway and Switzerland, totalling approximately €5 billion of investment [18]. The distribution of smart grid research and development (R&D) and deployment projects in Europe is shown in Figure 1.6 [18].

In the UK, the Low Carbon Networks Fund (LCNF) provided approximately £250 million of funding to 65 projects between 2010 and 2015. This was intended to stimulate the development and trial of the low-carbon technologies and infrastructure constituting smart grids, and to promote energy saving schemes. Examples of the projects undertaken include trials of energy storage, analysis based on the enhanced visibility provided by electrical measurement devices located at points on distribution networks which were not previously monitored, and measures to provide the additional network automation and control which may be required in the presence of high penetrations of distributed generation [19].

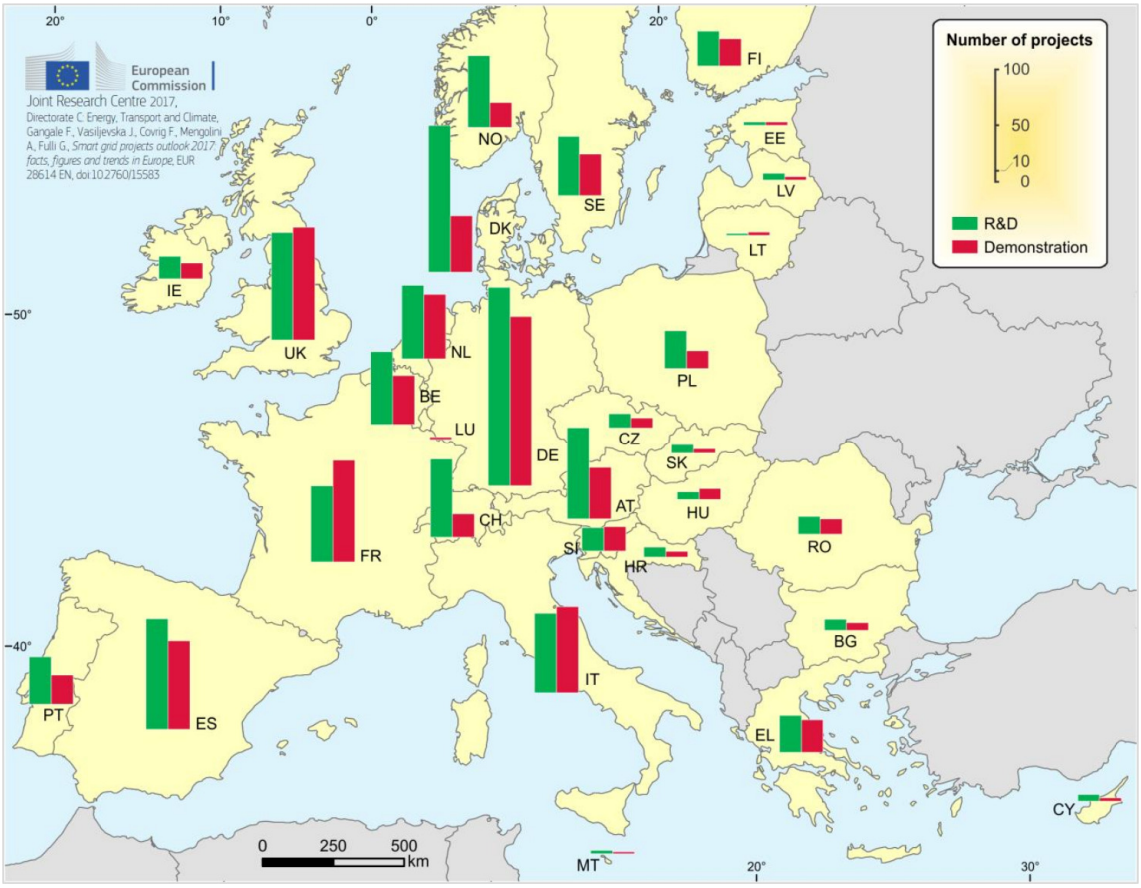

Figure 1.6: Smart grid R&D and demonstration projects in Europe [18]

1.1.4 - Smart electricity meters

In their most basic form, smart meters are distinguished from conventional utility meters by the facility to electronically communicate the values they measure and record to utilities, for the purpose of billing. This negates the requirement for manual meter reading, and provides the facility for more granular recording of energy consumption. Meters which fulfil this requirement are typically referred to as components of an automatic meter reading (AMR) infrastructure. More advanced smart electricity meters, capable of high-speed, two-way communication with utilities and other head-end systems, offer the facility of readings taken on demand, as well as the potential for demand-side management (DSM), for example by means of real-time pricing, or electrical measurements taken for the purpose of distribution network monitoring. Such meters are typically referred to as components of an advanced metering infrastructure (AMI) [13], [20]. The evolution of smart meter technology is shown in Figure 1.7 [21].

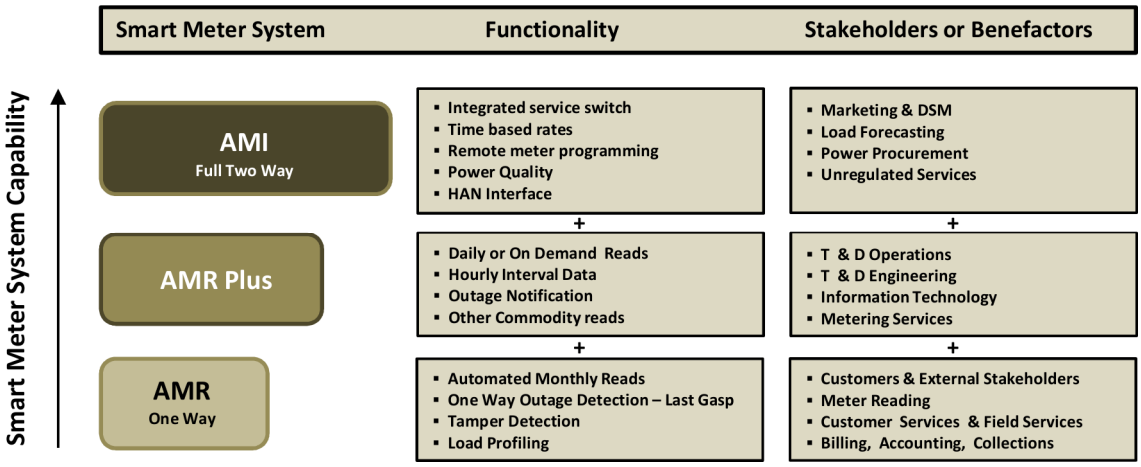

Figure 1.7: Smart meter technology evolution [21]

The fundamental elements of a smart meter, from acquisition of measurements of the electrical network to which it is connected, to communication with the utility or head-end system via a wide area network (WAN), are illustrated in Figure 1.8 [13].

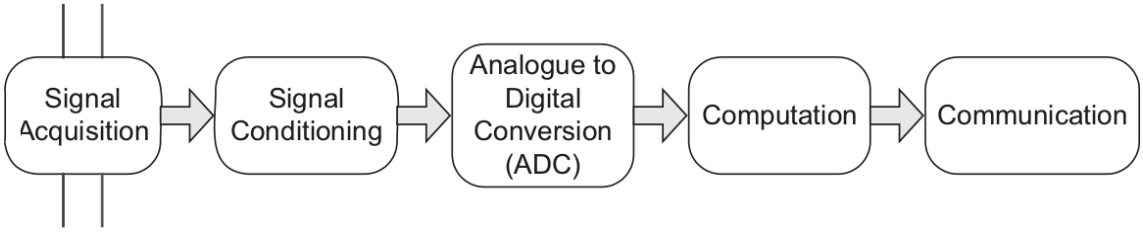

Figure 1.8: Functional block diagram of a smart meter [13]

AMI is considered to be a foundation investment in smart grids by enabling control at customer level, for example in the case of DSM, as well as by providing real-time visibility for the purpose of distribution network control and automation [20], [22]. This is shown in Figure 1.9 [20]

Globally, smart meter penetration is expected to reach approximately 53 % by the end of 2025 [23]. In Europe, legislation [24] under the EU's Third Energy Package mandates that, subject to a positive long-term cost-benefit analysis, member countries should equip 80 % of consumers with smart electricity meters by 2020. In the UK, there were approximately 16 485 000 smart meters operating in domestic and small commercial premises, as of the end of December 2019 [25].

From the perspective of both cyber security and security of supply, the adoption of AMI incurs significant potential vulnerabilities. These range from the compromise of consumer privacy by the inference of behaviour from energy consumption patterns, to the disruptive injection of false data, in the case that measurements from smart meters

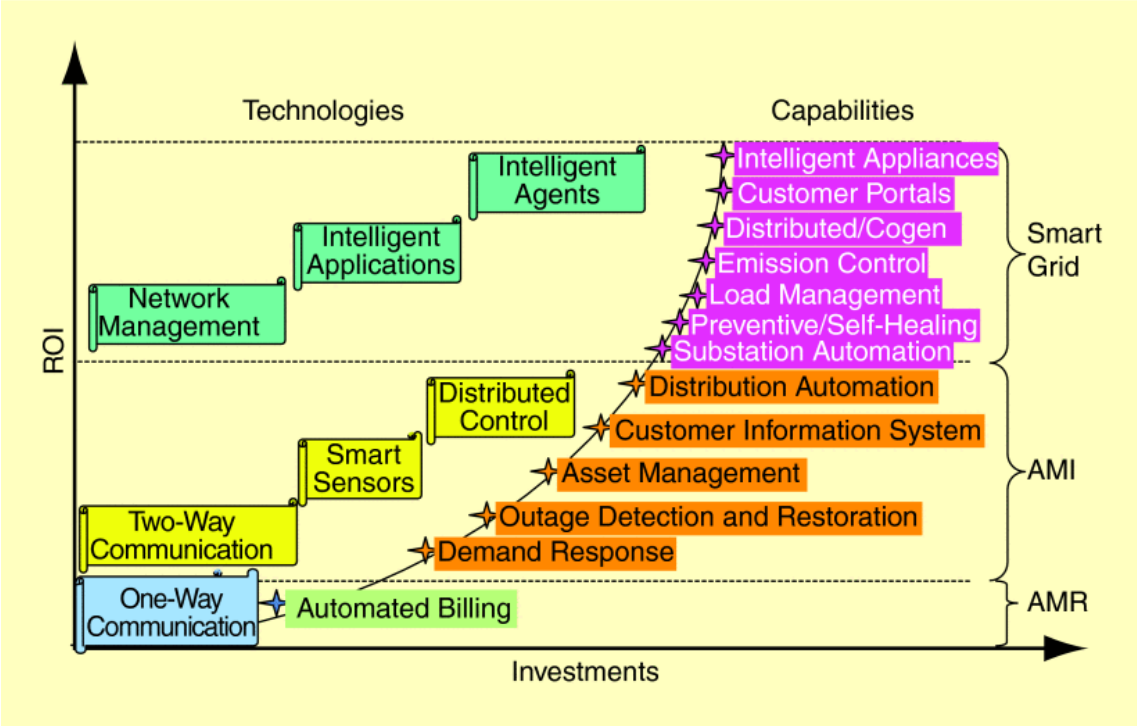

Figure 1.9: Smart metering and smart grid return on investments [20]

are used to inform distribution network control and automation. Where a remote supply disconnection facility is included within the smart meter, this represents a critical further vulnerability [26]–[28].

In the United States, the National Institute of Standards and Technology (NIST) has issued guidelines for security in smart grid infrastructure, including smart meters [29]. In turn, these guidelines cite existing standards for more general cyber security, for example the Federal Information Processing Standard (FIPS) *Minimum Security Requirements for Federal Information and Information Systems* [30], and *Security Requirements for Cryptographic Modules* [30], commonly known as FIPS 140-2. Such standards are readily applicable to AMI, owing to its close relation to existing, security-critical infrastructure, such as that for smart payment cards.

In 2012, the European Commission issued recommendations outlining the necessity for the mitigation of risks to privacy, personal data and security in the course of smart metering deployment [31]. An expert working group established by the European Commission, within its Smart Grids Task Force [32], has also issued broad cyber security guidance on smart grids, including AMI [33].

In the UK, the current *Smart Metering Equipment Technical Specifications* (SMETS 2) [34], issued by the Department of Energy & Climate Change (DECC), stipulate basic

security functions required of smart metering equipment, for example the support of specific cryptographic algorithms, and the secure storage of security credentials. The specification is supported by companion documents from other UK Government bodies, for example guidance on achieving certification under the National Cyber Security Centre's (NCSC) Commercial Product Assurance (CPA) scheme, issued by the former Communications-Electronic Security Group (CESG) [35]. This extends the DECC specification to outline the required behaviour and response of smart metering equipment in order to mitigate typical vulnerabilities and attacks.

Despite such guidelines and specifications, cyber security attacks have been demonstrated against commercially deployed smart meters in both the United States [36] and Europe [37], [38].

1.2 - Research objectives and structure

1.2.1 - Research objectives

The objective of the research described in this thesis was to investigate the impact of low-carbon technologies such as distributed, renewable generation on distribution networks, to demonstrate the use of smart metering in mitigating this impact, and to examine the issue of cyber security in the context of AMI. Particular contributions include:

- The development of a hardware smart meter test bed platform on which functions both within the capacity of existing smart meters, and expected to be within the capacity of future smart meters, may be tested.
- The development of a hardware-in-the-loop test rig, incorporating hardware smart meter test beds, the infrastructure required for WAN communication with the meters and for SCADA communication, and a Real Time Digital Simulator (RTDS) simulating a section of distribution network.
- The demonstration of a closed-loop control system which mitigates the impact of a high penetration of solar PV generation and electric vehicle charging on a section of distribution network, informed by real-time measurements from smart meters, and effected by a distribution transformer equipped with an on-load tap changer (OLTC).
- The demonstration of a cyber security attack in which a security vulnerability present in a commercially deployed smart meter is analysed, and exploited in a manner which permits unauthorised electronic access to the device.

1.2.2 - Thesis structure

Subsequent chapters are structured as follows:

- Chapter 2 examines the state of the art in the impact of low-carbon technologies such as distributed, renewable generation on distribution networks, the technical strategies available to mitigate these impacts, and their relative merits, the architecture of the control systems used to effect such strategies, and the cyber security issues pertinent to smart grids and AMI in particular.
- Chapter 3 describes the design, development and commissioning of a hardware-in-the-loop test rig to demonstrate the use of smart meter measurements for distribution network control, and incorporating multiple hardware smart meter test beds, the infrastructure required for WAN communication with the meters and for SCADA communication, and a Real Time Digital Simulator simulating a section of distribution network. The smart meter test bed platform developed permits the execution of custom firmware functions, and for the configuration of a wide range of measurement and communications parameters as required for a particular experiment.
- Chapter 4 describes the use of the smart meter test rig to demonstrate the implementation of real-time voltage control within a low voltage (LV) network. This employs the hardware, and builds on the foundation software and firmware, described in Chapter 3. A simplified LV network model is developed for execution on a Real Time Digital Simulator. The development of a voltage alarm firmware function for the smart meter test bed platform described in Chapter 3, and a voltage controller, is described. Finally, the operation of the controller is demonstrated in case studies illustrating scenarios of heavy loading, high levels of distributed generation, heavy, imbalanced loading, and the conflicting requirements of a combination of heavy loading and high levels of distributed generation.
- Chapter 5 describes the analysis of the cyber security vulnerabilities of a commercially deployed smart electricity meter resulting from inadequate provision for the protection of WAN communication, and for authentication when establishing connections with the local communications interface of the meter. These vulnerabilities are exploited, and are demonstrated to permit unauthorised electronic access to the meter. Recommendations are made of measures to mitigate the vulnerabilities identified and exploited.
- Chapter 6 provides a conclusion of the research undertaken, and identifies pertinent, future research avenues, further to this work.

2 - Literature review

2.1 - Introduction

The techniques employed for conventional network control, as well as the state of the art of the impact of distributed generation, strategies to mitigate this impact including the use of smart metering, and cyber security issues pertinent to smart grids and advanced metering infrastructure (AMI), are presented.

Subsequent sections are structured as follows:

- Section 2.2 examines the control techniques employed on conventional distribution networks, in the absence of a high penetration of distributed generation.
- Section 2.3 examines the impact of distributed generation on voltage regulation, power quality, and system protection, along with the potentially conflicting impact of electric vehicle (EV) charging.
- Section 2.4 examines control strategies to mitigate the impact of distributed generation on distribution networks, including the use of smart metering.
- Section 2.5 examines the architecture of schemes to mitigate the impact of distributed generation on distribution networks.
- Section 2.6 examines the basis for cyber security attacks on smart meters (SMs) and AMI, as well as the vulnerabilities of such systems, and published attacks.

2.2 - Conventional distribution network control

Voltage control has been employed in conventional distribution network control in order to provide a voltage at the connection point of customers which is compliant with applicable standards, for example *The Electricity Safety, Quality and Continuity Regulations 2002* [39] in the UK. Such control is required to accommodate the impact of varying demand on the voltage drop across transformers and conductors, as power is conveyed through the distribution network from high voltage (HV), through medium voltage (MV), to low voltage (LV). This is illustrated in Figure 2.1 [40].

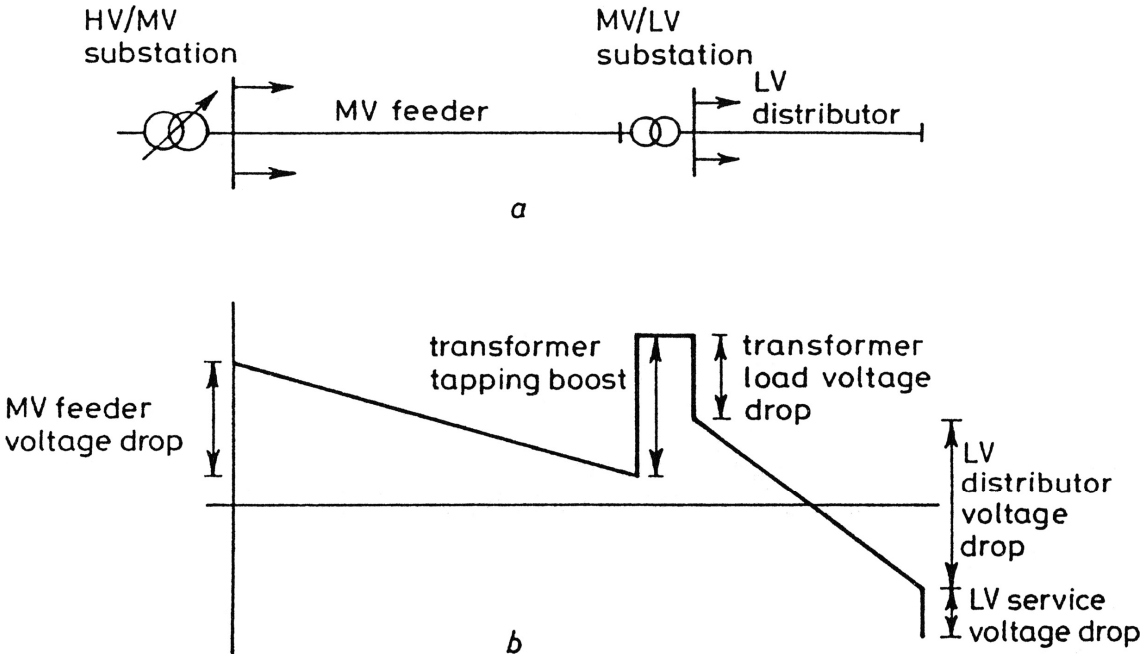

Figure 2.1: Voltage regulation on MV and LV networks. a: Simplified distribution network diagram. b: MV and LV network voltage variation [40]

The above figure shows the voltage drop across the MV and LV feeders and the MV/LV transformer, and the compensatory boost provided by the tap setting of the MV/LV transformer.

The principal mechanism of voltage control on conventional UK distribution networks is the variation of transformer tap setting. In the case of HV/MV, or primary transformers, this is typically achieved by means of on-load tap changers (OLTCs), operating automatically under load in order to maintain busbar voltage within an acceptable range. In the case of MV/LV transformers, this is typically achieved by means of manual, off-load tap selection [40], [41].

2.2.1 - Automatic voltage control

A conventional automatic voltage control (AVC) scheme for the control of OLTC-equipped HV/MV transformers is illustrated in Figure 2.2 [42].

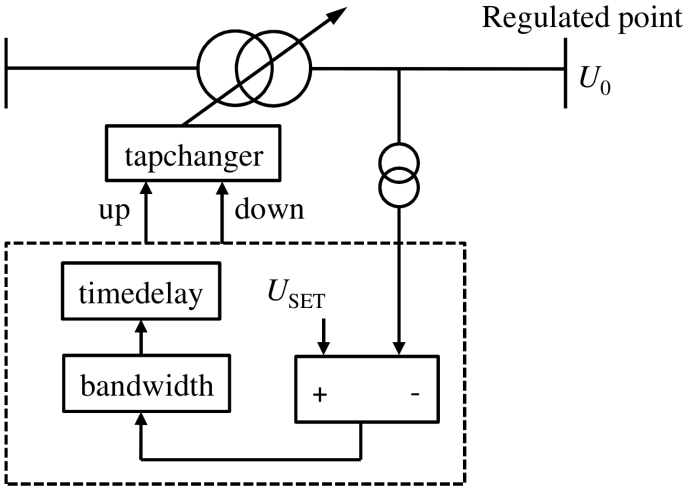

Figure 2.2: Basic AVC scheme [42]

Given the voltage set-point U_{SET}, the control scheme in the above figure acts to maintain the busbar voltage U_o within the range:

$$U_{LB} \leq U_0 \leq U_{UB} \tag{2.1}$$

where the lower boundary U_{LB} is defined as:

$$U_{LB} = U_{SET} - 0.5 \cdot bandwidth \tag{2.2}$$

and the upper boundary U_{UB} is defined as:

$$U_{UB} = U_{SET} + 0.5 \cdot bandwidth \tag{2.3}$$

The bandwidth element serves to prevent hunting of the control scheme. This can arise if a tap change performed to correct for what is deemed to be a low busbar voltage, results in what is deemed to be a high busbar voltage, or vice versa, resulting in a continuous sequence of alternate tap-change operations. Accordingly, a bandwidth of just under twice the transformer tap step is typically employed. The time-delay element serves to prevent the control scheme performing tap-change operations on the basis of brief voltage variations, and to limit the total number operations, with the associated wear on the tap changer mechanism and contacts [40].

2.2.2 - Line drop compensation

AVC schemes may be extended to account for the resistance and reactance of the feeder supplied by the transformer, and the current demand, known as line drop compensation (LDC) [40], [41]. This is illustrated in Figure 2.3 [42]:

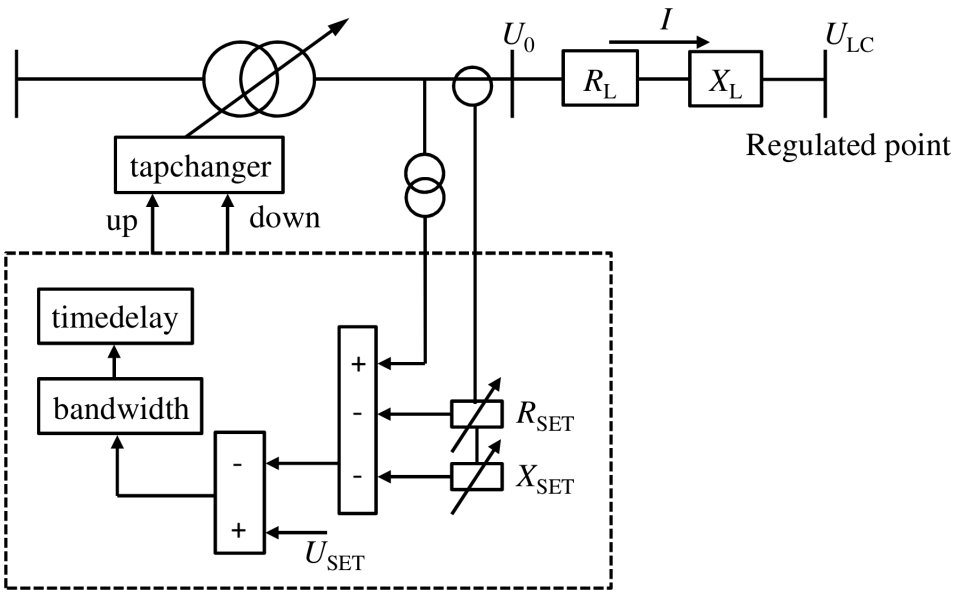

Figure 2.3: AVC scheme with LDC [42]

Given the voltage set-point U_{SET}, the control scheme in the above figure acts to maintain the voltage at the feeder-end load centre U_{LC} with the range:

$$U_{LB} \leq U_{LC} \leq U_{UB} \tag{2.4}$$

where the lower and upper boundaries are defined as per Equations (2.2) and (2.3) respectively. In addition to the busbar voltage, the load is also considered under this scheme, based on measured current, the resistive and reactive set-points R_{SET} and X_{SET}, derived from the ratios of the voltage and current transformers, and the feeder resistance and reactance, R_L and X_L.

2.2.3 - Voltage regulators and capacitor banks

In order to compensate for excessive voltage drop at critical points, voltage regulators and capacitor banks have sometimes been employed on UK distribution networks. The voltage regulators are typically autotransformers, equipped with OLTCs. The capacitor banks may be permanently connected and of a fixed value, or switched in order to

provide reactive power compensation and boost voltage according to demand [40]–[43].

2.3 - The impact of distributed generation

The principal impacts of distributed generation (DG) on distribution networks may be categorised as follows [44]–[50]:

- Voltage regulation: DG may cause a voltage rise at the point of connection. The additional demand of other low-carbon technologies, for example EV charging or heat pumps, if these are located elsewhere on a distribution network, may present a conflicting technical impact, compounding the issue of voltage regulation. Reverse power flow resulting from a high DG penetration may also result in undesirable behaviour in voltage regulation control schemes, for example LDC.
- Power quality: Transient voltage events such as dips and swells may result from sudden variation in the output of DG sources. DG sources interfaced to the network by means of power electronics may introduce harmonic distortion. Resonance or other interactions may also occur between DG sources and other elements of the distribution network, including voltage control systems. The uneven distribution of single-phase DG sources across phases, particularly on LV feeders, may result in voltage imbalance.
- Network losses: DG may reduce network losses by offsetting demand with local generation. However, if generation significantly exceeds local demand, with associated reverse power flow, losses may be increased. The thermal limits of distribution transformers and cables may limit the penetration of DG, as a result of increased power flow.
- System protection: DG may result in increased fault current levels on a distribution network. Furthermore, adding additional power sources to a distribution network may alter the pattern of power flow, and power flow in the opposite direction to conventional operation may occur. DG may also energise a network, or part of it, which is otherwise expected to be isolated from the upstream network.

Of the impacts listed above, the effect of DG on voltage regulation, the power quality issue of voltage imbalance, and system protection, along with the potentially conflicting impact of EV charging on distribution networks, are considered in further detail in the following sections.

2.3.1 - Voltage regulation

Injection of real power into a distribution network by a DG source results in a voltage rise at the point of connection [46], [51]. The regulatory limits prescribing voltage on a distribution network may result in voltage rise being the limiting factor to the penetration of DG. In a simple, radial feeder, the voltage rise caused by a DG source at its point of connection may be approximated as [45], [52], [53]:

$$\Delta V \simeq \frac{(P_G - P_L)R + (Q_G - Q_L)X}{V} \tag{2.5}$$

where P_G and Q_G are the real and reactive power output of the DG source, P_L and Q_L are the real and reactive power dissipation of the load, R and X are the resistance and reactance of the feeder, and V is the line voltage at the connection point of the DG source [45]. From this, it can be seen that the effect on voltage of DG sources located further from the substation will be more significant than those located closer to it. It can also be seen that whilst the injection of active power will result in a voltage rise, the injection or consumption of reactive power by the DG source will also result in an increase or decrease in voltage, respectively [46], [51]. At present, however, standards prescribing the operation and connection of small scale DG sources typically restrict their power factor to approximately unity, such as 1.00 ± 0.05 in the case of *Engineering Recommendation G83/2* in the UK [54], and an average, lagging power factor of no less than 0.90, at 50 % load, in the case of IEC 61727 [55].

Real power injected by DG sources serves to offset the power dissipation of local loads which would otherwise be served by the upstream network. If the power injection of DG sources exceeds the power dissipation of local loads then reverse power flow, relative to the direction of flow in the absence of DG, will occur. A simplified, radial feeder is illustrated in Figure 2.4 [56].

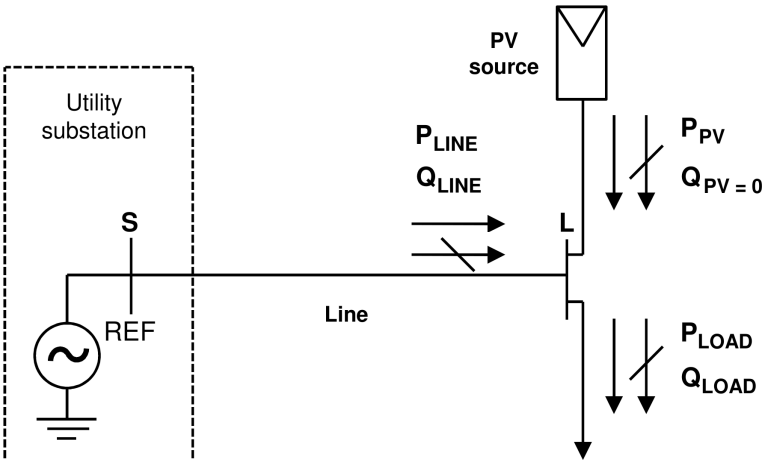

Figure 2.4: Simplified distribution system model [56]

Given a fixed load, the reduction and subsequent reversal of real power flow in such a network, as a result of increasing power injection, will cause the voltage at the point of connection to rise until a limit is reached. This is shown in Figure 2.5 [56].

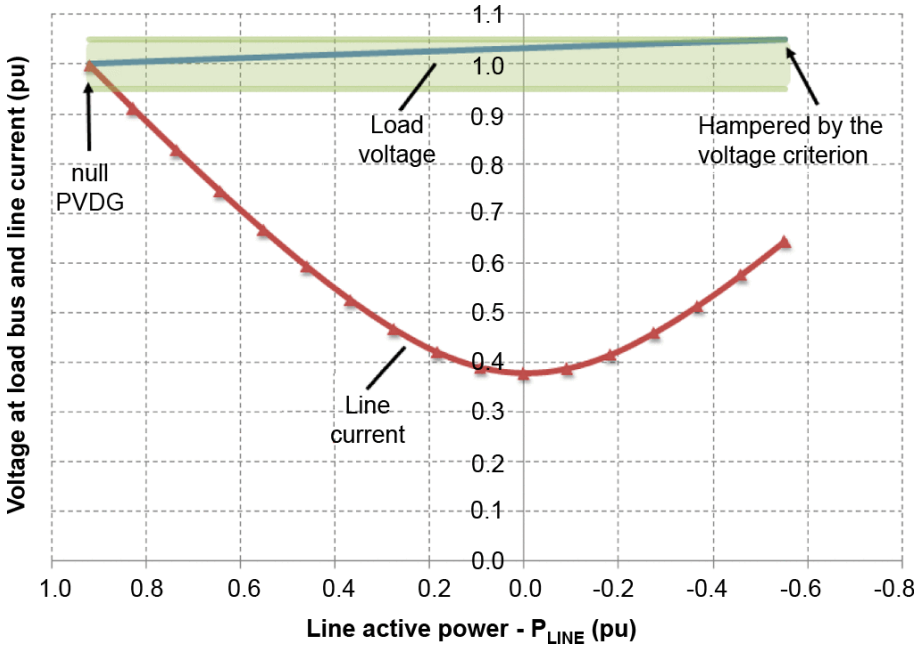

Figure 2.5: Voltage at the load bus and line current as a function of P_{LINE} [56]

The effect which DG may have on the voltage profile of a radial feeder under different levels of demand is shown in Figure 2.6 [50].

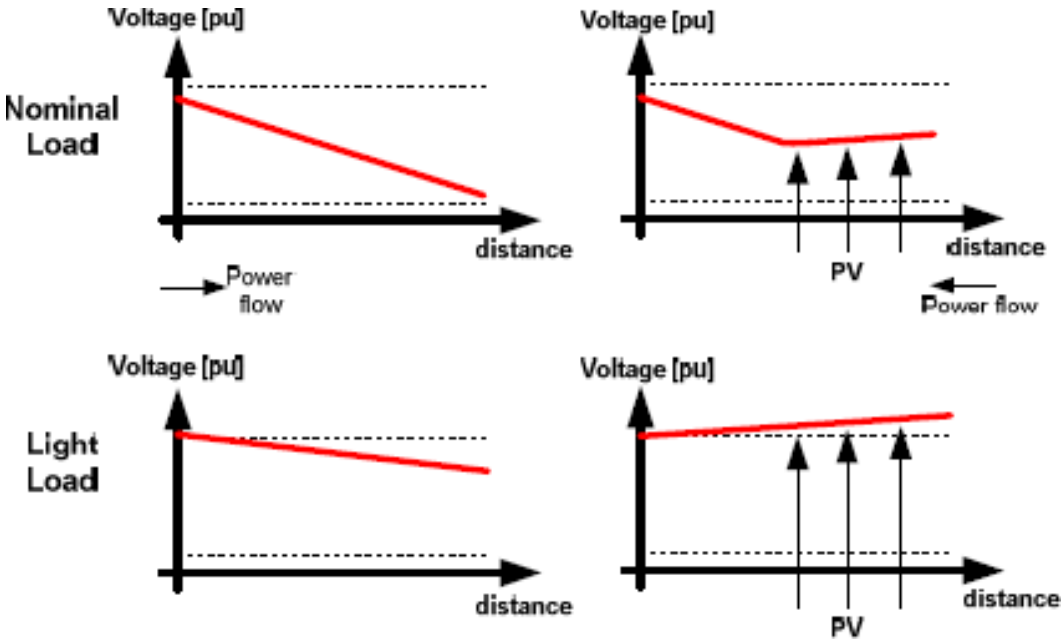

Figure 2.6: Voltage profile on an LV feeder. The second column shows the effect of solar photovoltaic (PV) inverters [50]

In [57], Ingram et al. present a generic, UK distribution network. This model extends from a 33 kV, three-phase source, to four 400 V, radial feeders, representative of urban, low voltage distribution systems. A single line, overview diagram of this network is illustrated in Figure 2.7 [45].

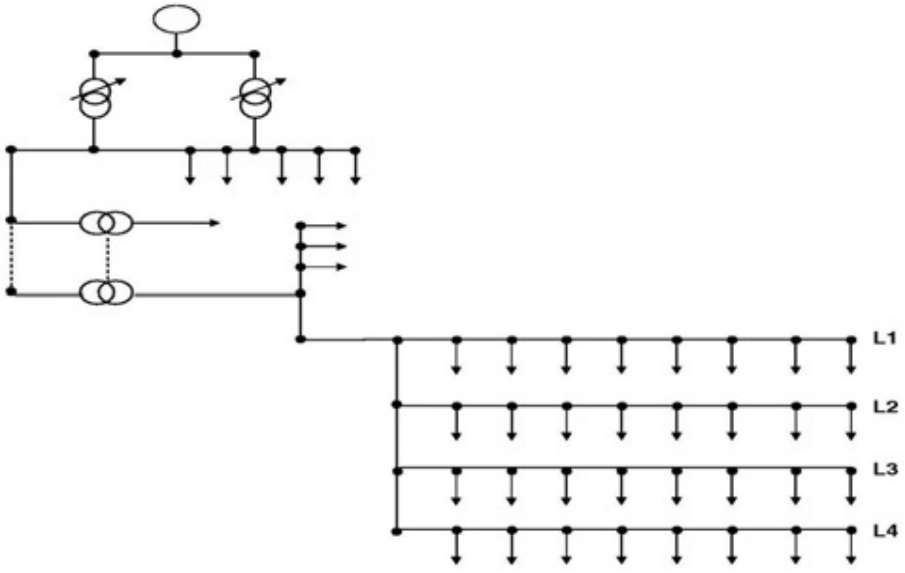

Figure 2.7: Single-line diagram of the UK Generic Network [45]

DG sources were modelled as single-phase, with a rating of 1.1 kW. DG Penetration is defined as the percentage of customers with these sources installed, such that 100 % penetration represents all customers having 1.1 kW of generation capacity, and 200 %

penetration represents all customers having 2.2 kW. A minimum load of 0.16 kVA per customer was considered. Of the four LV feeders, three were modelled as lumped loads, with the fourth represented in detail. The simulation study found that, assuming a uniform distribution of generation, an upper voltage limit of 10 % was exceeded at between 40 % and 50 % penetration of the 1.1 kW DG sources operating at rated output, under minimum load conditions, and dependent on whether a constant impedance or constant power model was used to represent system loads. Results of the low voltage feeder remote end voltages, for the constant impedance and constant power load models, are shown in Figure 2.8 and Figure 2.9 respectively [57].

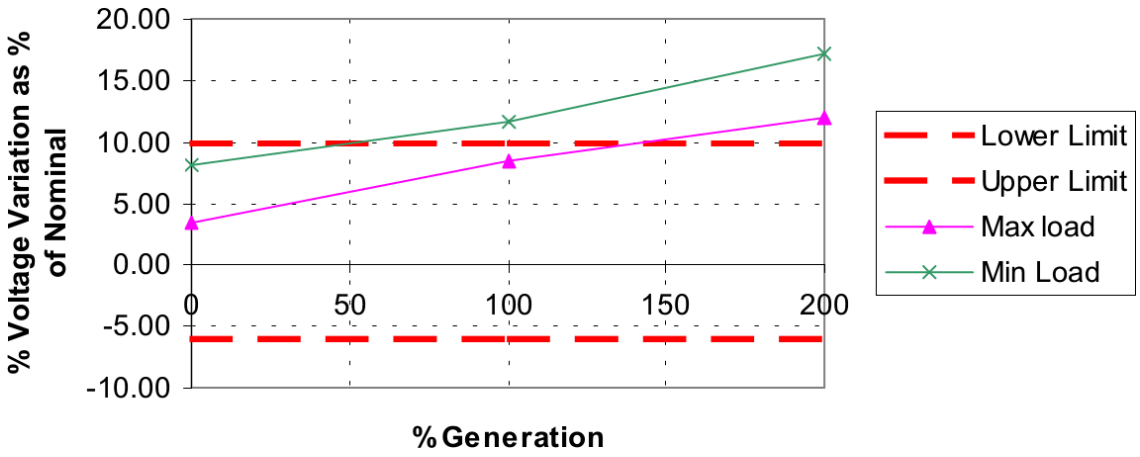

Figure 2.8: Voltage variation at the remote end of a 400 V feeder with increasing generation penetration, using a constant impedance equivalent load on the MV system [57]

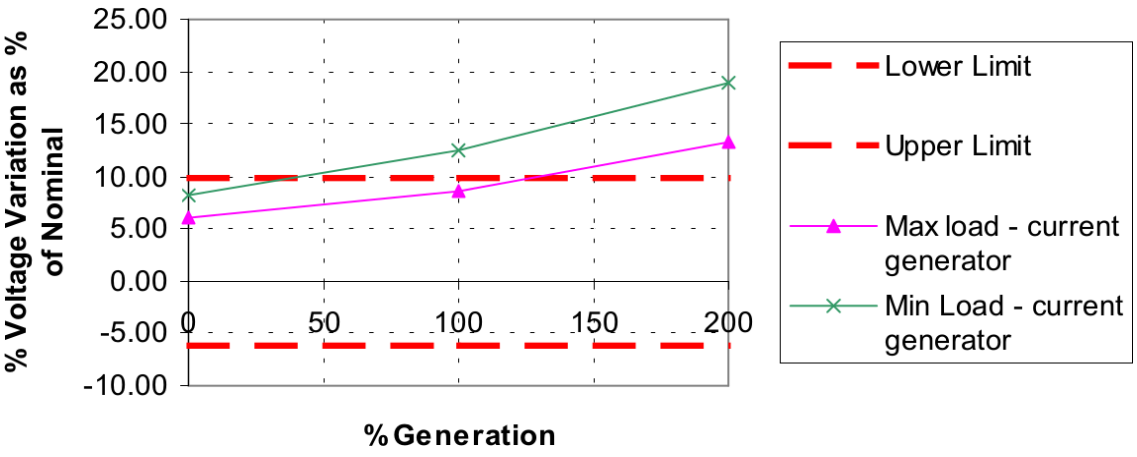

Figure 2.9: Voltage variation at the remote end of a 400 V feeder with increasing generation penetration, using a constant power equivalent load on the MV system [57]

The study of [57] further illustrated that local concentration of DG sources on a particular feeder results in an upper voltage limit being reached at the feeder end at a

lower level of DG penetration than can be achieved with uniform distribution of DG sources.

In [45], Trichakis et al. also performed a simulation study, using the generic, UK distribution network presented in [57] and illustrated in Figure 2.7. This study concluded that, assuming a uniformly distributed, minimum load of 61.44 kW at unity power factor, the maximum, uniformly distributed generation which could be supported by the network was 185 kW, before an upper voltage rise limit of 10 % was exceeded. The study further found that this voltage rise limited DG penetration before the cable and transformer thermal limits, and voltage regulation limits, were reached. Clustering of the DG sources to one of the four LV feeders was found to reduce the maximum generation which could be accommodated to 48 kW, whilst clustering of the DG sources at the ends of the LV feeders was found to limit the maximum generation to 28 kW, before a 10 % voltage rise limit was reached in both cases.

In [45], Trichakis et al. also performed a study based on an existing UK, urban, underground, LV distribution network. The network was modelled in Manitoba HVDC Research Centre's PSCAD. A single line, overview diagram of this network is illustrated in Figure 2.10 [45].

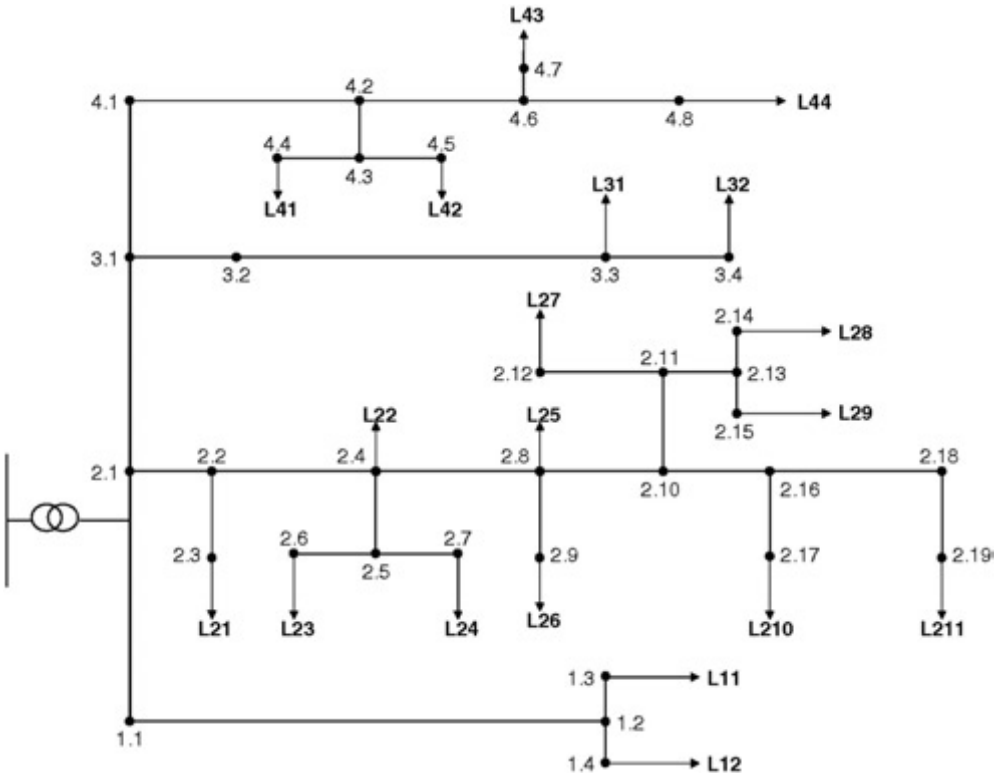

Figure 2.10: Single-line diagram of the case study public UK network [45]

The network illustrated in Figure 2.10 hosts 198 single-phase customers, as well as public street lighting. For the purpose of the study conducted, all demand is attributed to customer loads, with a minimum demand of 0.375 kW per customer at unity power factor. The maximum DG which can be accommodated on this network before a voltage rise limit of 10 % is reached is concluded to be 204 kW, or 1.03 kW per customer, with generation distributed uniformly across all customers, and under minimum loading. With the DG sources distributed uniformly across the 107 customers of the second LV feeder, the maximum generation which could be accommodated before this voltage rise limit was reached was found to be 85 kW, or 0.79 kW per customer.

In [58], Barbato et al. present the results of LV network monitoring by means of smart meters and MV/LV substation sensors, under the European FP7 project IDE4L. The network is located in the city of Brescia, Northern Italy, and hosted 299 customers, 118 with residential PV installations, across ten feeders. Figure 2.11 [58] shows the voltage of the second phase of Feeder 1 of this network, as well as the voltage measured at the connection points of two customers on the same phase, over one day.

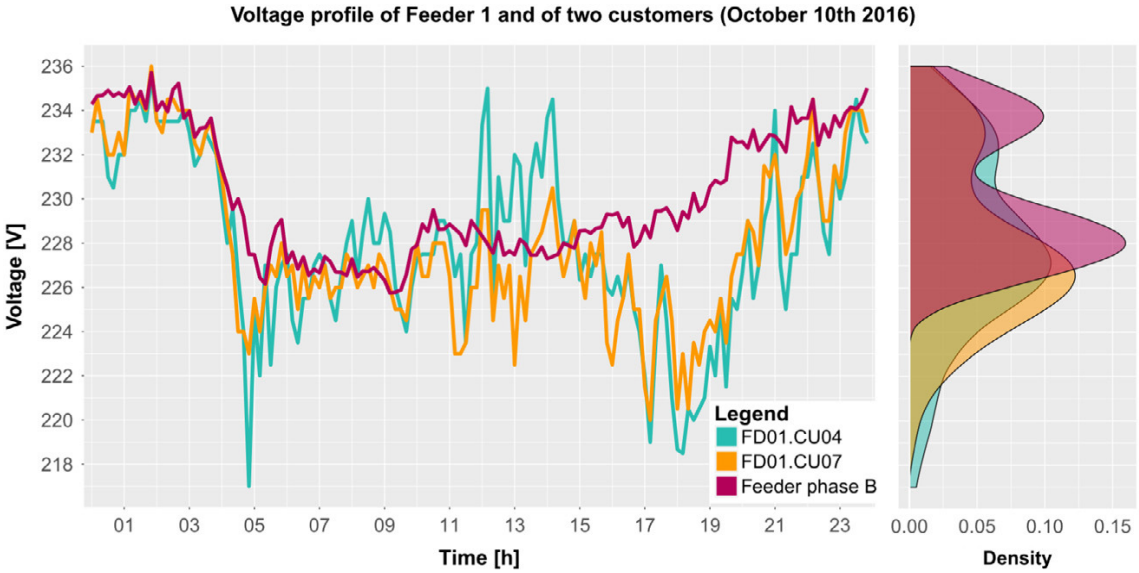

Figure 2.11: Voltage of Feeder 1-phase B compared with the voltage measured on customer 4 and 7 connected on the same phase. October 10th, 2016 [58]

It can be seen that the voltage at the connection point of customer CU04, with a PV installation, exhibits a significant rise during the afternoon period of maximum solar irradiance, compared to that of customer CU07, without a PV installation. Figure 2.12 [58] shows the voltages presented in Figure 2.11, over a period of one week. It is observed in [58] that, whilst PV generation is responsible for a significant voltage rise, the customer voltages recorded were within the 230 V ± 10 % range of EN 50160 [59].

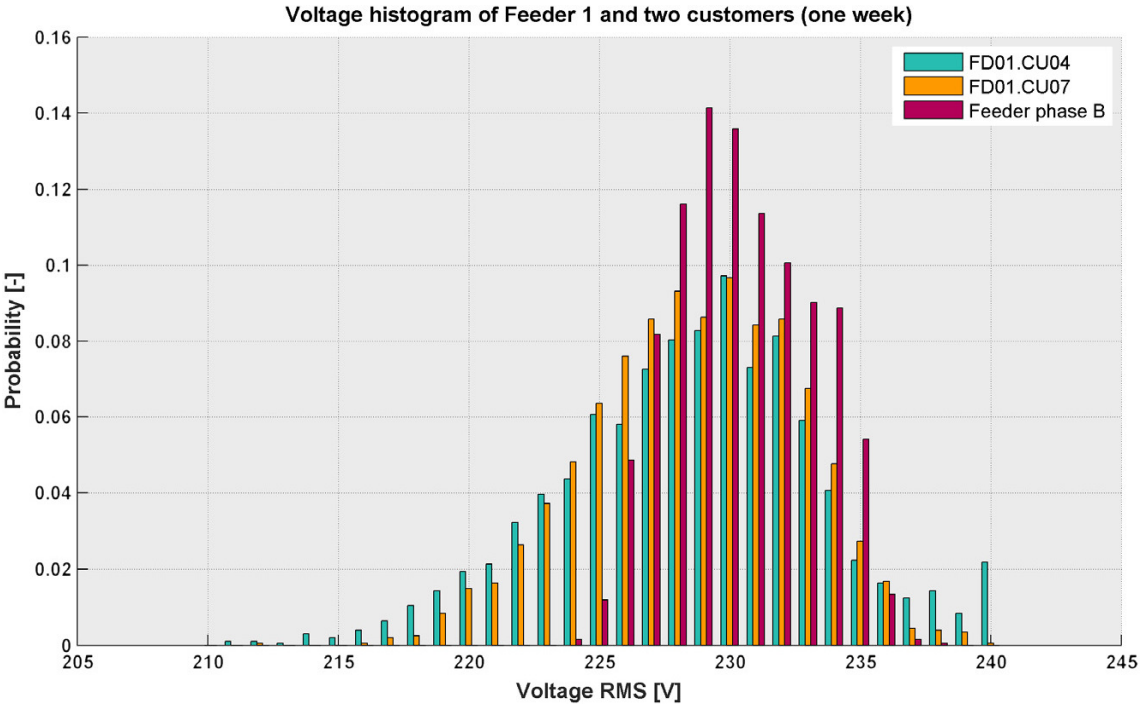

Figure 2.12: Histogram of one week of voltage measurements (Oct. 10th – Oct. 16th) [58]

The Low Voltage Network Solutions project [60], commissioned by distribution network operator (DNO) Electricity North West (ENWL), monitored substation voltage and imbalance, as well as a number of other parameters, on 200 substations across the ENWL network during 2012 and early 2013. Of these substations, 28 comprised pole mounted transformers, and 172 ground mounted, with a total of over 1000 LV feeders. With regard to the penetration of PV, the project found that 61 % of the substations assessed had between 0.2 % and 49 % of customers with PV installations, with an average PV installation capacity of 3 kW. Notably, the report found that in 7 % of the substations, busbar voltages were consistently above 253 V (1.1 p.u.), based on ten-minute sampling. Further to the project, and to estimate the impact of a greater penetration of PV generation, a probabilistic impact assessment was performed on 25 ENWL LV networks, with a total of 128 feeders [61]. Under this assessment, PV installations were modelled with random sizes, distributed according to the statistics of registered PV installations in the UK at the time of the study [62]. Irradiance was based on actual measurements recorded by Whitworth Meteorological Observatory at The University of Manchester. In considering the effect of a range of penetration levels of PV from 0 to 100 %, defined as the percentage of customers with the technology installed, a five-minute resolution of the PV data was used with a Monte Carlo method, and 100 simulations per penetration level. In the feeders with more than 25 customers connected, the percentage of feeders exhibiting technical issues of non-conformance with the one-week or ten-minute average voltage ranges of EN 50160 [59], or

exceeding the capacity of the transformer or conductors, at any level of penetration, is shown in Figure 2.13 [61]. Other technologies considered in the study, including EVs, are also shown.

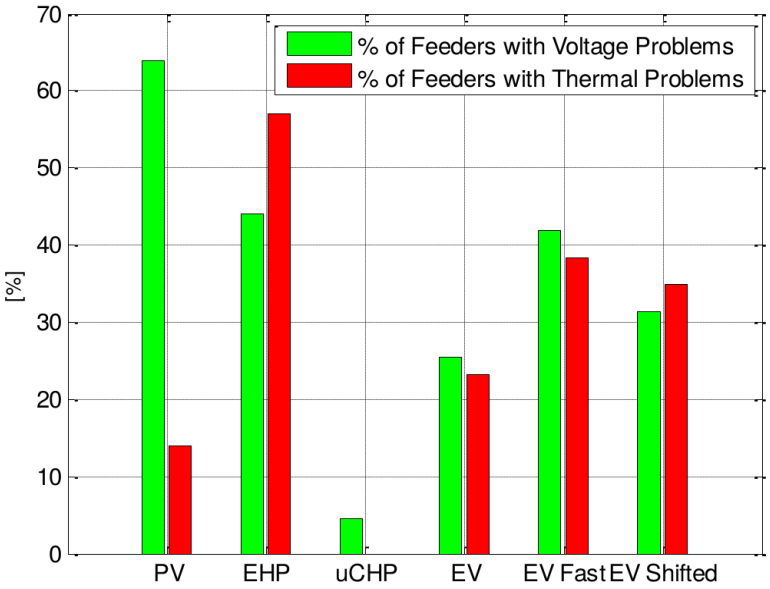

Figure 2.13: Feeders with technical problems per technology (more than 25 customers) [61]

The above figure shows that voltage issues were found in 64 % of the feeders modelled with up to 100 % of PV penetration. Figure 2.14 [61] shows the percentage of the occurrence of either voltage or thermal limits as the first issue in the case of increasing PV penetration on the feeders found to exhibit either technical issue. Again, other technologies considered in the study, including EVs, are also shown.

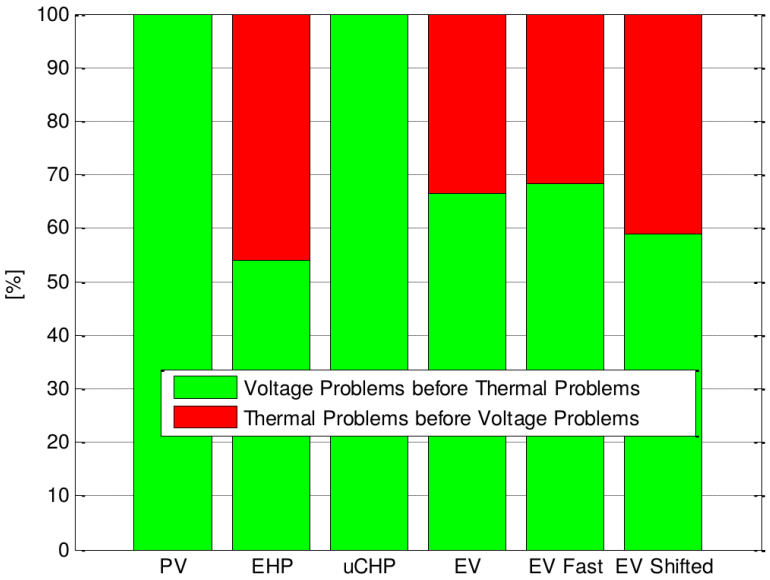

Figure 2.14: First technical issue among the feeders with problems per technology [61]

This above figure shows that, in all cases where a feeder is found to exhibit a technical issue, the voltage impact of PV generation is a more significant limit than the thermal constraints of the transformer and conductors.

2.3.2 - Voltage imbalance

The report *System Integration of Additional Micro-generation* [63], commissioned by the Department of Trade and Industry (DTI), asserts that the stochastic model presumed for the distribution of single-phase loads across the population of customers served by a three-phase feeder may reasonably be applied to the distribution of single-phase generation sources, such as PV systems, on an LV network. However, where imbalance in the distribution of single-phase DG sources across phases does exist, this can cause a voltage imbalance between phases [64]. This effect will be most pronounced at downstream points on radial feeders [65]–[67]. As well as resulting in increased losses from neutral conductor heating, a voltage imbalance is a particular issue for three-phase motors [64], [68] and variable-frequency drives [69]. Furthermore, the same power flow, imbalanced across phases, will result in less 'headroom' between the lowest or highest phase and prescribed limits, compared to a balanced condition [67], [70].

True voltage imbalance is defined in the UK [71], and Europe [59], as the ratio of the negative sequence voltage component to the positive sequence voltage component, expressed as a percentage. This is referred to as the voltage unbalance factor (% VUF):

$$\%\,\mathrm{VUF} = \frac{V-}{V+} \cdot 100 \tag{2.6}$$

The IEEE defines an approximation to this, the phase voltage unbalance rate [72], [73]:

$$\%\,\mathrm{PVUR} = \frac{\text{max voltage deviation from avg phase voltage}}{\text{avg phase voltage}} \cdot 100 \tag{2.7}$$

In the UK, Engineering Recommendation P29 defines a % VUF limit of 1.3 %, with up to 2 % permitted for less than one minute [71]. EN 50160 defines a range of 2 % for 95 % of the ten-minute average period over one week [59].

In [57], analysis of the impact of imbalanced connection of DG sources was conducted by only connecting generation sources to phase A of the 400 V feeder modelled in

detail. The resulting % VUF, for the constant impedance and constant power load models, are shown in Figure 2.15 and Figure 2.16 respectively [57].

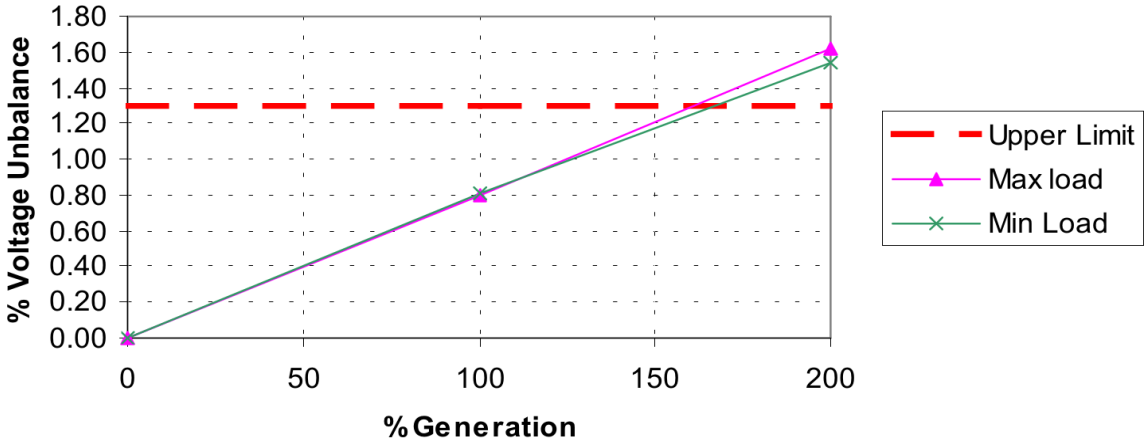

Figure 2.15: Voltage imbalance results due to connection of generation on one phase of a 400V feeder, using constant impedance equivalent load on MV system [57]

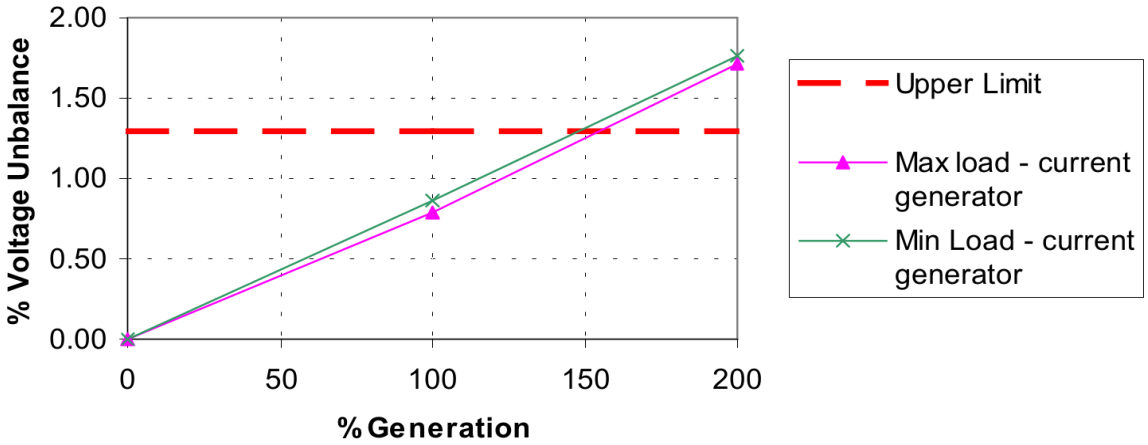

Figure 2.16: Voltage imbalance results due to connection of generation on one phase of a 400V feeder, using constant power equivalent load on MV system [57]

It can be seen from the above figure that the % VUF limit of 1.3 % defined by P29 [71] is exceeded with a penetration of 1.1 kW DG sources of approximately 150 %.

In [45], Trichakis et al. also examined the issue of imbalance, using the generic, UK distribution network presented in [57] and illustrated in Figure 2.7. It was found that, in the case of uniformly distributed, unity power factor DG sources, and at minimum, uniformly distributed unity power factor load conditions of 61.44 kW or 0.16 kW per customer, a maximum of 47.8 kW of generation could be supported on one phase of one feeder before a % VUF limit of 1.3 % was exceeded. In the case of the existing UK, underground, LV distribution network model also considered in [45] and illustrated in Figure 2.10, the maximum generation which could be supported, uniformly distributed

on one phase of the second feeder was approximately the same as for the generic, UK network, at 47.8 kW. This also reflects the maximum penetration of 150 % of 1.1 kW DG sources found in [57].

2.3.3 - System protection

In addition to the effect it may have on voltage, the introduction of distributed generation onto a distribution feeder may increase the magnitude of fault current flow in the feeder to which it is connected, and in adjacent feeders. It may also have the effect of changing the direction of fault current flow. Such impacts may require the uprating of assets such as transformers and conductors, and also have the potential to cause a number of issues with the operation of protection devices. Existing protection schemes predicated on one-way current flow may no longer be adequate to protect feeders hosting a high penetration of distributed generation, and an increase in the use of dedicated communication to coordinate protection may be required [49], [74]. Protection operation issues of particular concern are the following [44], [46], [75], [76]:

- Unintended islanding
- Protection blinding
- False tripping
- Reclosure impediment

These issues are considered in further detail in the following sections.

2.3.3.1 - Unintended islanding

Islanding occurs when a section of distribution network no longer connected to the upstream network continues to be energised by distributed generation connected to it. Although circumstances exist under which this may be desirable, it may present considerable hazards to equipment, those working on the network, and consumers, particularly if it is unintended. The most fundamental hazard is injury to consumers or those working on the network arising from an assumption that, since the local distribution network is no longer connected to the upstream network, it is no longer energised [49], [76], [77]. In the event that protection devices have isolated the section of distribution network from the upstream network due to the detection of a fault on the local network, DG sources may continue to contribute current to the fault, causing further damage [49]. A compounding issue is that, whilst it may be sufficient to cause damage, the fault current contribution of individual DG sources may not be sufficient

to trigger protection which would otherwise isolate the fault, in a timely manner [46], [74], [76].

Due to what may be a significant, step change in the load presented to DG sources on a section of network at the point that it becomes islanded, and also dependent on the control scheme of the individual DG sources, the voltage and frequency of the islanded network section may deviate rapidly and substantially from their values prior to disconnection from the upstream network. This presents a power quality issue which may damage assets and consumer equipment. It also presents a challenge to resynchronisation with the upstream network, prior to reconnection to it, and a considerable hazard if reconnection is attempted without resynchronisation. This requires dedicated protection infrastructure which would not have been required in the absence of DG sources [49], [74], [76], [77].

Deviation of voltage and frequency values following islanding of a section of network are currently the principal means by which islanding is detected [49], [77]. Standards prescribing the operation of DG sources, such as IEC 61727 [55] and IEEE 1547 [78], require the inclusion of islanding prevention measures in order that the sources quickly cease to energise a section of network if it becomes islanded. In the event of a rapid deviation of voltage and frequency values, 'passive' protection may be employed to isolate the DG source from the network when these values fall outside of an acceptable window. In the event that the match of load and DG capacity on the islanded network section is sufficiently good that the deviation of voltage and frequency occurs too slowly for islanding detection to occur in an acceptable time, 'active' protection may be employed. Under such a scheme, the control scheme of the otherwise voltage following DG source is designed to deviate more rapidly from the voltage and frequency values prior to islanding, by design. This enables the anti-islanding protection to detect values which fall outside of an acceptable window, and hence an islanded condition, more quickly than would otherwise be the case [49], [77].

In the case that auto-reclosing is employed, it is imperative that anti-islanding protection operates quickly enough that temporary faults are not sustained by the fault current contribution of DG sources during the dead time of the recloser. Such onerous timing requirements may preclude the use of voltage and frequency deviation to detect islanding, and instead require the use of dedicated communication between DG sources and distribution network protection equipment [74], [76].

2.3.3.2 - Protection blinding

Protection blinding, also known as protection under-reach, occurs as a result of the contribution of fault current from DG sources to a fault, in addition to the fault current from the upstream network. Consequently, the total current at the fault location will increase, while the contribution from the upstream network will decrease [44], [76]. Dependent on the impedance of the upstream network, the DG sources, and assets such as transformers and conductors, the current contribution of the upstream network may be reduced to such a degree in the event of a fault that protection does not detect it [74], [75]. This is illustrated in Figure 2.17 [44].

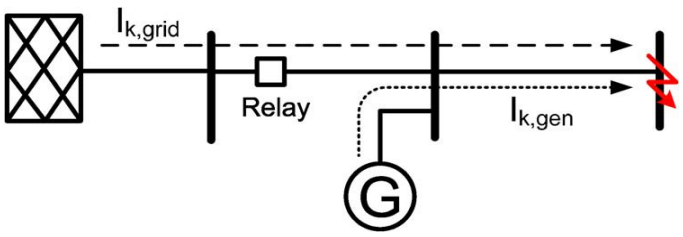

Figure 2.17: Principle of blinding of protection [44]

2.3.3.3 - False tripping

Where two or more feeders are supplied from a common substation bus, DG sources on one feeder may contribute fault current to a fault occurring on an adjacent feeder, via that bus. In addition to increasing the total fault current, the contribution of current from the feeder on which no fault is present may be sufficient to trigger the protection of that feeder, isolating it unnecessarily [44], [49], [75], [76], [79]. This is illustrated in Figure 2.18 [44]. Directional protection may be used to prevent erroneous tripping of this sort [44], [46], [49], [76], [80].

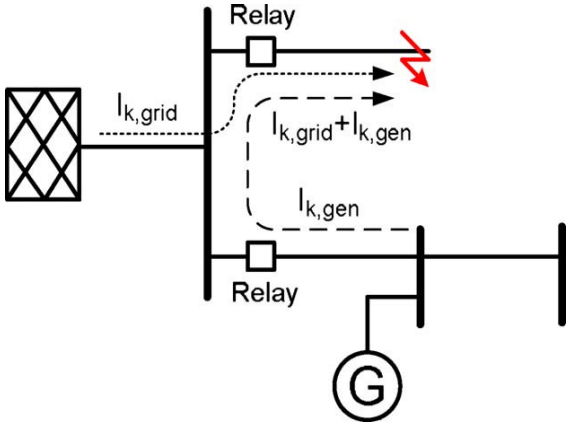

Figure 2.18: Principle of false tripping [44]

2.3.3.4 - Reclosure impediment

Since 80 % of faults occurring on distribution networks are temporary in nature, reclosers are widely employed, particularly to protect overhead circuits [44], [80]. However, DG sources may continue to supply fault current to a fault on a section of network during the dead time of the recloser protecting it, preventing arc extinction and sustaining the fault [44], [74]–[76].

In protection coordination schemes under which an upstream recloser is intended to prevent downstream protection devices such as fuses from operating in the case of temporary faults, the additional fault current contributed by DG sources may cause the downstream protection to operate before the recloser can operate [44], [49]. This is illustrated in Figure 2.19 [49].

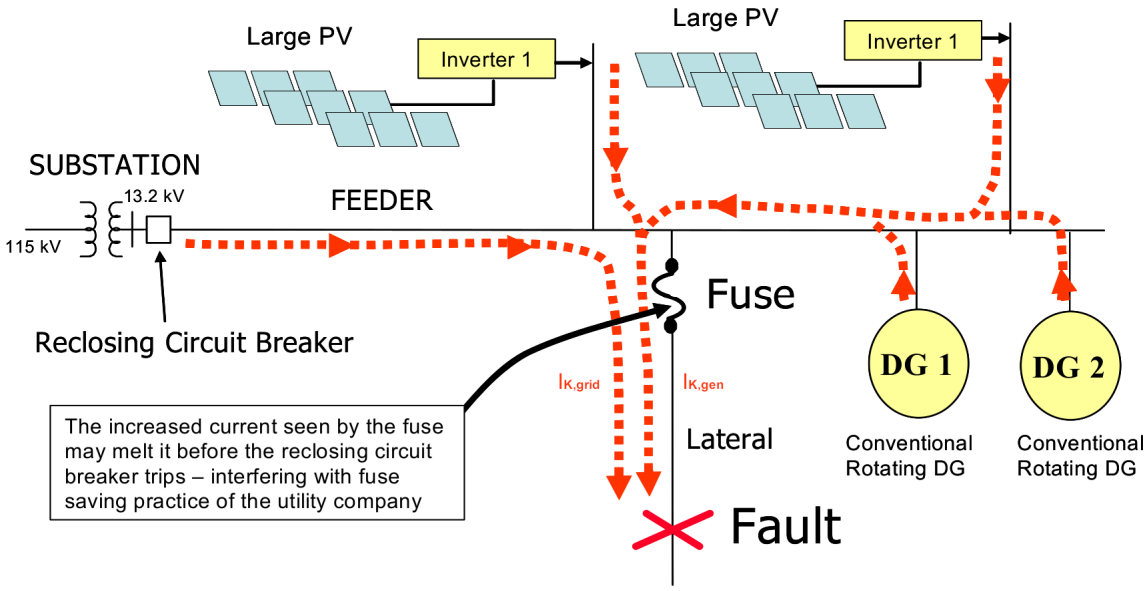

Figure 2.19: How fault contributions from other feeder energy sources such as PV can interfere with fuse and circuit breaker coordination in fuse-saving schemes [49]

Even during the dead time of a recloser, typically in the order of 0.3–0.6 s [81], significant deviation of voltage and frequency may occur in an islanded section of network, energised by DG sources present on it. This loss of synchronisation with the upstream network presents a significant hazard upon reconnection [74], [76], [77].

2.3.4 - The impact of electric vehicle charging

EV charging, not considering future vehicle-to-grid (V2G) technology, represents a significant potential load on distribution networks. A typical, residential charging point

has a rating of 16 A or 3.68 kW [82]. In [70], Rodriguez-Calvo et al. conclude that, since EV charging is expected to take place predominantly at night, during the period in which demand from other loads is typically lowest, it does not present such an immediate issue to voltage compliance as PV adoption. In [83], an aggregated charge profile for plug-in hybrid electric vehicle (PHEVs) is presented which reflects this, shown in Figure 2.20. However, it is noteworthy that such a profile is approximately an inverse of daily solar irradiance and, hence, potential PV output, and EV charging does have the potential to result in under-voltage conditions, particularly at the ends of long, radial LV feeders, or on already heavily loaded networks [84], [85].

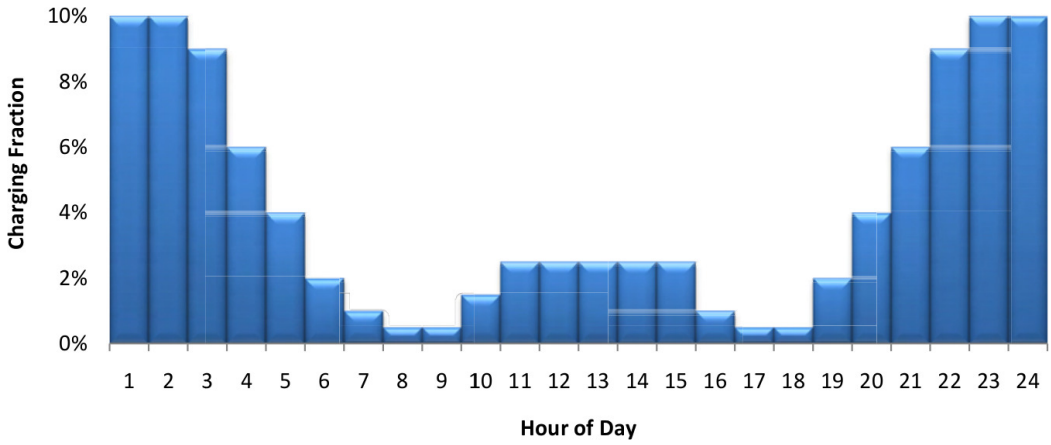

Figure 2.20: PHEV Charge Profile (Hour 1 represents 12:01 a.m. to 1:00 a.m. Hour 24 represents 11:01 p.m. to 12:00 a.m.) [83]

Even if the demand of EV charging does not result in under-voltage conditions on a distribution network, it has the potential to affect voltage regulation and balance.

In [84], a study of the impact of EV charging was undertaken, based on the generic and existing UK, LV distribution networks presented in [57] and [45], and illustrated in Figure 2.7 and Figure 2.10 respectively. Customer load, not including EV charging, was modelled according to half-hourly data provided by the UK Energy Research Centre (UKERC). The study considered a slow charging rate of 1.3 kW, and a fast rate of 9.6 kW, with a total of 66 customers using EVs, as per the penetration scenarios examined in the study. Figure 2.21 [84] shows the load effect of EV charging on a secondary transformer of the existing UK, LV distribution network, on both weekdays and weekends.

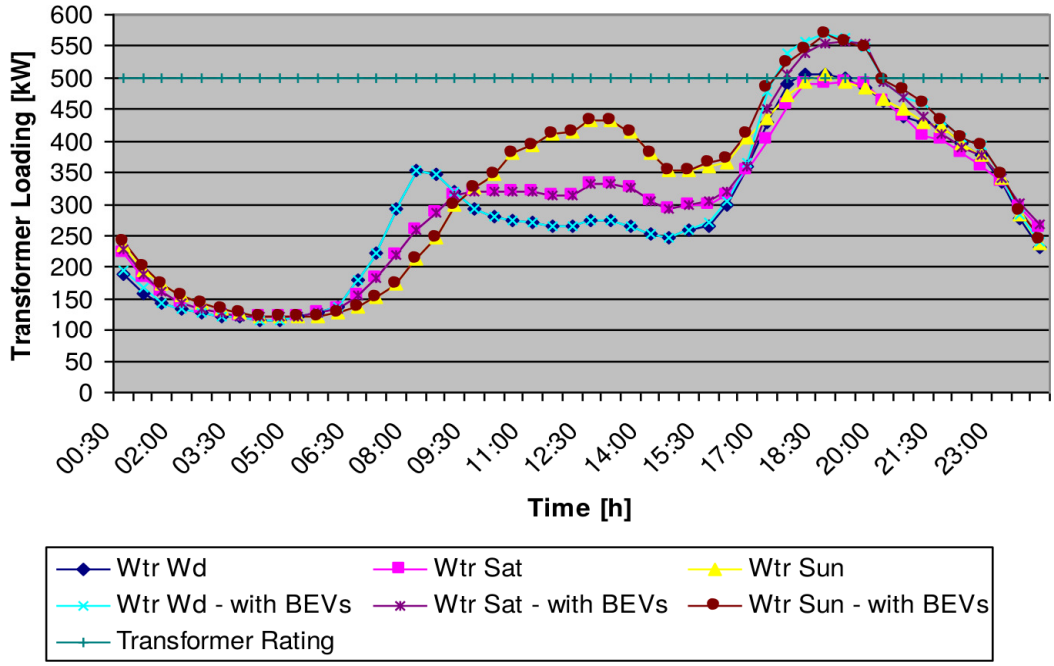

Figure 2.21: 100 % home slow-charging scenario for the UK existing LV distribution network during winter [84]

It can be seen from the above figure that the transformer rating is exceeded by EV charging under this scenario, on winter evenings. The study further found that EV charging resulted in transformer overloading in both autumn and winter when the generic UK network model was employed. Customer voltage was not found to exceed current UK voltage limits [39] under any of the scenarios considered. Under the worst-case scenario presented in Figure 2.21, the feeder end customer voltages were found to be approximately 236 V in the case of the generic UK network, and 239 V in the case of the existing UK network, with a substation voltage of approximately 250 V. With regard to voltage regulation, under the worst-case scenario, a voltage difference of approximately 6 % was found between the substation and feeder end in the case of the generic UK network, and approximately 4.7 % in the case of the existing UK network. The study also found that a maximum of approximately 48 kW of charging load may be accommodated on one phase of one of the 400 V feeders before a % VUF limit of 1.3 % [71] is exceeded. However, the report concludes that it is transformer loading which is expected to be the limiting factor with regard to EV penetration, although brief overloading may be tolerated by distribution transformers without the requirement for upgrading by the DNO.

Further to the Low Voltage Network Solutions project [60], commissioned by DNO Electricity North West (ENWL), and to estimate the impact of prospective EV adoption, a probabilistic impact assessment was performed on 25 ENWL LV networks, with a total of 128 feeders [61]. Under this assessment, EV profiles were created based on the

result of a one-year EV field trial conducted in Dublin. In the feeders with more than 25 customers connected, the percentage of feeders exhibiting technical issues of non-conformance with the one-week or ten-minute average voltage ranges of EN 50160 [59], or exceeding the capacity of the transformer or conductors, at any level of penetration, is shown in Figure 2.13 [61]. The figure shows that both issues of voltage non-conformance and issues of thermal overloading of network assets were found in approximately 25 % of the feeders modelled with up to 100 % of EV penetration. Figure 2.14 [61] shows the percentage of the occurrence of either voltage or thermal limits as the first issue in the case of increasing EV penetration on the feeders found to exhibit either technical issue. This figure shows that in this study, in all cases where a feeder is found to exhibit a technical issue, the thermal impact of EV adoption was slightly more significant than the voltage impact, presenting the limiting factor to EV penetration in approximately 65 % of cases.

2.4 - Strategies for distribution network voltage control

The principal strategies for voltage control in distribution networks hosting a large penetration of DG, also considering the potentially conflicting impacts of other low-carbon technologies (LCTs) such as EVs, may be categorised as follows [46], [85]–[90]:

- Network reinforcement: Reduction of the resistance and reactance of distribution network feeders reduces the effect of real and reactive power flow on voltage, as per Equation (2.5).
- Curtailment: The real power injection of DG sources may be constrained in order to limit the resulting voltage rise.
- Demand-side management (DSM): Appliances, domestic and commercial heating and cooling, and EV charging, may be controlled in order to optimally schedule their demand.
- On-load tap changers: By changing the distribution transformer tap position under load, busbar voltage may be controlled to reflect the balance of generation and demand on a feeder at a given time.
- Reactive power flow control: By absorbing reactive power, DG sources may mitigate the voltage rise resulting from real power injection, as per Equation (2.5). In the case that conflicting requirements exist, for example an over-voltage condition on a feeder resulting from a high penetration of PV and an under-voltage condition on an

adjacent feeder supplied by the same busbar resulting from high demand, injection of reactive power by switched capacitors may be employed to raise the voltage on the feeder exhibiting under-voltage, as per Equation (2.5).

- Storage: Local storage of real power from, for example, PV generation, may be used to limit the instantaneous real power injection into a feeder. Energy stored and consumed locally in this way does not contribute to active power flow in the feeder.

In all cases of active control, the distributed measurements offered by smart meters located at the periphery of the distribution network enhance the scope for, and effectiveness of, coordinated control [46], [85], [91].

Of the control strategies listed above, the use of OLTCs, reactive power flow control by DG sources, and energy storage, are considered in further detail in the following sections.

2.4.1 - On-load tap changers

On-load tap changers have not typically been used at secondary substation level in the UK and Europe [92], [93]. However, the requirement for voltage control in the presence of high DG penetration on distribution networks and, in particular, to mitigate the voltage rise associated with real power injection by these technologies, increasingly justifies the costs of additional transformer, communications and control infrastructure, and of the wear of tap-change operations [51], [94]. The implementation of OLTCs with electronic commutation in addition to [95] or replacing mechanical commutation [96]–[100], may mitigate these issues by offering faster commutation without mechanical wear or arcing. The use of decoupled OLTCs, capable of changing the tap position of each phase independently, has also been proposed [101], [102].

The performance of conventional AVC schemes, based on maintaining a constant busbar voltage, and LDC, in the presence of high penetrations of DG, have been examined in literature [42], [46], [49], [103], [104]. However, high penetrations of DG resulting in low load current and even reverse power flow may adversely affect such schemes [105]–[109]. Hence, control strategies have been presented which augment or supplant such control, as well as considering both time of day, significant due to the daily profile of solar irradiance, and the potential for distributed network voltage monitoring, even on LV networks, offered by technologies such as smart meters. In [103], a scheme by which historical voltage data from a feeder is used to augment more basic LDC control in the absence of real-time voltage measurements is proposed. In [106], conventional LDC is augmented by considering power flow direction. The use

of OLTCs in combination with reactive power control from DG sources, capacitors and distribution static compensators (DSTATCOMs) has also been examined [43], [110], [111], including with distributed voltage measurements [51], [112].

The DG DemoNet – Smart LV Grid project [113]–[116] considered three levels of OLTC control: That based only on voltage measurement at the local busbar, control based on distributed voltage measurements, and reactive power control of DG in addition to the OLTC. This was demonstrated in field trials on three Austrian LV networks.

In [117], Li et al. propose a scheme whereby voltage measurements from points distributed along the feeder served by a transformer are used to generate a reference value for an AVC relay controlling an OLTC. The algorithm for this function is shown in Figure 2.22 [117], where V_{ref} is the reference voltage provided to the AVC relay.

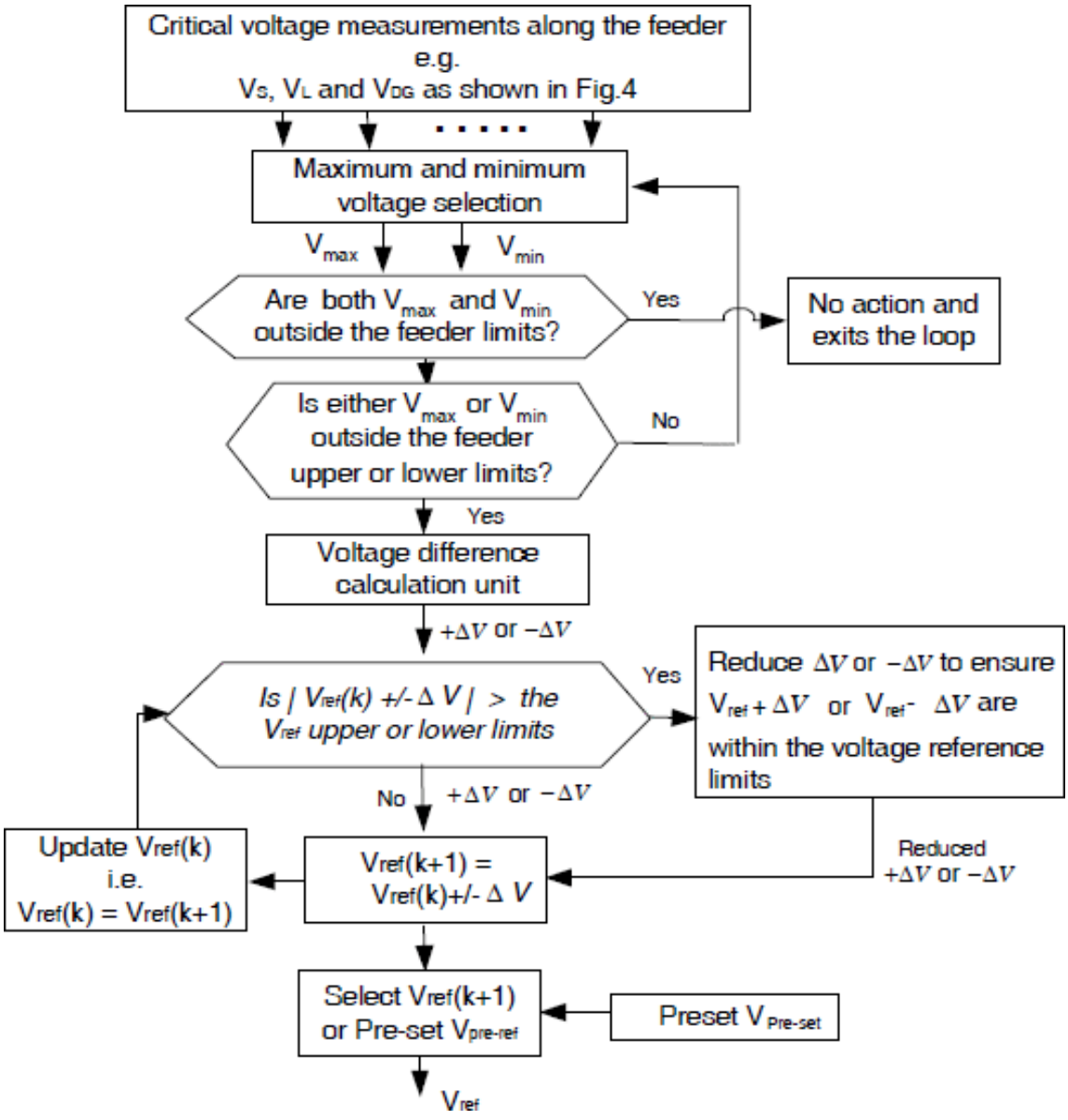

Figure 2.22: Automatic Voltage Reference Setting (AVRS) [117]

It can be seen that this scheme considers whether an existing conflict between concurrent over-voltages and under-voltages exists, and whether a tap-change operation will result in further voltage violations. In [118], a similar algorithm to that that proposed in [117] was demonstrated which also considers the effect of multiple prospective tap-change operations, prior to issuing a new voltage set-point reference. This scheme was demonstrated on a model of a section of Finnish distribution network supporting both static loads and controllable DG, simulated on a Real Time Digital Simulator (RTDS) in order that closed-loop testing of the control algorithm could be performed on commercial distribution network automation hardware. The operation of the algorithm is shown in Figure 2.23 [118].

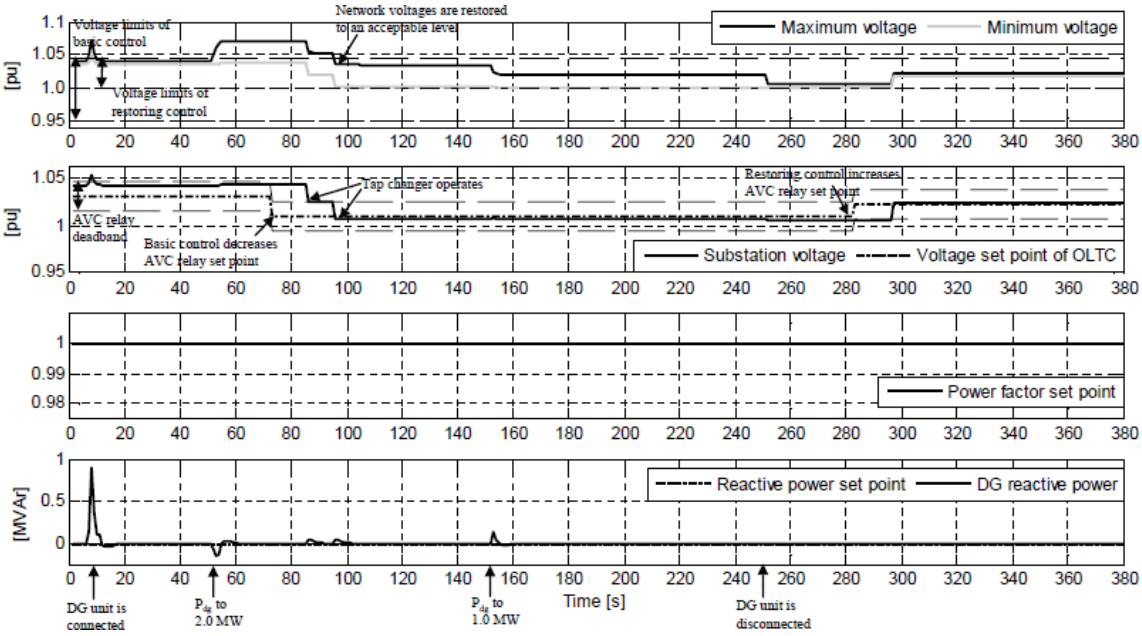

Figure 2.23: The operation of the control algorithm in minimum loading conditions when substation voltage is the primary control variable [118]

It can be seen that an increase in DG active power output results in an over-voltage condition to which the algorithm responds, issuing a voltage set-point which results in two tap-down operations, restoring the voltage to within limit. The disconnection of the DG subsequently results in an under-voltage condition to which the algorithm responds by issuing a voltage set-point which results in a single tap-up operation, restoring the voltage to within limits.

In [93], Long et al. specifically consider the application of OLTCs to LV feeder control, with three possible control schemes: constant set-point, time based, and remote monitoring based. Under the constant set-point scheme, tap changes are made in order to maintain a busbar voltage as close as possible to the set-point. The time-based scheme employs two set-points, representing peak and off-peak demand, and scheduled according to time of day and season. The remote monitoring scheme employs feeder end voltage readings, and categorises the proximity of these values to limits as green, orange, or red, representative of their severity. This is shown in Table 2.1 [119]. An OLTC voltage set-point for the next control cycle, $V_{set\ i+1}$, is calculated as shown below, where $V_{busbar\ i}$ is the current busbar voltage, and ΔV_i is a compensating voltage.

$$V_{set\ i+1} = V_{busbar\ i} - \Delta V_i \tag{2.8}$$

The compensating voltage ΔV_i is the product of the factor corresponding to the category of the maximum and minimum of all the feeder end voltages, taken from Table 2.1, and the voltage step of the OLTC.

Table 2.1: Compensating voltage factor according to the voltage zones [119]

		Maximum				
		Red >253V	Orange 253V≥. ≥248V	Green 248V>. ≥221V	Orange 221V>. ≥216V	Red <216V
Minimum	Red >253V	+3				
	Orange 253V≥. ≥248V	+2	+2			
	Green 248V>. ≥221V	+2	+1	0		
	Orange 221V>. ≥216V	+1	0	−1	−2	
	Red <216V	0	−1	−2	−2	−3

In [93], the performance of the remote monitoring scheme was compared to that of the simpler fixed, and time-based set-point schemes using a model of a real, UK, residential LV network, operated by ENWL. This consisted of six radial, LV feeders, with a total of 351 single-phase customers, simulated in EPRI's OpenDSS and MathWorks' MATLAB. Customers were modelled with realistic load and PV generation profiles, with PV penetration defined as the percentage of the total number of customers with a PV installation. The OLTC bandwidth, the difference between the busbar and set-point voltage at which the OLTC will operate, was set at 2.2 %. The tap changer delay, the period for which the bandwidth must be exceeded before the OLTC will operate, was set at 120 s. With an even penetration of PV, the average, annual effect on voltage compliance of the remote monitoring-based control (RMC), constant set-point control (CSC), and time-based control (TBC) schemes, compared to compliance in the case of only off-load tap changer provision, is shown in Figure 2.24 [93]. The average daily number of tap changes for this period is shown in Figure 2.25 [93].

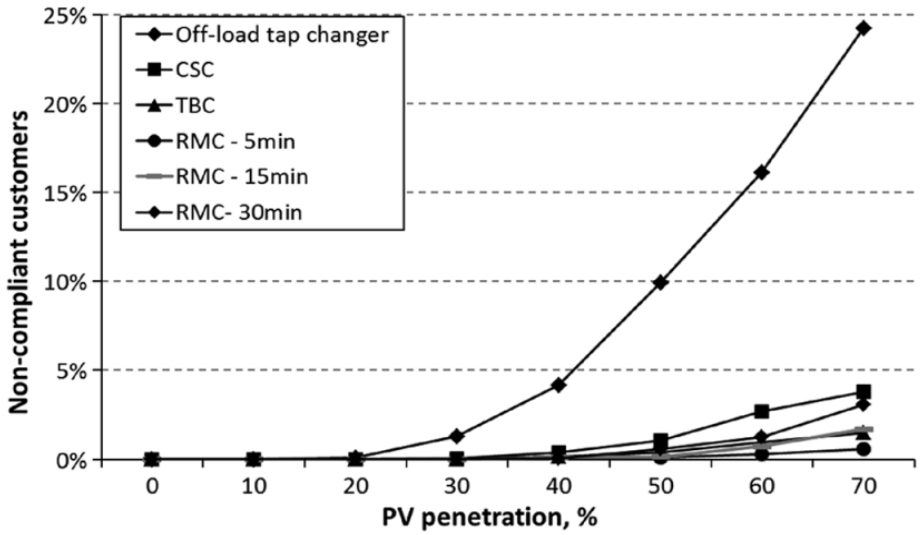

Figure 2.24: Average customers with voltage problems - even PV penetration [93]

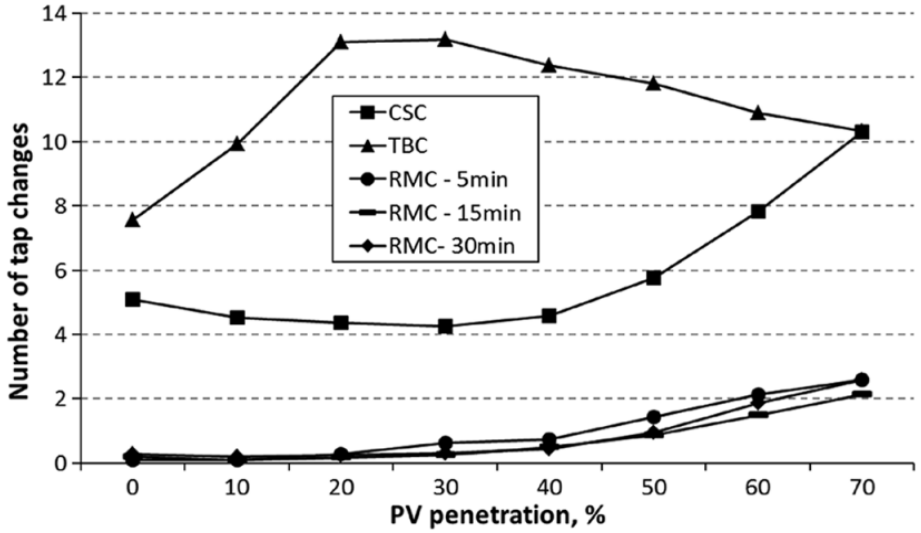

Figure 2.25: Daily average number of tap changes - even PV penetration [93]

It can be seen that under all control schemes, the OLTC significantly mitigates the voltage non-compliance issue of increasing PV penetration, when compared to an off-load tap changer, and that employing remote monitoring in the control algorithm both increases the degree of this mitigation and reduces the total number of tap-change operations required.

The remote monitoring based control scheme presented in [93] was deployed in a trial conducted by ENWL involving two secondary substations equipped with OLTCs [119]. Both had six feeders, with PV penetration of approximately 30 %. In this case, the OLTC bandwidth was set at 4.4 %, and the delay at 120 s. The set-point, busbar voltage, and tap position over the course of a midweek, May day at one of the two substations is shown in Figure 2.26 [93], [119].

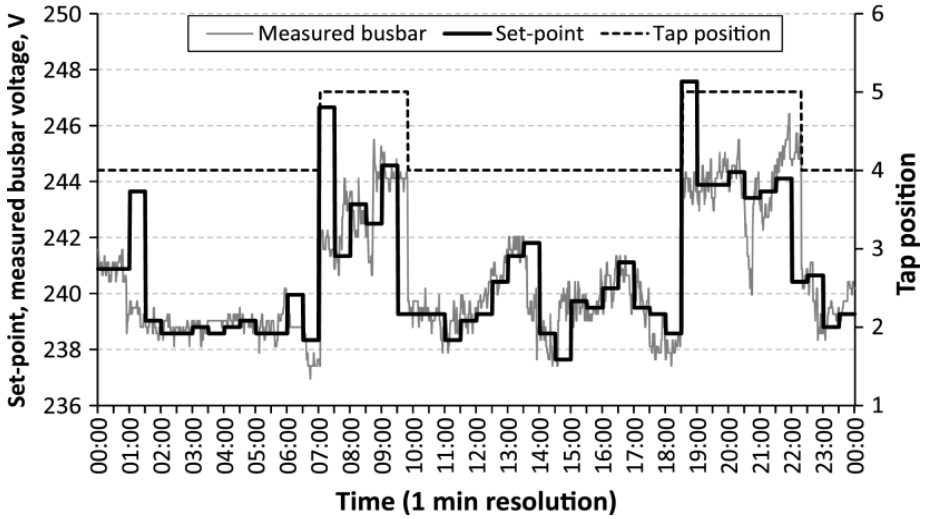

Figure 2.26: Actual tap operation at Landgate Substation [93], [119]

2.4.2 - Reactive power control of distributed generation

The X/R ratio in LV networks is low in comparison to MV networks, typically by an order of magnitude [120]–[122]. This reduces the capacity for voltage regulation by means of reactive power control [123]. The transfer of reactive power also results in increased system losses and loading of the DG sources [118], [124]. Indeed, the increased losses resulting from the power transfer associated with the use of reactive power exchange to limit voltage rise from real power injection may exceed the real power injection curtailment required to achieve the same effect [120].

In the case of reactive power control of DG sources such as PV inverters for the purpose of voltage regulation, the reactive power capacity of the DG source is limited by the total apparent capacity, and the active power output of the device. The operation envelope of such a DG source is shown in Figure 2.27 [51].

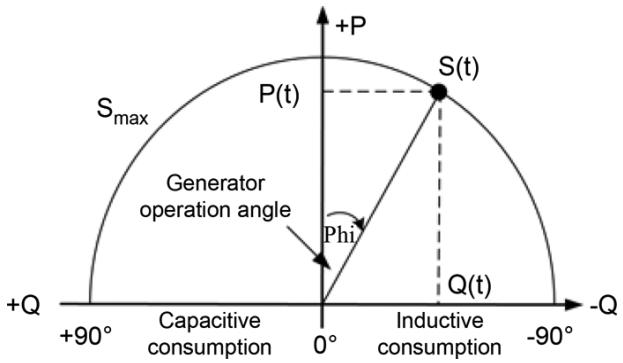

Figure 2.27: PQ-diagram of a generator (generator perspective) [51]

It can be seen from this figure that the vector sum of the active (P) and reactive (Q) power flows of the DG source must not exceed the total rating of the device (S). The limitation of active power export due to the use of reactive power flow for voltage control may have an undesirable economic impact [51].

In Germany, the capacity for reactive power absorption to aid voltage control is mandated for LV-connected PV inverters [125]. The standard, local reactive control rule is shown in Figure 2.28 [124], [125].

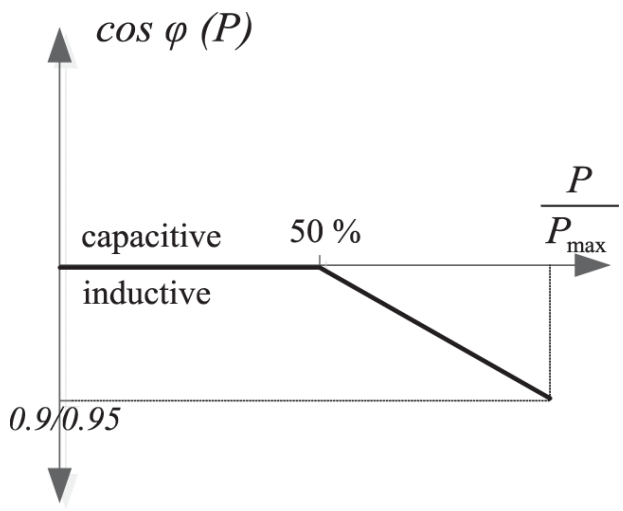

Figure 2.28: Standard local reactive control rule [124], [125]

Under this control scheme, above 50 % of rated output, the PV inverter absorbs reactive power, up to a power factor of 0.95, in order to mitigate the voltage rise at its point of connection resulting from real power injection.

In [124], [126]–[128], DG control schemes are proposed whereby the reactive power of a DG source is controlled in order to minimise the voltage rise at the point of connection. In [129], Carvalho et al. demonstrate such a DG control scheme on a simple MV feeder model representing a 20 km-long, 30 kV, 50 mm^2, aluminium, overhead line. The feeder is considered both without load, and with a load of 5 MW and 2 MVAr. In both cases, the effect on voltage of the control of the DG reactive power by means of the proposed control scheme, as well as the effect of a constant leading or lagging power factor, is examined for a range of DG active power outputs. This is shown in Figure 2.29 [129].

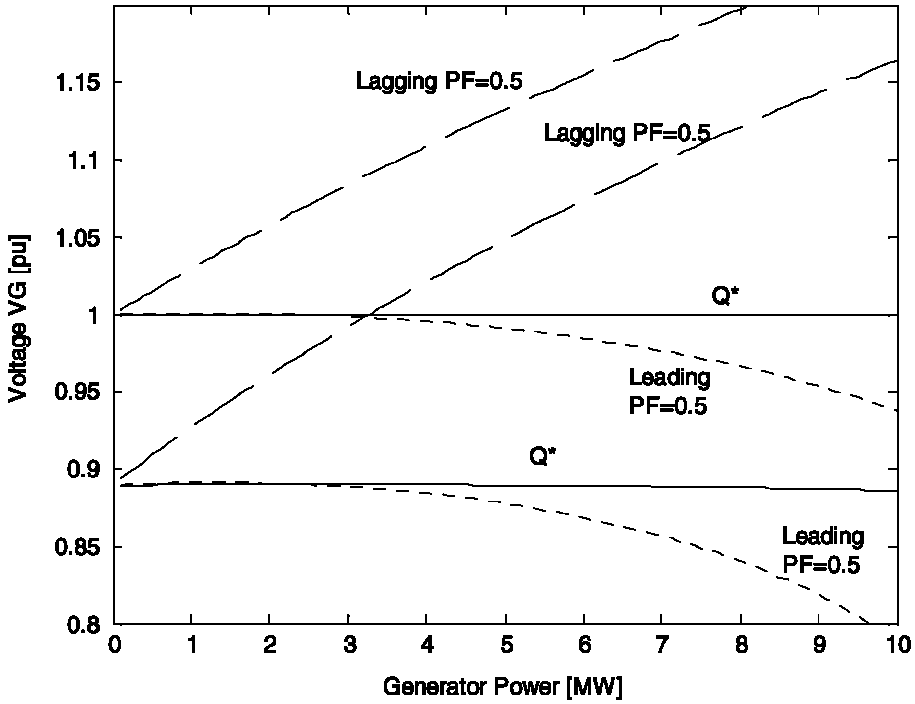

Figure 2.29: Bus voltage V_G evolution with generator power for fixed transformer secondary voltage [129]

The figure shows the effect of fixed leading or lagging power factor, and reactive power control, Q*, without load in the case of the upper curves, and with load in the case of the lower curves. It can be seen that, in this scenario, the local control of generator reactive power can be effective in the mitigation of voltage rise from the real power injection of DG.

In [43], Liu et al. demonstrate an adverse impact of the use of local voltage control by means of reactive power control of PV. The study considers a model of an approximately six mile-long, 12.5 kV representative feeder, employing an OLTC at the substation, and a voltage regulator approximately two miles from the substation. The feeder supports a total of 7 lumped loads, totalling approximately 11 MVA, and representative of a mix of residential and commercial demand. PV penetration is defined as the percentage of local load. Figure 2.30 [43] shows the feeder voltage with 50 % PV penetration, operating at rated power, and light loading, resulting in reverse active power flow.

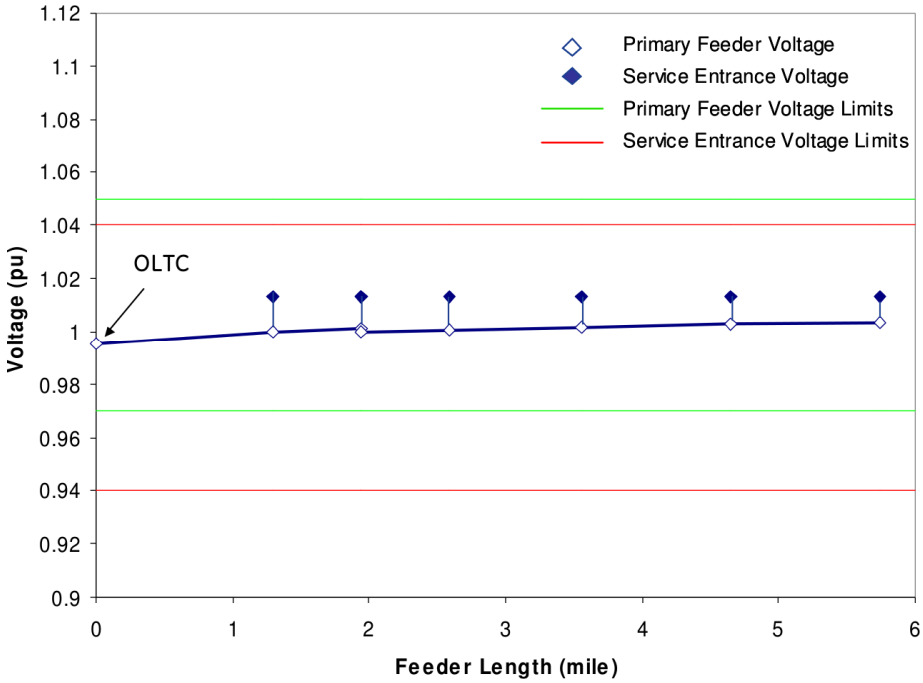

Figure 2.30: 50 % PV penetration voltage profile with inverters controlling voltage [43]

It can be seen that, despite the state of reverse power flow, voltage is well regulated along the length of the feeder. However, the absorption of reactive power in order to mitigate voltage rise results in considerable reactive power import to the feeder, with the consequence of increased feeder losses and increased reactive power demand from the upstream network. This is shown in Figure 2.31 [43].

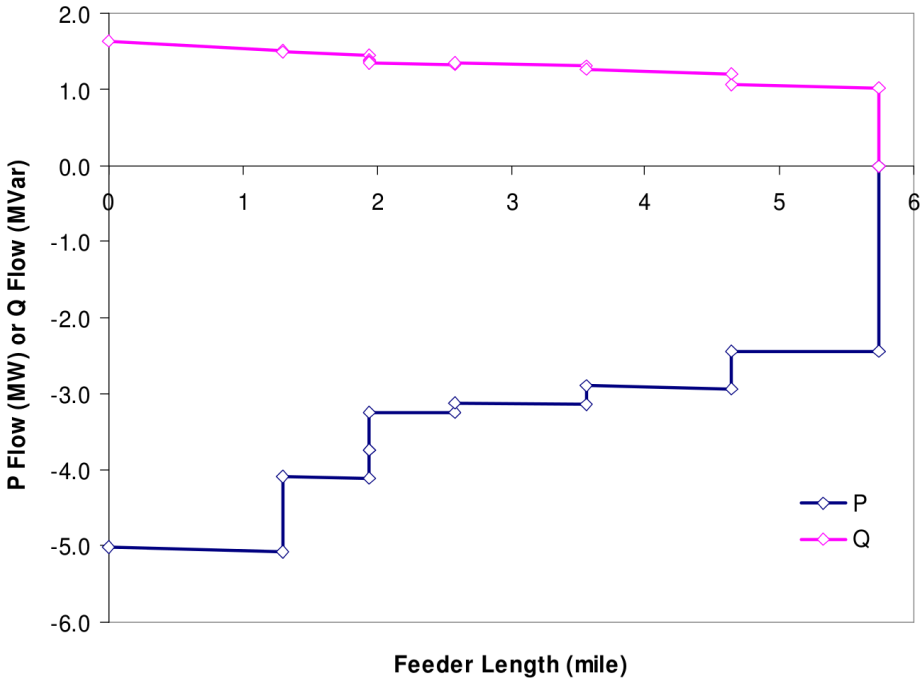

Figure 2.31: 50 % PV penetration power profile with inverters controlling voltage [43]

2.4.3 - Energy storage

Storage of surplus energy generated by DG at, or close to, the point of generation, negates the voltage rise that might otherwise result as a result of active power export, as well as the losses associated with power transfer, and the detrimental impact of, for example, reverse power flow [130]–[134].

Schemes have been presented in [130], [131], [135], [136] under which local battery storage is used to increase the PV hosting capacity of a network by mitigating effects such as voltage rise. In [123], this is achieved by the control of a combination of storage and PV inverter output. In [137], this is considered in the context of EVs, and in [138] in the case of public EV charging stations integrating energy storage.

In [139], a scheme under which battery storage is controlled to mitigate voltage rise, with the priorities of minimising OLTC operations and system losses, is presented. The scheme was demonstrated using a hardware-in-the-loop test rig in which a controllable AC source and a battery-based energy storage system were interfaced to an RTDS simulating a distribution network model.

In [140], a scheme for the integration of storage with a power electronic transformer at secondary distribution substation level was presented. However, in [141] it was concluded that placement of energy storage at customer level is more efficient than at grid level.

In [142], the use of energy storage to mitigate voltage imbalance on a network hosting PV generation is demonstrated, under simulation, and on a laboratory, hardware test rig.

2.5 - The architecture of distribution network control

2.5.1 - Centralised vs decentralised control

The architecture of systems used for distribution network control may be categorised according to the level of the electrical distribution network at which decisions are made. Existing networks are characterised by a centralised control architecture, in which control is effected primarily from a network control centre, or by automation at primary substations [87], [143], [144]. This is illustrated in Figure 2.32 [143].

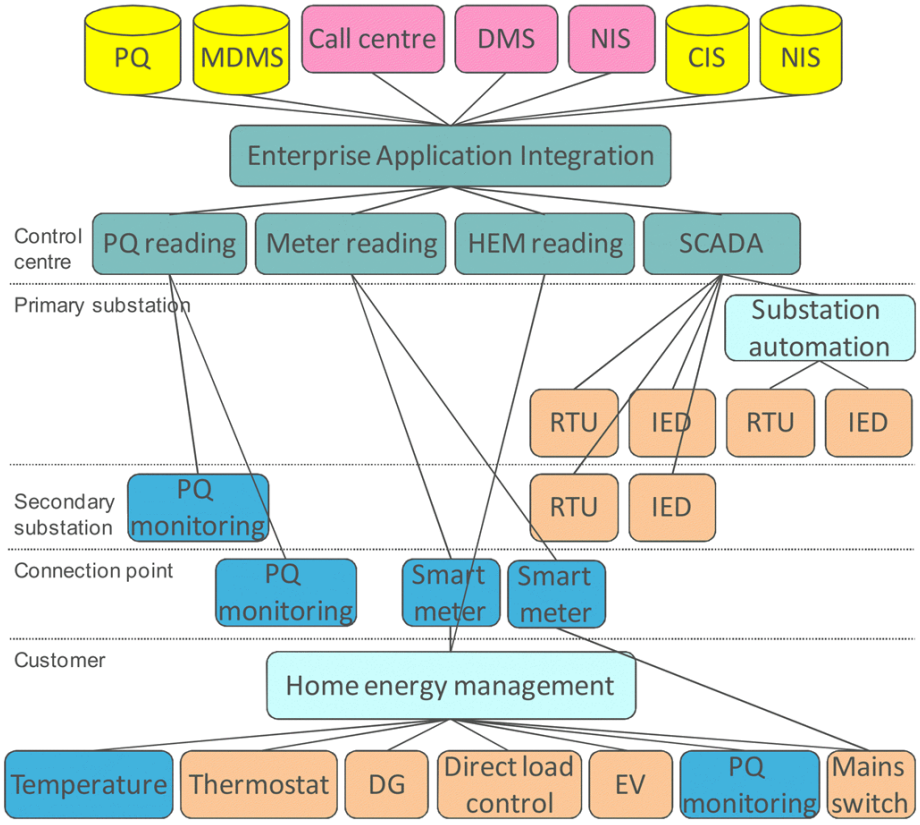

Figure 2.32: Centralised distribution network management system [143]

Under a decentralised control architecture, network monitoring data, for example from smart meters, is stored and processed, and control decisions effected, at lower levels of the distribution network than in the case of a centralised architecture, for example at secondary substation level [87], [143], [144]. This is illustrated in Figure 2.33 [143].

Under autonomous PV inverter control schemes, control is effected at the very periphery of the distribution network, based on local measurements [123], [124], [145], [146]. It is important to consider, however, the mutual interaction between devices effecting autonomous, local control, and between such devices and centralised control systems [147]. In contrast to such local automation, schemes have been proposed whereby control is effected by PV inverters, but directed by a more centralised agent, coordinating a number of sources [110], [128].

In the case of distribution substations with OLTCs, local automation may be employed which augments or replaces existing control techniques, such as LDC. In [148], the SuperTAPP n+ scheme demonstrated in a trial by EDF Energy for the control of a network hosting DG is described. Under this scheme, OLTC control is based on measurements taken locally to the substation. Similarly, in [106], conventional LDC is extended to accommodate the potential for reverse power flow caused by DG.

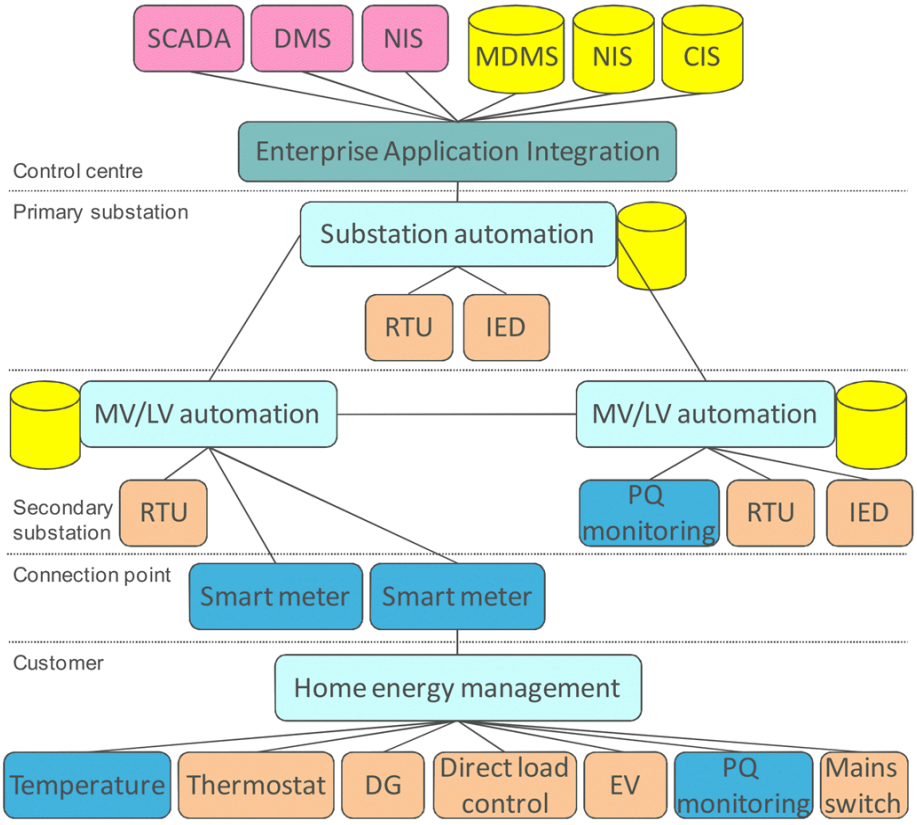

Figure 2.33: Decentralised distribution network management system [143]

Although processing may still take place at substation level, and control effected locally by, for example, an OLTC, distributed measurements may offer superior performance when compared to a control scheme based exclusively on local measurements. The DG DemoNet project [113]–[116] compared an OLTC control strategy based on local busbar voltage measurement with one based on distributed measurements from smart meters. Similarly, in [149], coordinated control schemes of this sort are compared with local control schemes such as AVC, in the case of OLTC-equipped substations, and an automatic voltage regulator (AVR) in the case of DG. Further schemes have been proposed whereby optimal, collective control of DG is based on distributed measurements [51], [105], [112], [121].

Multi-agent systems, under which multiple, intelligent agents, located within, for example, PV inverter controllers, communicate and cooperate in order to reach optimal decisions for distribution network control have also been proposed [88], [150]–[153].

2.5.2 - The architecture of schemes that have been deployed

In [154], Lu et al. present a control architecture under which LV network data from smart meters in customer premises and power quality (PQ) meters in street cabinets is communicated to a substation automation unit (SAU) at a secondary substation via DLMS/COSEM over OPERA broadband over power line (BPL) [155]. This was demonstrated under the INTEGRIS project [156]. The architecture of the project trial, conducted on part of a distribution network of A2A Reti Elettriche SpA (A2A), located in Brescia, Northern Italy, is illustrated in Figure 2.34 [154].

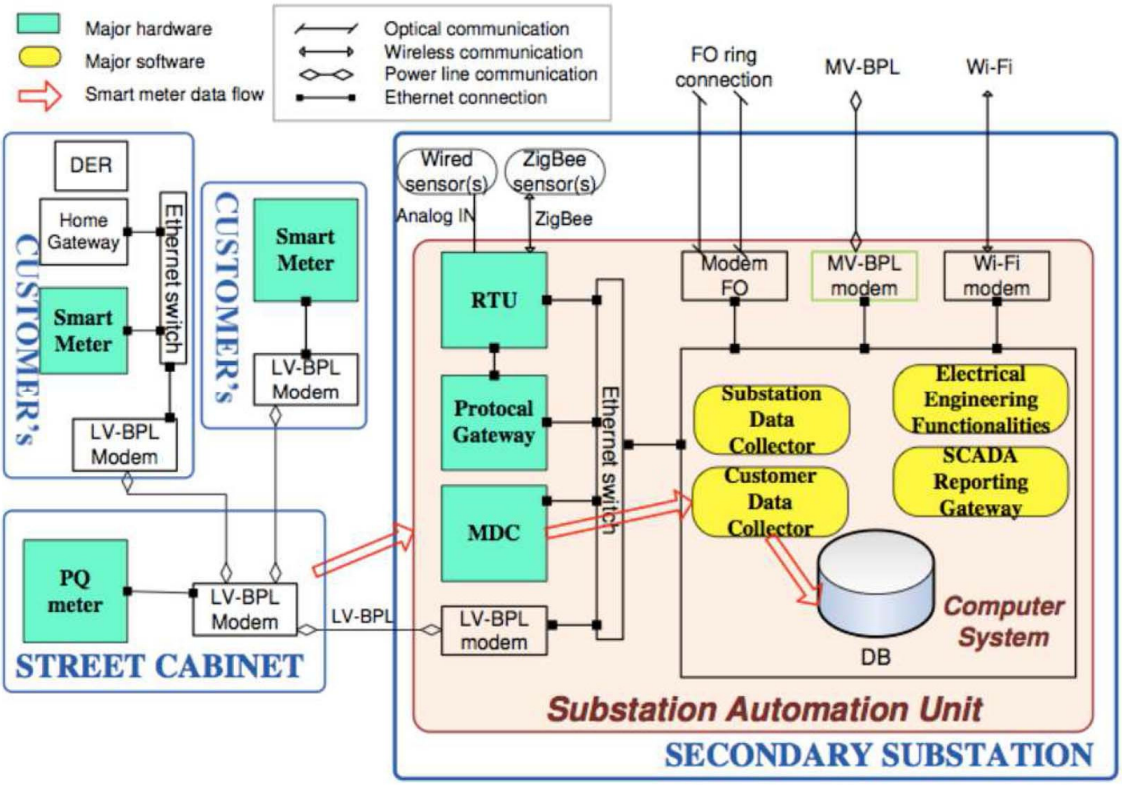

Figure 2.34: Internal components of SAU (in A2A field trial) [154]

Under this INTEGRIS trial, data was conveyed between secondary substations, and to the control centre, by means of a combination of fibre optic, BPL, and WiFi interfaces, and using the IEC 61850 protocol.

Under the LoVIA field trial [119], conducted by ENWL, LV network monitoring and control was achieved by means of metrology and communications units (MCUs) located at the mid and end points of LV feeders on the test network. These communicated with a remote terminal unit (RTU) located at the secondary substation by means of GPRS. DNP3 was used over a local interface between the RTU and the relay controlling the OLTC of the secondary substation transformer. This enabled local voltage control to be

effected by means of the OLTC, and based on measurements from the LV feeder. The architecture of the trial is illustrated in Figure 2.35 [119].

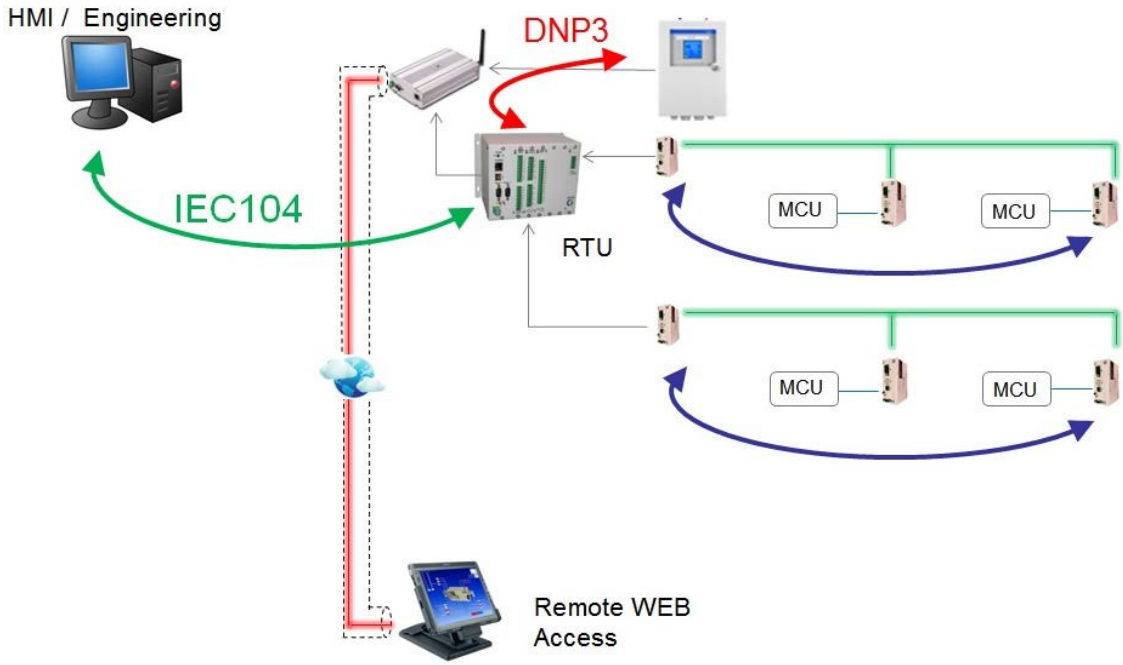

Figure 2.35: LoVIA project architecture [119]

2.6 - Smart meter and AMI security

2.6.1 - Conventional electricity meter security

Historically, the most common illegal interaction with electricity metering equipment has been local, physical tampering for the purpose of electricity theft. This has typically involved electrical bypass of the meter, attempts to stop or slow the recording of energy consumption by means of magnetic or radio frequency (RF) interference, or interference with timing mechanisms in the case of multiple rate tariffs [157]–[159]. In 2011 it was revealed that more than 120 000 of the 3.5 million prepayment meter customers had been affected by the purchase of counterfeit electricity top-ups [160]. It has been estimated that electricity theft in the UK costs consumers £440 million per year [161]. The consequence of meter bypassing, and covert tampering with the internal electronics of a conventional meter by means of a hole cut in the back of the enclosure, are both shown in Figure 2.36. These examples were both found by technicians visiting premises to replace conventional meters with SMs.

Figure 2.36: Left, conventional meter bypassing, and right, internal tampering (courtesy Mark Malins)

2.6.2 - Electricity distribution as a target for attack

Electricity distribution networks are an established target of terrorist activity. In 1996, six IRA members were each sentenced to 35 years imprisonment for plotting to target substations around London and South East England with explosive devices [162]. In 2006, an Australian man was sentenced to 20 years imprisonment by the New South Wales Supreme Court for plotting to bomb the electricity network supplying Sydney [163]. In 2015, the Russian hacker group Sandworm attacked the substations of three utility companies in Ukraine. By gaining access to SCADA systems, they were able to open circuit breakers resulting in power loss to more than 225 000 customers [164], [165].

Electrical systems are also a key strategic target during conflict between nation states. For example, Operation Desert Storm, conducted during the Gulf War, saw 215 sorties launched against electricity supply targets in Iraq, reducing generation capacity to less than 300 MW, and transmission to less than a quarter of its capacity prior to the conflict [166]. The *2008 Report to Congress of the U.S.-China Economic and Security Review Commission* asserted that:

'China is targeting U.S. government and commercial computers for espionage … Internet-connected networks operate the national electric grid and distribution systems

for fuel ... A successful attack on these Internet-connected networks could paralyze the United States.' [167]

Indeed, it may be the case that state-sponsored infiltration of the U.S. electricity transmission and distribution systems has already occurred [168].

In 2009 the Stuxnet worm was first detected. This malware exploits the use of default passwords and a Microsoft Windows Server service remote procedure call (RPC) handling remote code execution vulnerability, amongst others. It specifically targets Siemens S7 programmable logic controllers, with the United States and Israel suspected of authoring the worm to attack uranium enrichment facilities in Iran [169]–[171].

An attack against electricity distribution infrastructure which resulted in widespread loss of supply for a period of 24 hours in, for example, the UK, has the potential to cause considerable harm to personal and social welfare. The UK Government's *National Risk Register Of Civil Emergencies* [172] identifies the risk to other utilities, such as gas and other fuel distribution, water and sewerage, as well as to telecommunications and financial services, from a widespread loss of electricity supply. Regional risk assessments [173], [174] identify the primary impacts of such an event, including fatalities from, for example, hypothermia in the elderly and vulnerable as a result of inadequate heating, property fires resulting from the use of candles and open fires, disruption to transport, disruption to the food chain as a result of problems storing, transporting and cooking food, and increased crime.

2.6.3 - Smart meters and AMI as targets for attack

Advanced metering infrastructure (AMI), as an important component of the smart grid vision of future energy distribution networks, represents a significant target for attack, as well as presenting unique vulnerabilities. Examples of the groups who may be responsible for attacks on smart meters as part of AMI, their motivations, and tools, are presented in Table 2.2 [175].

Table 2.2: AMI potential attackers, their motivation and the tools they use [175]

Attacker	Motivation	Tool
Customers	Personal reasons	Personal knowledge or assistance from criminals
Criminals	Financial, sabotage or terroristic	Creating software and hardware to tamper with AMI
Insiders	Various	Unethical use of the system's trust, illegal use of their authority and knowledge
Institutions	Using private information for various reasons, denial of service	Using expertise, authority, resources and vulnerabilities of system or its components

In [175], counter-measures against the physical tampering attacks typically employed against conventional meters, when employed against smart meters, are presented. However, the advent of advanced meter reading (AMR) and AMI introduces the threat of attacks which exploit the requirement for communication of SMs with devices outside of customer premises. These are illustrated in Figure 2.37 [176].

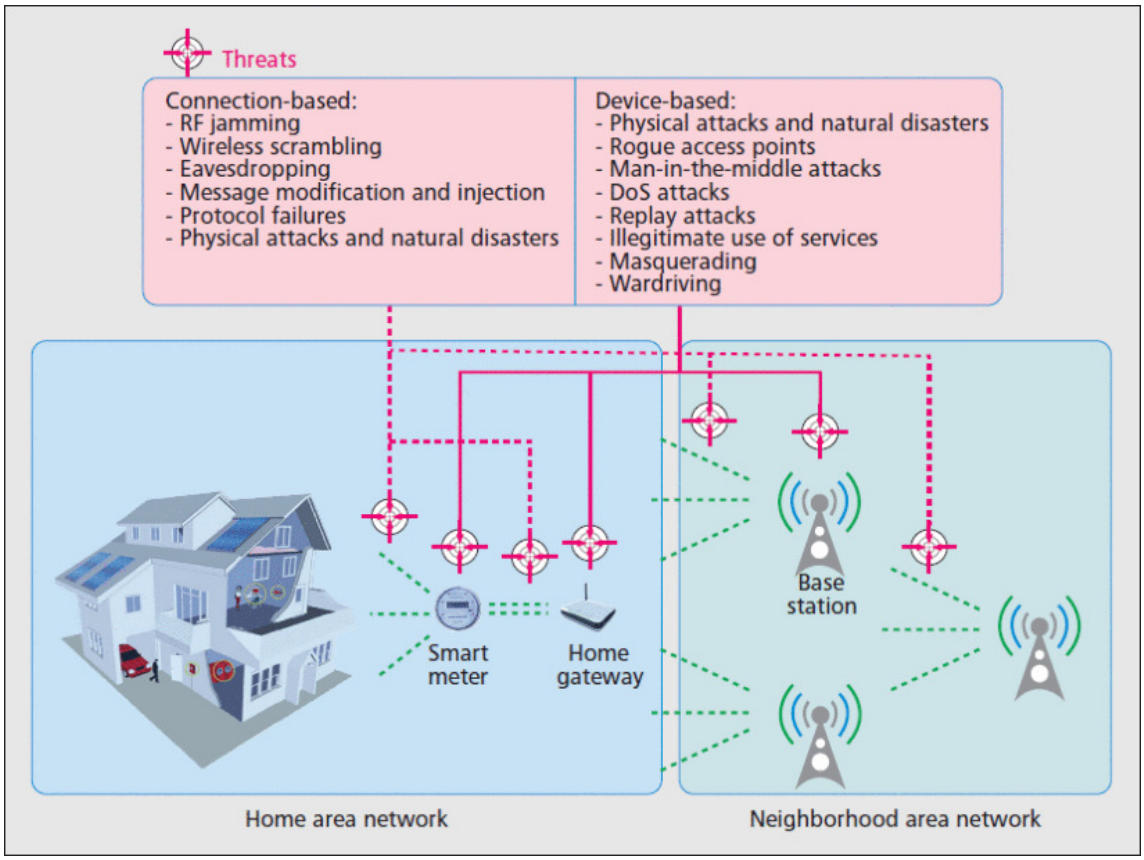

Figure 2.37: Smart grid distribution and corresponding threats [176]

The principal attacks against AMI systems may be categorised as follows [26], [27]:

- Theft of data: For example, the theft of customer consumption data, or encryption keys stored within a SM.
- Theft of energy: Energy consumption is inaccurately reported, or falsely attributed.
- Denial of Energy: Malicious use of the remote, electrical disconnect facility of many SMs.
- Disruption of network control: For example, providing false measurements in the case that these are used for operational purposes, or generating rapidly fluctuating load conditions by cyclically operating the remote supply disconnection facility.

These categories are considered in further detail in the following sections.

2.6.3.1 - Theft of data

The interception of data communicated by smart meters may allow an attacker to infer details of customer behaviour, for example domestic occupancy [177]–[180]. This was demonstrated in a presentation given by Carluccio and Brinkhaus on an attack on a domestic smart meter installation in Germany [181], [182]. Here, communication between the SM and the head-end of the meter operator was intercepted, and customer behaviour deduced from energy consumption profiles. False consumption data was also successfully issued to the energy supplier.

The impersonation of another customer or SM, using stolen data, has further implications for energy theft [183]–[185].

Data encryption is a key element of achieving confidentiality, by preventing eavesdropping and data tampering. Data integrity is further protected by authentication techniques, ranging from password authentication to digital certification [26], [183], [186].

2.6.3.2 - Theft of energy

The mechanisms of electrical bypass of the meter tails employed against conventional meters apply equally to SMs. Furthermore, SMs present further vulnerabilities as a result of communication, hardware or firmware compromise, in order to misrepresent energy consumption. However, approaches have been presented to detect energy theft by means of identifying anomalies in energy consumption patterns. In [157], a machine

learning method is presented which identifies anomalies in the consumption profiles of customers on an individual level. In [187], such anomalies are identified considering the aggregated energy consumption of a number of customers.

2.6.3.3 - Denial of energy

SMs incorporating a remote supply disconnection facility as mandated in the UK [34], for example, present a vulnerability not present in conventional meters. An attack in which control was gained over this facility might result in the denial of energy to a large number of customers [26], [28], or destabilisation of the distribution, or even transmission networks, by imposing rapid changes in load across a wide area [188]. If compromised, the firmware of a meter may be modified or replaced in order to alter the behaviour of the meter or further infect other devices [28], [178], [183]. This also has implications for the theft of data and energy.

2.6.3.4 - Disruption of network control

If measurements from smart meters are used to inform distribution network control decisions, false data injection, for example in the case of a man-in-the-middle (MITM) attack, may lead to necessary control action not being taken, or unnecessary control action being taken [189]–[192]. In [188], simulation case studies undertaken by Wei and Wang illustrate the effect of data-centric attacks on both data exchanged between smart meters and a control centre, for operational purposes, and SCADA data used for circuit breaker control. These resulted in power quality issues and erroneous protection operation in the simulated distribution network. Schemes to detect and mitigate the effects of false data injection attacks have been proposed [190], [193]. However, Overman et al. [194] assert that whilst such systems must include measures to identify and prevent cyber security intrusion, they must also be designed to tolerate such attacks to some extent.

2.6.4 - Vulnerabilities and constraints of smart meters and AMI

The cyber security vulnerabilities of SMs, beyond those applicable to conventional meters, may be categorised as follows [26], [195]:

- Insecure wide area network (WAN) interface: If not protected by, for example, well-implemented encryption, communication between the SM and the head-end system may be intercepted, modified or falsely injected [183], [185].

- Insecure local interface: For example, access might be gained to a local, optical interface intended for meter reading and configuration using authentication credentials or encryption keys captured by bus snooping [178].

- Bus attacks: Data conveyed between components within the SM may be captured, modified or falsely injected. Data captured might include authentication credentials or encryption keys. Data related to consumption might be modified or falsely injected, for the purpose of energy theft. Data related to the identity of the meter might be modified or falsely injected, for the purpose of impersonation [183]–[185].

- Power or clock glitching: Modulation of the power or clock signals internal to the SM may result in firmware not behaving as designed, for example skipping instructions in the course of authentication or encryption [183], [184].

- Poor implementation of cryptography: This might include the use of cyphers with known vulnerabilities, the use of short or predictable keys, or the use of low-entropy random number generation. It might also include vulnerability to replay attacks, under which encrypted data, for example authentication credentials, is captured and subsequently retransmitted in the course of an attack [183], [185].

- Firmware flaws: For example, vulnerability to buffer overflow or format string attacks, under which data is written to memory locations in a manner not intended by the firmware design, or an insufficiently robust mechanism for firmware update [183], [196].

- Key and password management: For example, keys and passwords stored in non-volatile memory within components of the smart meters may be exposed by extracting the firmware from these devices, or captured during transmission between them. This may expose multiple SMs to attack if common keys or authentication credentials are used [28], [183], [197].

Constraints of SMs, pertinent to cyber security, include [198]:

- Cost: Commercially deployed SMs are necessarily a mass-produced device and, as such, are cost-optimised. Accordingly, a compromise is made between cost and security. This might preclude, for example, the use of dedicated security hardware such as a cryptoprocessor [199].

- Technical limitations: In addition to being limited by cost, the technical capacity of SMs may be limited by physical, communications, and power dissipation requirements. For example, well-established Internet security protocols which might be applied to AMI systems, such as IPsec or SSL/TLS, or elliptic curve cryptography,

are not necessarily scalable for implementation on resource-constrained SMs [28], [200], [201].

- Type approval: SMs may require type approval and/or certification to be used for legal metrology, for example under *The Meters (Certification) Regulations 1998* in the UK [202]. This may limit the scope for upgrade or modification of the devices, for example to patch a known security issue.
- Location: The location of SMs, in customer premises, is an uncontrolled, insecure environment. Access to the meter, for example for the purpose of physical tampering, is unrestricted and unmonitored.

In addition to those applicable to SMs, limiting factors pertinent to cyber security and applicable to AMI systems include [198]:

- Limited communications: For example, low available bandwidth over low-power RF links such as power line carrier (PLC), or high contention for a mobile telephone network cell. This might preclude the use of security protocols imposing a large overhead, or the frequent exchange of certificates [203].
- Public communications: For example, the use of the public, cellular telephone network for communication. As well as limiting the scope for isolation of AMI traffic from other services, this might mandate the use of specific protocols, for example GPRS.
- Data management: An AMI system hosting large numbers of SMs will need to process and store a large volume of data, as well as accommodating the cryptographic overhead associated with communication with them [197]. In addition, multiple, geographically disparate parties may require role-based access to AMI head-end data, for example energy retailers and DNOs. This requires management of what data is available to which parties, and how it is securely conveyed [183], [204].

2.6.5 - The security of existing smart meter and AMI schemes

A survey by the 7th Framework Programme Meter-ON project [205] examined 15 smart meter deployment projects across ten European countries, totalling a projected deployment of approximately 100 million meters by 2020. In the case of five of these projects, it was found that no encryption of data between the meters, data concentrators and back-office systems was employed, and in the case of four of these projects no security event logging was performed. Furthermore, it has been suggested that the majority of cyber security breaches are not reported by organisations due to

reputational concerns [206]. However, valuable conclusions regarding cyber security have been drawn from SM deployments which have already taken place [207].

2.6.6 - Published smart meter and AMI attacks, and tools

The extraction of symmetric AES-128 encryption keys from a commercially deployed SM was presented by Vidal and Illera [37], [38]. The keys, used to encrypt PLC communication by the device, were eavesdropped during transmission between processor and PLC devices at printed circuit board (PCB) level within the device, along with the unique identification number of the meter. If the same keys are used across multiple meters, then they may be used to gain illegitimate access to these devices [197]. Furthermore, access to the bus on which the unique identification number of the meter is communicated at PCB level may permit a man-in-the-middle (MITM) attack, under which a false identification number is introduced in order to impersonate another SM [195]. PCB-level access to a SM also presents the opportunity for other data manipulation and key extraction attacks [195], [208], though schemes have been proposed to address the issue of insecure key management, for example [196], [209].

In [36], Lawson presents an attack involving the extraction of firmware from the microcontroller of a smart water meter radio module. This is achieved by connection to the unprotected JTAG interface of the device. The defeat of rudimentary tamper protection is also described. This is shown in Figure 2.38 [36].

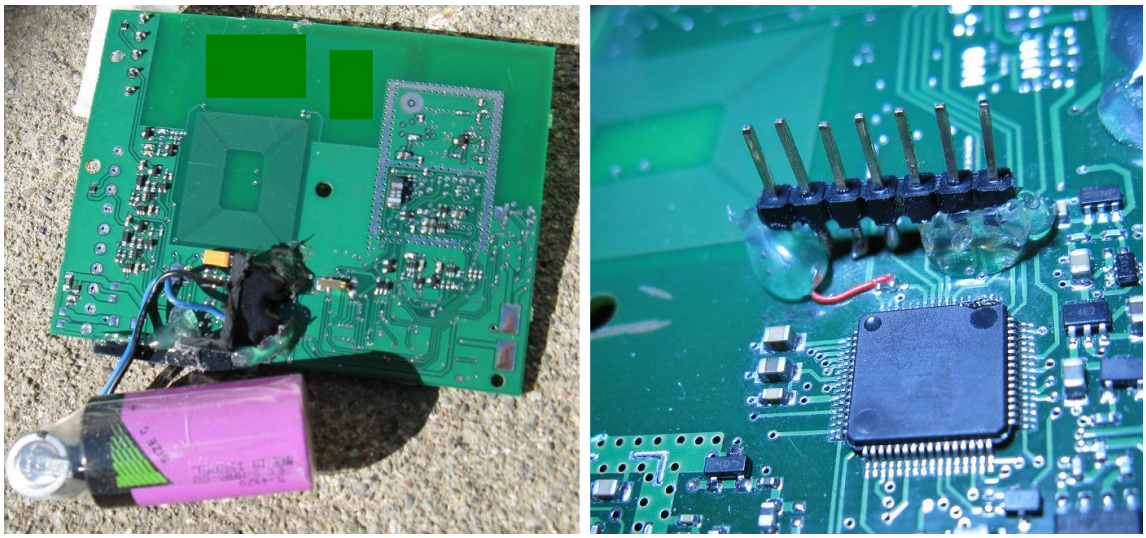

Figure 2.38: Attack on a smart water meter by connection to the unprotected JTAG interface of the microcontroller [36]

A practical demonstration of a denial-of-service (DoS) attack against two SMs is presented in [210], and in [211] a DoS attack involving multiple mesh-connected SMs is simulated.

In [212], Davis presents a worm, an example of self-replicating malware, targeting mesh-connected SMs. In a simulated attack, this infected over 15 000 meters in under 24 hours.

In [213], communication between the local, optical interface of a commercially deployed SM and the vendor-specific management software is intercepted and used to determine the authentication token calculation algorithm. This was demonstrated to reduce the predicted time required for a brute-force password attack on the authentication protocol used by the optical interface of the SM of over four years, to under four hours.

A framework for fuzzing, an attack technique whereby semi-random data is transmitted to a target in order to expose insecure behaviour or instabilities, designed to exploit SMs using the DLMS/COSEM protocol, is presented in [214].

A framework and toolkit for exploiting vulnerabilities in Zigbee networks, widely used for home area network (HAN) communication [215], [216], is publicly available [217].

In [178], Mo et al. propose attack schemes targeting the local interface of a smart meter. These include data spoofing, under which false data is presented to a smart meter, a replay attack, under which legitimate traffic is recorded and then replayed to the meter, and a delay attack, under which traffic is intercepted and then provided to the meter ‘out of date’. An open source toolkit for penetration testing SMs using the C12.18 and C12.19 protocols over a local, optical interface, is publicly available [218].

3 - Design and development of the smart meter test rig

3.1 - Introduction

The design, development and commissioning of a hardware-in-the-loop test rig, incorporating hardware smart meter test beds, the infrastructure required for WAN communication with the meters by means of GPRS and for SCADA communication, and a Real Time Digital Simulator (RTDS) simulating a section of distribution network, is described. The test rig was developed in order to examine the use of AMI as a component of a distribution network control, or smart grid scheme.

Subsequent sections are structured as follows:

- Section 3.2 outlines the logical design of a smart meter test bed platform, intended to be representative of smart meter designs which are currently seen, or which might conceivably be seen, in commercially deployed smart meters in the UK. The logical design of a test-rig architecture which employs these test beds as part of distribution network control, or smart grid scheme, is also presented.
- Section 3.3 describes the development of the hardware and foundation firmware for the smart meter test bed platform, based in the logical architecture presented in Section 3.2.1.
- Section 3.4 describes the development of the test rig, including configuration of the RTDS, and of the SCADA server and controller machines, and the software development of the GPRS server. The physical architecture of the test rig is also described, based on the logical architecture presented in Section 3.2.2.
- Section 3.5 describes the design and execution of a commissioning test, conducted to verify the correct operation of all the hardware, firmware and software elements within the smart meter test rig. This test demonstrates a simple, real-time voltage control scheme, effected using a transformer equipped with a SCADA-controlled OLTC within a simulated network, and informed by voltage readings from one of the smart meter test beds.

- Section 3.6 discusses the work undertaken, in the context of existing research in this field, and summarises the advancements and contributions made. The limitations of the approach taken are also considered.
- Section 3.7 summarises and concludes the work presented in this chapter.

3.2 - Smart meter test bed platform and test rig design

3.2.1 - Smart meter test bed platform

The design of the smart meter test bed platform was intended to be representative of smart meter designs which are presently seen, or which might conceivably be seen, in commercially deployed smart meters in the UK. Accordingly, a custom architecture was designed and implemented for the purpose of this research, which reflects constraints specific to domestic and light commercial smart meters such as cost, physical size and power consumption. The design is also such that a wide range of supply monitoring, data processing, and communications configurations may be applied. The logical architecture of the smart meter test bed platform is illustrated in Figure 3.1.

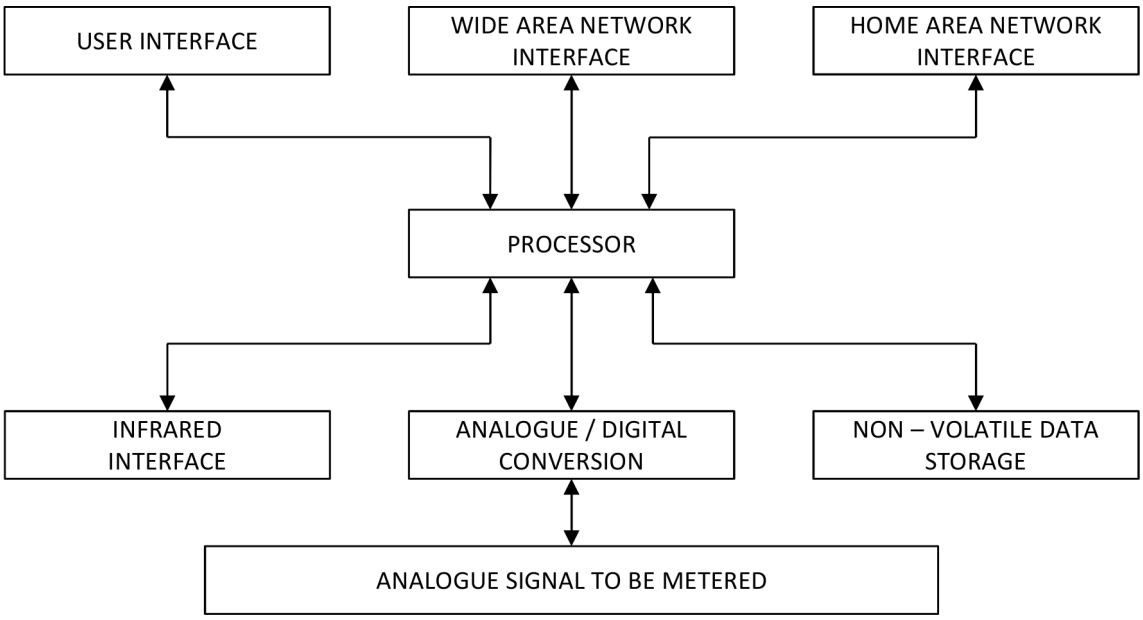

Figure 3.1: Logical architecture of the smart meter test bed platform

The choice of elements included, and the logical architecture of the smart meter test bed platform, was informed by existing, commercially deployed smart meters, and by the first version of the UK *Smart Metering Equipment Technical Specifications* (SMETS

1) [219], published by the former Department of Energy & Climate Change. A number of further elements may be found in commercially deployed meters, and specified in SMETS 1, for example a contactor for remote supply disconnection, an output signal for the control of auxiliary load switches, and tamper detection hardware. However, these elements were not directly relevant to the research conducted using the smart meter test beds, nor will their absence affect this research, and hence were not included.

The core of the meter architecture is a single processor. The need for numerous PCB-level hardware interfaces, such as SPI and UART serial, as well as low power consumption and relatively modest computational power requirements, make a microcontroller the typical choice for commercially deployed meters. Microcontrollers also contain non-volatile memory and RAM, such that external memory may not be required for operation of the device, although in practice it will typically be required for the mass storage of data such as meter readings. The architecture presented in Figure 3.1 includes non-volatile storage for this purpose.

A two-channel analogue to digital converter is included for the acquisition of current and voltage values.

Two radio frequency interfaces are included in the architecture presented in Figure 3.1: a home area network (HAN) interface and a wide area network (WAN) interface. The HAN interface was included for local communication with, for example, simulated controllable loads, for the purpose of DSM. The WAN interface was included for communication with a remote, head-end system, by means of a cellular telephone network connection.

The architecture includes two interfaces for local user interaction with the meter test bed. These are a user interface, comprising an LCD display, feedback LEDs and user-accessible switches, and an infrared communication interface. Both the user interface and infrared communication interface are included for the purpose of monitoring and debugging.

3.2.2 - Test rig

The architecture of the smart meter test rig is intended to represent the fundamental elements of a distribution network control or smart grid system incorporating AMI. Its design is informed by the architectures of systems examined in Section 2.4 and Section 2.5. The WAN communication scheme is typical of that employed for smart metering in

the UK. As such, smart meter test beds individually establish concurrent connections with a server over the WAN. The closed-loop, logical architecture of the test rig is illustrated in Figure 3.2.

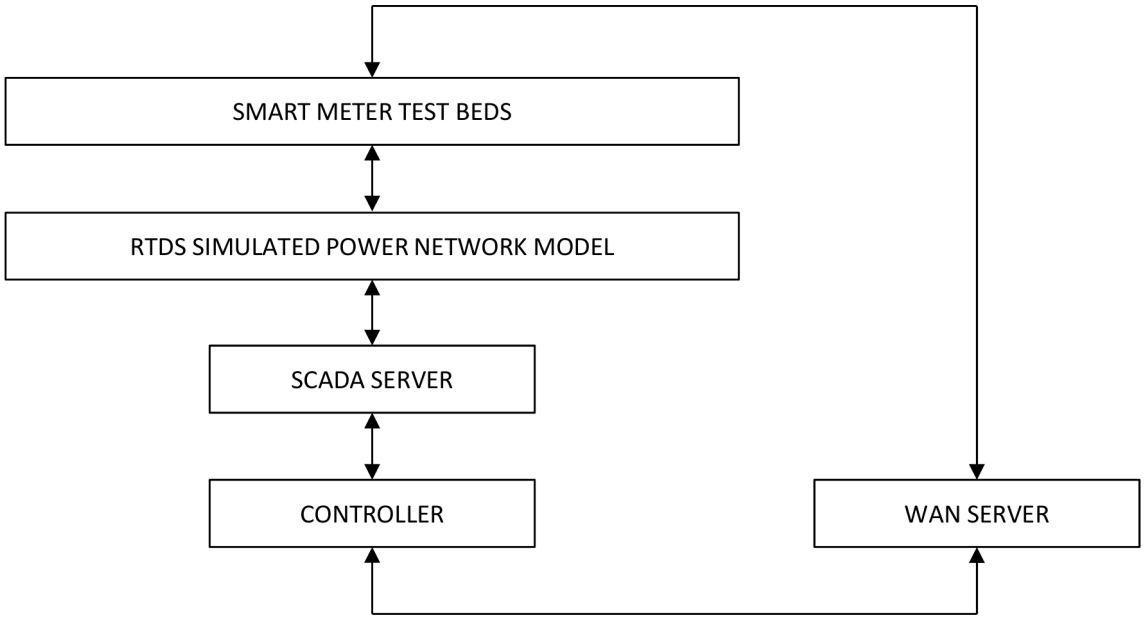

Figure 3.2: Logical architecture of the smart meter test rig

The simulated power network model is hosted on a Real Time Digital Simulator (RTDS), manufactured by RTDS Technologies. This hardware device performs electromagnetic transient simulation, with a minimum time-step of 50 μs. In addition, values from within the simulated model can be realised as analogue signals using DAC cards connected to the simulator, and SCADA data exchanged with appropriate devices within the simulated model over a LAN connection. By means of the DAC cards of the RTDS, the smart meter test beds are provided with analogue voltage signals representative of the instantaneous voltage and current at a specific point in the simulated network. By means of the SCADA interface of the RTDS, control directives may be issued to appropriate devices within the network via the SCADA server, for example an OLTC.

The controller is the endpoint of data received from the smart meter test beds, via the WAN server. On the basis of this data, the controller issues directives to devices within the RTDS simulated power network model, such as OLTCs, via the SCADA server.

The SCADA server acts as a master station, providing protocol conversion and data buffering. Translation from one SCADA protocol to another is required for communication between the RTDS and controller device. It also permits data to be received from the controller with non-deterministic timing, but buffers this data for

exchange with the SCADA interface of the RTDS at regular polling intervals, for example one-second.

The WAN server manages concurrent connections with multiple smart meter test beds, including performing registration of the devices upon connection, maintaining current connections, and handling disconnection. The WAN server also issues instructions for administration, or from the controller, for example a request for voltage readings to be taken by all connected meters or a sub-set thereof, and buffers data received from connected meters for transmission to the controller, for example the results of voltage readings.

3.3 - Smart meter test bed platform development

3.3.1 - Hardware

The hardware design of the smart meter test bed platform was designed and implemented for the purpose of this research, based on the logical architecture described in Section 3.2.1 and illustrated in Figure 3.1. Figure 3.3 illustrates the physical architecture of the smart meter test bed platform including the hardware elements, the interfaces between them, and which of these interfaces have hardware interrupts associated with them. These interrupts are used to trigger interrupt service routines and a return of the microcontroller from a dormant, low power state.

In order to permit alternative communication or sample acquisition devices to be used with the core hardware of the meter, the design is physically separated into two PCBs: a motherboard and a daughterboard. Data and power buses are conveyed between the two boards by means of a header.

The hardware of the processor, memory and supporting devices, the local interfaces, the WAN and HAN interfaces, and the ADC and associated filtering, are described in further detail in the following sections.

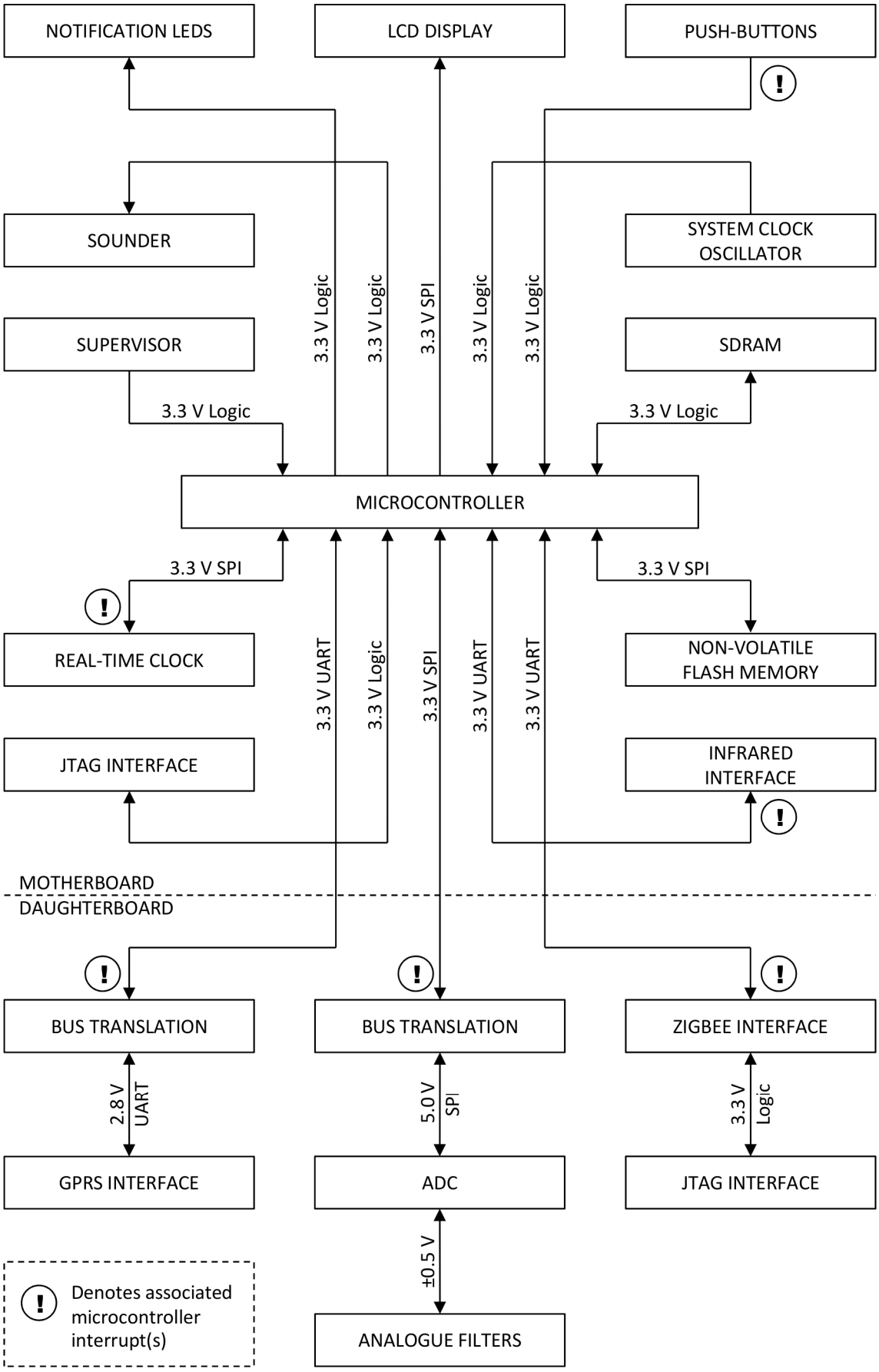

Figure 3.3: Physical architecture of the smart meter test bed platform

3.3.1.1 - Processor, memory and supporting devices

The processor used in the design is an 8-bit, Atmel AVR XMEGA microcontroller. This device contains 128 kB of flash memory for program storage, 8 kB of flash memory for bootloader storage and 2 kB of EEPROM. It also contains 8 kB of internal SRAM. In addition to the internal RAM, external SDRAM was used in conjunction with a dedicated interface within the microcontroller which permits the memory address space used to address the internal RAM to be extended contiguously into the external RAM.

The RAM used in the design is 3.3 V, synchronous, dynamic memory with a capacity of 64 Mb, arranged as 4 x 4 x 4 Mb, and with a maximum clock speed of 133 MHz.

The microcontroller includes four hardware SPI interfaces. These are allocated to the LCD controller, the real-time clock, non-volatile memory and the ADC. The clock prescaler stages within the microcontroller permit an independent serial clock (SCK) frequency to be assigned to each of the SPI interfaces of up to half of the system clock frequency. The microcontroller also includes four USARTs. Three of these are allocated to the infrared interface, WAN interface, HAN interface. The microcontroller provides multiple levels of interrupt priority for the USART interfaces, if used asynchronously, in addition to those used for generic logic interrupts.

A processor supervisor device, powered by the 3.3 V bus which also powers the microcontroller, is used to hold the microcontroller in a state of reset during power-on or in the event of the 3.3 V bus falling below a lower voltage limit. The supervisor will assert the reset signal of the microcontroller, a 3.3 V logic level, until the voltage of the bus has exceeded 2.93 V for a period of at least 200 ms. During operation, the supervisor will also re-assert the reset signal of the microcontroller if the voltage falls below the lower voltage limit of 2.93 V.

An external, active, ceramic oscillator provides a 12.000 MHz system clock signal to the microcontroller with a stability of ±25 ppm at a temperature of 21˚c. The oscillator is powered from the 3.3 V bus and has a 3.3 V logic level output.

A 64 Mb, 3.3 V flash device is used to provide non-volatile storage. This device permits a maximum SPI clock frequency of 66 MHz and page sizes of 1024 or 1056 bytes.

A real-time clock device, powered from the 3.3 V bus, is used with an external battery to maintain timekeeping when the meter test bed is not energised. This device has an

accuracy of ±2 ppm at RTP. In addition to a 3.3 V SPI interface for communication it provides a logic level interrupt signal to the microcontroller.

3.3.1.2 - Local interfaces

Four LEDs, two pushbuttons, a sounder and a graphic LCD are provided for direct interaction with the meter test beds by an operator. The LEDs are driven with low power bipolar transistors, with two controlled by general-purpose logic outputs of the microcontroller and one each controlled by the WAN and HAN modules. The sounder is also driven with a low power bipolar transistor controller by a general-purpose logic output of the microcontroller. The LEDs and sounder are powered from the 5.0 V bus. The two push buttons drive general-purpose logic inputs of the microcontroller. The inputs driven by the pushbuttons are also configured to be hardware interrupts. The LCD used is a 128 x 64-pixel device with an integrated controller, such that it can be driven by the microcontroller using a 3.3 V SPI interface. The LCD is powered from the 3.3 V bus. An LED backlight for the display, powered from the 5.0 V bus, is driven with a bipolar transistor controlled by a general-purpose logic output of the microcontroller.

The infrared interface is a bidirectional transceiver module which integrates an optoelectronic source, detector, buffer and switching devices. It is connected to the microcontroller with a 3.3 V UART interface and supports a maximum data rate of 115 kb/s. The infrared module is powered from both the 3.3 V bus, supplying the detector and logic elements, and the 5.0 V bus, supplying the infrared source device. Since the USART interface of the microcontroller to which the infrared module is connected is configured asynchronously, a hardware interrupt is also associated with the receive register of the microcontroller USART interface.

3.3.1.3 - WAN and HAN interfaces

The WAN interface is an integrated GSM and Class 10 GPRS transceiver module manufactured by Telit, and which can operate at both 900 and 1800 MHz. The WAN transceiver has a typical sensitivity of -108 dBm at 900 MHz and -107 dBm at 1800 MHz, and a transmission power of 22 dBm at 900 MHz and 30 dBm at 1800 MHz.

The WAN transceiver is powered from a dedicated 3.8 V bus. Since the operating voltage of the logic interface of the WAN module is 2.8 V, level translation is required for communication with the 3.3 V microcontroller. This is achieved by means of an active bus translation device which, in addition to performing voltage level translation, includes Schmitt triggers which increase the slew rate of logic signal edges. The WAN

transceiver is connected to the microcontroller, via the bus translation stage, by means of a bidirectional UART interface which employs RTS/CTS hardware flow control. Hence, bus translation is performed upon four logic lines, with two in each direction between the transceiver and microcontroller. A fifth logic signal from the microcontroller is used to assert the reset signal of the WAN transceiver. This logic signal is used to drive a low-power bipolar transistor connected to the internally biased reset line of the WAN transceiver in open-collector configuration. In addition to the UART interface, two further logic signals are provided by the transceiver module. The first is an operating state signal which is used to drive one of the notification LEDs. The second is a logic signal indicating the stability of the power supply to the WAN transceiver. As the slew rate of this signal is not critical, discrete level translation is used to convert it to a 3.3 V logic signal for presentation to the microcontroller.

Power, voltage, data and clock signals are conveyed directly from the transceiver module to a SIM card holder. The RF interface of the transceiver module is connected to a coaxial PCB antenna connector by means of a controlled impedance trace.

The HAN interface is an integrated, 2.4 GHz transceiver module manufactured by MeshNetics, which conforms to the IEEE 802.15.4 specifications for physical interface and media access, and which supports higher communications layers prescribed by the Zigbee protocol by means of firmware. The HAN transceiver has a typical sensitivity of -104 dBm and a transmission power of 20 dBm. It is powered from the 3.3 V bus and has 3.3 V logic interfaces enabling direct electrical connection between the UART interface of the transceiver and the USART interface of the microcontroller. In addition to the bidirectional UART interface, RTS/CTS hardware flow control is employed. A logic signal from the microcontroller is assigned to assert the reset line of the HAN transceiver. Since this line may also be driven by a programmer or debugger connected to the JTAG interface of the transceiver module the logic signal for the microcontroller is connected via a transistor in open-collector configuration in order to prevent possible contention. Finally, a logic-level status signal is provided by the HAN transceiver which is used to drive one of the notification LEDs.

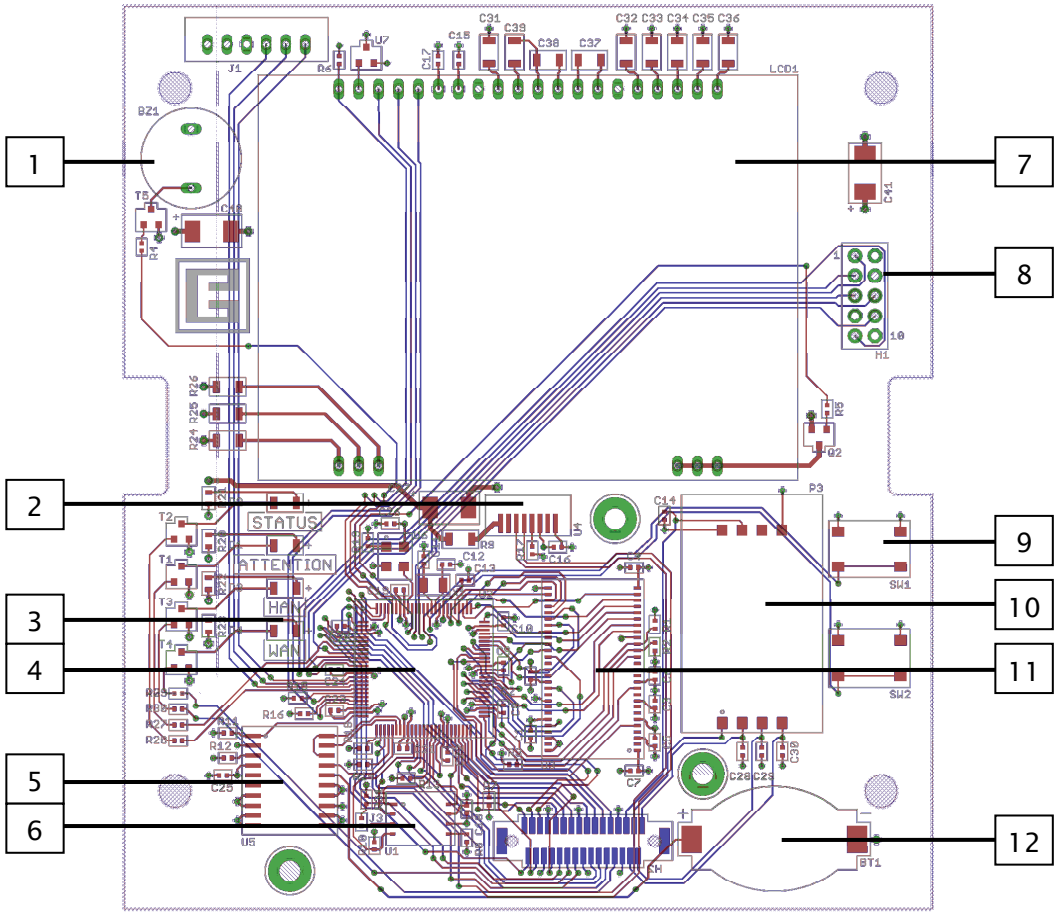

Figure 3.4: Smart meter test bed platform motherboard PCB design

Figure 3.4 shows the design of the smart meter test bed platform motherboard PCB. Figure 3.5 shows this PCB after manufacture and assembly. The elements indicated in both of these figures are as follows:

1: Sounder
2: Infrared interface
3: Notification LEDs
4: Microcontroller
5: Real-time clock
6: Non-volatile flash memory
7: LCD display
8: JTAG programming interface
9: Push buttons
10: SIM card holder
11: SDRAM
12: Real-time clock battery

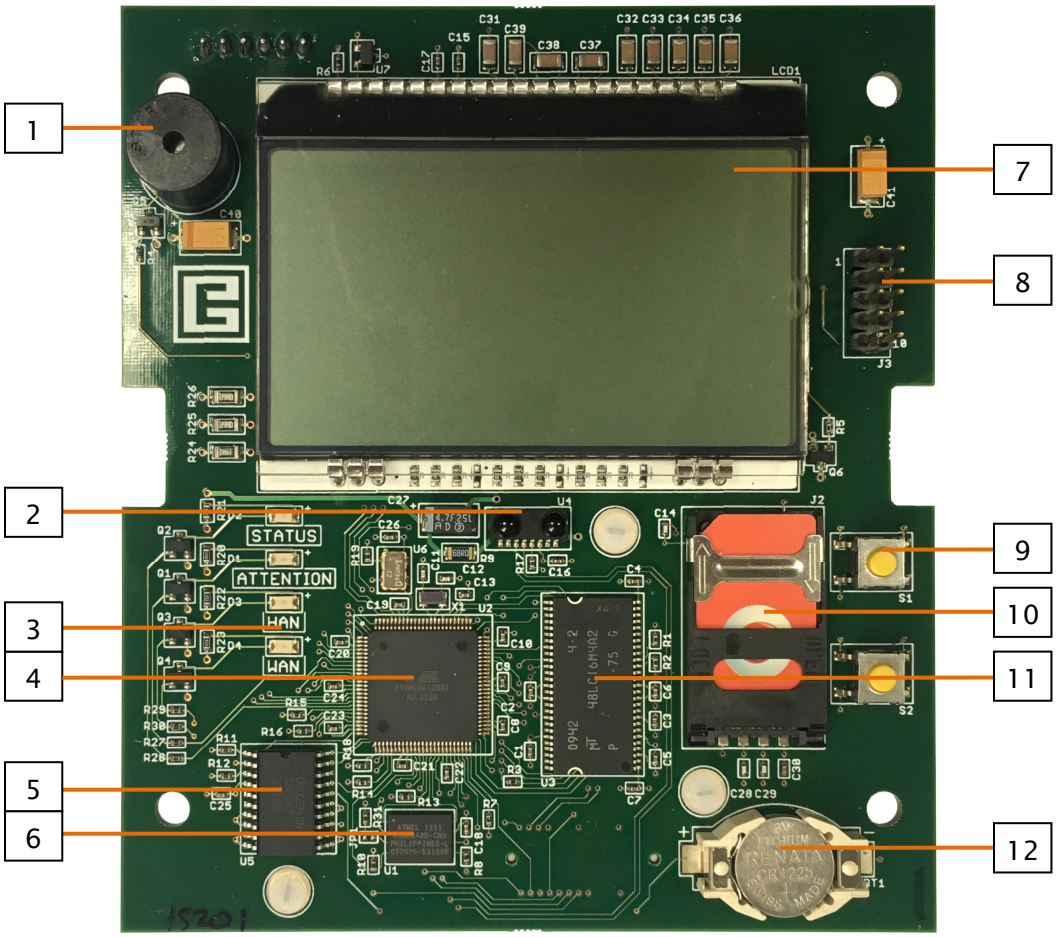

Figure 3.5: Assembled smart meter test bed motherboard

3.3.1.4 - ADC and filtering

The ADC employed is an Analog Devices ADE7753, a two-channel, 16-bit, second-order, delta-sigma device with a maximum sampling frequency of 31.25 kHz given a maximum system clock frequency of 4.0 MHz. It integrates a programmable-gain amplifier (PGA) for both channels, a temperature sensor and signal processing stages which include RMS calculation. Both channels have a maximum input voltage of ±0.5 V. The functional block diagram of the ADC is illustrated in Figure 3.6 [220]. The ADC is configured with one channel performing acquisition of voltage samples and the other channel performing acquisition of current samples. Anti-aliasing filters are applied to the input signals of both ADC channels. These filters are first-order RC networks with both R and C elements socketed in order that the filter characteristic can be configured for the sampling rate used in a particular experiment.

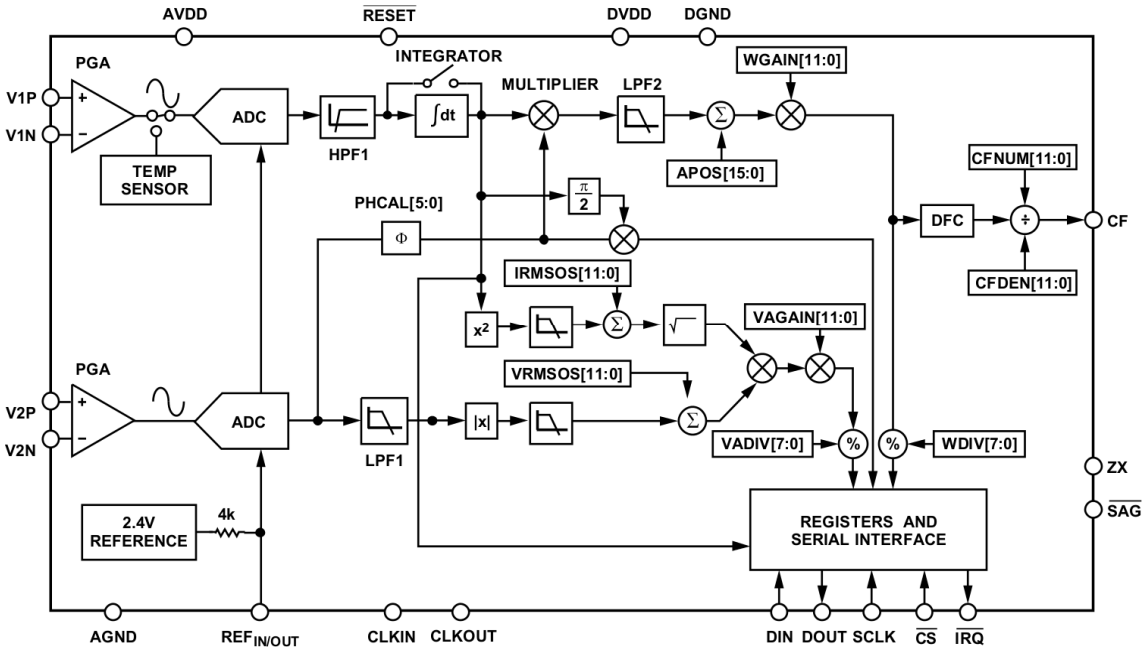

Figure 3.6: ADC functional block diagram [220]

The voltage channel signal path includes an attenuation network, preceding the anti-aliasing filter. The attenuation network is a resistive potential divider which matches the peak voltage range of an input signal taken from the phase and neutral bus bars within the meter, when monitoring a 230 V single-phase supply, to the input range of the ADC. Both R elements in the attenuation network are socketed in order that the input range can be configured for a particular experiment. In order that a low voltage input signal within the input voltage range of the ADC can also be used, for example from a signal generator or real-time digital simulator, provision is made for this to be connected directly to the input of the anti-aliasing filter. The voltage channel input stages are illustrated in Figure 3.7.

In order that a Manganin shunt resistor may be used as a current sensing transducer, the current channel signal path includes a phase correction filter, preceding the antialiasing filter. The phase correction filter is a first-order RC network which permits compensation for the phase shift in an input signal incurred from the parasitic inductance of a shunt resistor. Both R and C elements of this network are also socketed in order that they may be configured as required. As in the case of the voltage channel, provision is made that a low voltage signal within the range of the ADC input may be connected directly to the antialiasing filter. The current channel input stages are illustrated in Figure 3.8.

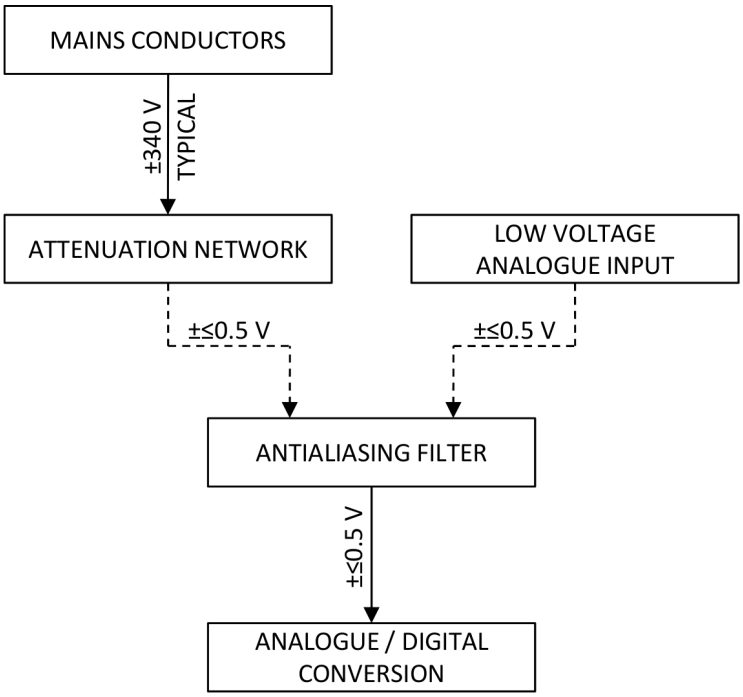

Figure 3.7: Voltage channel input stages

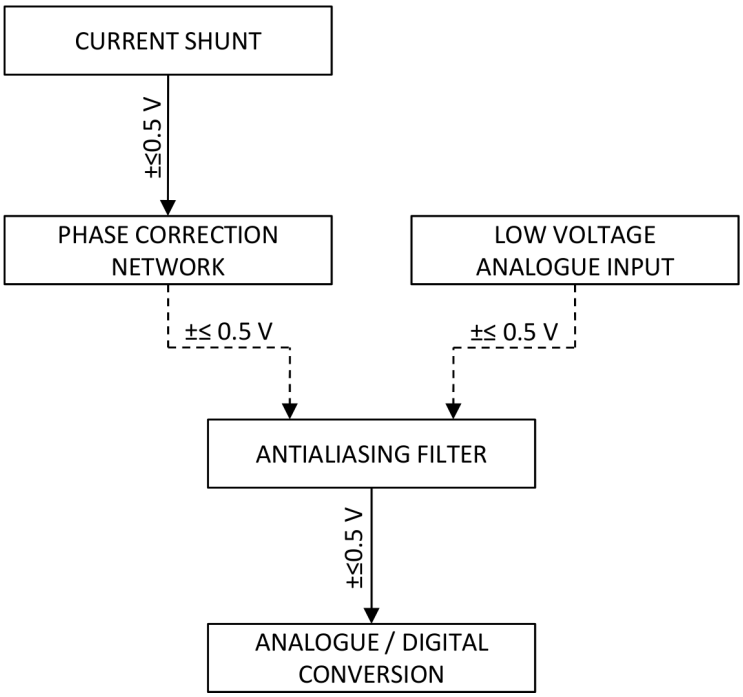

Figure 3.8: Current channel input stages

An integrated voltage reference is used to provide a 2.5 V reference to the ADC with an accuracy of ±1 mV and a maximum thermal drift of 3 ppm/°C. Since the operating voltage of the logic interfaces of the ADC is 5.0 V, level translation is required for communication with the 3.3 V microcontroller. This is achieved by means of an active bus translation device which, in addition to performing voltage level translation,

includes Schmitt triggers which increase the slew rate of logic signal edges. The ADC is connected to the microcontroller, via the bus translation stage, by means of a bidirectional SPI interface with a maximum clock rate of 10 MHz. Since this is a synchronous bus, an additional hardware interrupt line is also used. Hence, bus translation is performed upon five logic lines. These are clock, chip select and data from the microcontroller to the ADC, and data and interrupt from the ADC to the microcontroller.

The main clock of the ADC is derived from a local 3.579 545 MHz crystal.

The digital stages of the ADC are powered from the general 5.0 V bus, whilst the voltage reference device and analogue stages of the ADC are powered from an isolated 5.0 V bus in order to reduce the acquisition of supply-borne noise.

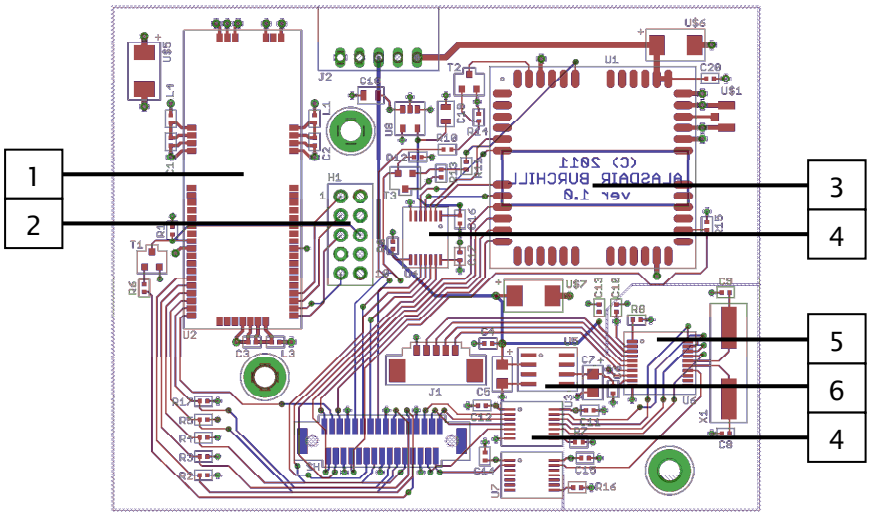

Figure 3.9: Smart meter test bed platform daughterboard PCB design

Figure 3.9 shows the design of the smart meter test bed platform daughterboard PCB. Figure 3.10 shows this PCB after manufacture and assembly. The elements indicated in both of these figures are as follows:

1: Zigbee interface
2: JTAG programming interface
3: GPRS interface
4: Bus translation devices
5: ADC
6: Voltage reference source

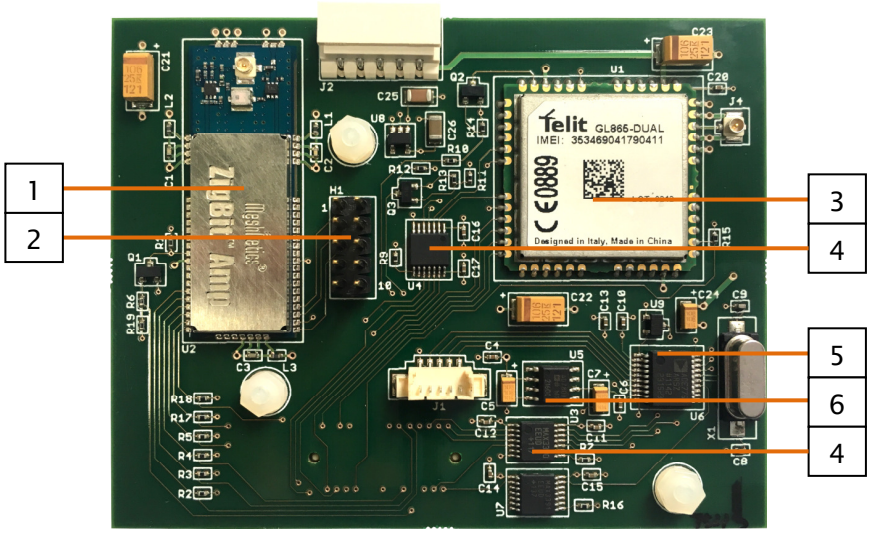

Figure 3.10: Assembled smart meter test bed daughterboard

3.3.1.5 – PCB design and assembly

The motherboard and daughterboard of the test bed were designed using CadSoft's EAGLE PCB EDA package. Both are 4-layer boards, with internal power and ground planes. In the case of the daughterboard, the ground plane is further divided into digital and analogue sections, with an isolated analogue ground plane beneath the input signal filters for both channels, the voltage reference device, and the ADC. This provides enhanced immunity from coupled and induced noise for the analogue components.

The motherboards and daughterboards were fabricated, and the surface-mount components assembled, by Newbury Electronics Ltd. The through-hole components were then assembled onto the boards manually. The motherboard and daughterboard connect back-to-back, by means of PCB headers, and are mechanically joined by nylon screws and spacers. The outline of the motherboard, and display and switch positions, are such that it fits into a commercially available smart meter enclosure sourced from Cixi Feiling Appliance Corp. Ltd.

3.3.2 - Firmware

Foundation firmware was developed for the smart meter test beds in order to provide a platform upon which further firmware functions could be added, as required, for a particular experiment. The foundation firmware comprises:

1. Drivers for the internal components of the microcontroller, for example the SPI interfaces.
2. Libraries for the hardware components of the meter which are external to the microcontroller, for example the ADC.
3. Initialisation routines to enable and configure internal components of the microcontroller, for example the system clock.
4. Initialisation routines to enable and configure the hardware components of the meter which are external to the microcontroller, for example the ADC
5. Buffers for the microcontroller USART interface used for communication between the microcontroller and the WAN hardware module.
6. Interrupt service routines for the microcontroller communications interfaces and other interrupt triggers, for example the microcontroller timer overflow.
7. A routine for establishing a connection to the WAN server of the test rig using the WAN interface of the meter.
8. A routine to perform the graceful shutdown of the HAN and WAN interfaces prior to de-energisation of the meter.

The implementation of these elements is described below:

1. C drivers supplied by the manufacturer of the microcontroller, Atmel, are used to control the low-level hardware elements of the microcontroller. The drivers used are:

    - CPU: Used to trigger a soft-reset of the microcontroller and provide reset cause reporting if a reset occurs that was not intentionally triggered.
    - PMIC: Used to configure and control the microcontroller Programmable Multilevel Interrupt Controller.
    - SLEEP: Used to configure and enter the low power sleep modes of the microcontroller.
    - SPI: Used to configure and operate the microcontroller SPI interfaces.
    - TC: Used to configure and operate the microcontroller Timer/Counter.
    - USART: Used to configure and operate the microcontroller USART interfaces.

In addition to the drivers, a software service module, CLOCK, supplied by Atmel and written in C, is used to simplify the configuration and control of the system clock.

2. Libraries were written to provide a reference for the registers within hardware components of the meter, external to the microcontroller. Those included in the foundation firmware are:

   - `ade77553.h` This contains a reference of the register addresses of the ADC used in the meter.
   - `st7565r.h` This contains a reference of the internal registers of the LCD controller used in the meter.

3. The file `brazil_board.h` assigns identifiers to the microcontroller communications interfaces used by hardware components of the meter external to the microcontroller. It also assigns identifiers to the hardware ports of the microcontroller at pin level. For example, the microcontroller SPI interface used for communication with the ADC is assigned a designator using the directive `#define ADC_SPI &SPIF`, whilst the microcontroller pin used as MOSI within the ADC SPI interface is assigned a designator using the directive `#define ADC_MASTER_MOSI IOPORT_CREATE_PIN(PORTF,5)`. The file `conf_board.h` is used to define the configuration of the electronic hardware of the smart meter test beds. The components of the meter which are external to the microcontroller, and which are enabled as an option in the foundation firmware, are selected by `#define` directives within the file `conf_board.h`. These components are:

   - ADC
   - LCD display
   - GPRS interface

   For example, the ADC is enabled using the directive `#define CONF_BOARD_ADC`. The file `init.c` is used to define the parameters of a hardware component required to initialise it. If a component is enabled in `conf_board.h`, the function `board_init` within `init.c`, and called from the top-level function `main.c`, configures the microcontroller port pins by setting pin direction, initial logic level, and activating pull-up or pull-down resistors as required. The function `board_init` within `init.c` also configures the microcontroller port pins assigned to the push buttons, notification LEDs and sounder by default.

The system clock settings of the microcontroller are configured with `#define` directives within the file `conf_clock.h`. In this way, the system clock source can be defined and a prescaler applied, if required for a particular experiment. The foundation firmware defines the system clock source to be the internal 32 MHz RC oscillator of the microcontroller, with no scaling applied.

4. The microcontroller SPI port assigned to the ADC, defined in `brazil_board.h`, is initialised as a bus master within the foundation firmware, with a clock frequency of 1 MHz. It is further configured with a clock polarity of 0 and clock phase of 1, i.e. the clock signal generated by the microcontroller will have a quiescent state of logic low and data transfer governed by the clock signal will occur on the falling edge of the signal. The interrupt enable register within the ADC, IRQEN, is cleared by default within the foundation firmware and all other ADC registers are left in the default state.

   The microcontroller SPI port assigned to the LCD display, defined in `brazil_board.h`, is initialised as a bus master within the foundation firmware, with a clock frequency of 8 MHz. It is further configured with a clock polarity of 1 and clock phase of 0, i.e. the clock signal generated by the microcontroller will have a quiescent state of logic high and data transfer governed by the clock signal will occur on the rising edge of the clock. Following initialisation of the SPI interface which drives it, a sequence of configuration commands is sent to the LCD display. These commands initialize the boost converter within the display, and configure settings such as contrast, and on which line the first pixel to be addressed resides.

   The microcontroller USART port assigned to the GPRS module, defined in `brazil_board.h`, is initialized as an asynchronous interface with a bit rate of 9600 b/s, a word size of 8 bits, 1 stop bit and no parity check bit. Following initialization of the USART interface, a sequence of configuration commands, in the Hayes/AT format, is sent to the GPRS module. These commands perform the following functions:

   i. Set the AT command echoing policy

   ii. Set the flow control policy of the UART interface used to communicate with the microcontroller of the smart meter

   iii. Define a packet data protocol (PDP) context for subsequent GPRS connection.

   iv. Configure the socket to be used for subsequent connection, specifying packet size, socket inactivity timeout, connection timeout (the maximum period to wait

for the acceptance of a connection before raising an error), and data sending timeout (the maximum period to wait before transmitting the contents of the transmit buffer, even if the number of bytes to send is less than the defined packet size).

v. Activate the PDP context defined by function 3.

The parameters set by these commands in the foundation firmware are given in Table 3.1.

Table 3.1: Foundation firmware GPRS settings

AT command echoing:	Disabled
Flow control:	Hardware, mono-directional (CTS only)
PDP type:	IP
PDP header compression:	Disabled
PDP data compression:	Disabled
TCP/UDP packet size:	300 B
Socket inactivity timeout:	90 s
Socket connection timeout:	600 s
Socket sending timeout:	50 s

5. Two dynamically allocated, 1 kB arrays are created in the foundation firmware to buffer data received from, and awaiting transmission to, the GPRS module. These arrays are operated as circular buffers. Functions to instantiate the buffer structure and to perform operations on the buffer, such as adding or removing elements, are defined within the file `ring_buffer.h`.

6. Generic, prototype interrupt service routines were implemented to handle data flow between any of the USART interfaces of the microcontroller, when used asynchronously, and circular buffers allocated to a hardware module external to the microcontroller, for example the GPRS module. Separate interrupt service routines were implemented to handle data awaiting transmission from, and data which has been received to, the microcontroller. Flow diagrams describing the operation of both the transmit and receive buffers are illustrated in Figure 3.11.

   Upon reception of data by a USART interface of the microcontroller the USART RX interrupt is triggered, and an instance of the USART RX interrupt service routine copies the received data to the circular input buffer associated with the USART interface upon which data has been received. The USART RX interrupt is then cleared. When the hardware transmission buffer of a USART interface of the

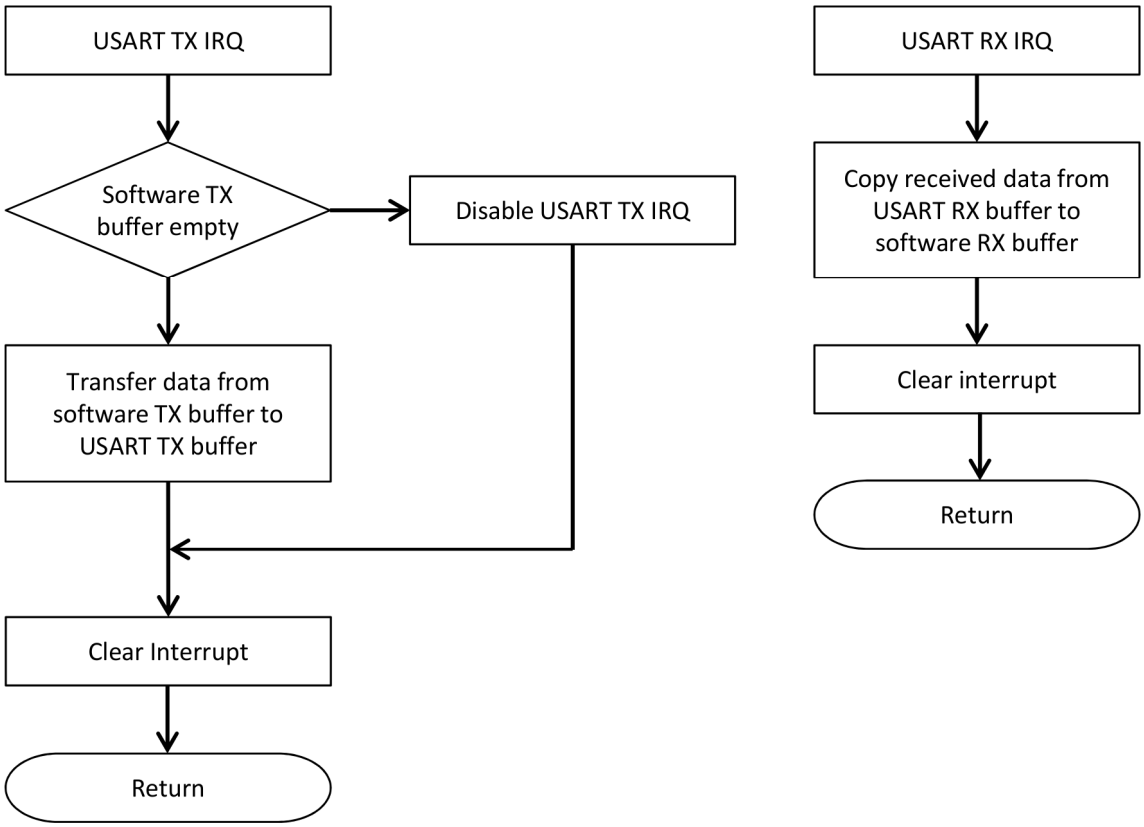

Figure 3.11: Generic USART interrupt service routines

microcontroller becomes empty the USART TX interrupt is triggered and an instance of the USART TX interrupt service routine copies data from the circular output buffer associated with the USART interface to which data is being sent, to the hardware transmission buffer. The USART TX interrupt is then cleared. If the circular output buffer is found to be empty when the USART TX interrupt is triggered, then this interrupt is disabled. The interrupt is re-enabled as soon as data is added to the circular output buffer.

Within the foundation firmware, the only hardware device external to the microcontroller which is enabled, and which is connected to the microcontroller with an asynchronous interface, is the GRPS module. Hence, a single instance of each of the USART RX and USART TX interrupt service routines are instantiated for this device.

In addition to interrupt routines triggered by communications events, a generic, prototype interrupt service routine was implemented within the foundation firmware which can be augmented to handle events such as button presses and timer overflows. A flow diagram describing the operation of this prototype interrupt service routine is illustrated in Figure 3.12.

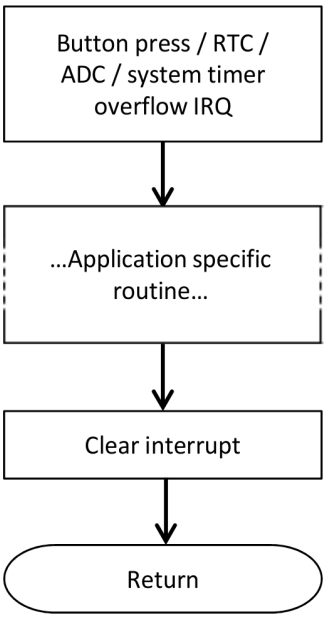

Figure 3.12: Generic, prototype interrupt service routine

Within the foundation firmware, this prototype routine is instantiated and augmented in order to service interrupt requests by the system timer internal to the microcontroller.

7. Following the successful configuration and initialisation of the GPRS module, including the creation and activation of a valid PDP context, the foundation firmware attempts to establish a TCP/IP connection with port 7048 of the GPRS server. The GPRS interface is left in a state such that further functions and communication may be performed, as required, for a particular experiment.

8. A function was included within the foundation firmware which terminates an open TCP/IP connection if one exists, deactivates the associated, active PDP context, and releases the bound socket.

3.4 - Test rig development

3.4.1 - Real Time Digital Simulator

The Real Time Digital Simulator (RTDS) employed is a physically self-contained machine manufactured by RTDS Technologies, which contains interchangeable cards for the real-time simulation of electrical networks as well as peripheral functions such as supervision of the unit and SCADA communication. A Giga Transceiver Analogue Output (GTAO) card, manufactured by RTDS Technologies, is used in conjunction with

the Giga Processor (GPC) cards of the RTDS unit in order to provide analogue signals to the current and voltage inputs of the smart meters, as described in Section 3.3.1.4. The analogue outputs of the GTAO card are single-ended with a range of ±10 V. The values of current and voltage signals from metered points with the simulated network are therefore scaled in order to fall within this range before being presented to the GTAO interface. The output values are refreshed on each 50 µs time-step of the network simulation performed by the RTDS, yielding an effective signal bandwidth of 10 kHz in accordance with the Nyquist–Shannon sampling theorem.

A Giga Transceiver Network Interface (GTNET) card, manufactured by RTDS Technologies, is used in conjunction with the GPC cards in order to provide a SCADA interface over Ethernet between hardware external to the RTDS and devices in networks simulated within the RTDS, such as transformer tap changers.

A Giga Transceiver Workstation Interface Card (GTWIF), manufactured by RTDS Technologies, is used in conjunction with the manufacturer's proprietary software package, RSCAD. This permits the layout and compilation of simulated networks, the upload of compiled networks to the GPC cards, and the control of a simulation during execution. The software package runs on a physically separate x86-64 desktop computer running the 32-bit edition of Debian GNU/Linux.

3.4.2 - SCADA server

The SCADA Server is a physically separate machine which acts as a bridge between the Giga Transceiver Network Interface (GTNET) card of the RTDS unit and the system controller. The GTNET card supports DNP3 for SCADA communication as a slave device only, and hence a DNP3 master station is required in order to connect to, and exchange data with, the card. The role of DNP3 master station is fulfilled by the software package PeakHMI, produced by Everest Software. A table of data points is created within the PeakHMI software which represents values to be read from, or written to, the GTNET DNP3 slave. These data points are created as required for a particular experiment. However, examples include a binary value to be written to the GTNET card to set the state of a circuit breaker, or a floating-point value to be read from the GTNET card in order to obtain the output value of a current transformer when these devices are used in a power network simulated within the RTDS. The DNP3 master station exchanges data between the table of data points and the DNP3 slave device once every second.

In addition to the DNP3 master station, the PeakHMI software package hosts an OPC server with access to the table of data points referred to by the DNP3 master station. The OPC server permits human-readable references to be assigned to points within the data table, and permits an OPC client connected to the server to request a list of the data points and to access them for reading, writing or both.

The SCADA server is an x86-64 desktop computer running the 32-bit edition of Microsoft Windows 7. It also runs the 32-bit edition of version 2.6 of the ActiveState Python distribution.

3.4.3 - GPRS server

The GPRS server is a physically separate, internet-facing system running a software server written in Python which accepts connections from the smart meter test beds. The server employs multithreading in order to support concurrent connections from multiple smart meter test beds. It also performs basic handling of data streams to and from the meters to which further functions can be added, as required, for a particular experiment.

The main process within the server instantiates a TCP/IP listening socket and binds it to port 7048. Upon receiving a connection request, the main process verifies that the maximum number of concurrent connections has not been exceeded and, if this is the case, accepts the connection. If the maximum number of concurrent connections has been reached, the request for a connection will be declined. Following the acceptance of a connection, the main process instantiates a new object of the class `Meter`, which stores the remote IP address and port of the connected meter as well as its serial number, a record of the current status of the meter, and a data structure to contain received data. The main server process adds the `Meter` object to the list of connected devices and instantiates a new handler thread to which it passes the `Meter` object.

The meter handler thread allocated to a particular meter buffers the data stream received over the connection with the meter and reassembles the data frames contained within it. STX/ETX frame encapsulation is employed for data transmitted between the server and connected meter and, as such, the handler thread will discard any data received until the start of a frame is signalled by the reception of an STX character. The handler will then reassemble the frame, which may span multiple TCP/IP packets, until the end of the frame is signalled by reception of the ETX character. Data subsequent to an ETX character within a TCP/IP packet it not lost, but rather is parsed for further complete or partial data frames. A default limit of 1 kB is placed on the

received data frames and frames exceeding this will be considered as malformed and hence discarded. Occurrences of the frame encapsulation characters within the data conveyed by a frame are handled in the same manner as the point-to-point protocol (PPP), a variant of the ISO high-level data link control (HDLC) protocol. Under this scheme, the instance of the reserved character within the data is replaced by the escape character 0x7D, followed by the original character bitwise XORed with 0x20.

In order to handle scheduled events, such as requests for readings to be transmitted to connected meters, the main process instantiates an event scheduler process with a default clock tick period of 1 s. To prevent connections with meters being closed unintentionally as a result of timeouts being triggered at any point along the length of the TCP/IP connection route, a default broadcast is made to all meters in the list of connected devices on every clock tick.

Figure 3.13 illustrates the execution of the GPRS server. In this example, the main process first instantiates the event scheduler process. Connections from two meters are then accepted with a handler process being instantiated for each. One connection is then lost, whilst one persists beyond the period covered by the figure. The default poll, broadcast to all connected meters by the event scheduler, is also shown.

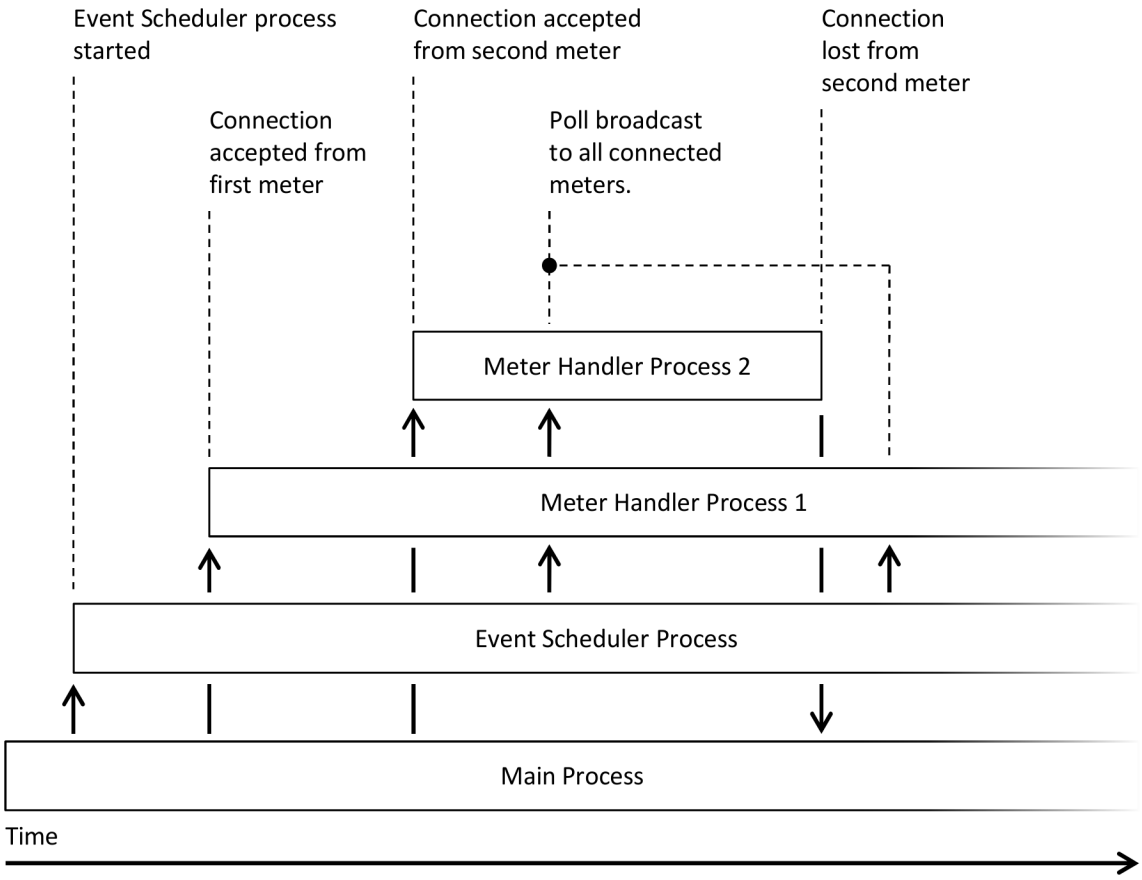

Figure 3.13: GPRS server core processes

The GPRS server is an x86-64 desktop computer running the 64-bit edition of Debian GNU/Linux. It also runs the 64-bit edition of version 2.7 of Python for Linux.

3.4.4 - Controller

The controller is an x86-64 desktop computer running the 64-bit edition of Debian GNU/Linux. It also runs the 64-bit edition of version 2.7 of Python for Linux and version 1.2.0 of OpenOPC. Python control schemes are executed on the controller, as required, for a particular experiment.

3.4.5 - Physical architecture

The physical architecture of the smart meter test rig is based on the logical architecture described in Section 3.2.2 and illustrated in Figure 3.2, and is illustrated in Figure 3.14. The connections between the RTDS GTWIF card and the RTDS workstation, as well as between the RTDS GTNET card, SCADA server, GPRS server and controller, are 100 Mb/s Ethernet links using an unmanaged switch. Communication between the cards within the RTDS unit is by means of optical links. In the case of all interfaces shown in Figure 3.14, significant protocols are specified, with N/S denoting that a non-standardised or application-specific protocol is used.

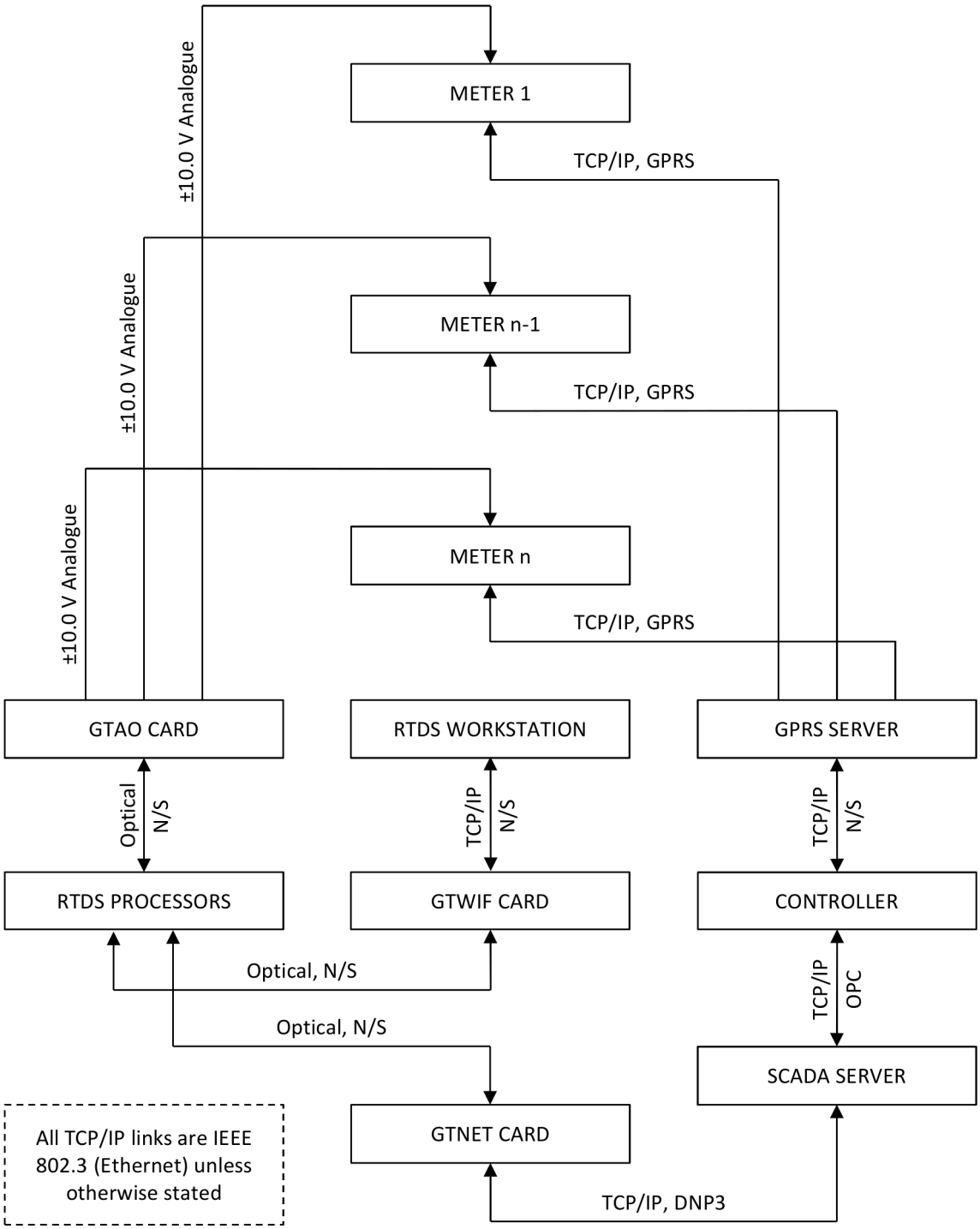

Figure 3.14: Physical architecture of the smart meter test rig

For the purpose of further research using the test rig, four smart meter test beds were manufactured. The RTDS unit and these smart meter test beds are shown in Figure 3.15. The mother and daughter boards of the meter are shown installed within enclosures, and powered from a laboratory power supply. The coaxial BNC leads conveying the voltage and current signals from the RTDS unit to the meters can also be seen.

Figure 3.15: RTDS unit and smart meter test beds

3.5 - Commissioning

In order to verify the correct operation of all the hardware, firmware and software elements within the smart meter test rig, a commissioning test was implemented. For the purpose of the test, only one of the four smart meter test beds was used.

3.5.1 - Commissioning test design

A simple, closed-loop test was designed to demonstrate the correct functioning of the test rig, based on the principle of voltage regulation by means of a transformer equipped with a SCADA-controlled OLTC. A single smart meter test bed was used to monitor the bus voltage of this transformer within a network simulated by the RTDS, using an analogue output. A controller script was written in Python which received voltage readings from the smart meter test bed via the GPRS server at one-second intervals and, if the readings violated preset limits, issued tap-change directives to the OLTC within the simulated network via the SCADA server. This was tested by manually triggering a step change in the supply voltage of the transformer within the simulated network.

3.5.2 - Simulated network

A simple network was created in RSCAD, consisting of a nominal 11 kV supply, a 500 kVA, 11 kV/415 V transformer, and a dynamic load for which real and reactive demand can be set during runtime. Circuit breakers were also included on both the primary and secondary sides of the transformer. The transformer incorporated a tap changer with positions from 0.80 p.u. to 1.25 p.u., with intervals of 0.05 p.u. The voltage of phase A, relative to neutral, was routed as an analogue output signal from the RTDS unit. This output was scaled by a ratio of 100:1, such that 500 V within the simulated network represented a full-scale output of 5 V from the RTDS unit. This output was provided as an input to the voltage channel of the smart meter test bed. A DNP3 SCADA slave station with three points was also created within the simulated network. These points were associated with the input registers ‘TapUp’ and ‘TapDown’, triggering the OLTC to tap up and down respectively, and the output register ‘TapPos’, returning the current tap position. The schematic of this network is shown in Figure 3.16.

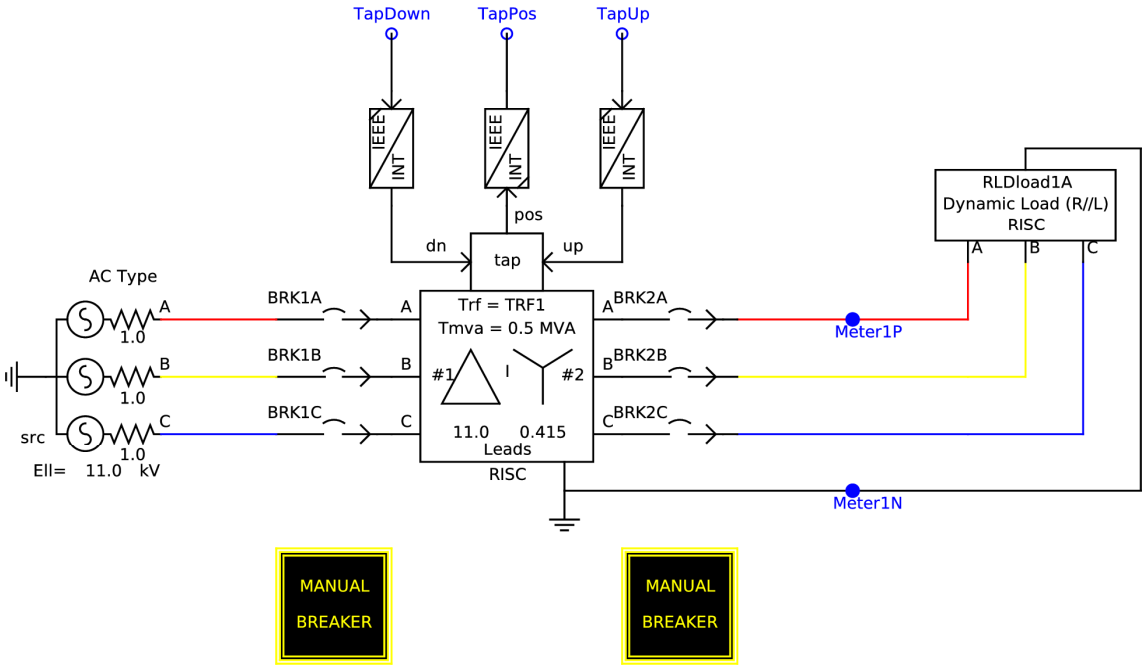

Figure 3.16: Commissioning test network schematic

In order to control the simulated network during the test, a runtime control screen was also created in RSCAD. This enabled the supply voltage of the transformer to be varied in the range 10.5 kV to 11.5 kV, and the real and reactive load on the transformer to be varied in the ranges 0–500 kW and 0–500 kVA respectively. It also enabled the circuit breakers within the network to be controlled, and the voltage at the metering point to be monitored. The runtime control screen is shown in Figure 3.17.

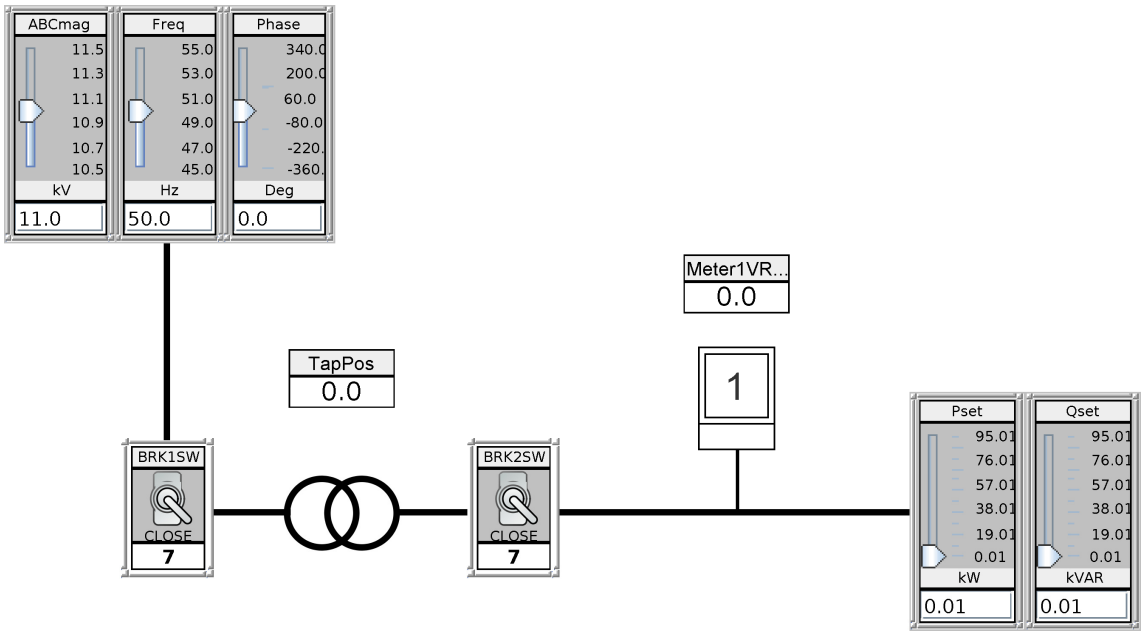

Figure 3.17: Commissioning test network runtime control

3.5.3 - Voltage control script

A simple voltage controller was written in Python. The voltage controller requests voltage readings at one-second intervals from the GPRS server, if a meter is connected. If a received voltage reading exceeds an upper limit of 235 V, or falls below a lower limit of 225 V, then the controller instantiates a 'Tap Changer' process, passing it the directive to tap up or down. The 'Tap Changer' process attempts to establish a connection with the OPC master station of the SCADA server as an OPC client and, if successful, issues a tap-up or tap-down directive, as appropriate, to the OPC master station. Upon reception by the OPC master station, the DNP3 master station of the SCADA server forwards the directive to the DNP3 slave station within the simulated network. After the tap-change directive has been issued, 'TapPos', as reported by the OPC master station via the DNP3 master station, is monitored. If 'TapPos' reflects the requested change then the 'Tap Changer' process returns the new tap position and terminates. If the tap position has not changed to reflect the request, or the process fails at any stage, the 'Tap Changer' process returns an error and terminates. Following the termination of a 'Tap Changer' process with success, the voltage controller will continue to monitor voltage readings and respond accordingly. Following the termination of a 'Tap Changer' process with an error, the voltage controller will instantiate another 'Tap Changer' process in order to attempt to effect the tap change. The 'Voltage Controller' and 'Tap Changer' processes are illustrated in Figure 3.18.

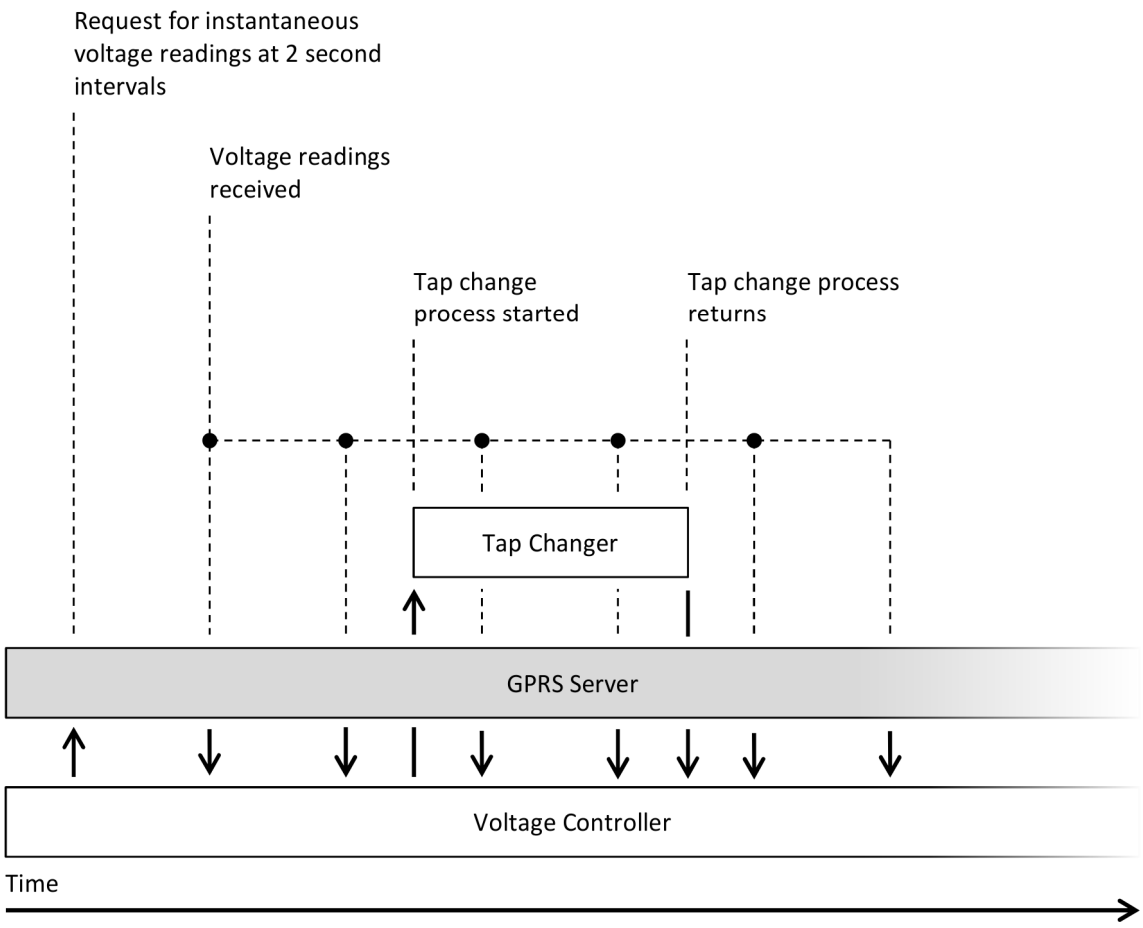

Figure 3.18: Voltage controller processes

3.5.4 - Test setup

The simulated network was compiled and executed on the RTDS with control of the simulation transferred to the runtime screen shown in Figure 3.17. A balanced load of 100 kW was applied to the transformer in the simulated network with the transformer tap position at 1.0 p.u. This yielded a voltage of approximately 228 V between the metered points. The GPRS server and SCADA servers were then started. A single meter was energised, with its voltage channel input connected to the RTDS GTAO card output associated with metered points in the test network. Finally, the voltage controller script was executed.

3.5.5 - Commissioning test results

In the first test, the supply voltage was changed from a starting value of 11.0 kV to 10.5 kV using the runtime control screen. The voltage controller responded to the metered voltage falling below the lower limit by instantiating a 'Tap Changer' process which, in turn, increased the tap position to 1.05 p.u. and returned the metered

voltage to within the prescribed limits. The metered voltage during this process is shown in Figure 3.19.

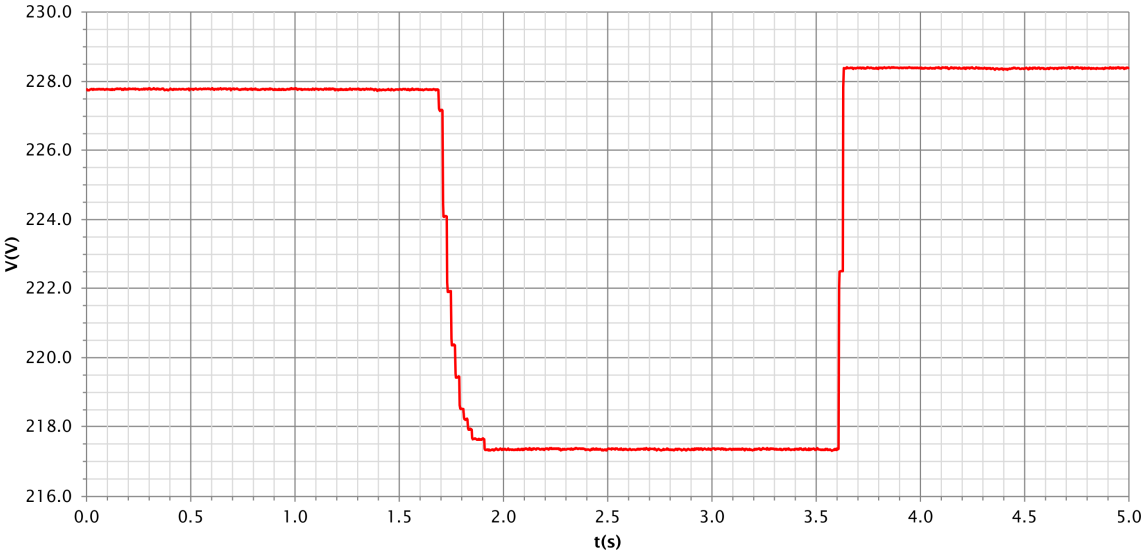

Figure 3.19: Tap up following metered under-voltage

In the second test, the supply voltage was changed from a starting value of 11.0 kV to 11.5 kV using the runtime control screen. The voltage controller responded to the metered voltage exceeding the upper limit by instantiating a 'Tap Changer' process which, in turn, decreased the tap position to 0.95 p.u. and returned the metered voltage to within the prescribed limits. The metered voltage during this process is shown in Figure 3.20.

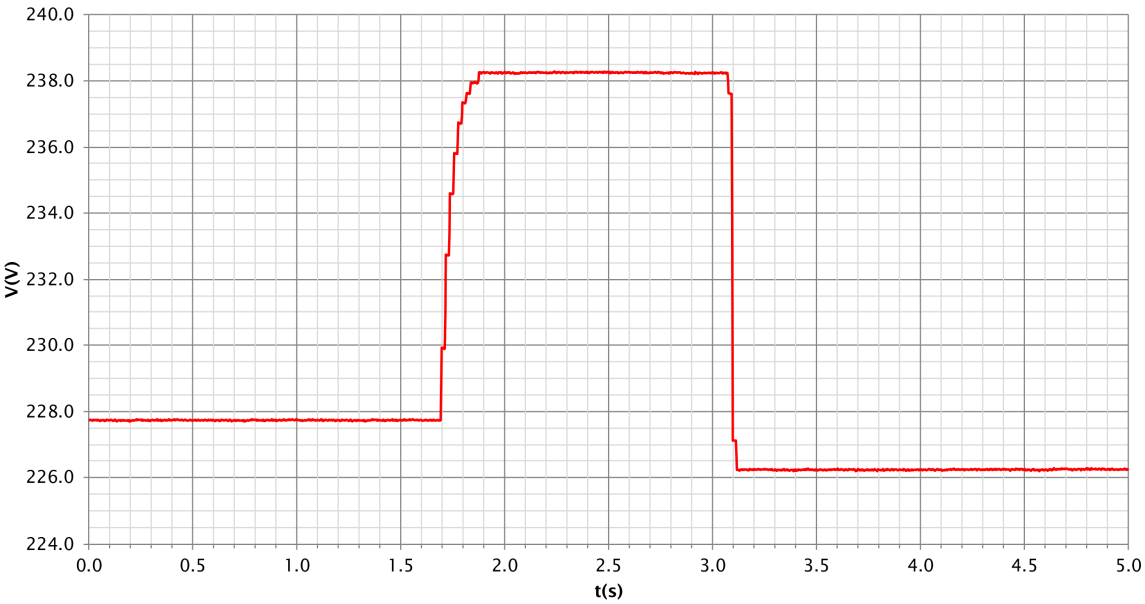

Figure 3.20: Tap down following metered over-voltage

3.6 - Discussion

The smart meter test rig developed permits analysis of the effectiveness of real-time voltage control informed by measurements taken by smart meters distributed across a radial distribution network, including the effect of real-world communications.

AVC schemes based on maintaining a constant MV busbar voltage in the presence of a limited penetration of DG, including those incorporating LDC, have shown effectiveness in simulation studies [42], [46], [49], [103], [104]. However, without control informed by distributed measurements, low load current and even reverse power flow resulting from a high penetration of DG may limit the usefulness of such systems [105]–[109]. In [117] voltage measurements from two points in a distribution network simulated on an RTDS were used to inform an AVC in real time. However, the limited number of monitoring points was a constraint of the hardware employed in this study, and the effect of real-world communications delays in limiting the response time of the system was not considered. Four smart meter test beds have been manufactured for the purpose of this research, constraining monitoring to a maximum of four distributed monitoring locations, though practically the number of smart meters which may be hosted by the test rig is limited only by the number of RTDS analogue output channels (12 per GTAO card).

In [93] the application of OLTCs to LV feeder control is examined, with constant set-point, time based, and remote monitoring-based control schemes considered. This study demonstrated that the OLTC combined with remote measurements offered the greatest mitigation of the effect of voltage non-compliance caused by PV penetration, whilst minimising the number of tap changes. However, this study did not consider the real-world limitations of communicating measurements from smart meters to a controller. The remote monitoring scheme presented in [93] was deployed in the real-world LoVIA field trial [119]. LV network monitoring was achieved by metrology and communications units (MCUs) distributed along the LV feeders on the test network. This limited the application of metrology to points on the distribution network providing exposed conductors to which monitoring equipment could be attached, for example in the substation and in street cabinets. As such, it was not possible in the trial of [119] to employ measurements at the point of common coupling (PCC), the connection point of the customer. As per equation (2.5), the feeder and supply cable between a given customer and the nearest monitoring point in this trial limited the accuracy to which the voltage at the customer's premises could be established, the uncertainty increasing with distance. The test rig developed in this work allows measurements to be taken by means of the smart meters from any point in the

distribution network simulated on the RTDS, without limitations of access to connection points. The performance of the system described in [119] is further limited by the intrinsic minimum response time of the voltage monitoring 'nodes' employed for the study, which present measurements as one-minute averages. Similarly, in the DG DemoNet – Smart LV Grid project [113]–[116], field trials of an OLTC controller informed by commercial smart meters were conducted on three Austrian LV networks. However, measurement granularity was limited by the commercial meters to a 5-minute moving-average value. The smart meter test beds developed in this work as part of the test rig may be configured such that voltage measurements are transmitted immediately, or averaged over an arbitrary number of samples or period of time, permitting the response of the system to be examined without limitations imposed by third-party hardware. The system employed for communication with the smart meters in the DG DemoNet – Smart LV Grid project was further limited by the fixed broadband over power line (BPL) communications protocol employed by the commercial meters, incurring a typical overhead of 1 s. The smart meter test beds developed in this work employ a cellular network interface, which reflects the preferred communications system for smart meter deployments in the UK, and permit the real-world communications and processing delays incurred in a real-time control system incorporating smart meters to be evaluated. These delays are non-deterministic factors, not adequately examined in existing studies.

The principal limitations of the test rig developed in this work are those of the necessary simplification of the distribution network simulated by the RTDS, due to finite processing capacity, and the small population of meters manufactured. A simplified power network simulation cannot fully reflect chaotic behaviours of real-world generation sources and loads, particularly at the level of LV where, at the periphery of the distribution network, the aggregated power figures based on diversified generation and demand are a weaker approximation of true power profiles. An advantage of the simulated distribution network, however, is that smart meters may always be preferentially allocated to network locations which are expected to experience the greatest voltage deviations, for example end points on radial feeders or long radial tees. In this way, the provision of smart meter measurements from all customers on a distribution network is not required, since a smaller population of meters may be allocated to such critical locations. However, a small population of smart meters does have the consequence of limiting the scope for examining the impact of communications congestion and processing overhead, if a smart metering head-end system is to support end-to-end communications with a large number of meters.

3.7 - Conclusion

A smart meter test bed platform has been developed which permits the control of sample acquisition, processing and communication parameters. A Real Time Digital Simulator has been employed to simulate a section of distribution network, and to provide analogue output signals representative of values within a simulated network in real-time. A test rig has been assembled which integrates these components in the form of a closed-loop control system, whereby SCADA-controllable assets within the simulated network may be directed by a controller informed by readings acquired by the smart meter test beds. Finally, a simple voltage control application has been implemented using one of the smart meter test beds, which successfully demonstrated the correct operation of the test rig, for the purpose of commissioning.

4 - Distribution network voltage control using smart meters

4.1 - Introduction

The use of the smart meter test rig to demonstrate the implementation of real-time voltage control within an LV network is described. This employs the hardware, and builds on the foundation software and firmware, described in Chapter 3.

Subsequent sections are structured as follows:

- Section 4.2 describes the development of a simplified LV network model for execution on a Real Time Digital Simulator (RTDS), and based on an existing generic distribution network model. The model extends from an 11 kV source to four LV feeders. The network model includes a distribution transformer equipped with an on-load tap changer (OLTC), and generation and load blocks which are controllable in order to simulate variation in the magnitude of generation and demand at different points within the network. The network also contains metering points allowing signals from the simulated network to be routed to the smart meter test beds via the hardware digital to analogue converters of the RTDS.
- Section 4.3 describes the implementation of a voltage alarm function to augment the foundation firmware of the smart meter test beds described in Chapter 3. This enables the smart meters to report, by exception, the detection of a measured voltage which violates prescribed limits.
- Section 4.4 describes the implementation of an automatic voltage controller. This implements an algorithm to assess the present voltage conditions measured within the simulated network by the smart meters and estimates the future voltage conditions if a tap change is performed. Based on the outcome of this algorithm and the availability of tap positions, the voltage control process will determine if a tap change should be requested, conduct the tap-change process over SCADA if necessary, and assess the subsequent network voltage conditions.
- Section 4.5 describes the configuration of instruments used in the experiment to demonstrate real-time voltage control, and of the telecommunications infrastructure employed. It also describes the test parameters used.

- Section 4.6 presents four test scenarios, illustrating the response of the voltage control system to voltage excursions on a simulated LV network exhibiting heavy loading and containing a high penetration of distributed generation. The four scenarios demonstrate the scope for voltage regulation using the on-load tap changer in the case of:

  1. Heavy loading, for example from a high penetration of electric vehicle charging.
  2. High levels of distributed generation, for example from a high penetration of solar PV installation.
  3. Heavy, imbalanced loading.
  4. The conflicting requirements of a combination of heavy loading and high levels of distributed generation.

- Section 4.7 discusses the work undertaken, in the context of existing research in this field, and summarises the advancements and contributions made. The limitations of the approach taken are also considered.

- Section 4.8 summarises and concludes the work presented in this chapter.

4.2 - LV network model

4.2.1 - Simulation topology

The LV distribution network model developed was based on the generic, UK distribution network, presented by Ingram et al. [57]. For the purpose of this research, a single 11 kV/LV transformer was considered, fed by an 11 kV source. Circuit breakers are included in the model between the 11 kV source and the transformer, and between the transformer and the LV bus, as a means of switching the supply to the simulated network during the process of testing. Four feeders are modelled, diverging radially from the LV bus. Along each of these feeders a grouped load/source block is modelled at the centre and end of the feeder. These are separated from each other, and from the LV bus, by simulated cable sections. The topology of the network is illustrated in Figure 4.1.

The network model was constructed in RTDS Technologies' RSCAD software, and simulated with a time-step of 75 μs. The model permits two cases, each describing the load and generation power of the individual loads and sources within each load/source

block, to exist concurrently. By switching between these cases during runtime the response of the voltage control system to the effects of a change in power flow within the simulated network can be observed.

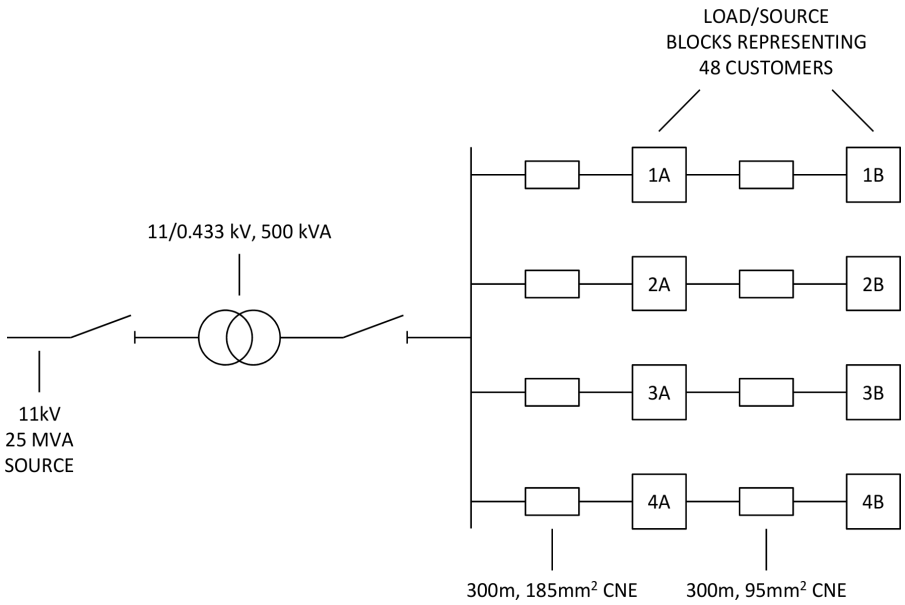

Figure 4.1: LV distribution network topology

4.2.2 - Network source and transformer configuration

The 11 kV source was assigned a rating of 25 MVA. This was simulated using an infinite bus voltage source combined with a positive sequence impedance. In order to conserve simulation capacity, a purely resistive series impedance, R, was employed for each phase, and calculated as follows:

$$R = \frac{V^2}{P} = \frac{11\,000^2}{25\,000\,000} = 4.84\,\Omega \tag{4.1}$$

Where *V* is the line voltage, and *P* is the source rating.

The transformer was further modelled as ideal, neglecting magnetising inductance and potential core saturation, with a rating of 500 kVA. It was assigned a Dy11 winding configuration with a leakage inductance of 0.05 p.u. and no-load losses of 0.001 p.u. The transformer is equipped with an OLTC, with a range of 87.5 % to 112.5 % in increments of 2.5 %, and assumed to be electronically-commutated. The tap changer has inputs which trigger tap changes up or down on the rising edge of a pulse and an output which return the current tap position. The source and transformer schematic from RSCAD are shown in Figure 4.2.

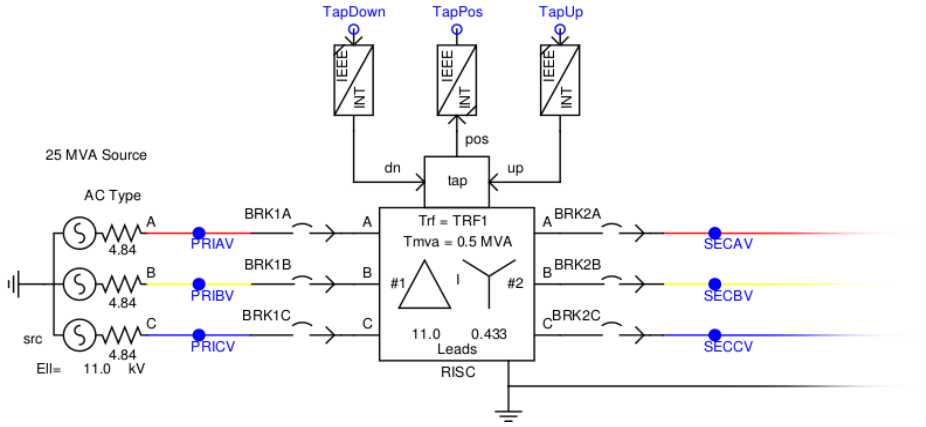

Figure 4.2: Distribution network source and transformer

4.2.3 - Cable modelling

Two cable section models were used in the simulated network. The first, used between the LV bus and the first load/source block on each feeder, was modelled as 300 m length of 185mm^2 CNE type cable with an impedance of 0.164 + j0.074 Ω/km for the phase conductors and 0.164 + j0.014 Ω/km for the neutral conductors, as per [57]. The cable section model was therefore constructed with a phase and neutral series resistance of 49.2x10^{-3} Ω and series inductance calculated as follows:

Phase conductor: $$L = \frac{X}{\omega} \cdot 0.3 = \frac{0.074}{2 \cdot \pi \cdot 50} \cdot 0.3 = 70.7 \times 10^{-6}\ \mathrm{H} \quad (4.2)$$

Neutral conductor: $$L = \frac{X}{\omega} \cdot 0.3 = \frac{0.014}{2 \cdot \pi \cdot 50} \cdot 0.3 = 13.4 \times 10^{-6}\ \mathrm{H} \quad (4.3)$$

The second cable section, used between the first and second load/source block on each feeder, was modelled as a 300 m length of 95mm^2 CNE type cable with a cable impedance is 0.32 + j0.075 Ω/km for the phase conductors and 0.32 + j0.016 Ω/km for the neutral conductors. The cable section model was therefore constructed with a phase and neutral series resistance of 96x10^{-3} Ω and series inductance calculated as follows:

Phase conductor: $$L = \frac{X}{\omega} \cdot 0.3 = \frac{0.075}{2 \cdot \pi \cdot 50} \cdot 0.3 = 71.6 \times 10^{-6}\ \mathrm{H} \quad (4.4)$$

Neutral conductor: $$L = \frac{X}{\omega} \cdot 0.3 = \frac{0.016}{2 \cdot \pi \cdot 50} \cdot 0.3 = 15.3 \times 10^{-6}\ \mathrm{H} \tag{4.5}$$

The schematic of the cable section models is shown in Figure 4.3.

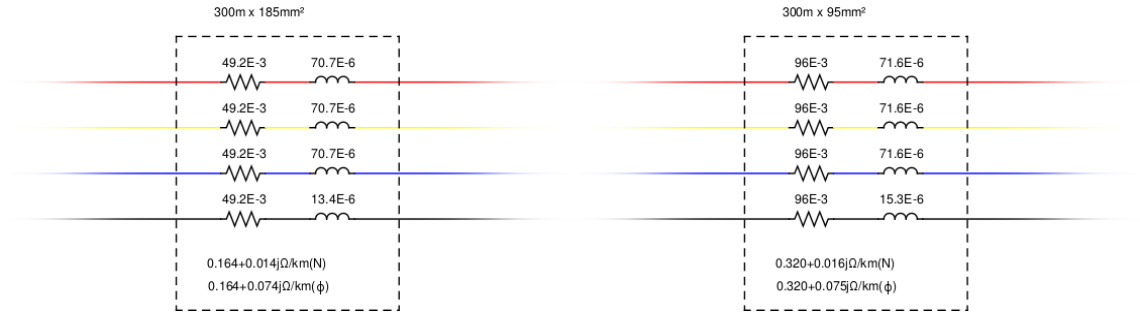

Figure 4.3: Cable section models

4.2.4 - Load/source block design

The load/source blocks, modelled at the centre and end of each of the four LV feeders are comprised of single-phase dynamic load models, provided by RSCAD, and power injection subsystems developed for the purpose of this study. Both the load and source elements were connected phase-neutral.

Each single-phase load and source within the load/source block was assigned three inputs. Two of these define set-points for real power flow, designated ‘A’ and ‘B’, and a third input, designated ‘SCENE’, selects which of ‘A’ and ‘B’ to assign as the current set-point. In this way, the set-points for two possible cases can be entered for all load and source elements in the network and a switch made between the two cases, affecting all load and source elements, controlled by the global variable ‘SCENE’.

4.2.5 - Dynamic load module control

The dynamic load modules are preceded by a selector which, based on the ‘SCENE’ input, defines which of inputs ‘A’ and ‘B’ are provided as the set-points to the module in the case of real and reactive power. The selectors controlling the real and reactive power set-points of the red phase load module in load/source block 1A are shown in Figure 4.4.

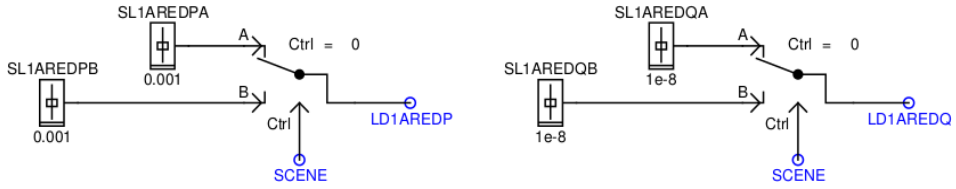

Figure 4.4: Load module set-point selectors

4.2.6 - Power injection subsystem design and control

Real power injection within the load/source blocks is achieved using a controlled voltages source connected to each feeder phase via series inductors, as shown in Figure 4.5.

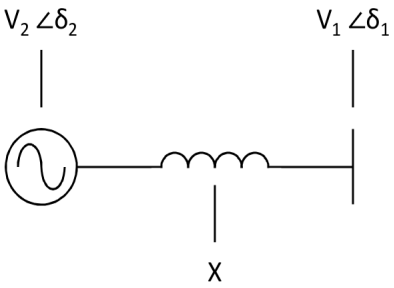

Figure 4.5: Power injection circuit

The relationship between voltage, phase and reactance in this circuit is defined as follows:

$$\sin(\delta_1 - \delta_2) = \frac{XP}{V_1 \cdot V_2} \tag{4.6}$$

$$\cos(\delta_1 - \delta_2) = \frac{XQ}{V_1(V_1 - V_2)} \tag{4.7}$$

Where V_1 and δ_1 are the voltage and phase of the controlled source, V_2 and δ_2 are the voltage and phase of the feeder, X is the series reactance, and P and Q are the real and reactive power flow. Rearranging these equations yields the expressions for real and reactive power transfer between voltage source and feeder:

$$P = \frac{V_1 \cdot V_2 \cdot \sin(\delta_1 - \delta_2)}{X} \tag{4.8}$$

$$Q = \frac{V_1(V_1 - V_2) \cdot \cos(\delta_1 - \delta_2)}{X} \tag{4.9}$$

In order to control active power flow into the feeder, the phase of the controlled source relative to the feeder is increased, whilst the voltage of the controlled source is matched to that of the feeder. The phase angle can therefore be expressed as follows:

$$\delta = \sin^{-1}\left(\frac{XP}{V^2}\right) \tag{4.10}$$

Where δ is the phase of the controlled source with respect to the feeder, and V is the matched voltage of the controlled source and feeder. In this application, only active power flow is controlled, and the reactive power flow is not regulated. As in the case of the dynamic load modules, the power injection subsystems are also preceded by a selector which, based on the 'SCENE' input, defines which of input 'A' and 'B' are provided as the real power set-point to the subsystem. A source capacity of 100 kVA is used. Hence the reactance is obtained as follows:

$$X = \frac{V^2}{P} = \frac{230^2}{100\,000} = 0.529\,\Omega \tag{4.11}$$

The RMS voltage of the feeder phase into which power is to be injected is calculated in the metering subsystem of the simulation and, hence, is available to reference in this subsystem. In order to synchronise the controlled source with the feeder, a zero-crossing detector is used to monitor the voltage of the phase to which is in connected, relative to neutral, and trigger a ramp generator. A constant is included in the subsystem to compensate for the simulation time-step delay, Δt, incurred as a result of signal exchange between processors used for power system and control simulation within the RTDS hardware. This is added to the phase of the controlled source. In the case of the subsystem described here, with a time-step of 75 µs, an average delay of 1.5 time-steps is incurred. The compensation constant is therefore calculated as follows:

$$COMP = \omega\Delta t = 2 \cdot \pi \cdot 50 \cdot 0.000\,075 \cdot 1.5 = 0.0353\,\mathrm{rad} \tag{4.12}$$

This compensation constant is added to the calculated value of δ and the output of the ramp generator, and sine of the total angle is calculated. The result of the sine calculation is then scaled to match the voltage of feeder, and the final value used to

control the voltage source. The complete power injection subsystem is shown in Figure 4.6.

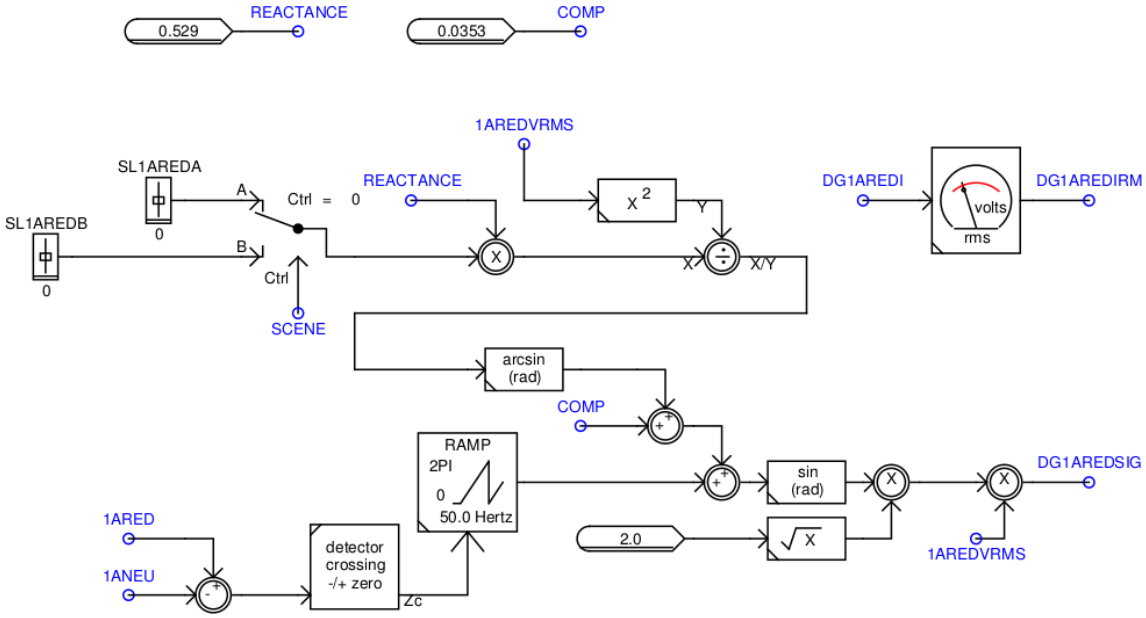

Figure 4.6: Power injection subsystem

The schematic of load/source block 1A is shown in Figure 4.7.

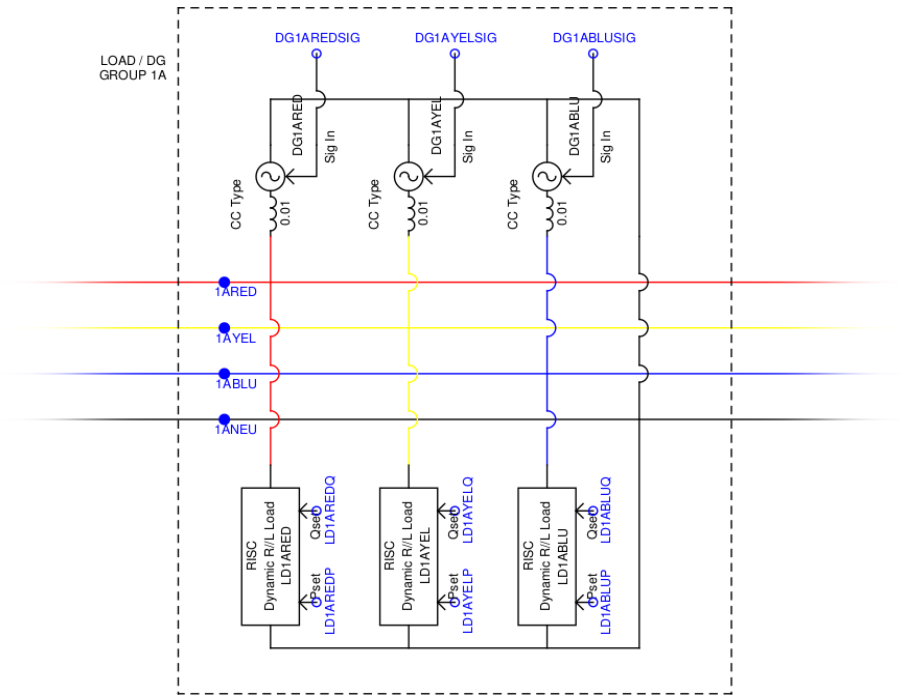

Figure 4.7: Load/source block schematic

2.6 - LV network simulation control

An RSCAD runtime environment was developed in order to control the simulated network during testing. The control interface for the 11 kV source and 11 kV/LV transformer is shown in Figure 4.8. This interface includes controls for the 11 kV source voltage and circuit breakers on the primary and secondary sides of the 11 kV/LV transformer, monitoring of the OLTC tap position, and monitoring of the LV bus. It also includes a control for the global variable 'SCENE' which sets which of case 'A' or 'B' is currently in use.

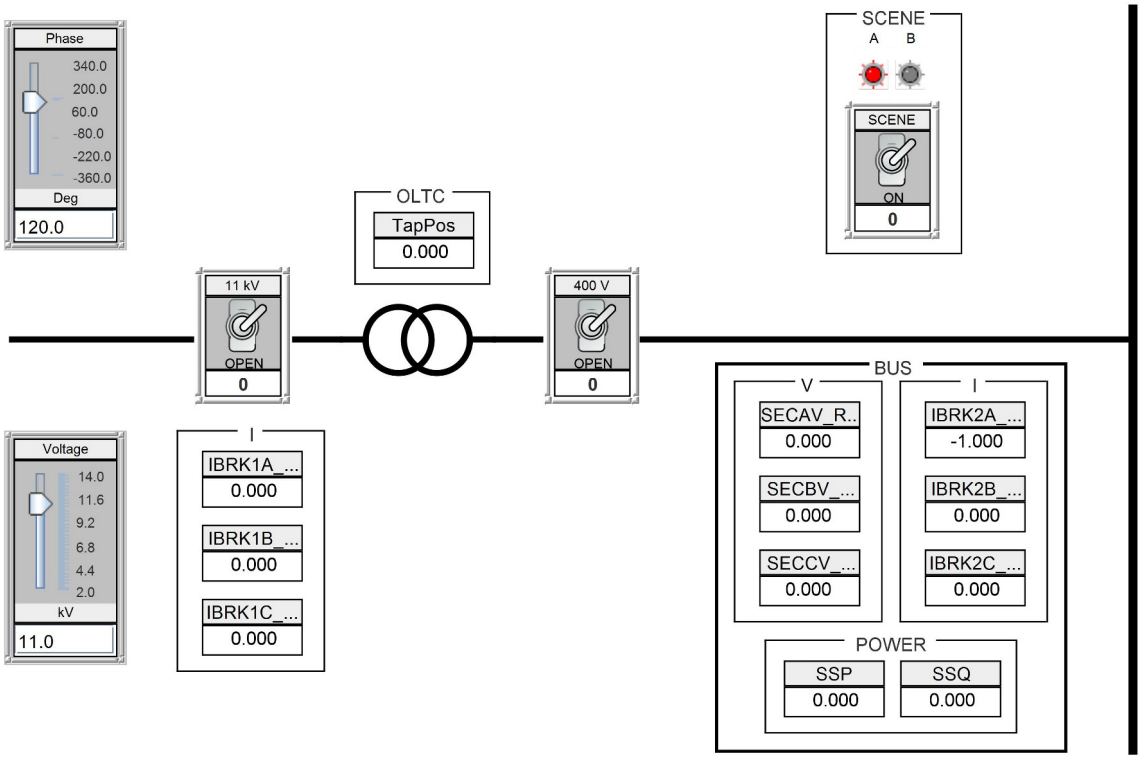

Figure 4.8: Network source, transformer and scene control

The control interface for load/source block 1A is shown in Figure 4.9. This interface includes controls for the active and reactive power of the dynamic load models, and the set-points of the active power injection subsystems. These controls are duplicated for cases 'A' and 'B', and the current case highlighted in red. The control interface also includes monitoring of the feeder voltage at the load/source block location and the delivered current of the active power injection subsystems.

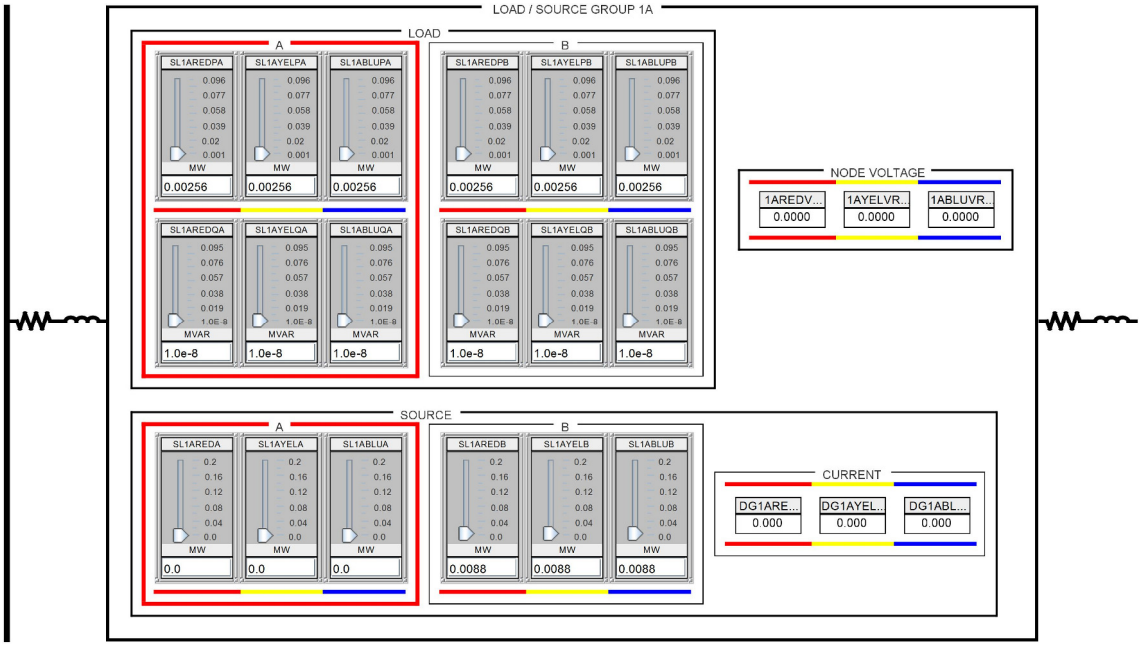

Figure 4.9: Load/source block control

4.3 - Development of the smart meter voltage alarm function

In addition to the RMS voltage measurement function implemented in the foundation firmware of the smart meters and described in Chapter 3, a voltage alarm function was implemented in order that the smart meters could report, by exception, the detection of a measured voltage which violates prescribed limits. As with the RMS voltage measurement function, this function is executed upon reception of a command from the GPRS server, to which the smart meters are connected. Upon execution, the voltage alarm function is passed a reference to the SPI interface buffer created for the ADC, a reference to the interrupt register assigned to the ADC and a reference to the prescribed voltage limits stored within the non-volatile memory of the meter. The function first enables triggering of the ADC interrupt on the zero-crossing of the measured voltage signal. The voltage alarm function then buffers three RMS readings from the voltage channel RMS register within the ADC. These reads are synchronised to the zero-crossing of the measured voltage signal, and hence correspond to three half-cycles. The three values are then averaged, and the result compared to the prescribed voltage limits. If the average value is within the prescribed voltage limits, the process repeats. If the average value violates the prescribed voltage limits, the ADC interrupt triggering on the zero-crossing of the measured voltage signal is disabled, the average value returned to the calling function, and the voltage alarm function terminated. The procedural flow of the voltage alarm process is illustrated in Figure 4.10.

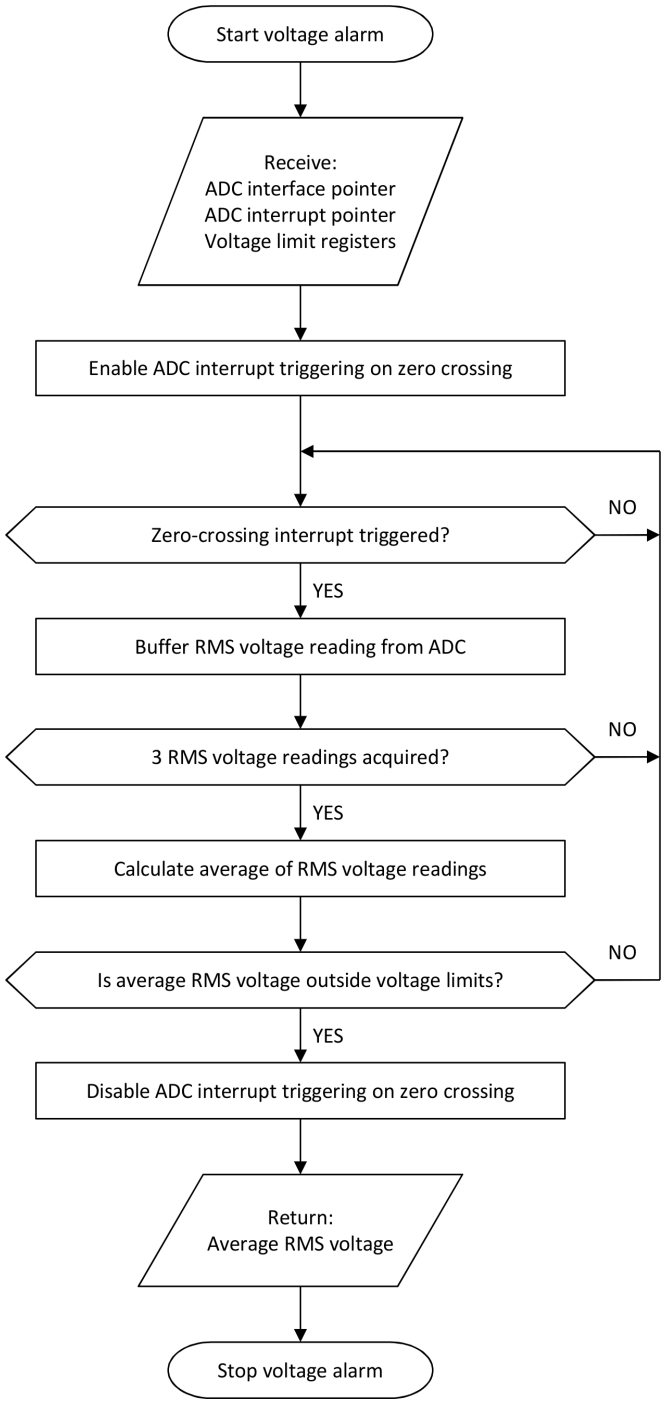

Figure 4.10: Voltage alarm procedural flow

4.4 - Development of the automatic voltage controller

A voltage control process was implemented in Python to execute on the controller hardware of the test rig, herein referred to as the AVC or Automatic Voltage Controller, which fulfils the function of 'controller' within the test-rig, as described in Chapter 3.

This controller directs the operation of the smart meter test beds by means of the GPRS server, receives measurement from the smart meter test beds, and issues directives to the OLTC within the RTDS simulated power network model, via the SCADA server. The core algorithm used to determine what voltage control behaviour, if any, should be taken within this process is based on that proposed in [221] and [117]. As such, in the event of a voltage or voltages outside of the prescribed limits being detected, the algorithm first evaluates whether conflicting voltage issues exist. If this is the case, it is anticipated that the use of the tap changer to restore the voltage at one metered point to within the prescribed limit will increase the degree to which the voltage at one or more of the other metered points violates the opposing limit, and hence no further action is taken. If no conflicting voltage issues exist, the algorithm verifies whether the tap changer is already at the highest position, in the case of an under-voltage condition, or the lowest position, in the case of an over-voltage condition, in which cases no further action is taken. The algorithm then estimates whether a change in tap changer position would cause the voltage at other metered points in the network, currently with the prescribed voltage limits, to violate those limits. If this would be the case, then no remedial action is attempted. The estimated voltage at a given point following a tap change is taken as the product of the current voltage and the ratio of the prospective tap position to the current tap position. For example, given a current voltage at a meted point of 230.00 V, a prospective tap position of 95.0 % and a current tap position of 97.5 %, the resulting voltage would be estimated as follows:

$$230.00 \cdot \frac{95.0}{97.5} = 224.10\,\mathrm{V} \tag{4.13}$$

Finally, if it is estimated that a change in tap changer position would not cause the voltage at other metered points in the network, currently within the prescribed voltage limits, to violate those limits, then the algorithm will initiate a tap change.

Upon instantiation, the AVC process is passed an array of references to the handler processes of all connected meters. It is also passed a reference to the socket allocated to the connection with the OPC SCADA server, references to objects containing the voltage limits, and the parameters and current position of the OLTC. If the algorithm determines that a tap change should not take place, then the process returns a failure and terminates. If the algorithm determines that a tap change should be executed then a tap-change directive is issued to the OPC SCADA server, the process returns a success and then terminates. The procedural flow of the AVC process is illustrated in Figure 4.11 and Figure 4.12.

This page intentionally left blank

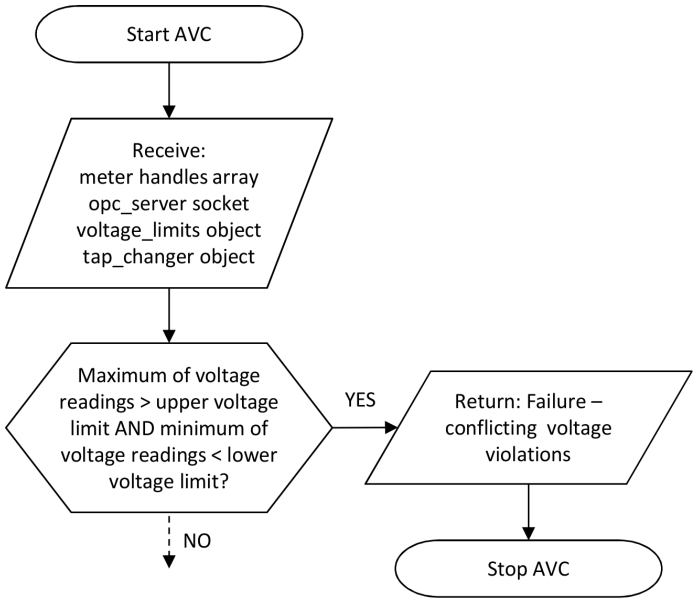

Figure 4.11: AVC process procedural flow (continued in Figure 4.12)

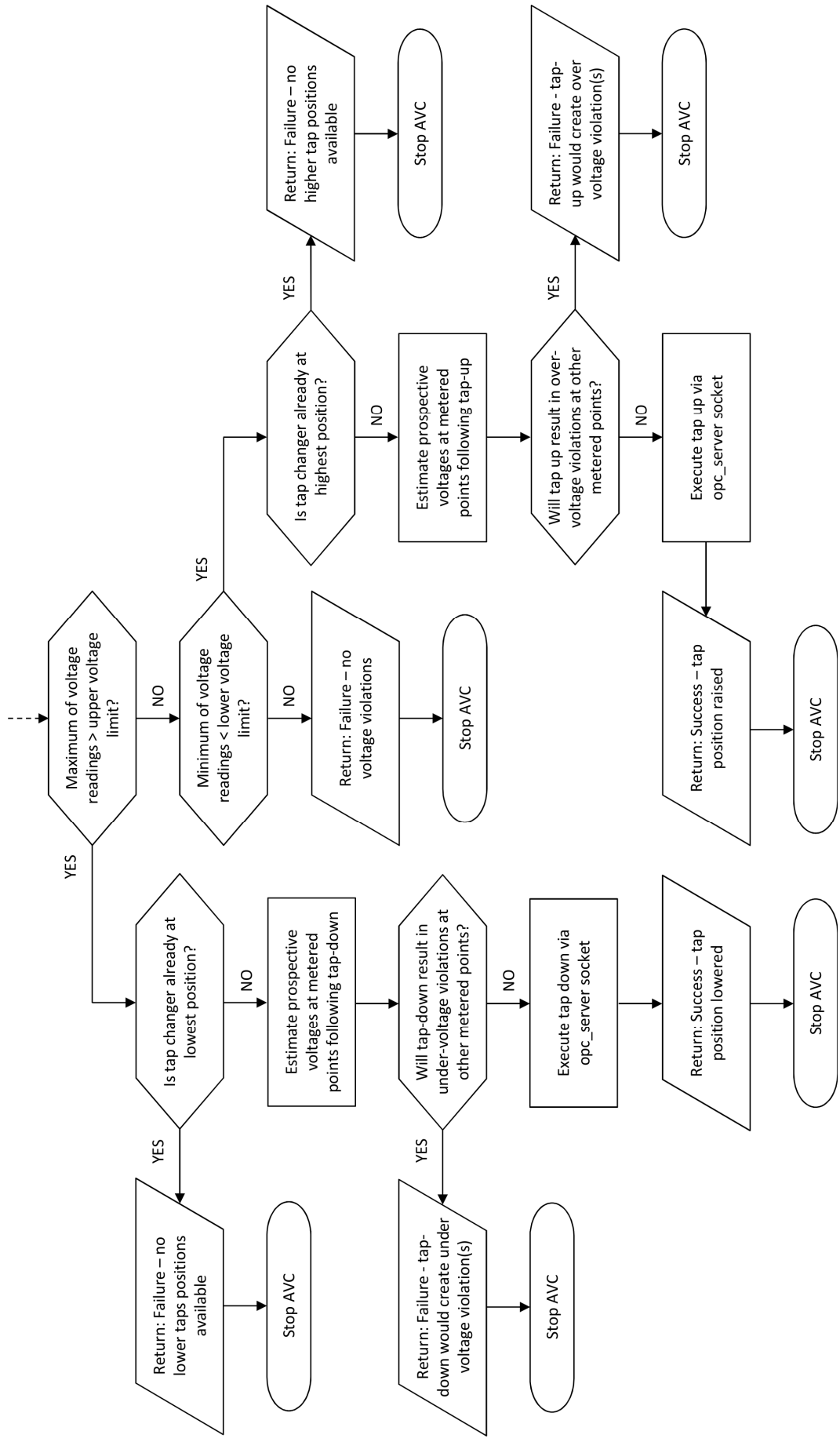

Figure 4.12: AVC process procedural flow (continued from Figure 4.11)

In order to utilise the AVC process, the event scheduler, included in the foundation firmware, issues a command to all connected meters to enable voltage exception reporting by executing the voltage alarm function. Upon receiving an alert of a voltage limit violation from one of the connected meters, the event scheduler sends a command to all connected meters to disable voltage exception reporting, in order to prevent multiple further notifications. The event scheduler then requests a read from all connected meters in order to obtain a current snapshot of the voltages at all monitored points in the LV distribution network. Once these read requests have been fulfilled, the event scheduler instantiates the AVC process. Upon termination of the AVC process, the event scheduler requests a read from all connected meters in order to obtain a current snapshot of the voltages at all monitored points in the LV distribution network following AVC execution. Finally, in order to address further voltage limit violations, the event scheduler sends a command to all connected meters to enable voltage exception reporting.

An example of the execution sequence of server processes in the case that two meters are utilised is illustrated in Figure 4.13.

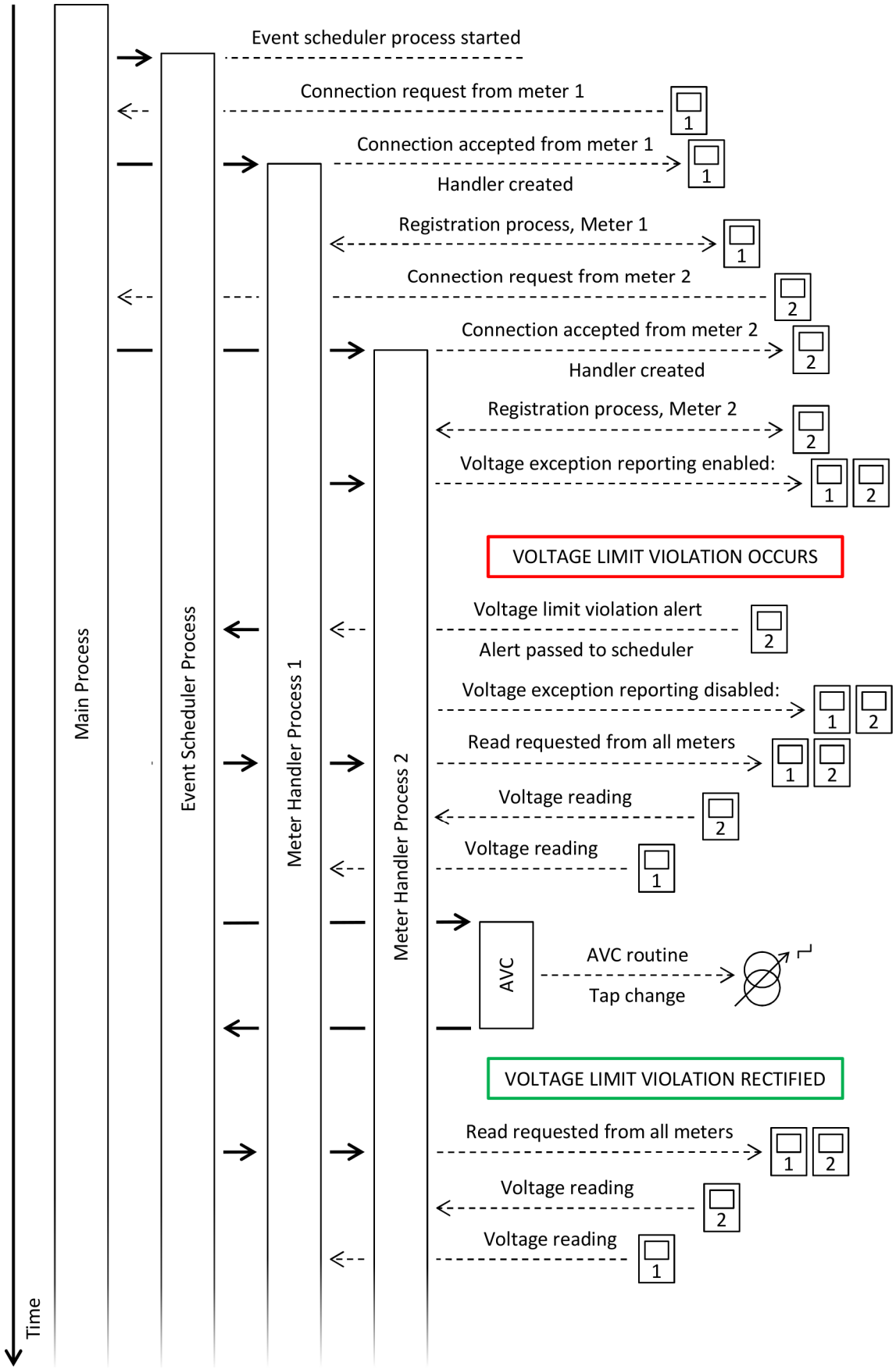

Figure 4.13: Example execution sequence of server processes

4.5 - Experimental setup

4.5.1 - Configuration of measuring equipment

An 8 channel Yokogawa DLM4038 mixed signal oscilloscope was used to acquire synchronised measurements of both the voltage at the metered points within the simulated network and the execution of the server processes. In addition to the voltage signals taken directly from the metered points within the simulated network and presented on analogue output (GTAO) channels of the RTDS, the RMS values of these signals were also calculated within the RTDS simulation and presented on analogue output channels of the RTDS. This enabled direct recording of the RMS voltage values using the oscilloscope. In order to measure the timing of server events, a call was added to the server software to toggle bit 0 of the parallel port interface of the GPRS server machine on the following events:

A - Voltage limit violation alert received (followed by command sent to all connected meters to disable voltage exception reporting).

B - Acknowledgment of reset received from all meters (followed by voltage read command sent to all connected meters).

C - Voltage read received from all meters (followed by instantiation of AVC process and execution of tap position change, as appropriate).

D - Termination of AVC process (followed by voltage read command sent to all connected meters).

E - Voltage read received from all meters.

The parallel port pin assigned to bit 0 was connected to the oscilloscope via a pull-down resistor. The arrangement of measurement connections is illustrated in Figure 4.14.

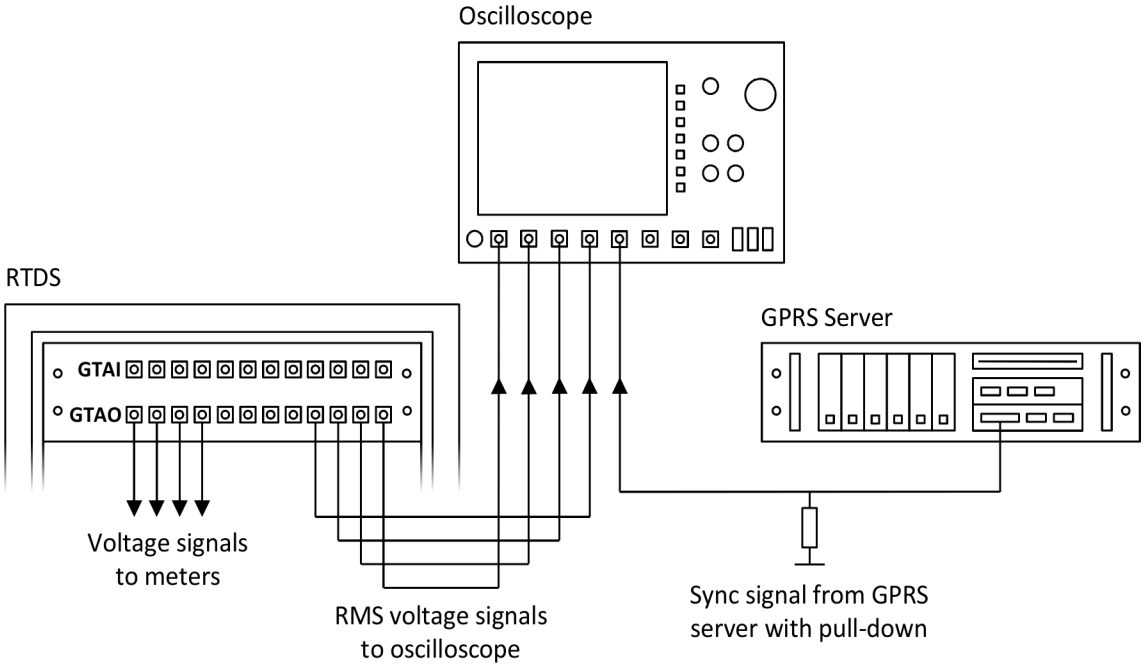

Figure 4.14: Connection of measurement equipment

4.5.2 - Telecommunications system

The GPRS connections between the smart meters and the GPRS server were made using the Vodafone UK cellular telecommunications network. The base station used was operating in the 1800 MHz band at Vodafone site reference 31823 and had a maximum transmission power of 25.8 dBW. The base station antenna was mounted approximately 41 m above ground level. The smart meters were located in the basement of the East Building of the Department of Engineering at Cardiff University, approximately 2 m below ground level. The antennas used on the smart meters were vertically polarised, quad-band elements with a gain of +4 dBi. The average received signal strength recorded by the GPRS receivers within the smart meters was -55 dBm. The locations of the smart meters and the cellular base station are shown in Figure 4.15 [222], indicated in red and green, respectively.

Figure 4.15: Locations of smart meters and cellular base station [222]

Figure 4.16 [223] shows an aerial perspective view of the locations of the smart meters and the cellular base station, indicated in red and green, respectively.

Figure 4.16: Aerial perspective view of smart meter and cellular base station locations [223]

4.5.3 - Test parameters

The voltage limits within the smart meter firmware and server software were set to a lower limit of 216.2 V and an upper limit of 253.0 V. These represent 230 V -6 % and +10 % respectively, as per *The Electricity Safety, Quality and Continuity Regulations 2002* [39]. All voltage signal values provided to the smart meters were taken between phase and neutral in the simulated network. Each scenario was tested 50 times in order that statistical analysis of the timing of server events, and time taken to restore network voltages to within prescribed limits, could be performed. The experimental time window for capture of the results presented was between 16:58 and 20:31.

4.6 - Test scenarios

4.6.1 - Scenario 1: High demand

Scenario 1 demonstrates the response of the voltage control system to demand from a high penetration of electric vehicle charging. Case A represents a base load of 1.3 kW/customer, reflecting maximum nominal customer demand [57], distributed uniformly across phases and across the extent of the simulated network. Case B represents the addition of a 10 % penetration of 3.5 kW/customer electric vehicle

charging, reflecting the maximum typical domestic electric vehicle charging power [82], distributed uniformly across phases and across the extent of the simulated network. The loads at each of the grouped load/source blocks for cases A and B are shown in Figure 4.17.

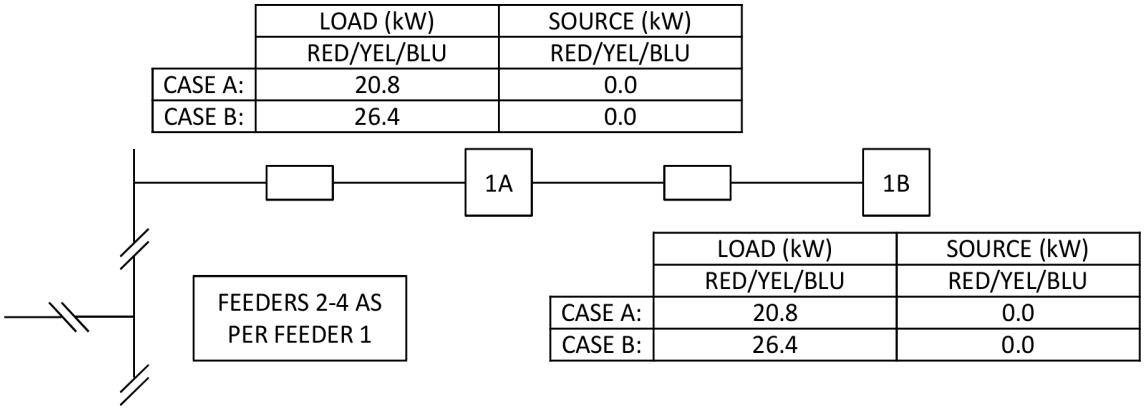

Figure 4.17: Scenario 1 load powers

Two smart meter test beds were utilised in this scenario. They were both assigned connections to the red phase at the locations in the simulated network shown in Figure 4.18.

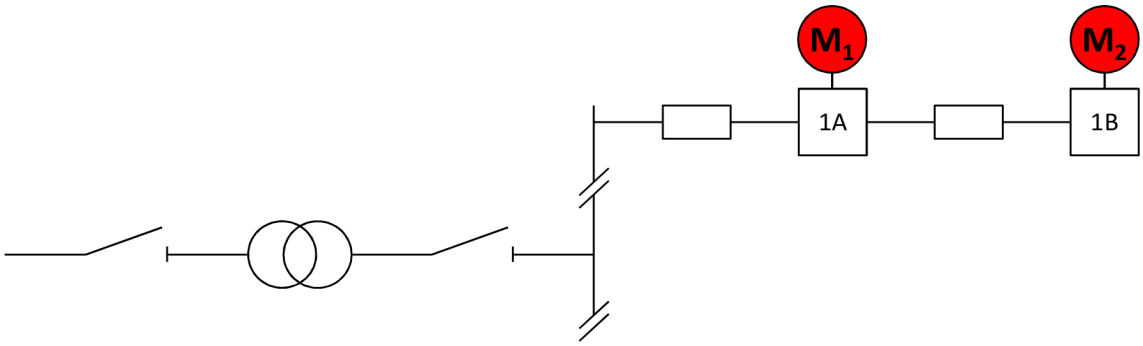

Figure 4.18: Scenario 1 meter locations

The voltages of all phases at each of the grouped load/source blocks in cases A and B are shown in Figure 4.19. Since all elements in the modelled network are balanced, the phase voltages are equal. Voltages which violate the prescribed limits are highlighted.

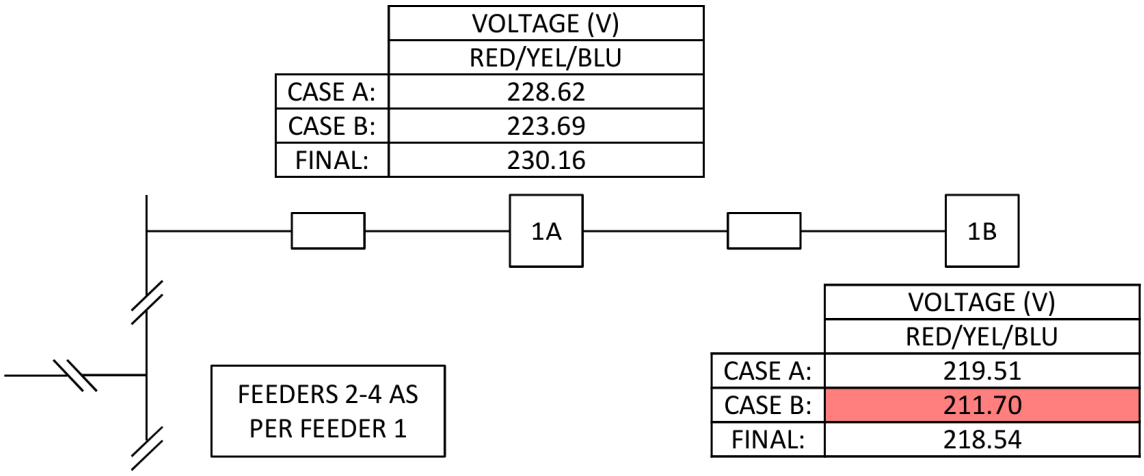

Figure 4.19: Scenario 1 network voltages

As a result of the additional loading added in case B, the voltage at grouped load/source blocks 1B fell below the lower voltage limit. The predicted voltages at the metered points as a result of an increase in tap changer position in response to the under-voltage condition, estimated by the AVC process, are shown in Table 4.1.

Table 4.1: Scenario 1 measured and predicted voltages

		Voltage (V)	
METER NUMBER:	METER LOCATION:	CASE B:	PREDICTED:
1	1A (RED PHASE)	223.69	229.58
2	1B (RED PHASE)	211.7	217.27

Since the predicted voltages indicated that the tap changer position could be increased without causing further voltage limit violations, the AVC executed an increase in tap changer position. The final resulting voltages are shown in Figure 4.19.

The profiles of the voltages at the metered points in scenario 1, with respect to time, are shown in Figure 4.20. The voltage limit violation at grouped load/source block 1B, following the transition from case A to case B, occurs at 0.00 s. In addition, the mean, and lower and upper quartile times of server events A to E, as specified in Section 4.5.1, are shown.

The mean, and lower and upper quartile times to achieve restoration of the voltage at all metered points to within the prescribed voltage limits are shown in Table 4.2.

Table 4.2: Scenario 1 restoration times

	L.Q.	$\bar{x}$	U.Q.
Restoration time (s):	2.74	2.89	3.06

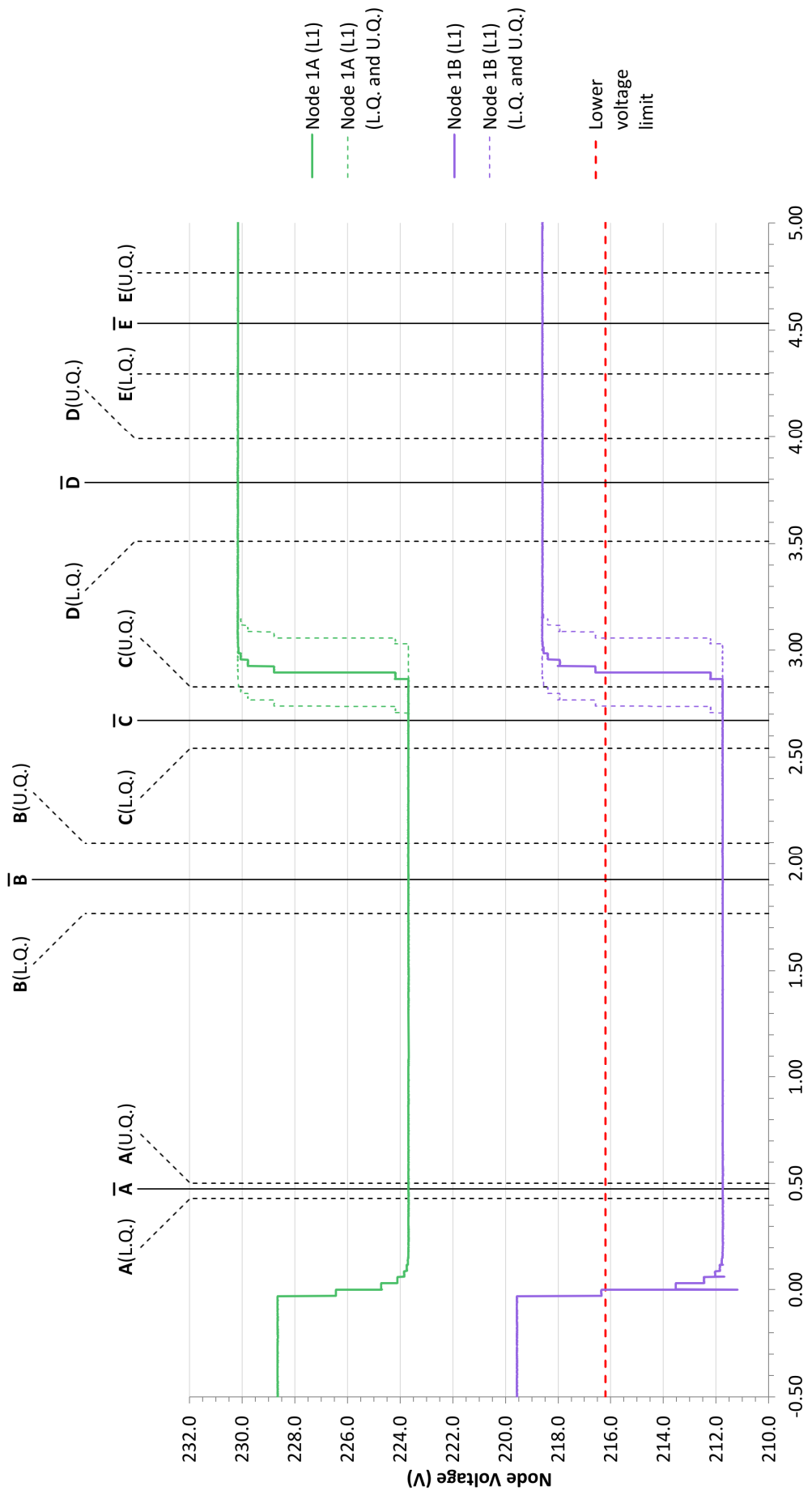

Figure 4.20: Scenario 1 voltage profiles and server events

4.6.2 - Scenario 2: High levels of distributed generation

Scenario 2 demonstrates the response of the voltage control system to high levels of distributed generation, from a high penetration of solar photovoltaic installations. Case A represents a load of 0.16 kW/customer, reflecting the minimum nominal customer demand [57], distributed uniformly across phases, and across the extent of the simulated network. Case B represents the addition of a 50 % penetration of 1.1 kW/customer generation, reflecting the PV penetration threshold at which voltage violations occurred in the study of [57], distributed uniformly across phases, and across the extent of the simulated network. The load and generation at each of the grouped load/source blocks for cases A and B are shown in Figure 4.21.

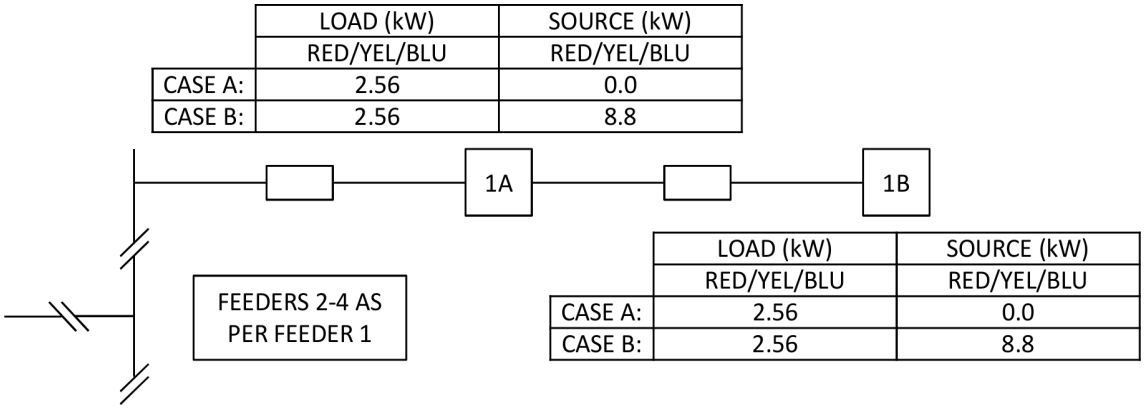

Figure 4.21: Scenario 2 load and generation powers

Two smart meter test beds were utilised in this scenario. They were both assigned connections to the red phase at the locations in the simulated network shown in Figure 4.22.

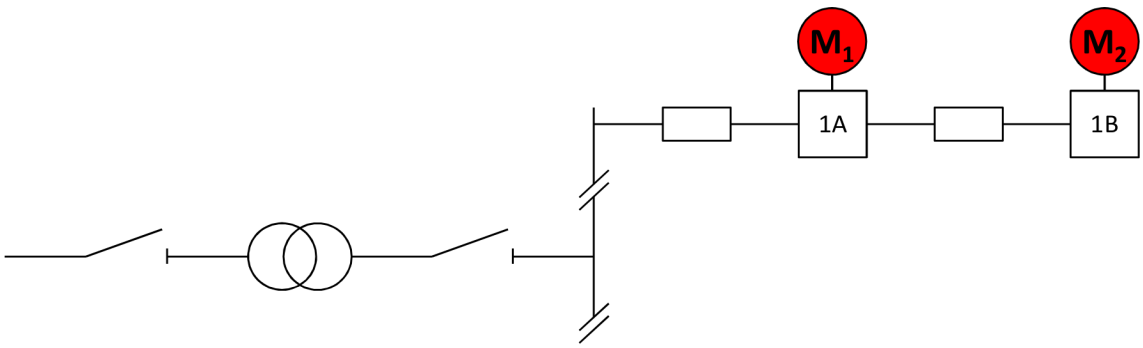

Figure 4.22: Scenario 2 meter locations

The voltages of all phases at each of the grouped load/source blocks in cases A and B are shown in Figure 4.23. Voltages which violate the prescribed limits are highlighted.

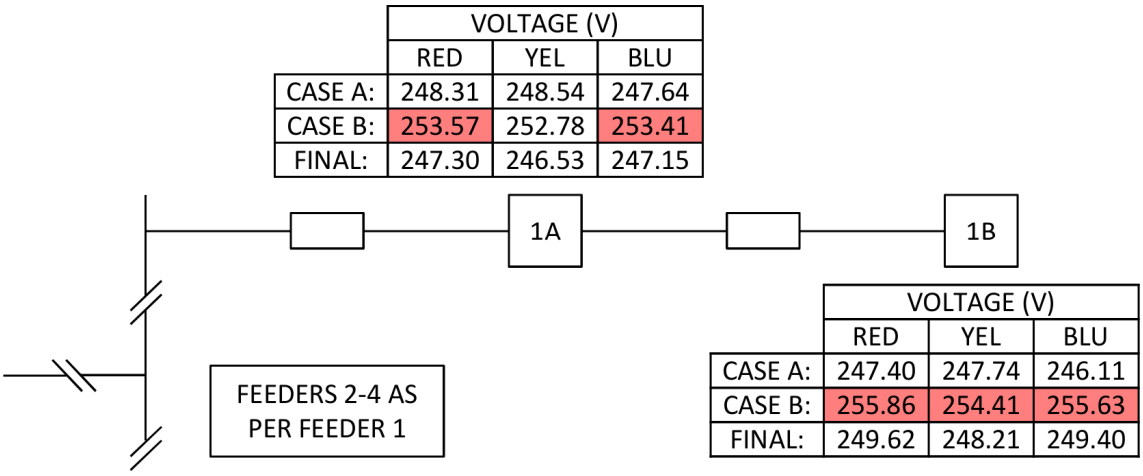

Figure 4.23: Scenario 2 network voltages

As a result of the additional generation added in case B, the red phase voltage at grouped load/source blocks 1A and 1B exceeded the upper voltage limit. Despite being balanced by design, a small imbalance exists between the phase voltages as a result of the disparity between their fundamental relative phases and the discrete time-step on which execution of the constituent elements of the source models used for power injection practically takes place within the RTDS. The predicted voltages at the metered points as a result of a decrease in tap changer position in response to the over-voltage condition, estimated by the AVC process, are shown in Table 4.3.

Table 4.3: Scenario 2 measured and predicted voltages

		Voltage (V)	
METER NUMBER:	METER LOCATION:	CASE B:	PREDICTED:
1	1A (RED PHASE)	253.57	247.07
2	1B (RED PHASE)	255.86	249.30

Since the predicted voltages indicated that the tap changer position could be decreased without causing further voltage limit violations, the AVC executed a decrease in tap changer position. The final resulting voltages are shown in Figure 4.23.

The profiles of the voltages at the metered points in scenario 2, with respect to time, are shown in Figure 4.24. The voltage limit violations at grouped load/source blocks 1A and 1B, following the transition from case A to case B, occur at 0.00 s. In addition, the mean, and lower and upper quartile times of server events A to E, as specified in Section 4.5.1, are shown.

The mean, and lower and upper quartile times to achieve restoration of the voltage at all metered points to within the prescribed voltage limits are shown in Table 4.4.

Table 4.4: Scenario 2 restoration times

	L.Q.	$\bar{x}$	U.Q.
Restoration time (s):	2.01	2.20	2.27

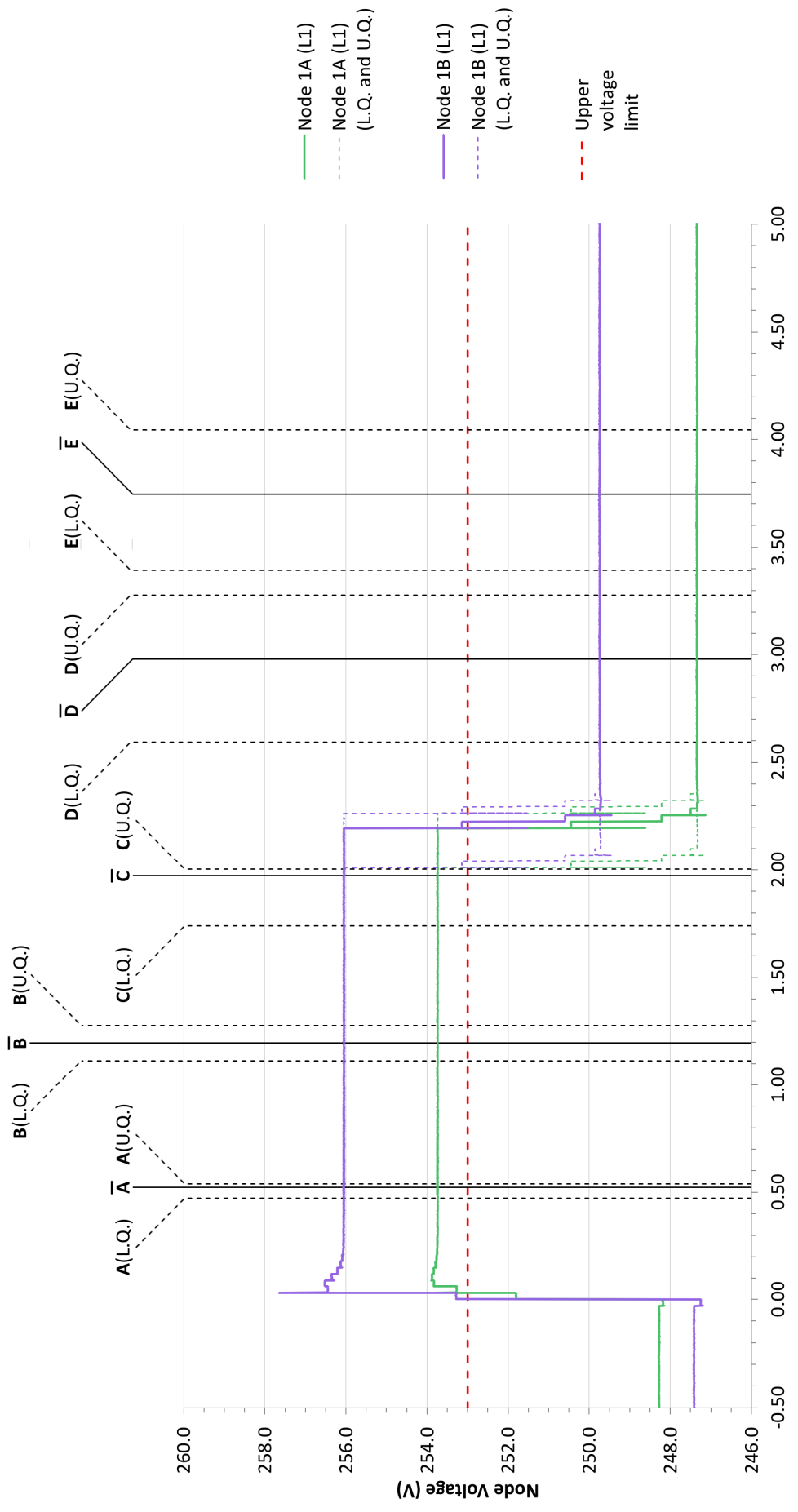

Figure 4.24: Scenario 2 voltage profiles and server events

4.6.3 - Scenario 3: Heavy, imbalanced loading

Scenario 3 demonstrates the response of the voltage control system to heavy loading from a high penetration of electric vehicle charging which is not distributed evenly across phases. This is based on Scenario 1. Case A represents a load of 1.3 kW/customer, distributed uniformly across phases, and across the extent of the simulated network. Case B represents the addition of a 5 % penetration of 3.5 kW/customer electric vehicle charging, distributed across the red, yellow and blue phases with a ratio of 2:2:1, within all load/source blocks. The loads at each of the grouped load/source blocks for cases A and B are shown in Figure 4.25.

	LOAD (kW)			SOURCE (kW)
	RED	YEL	BLU	RED/YEL/BLU
CASE A:	20.8	20.8	20.8	0.0
CASE B:	24.16	24.16	22.48	0.0

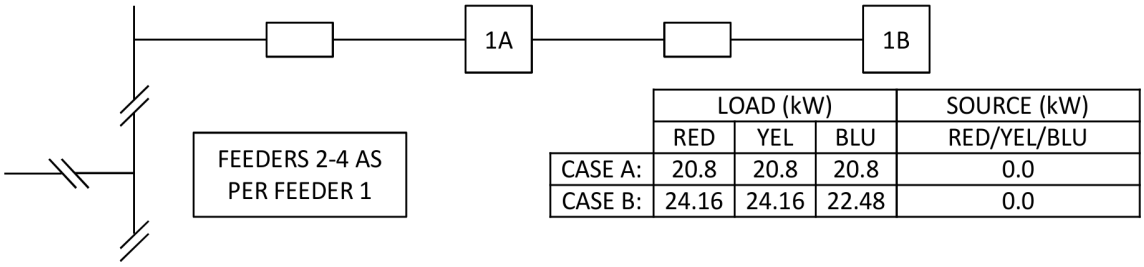

	LOAD (kW)			SOURCE (kW)
	RED	YEL	BLU	RED/YEL/BLU
CASE A:	20.8	20.8	20.8	0.0
CASE B:	24.16	24.16	22.48	0.0

Figure 4.25: Scenario 3 load and generation powers

Three smart meter test beds were utilised in this scenario. They were assigned connections to the red, yellow and blue phases, respectively, at the location in the simulated network shown in Figure 4.26.

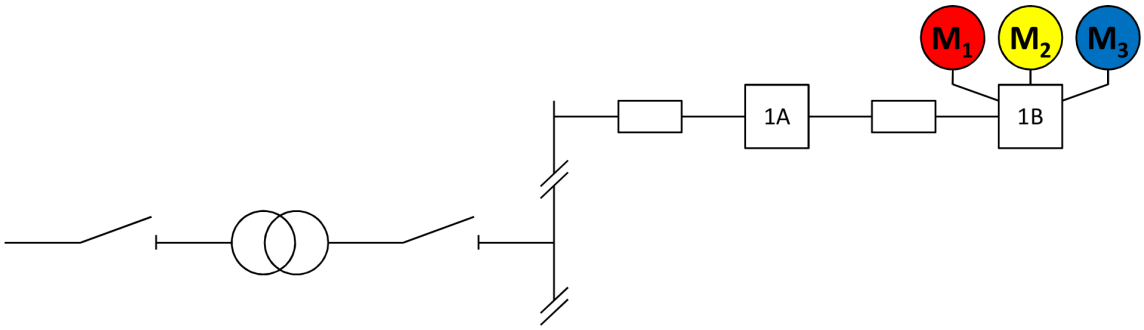

Figure 4.26: Scenario 3 meter locations

The voltages of all phases at each of the grouped load/source blocks in cases A and B are shown in Figure 4.27. Voltages which violate the prescribed limits are highlighted.

	VOLTAGE (V)		
	RED	YEL	BLU
CASE A:	228.62	228.62	228.62
CASE B:	225.41	225.22	227.98
FINAL:	231.85	231.68	234.34

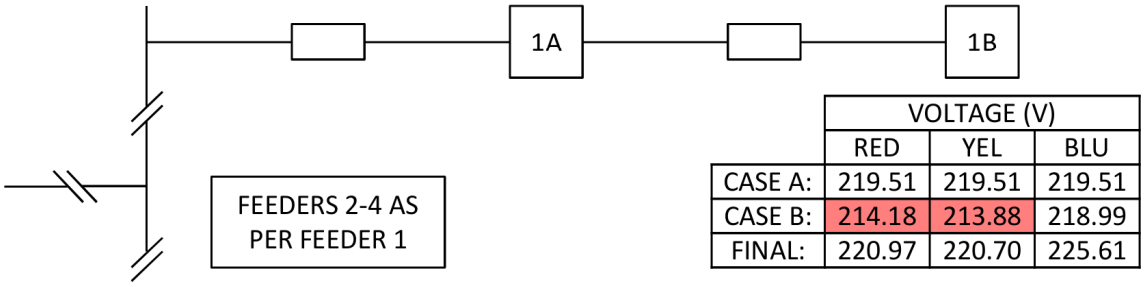

	VOLTAGE (V)		
	RED	YEL	BLU
CASE A:	219.51	219.51	219.51
CASE B:	214.18	213.88	218.99
FINAL:	220.97	220.70	225.61

Figure 4.27: Scenario 3 network voltages

As a result of the additional loading added in case B, the voltages of the red and yellow phases at grouped load/source block 1B fell below the lower voltage limit. The predicted voltages at the metered points as a result of an increase in tap changer position in response to the under-voltage condition, estimated by the AVC process, are shown in Table 4.5.

Table 4.5: Scenario 3 measured and predicted voltages

		Voltage (V)	
METER NUMBER:	METER LOCATION:	CASE B:	PREDICTED:
1	1B (RED PHASE)	214.18	219.82
2	1B (YEL PHASE)	213.88	219.51
3	1B (BLU PHASE)	218.99	224.75

Since the predicted voltages indicated that the tap changer position could be increased without causing further voltage limit violations, the AVC executed an increase in tap changer position. The final resulting voltages are shown in Figure 4.27.

The voltage imbalance caused by the additional imbalanced loading may be expressed as a percentage figure approximated by the phase voltage unbalance rate, presented in equation (2.7). The voltage imbalances at locations 1A and 1B as a result of the additional imbalanced loading are as follows:

Location 1A:
$$\%\,\mathrm{PVUR} = \frac{1.78}{226.20} \cdot 100 = 0.79\,\% \tag{4.14}$$

Location 1B:
$$\%\,\mathrm{PVUR} = \frac{3.31}{215.68} \cdot 100 = 1.53\,\% \tag{4.15}$$

The voltage imbalances at locations 1A and 1B following the tap change operation directed by the AVC are as follows:

Location 1A:
$$\%\,\mathrm{PVUR} = \frac{1.72}{232.62} \cdot 100 = 0.74\,\% \tag{4.16}$$

Location 1B:
$$\%\,\mathrm{PVUR} = \frac{3.18}{222.43} \cdot 100 = 1.43\,\% \tag{4.17}$$

The increase in tap changer position resulted in a reduction in the degree of voltage imbalance, in addition to restoring all voltages to within limits, and the final imbalance is within the limits of EN 50160 [59] and the short-term limit of Engineering Recommendation P29 [71]. However, the final imbalance still slightly exceeds the 1.3 % long-term limit of Engineering Recommendation P29.

The profiles of the voltages at the metered points in scenario 3, with respect to time are shown in Figure 4.28. The voltage limit violation at grouped load/source block 1B following the transition from case A to case B, occurs at 0.00 s. In addition, the mean, and lower and upper quartile times of server events A to E, as specified in Section 4.5.1, are shown.

The mean, and lower and upper quartile times to achieve restoration of the voltage at all metered points to within the prescribed voltage limits are shown in Table 4.6.

Table 4.6: Scenario 3 restoration times

	L.Q.	$\bar{x}$	U.Q.
Restoration time (s):	2.75	2.90	3.10

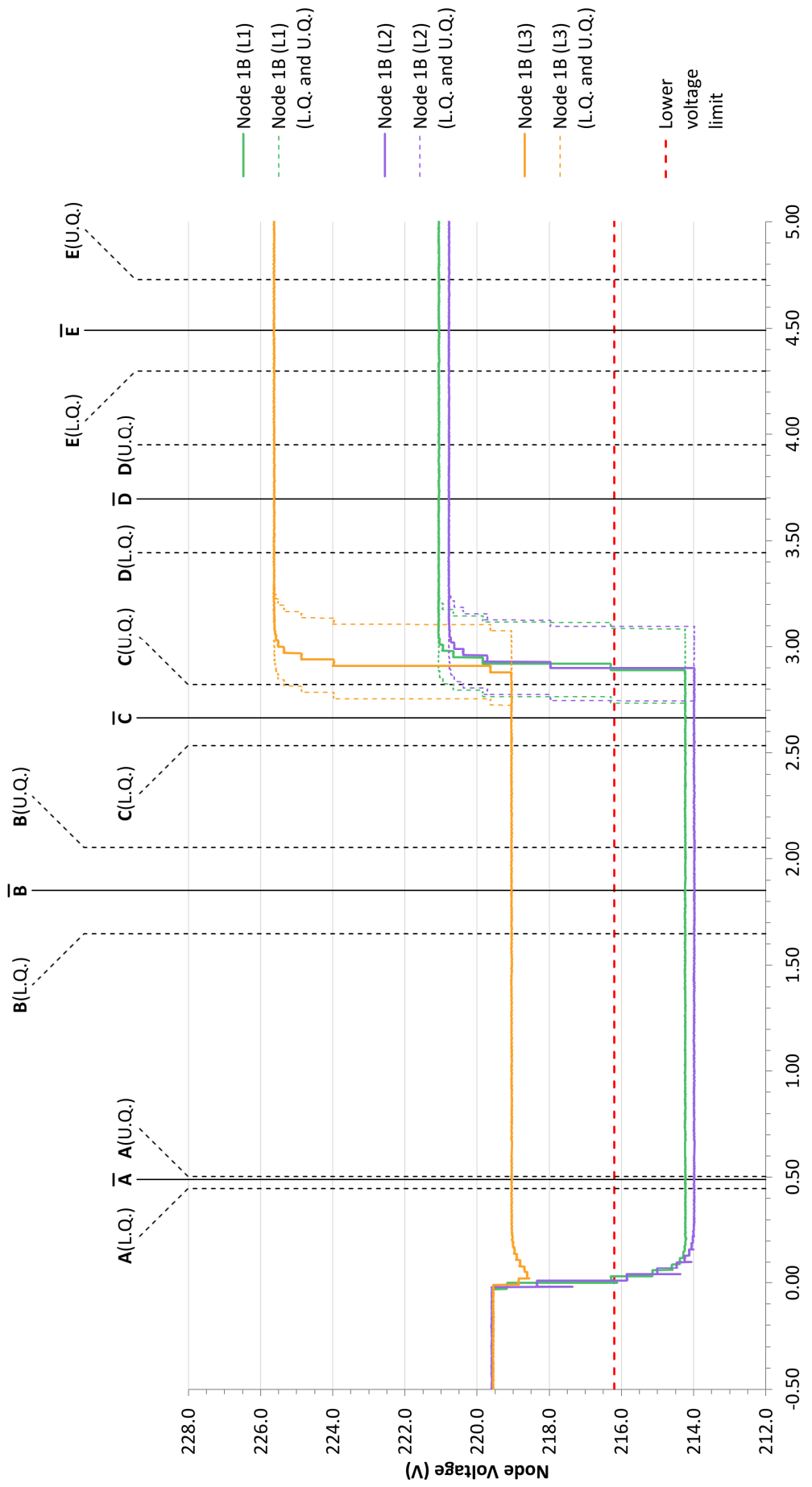

Figure 4.28: Scenario 3 voltage profiles and server events

4.6.4 - Scenario 4: Heavy loading and high levels of distributed generation

Scenario 4 demonstrates the response of the voltage control system to the conflicting requirements of a combination of heavy loading from a high penetration of electric vehicle charging, and high levels of distributed generation from a high penetration of solar photovoltaic installations, on adjacent feeders. This is based on scenarios 1 and 2. Case A represents a load of 1.3 kW/customer, distributed uniformly across phases within all load/source blocks on feeders 1 and 2, a load of 0.16 kW/customer distributed uniformly across phases within all load/source blocks on feeders 3 and 4, and a 75 % penetration of 1.1 kW/customer generation distributed uniformly across phases within all load/source blocks on feeders 3 and 4. Case B represents the addition of a 15 % penetration of 3.5 kW/customer electric vehicle charging, distributed uniformly across phases within all load/source blocks on feeders 3 and 4. The loads at each of the grouped load/source blocks for cases A and B are shown in Figure 4.29.

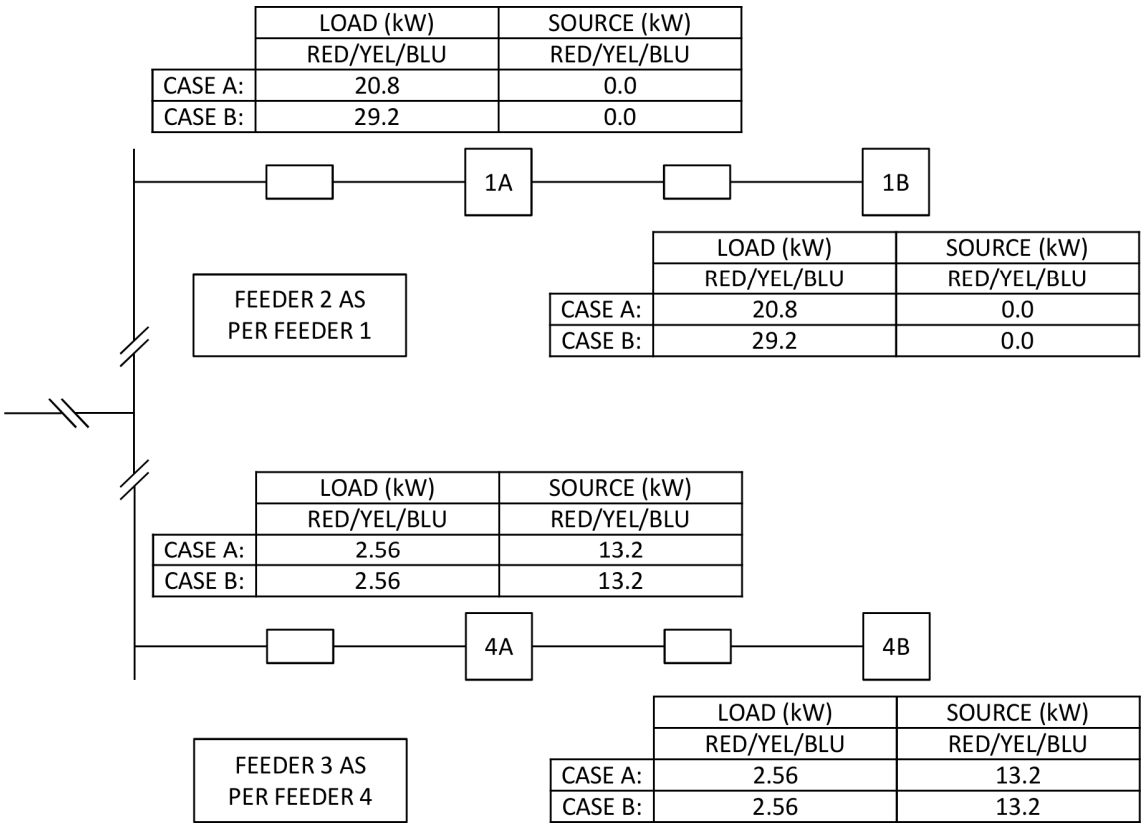

Figure 4.29: Scenario 4 load and generation powers

Four smart meters were utilised in this scenario. They were assigned connections to the red phase at the locations in the simulated network shown in Figure 4.30.

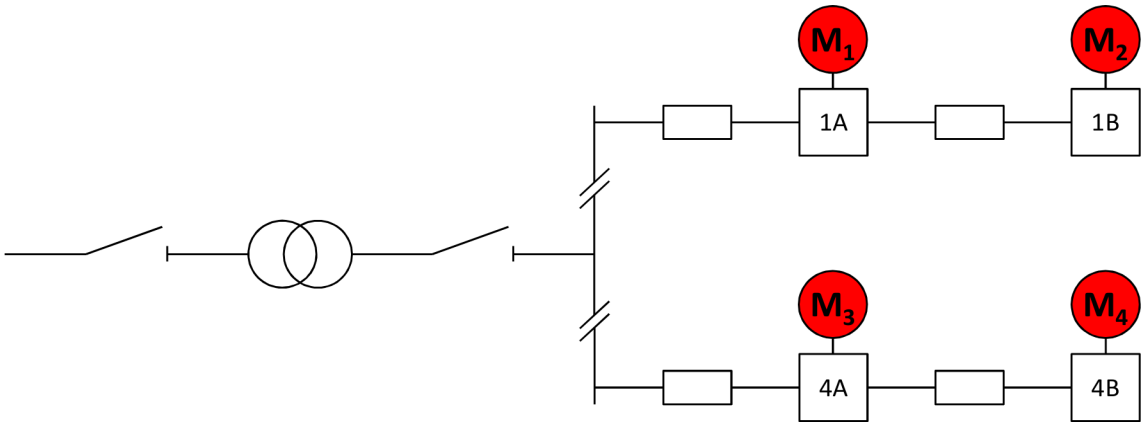

Figure 4.30: Scenario 4 meter locations

The voltages of all phases at each of the grouped load/source blocks in cases A and B are shown in Figure 4.31. Voltages which violate the prescribed limits are highlighted.

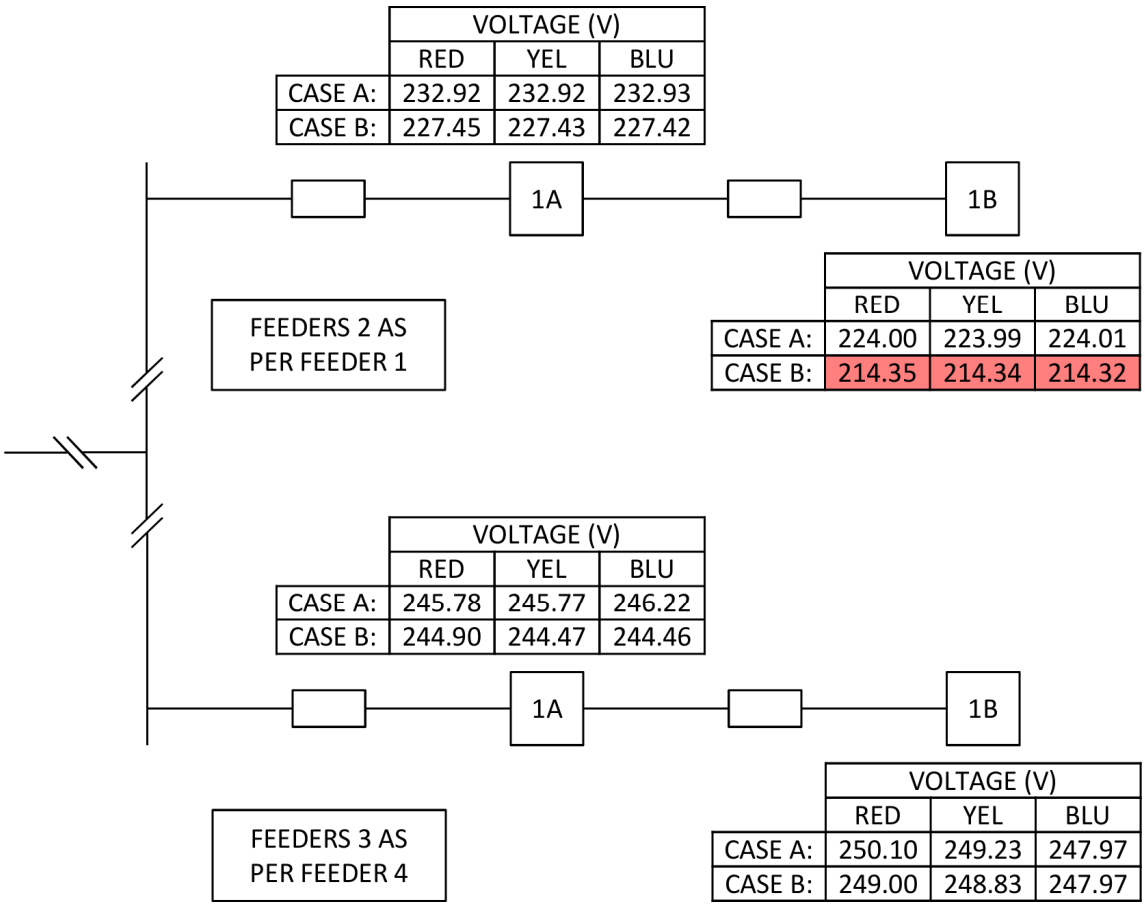

Figure 4.31: Scenario 4 network voltages

As a result of the additional loading added to feeders 1 and 2 in case B, the voltages at grouped load/source block 1B fell below the lower voltage limit. Despite being balanced by design, a small imbalance exists between the phase voltages as a result of

the disparity between their fundamental relative phases and the discrete time-step on which execution of the constituent elements of the source models used for power injection practically takes place within the RTDS. The predicted voltages at the metered points as a result of an increase in tap changer position in response to the under-voltage condition, estimated by the AVC process, are shown in Table 4.7.

Table 4.7: Scenario 4 measured and predicted voltages

		Voltage (V)	
METER NUMBER:	METER LOCATION:	CASE B:	PREDICTED:
1	1A (RED PHASE)	227.45	233.44
2	1B (RED PHASE)	214.35	219.99
3	4A (RED PHASE)	244.90	251.34
4	4B (RED PHASE)	249.00	255.55

Since the predicted voltages indicated that an increase in the tap changer position would result in further voltage limit violations, the AVC did not execute any change to tap changer position.

The profiles of the voltages at the metered points in scenario 1, with respect to time, are shown in Figure 4.32. The voltage limit violation at grouped load/source block 1B, following the transition from case A to case B, occurs at 0.00 s. In addition, the mean, and lower and upper quartile times of server events A to C, as specified in Section 4.5.1, are shown.

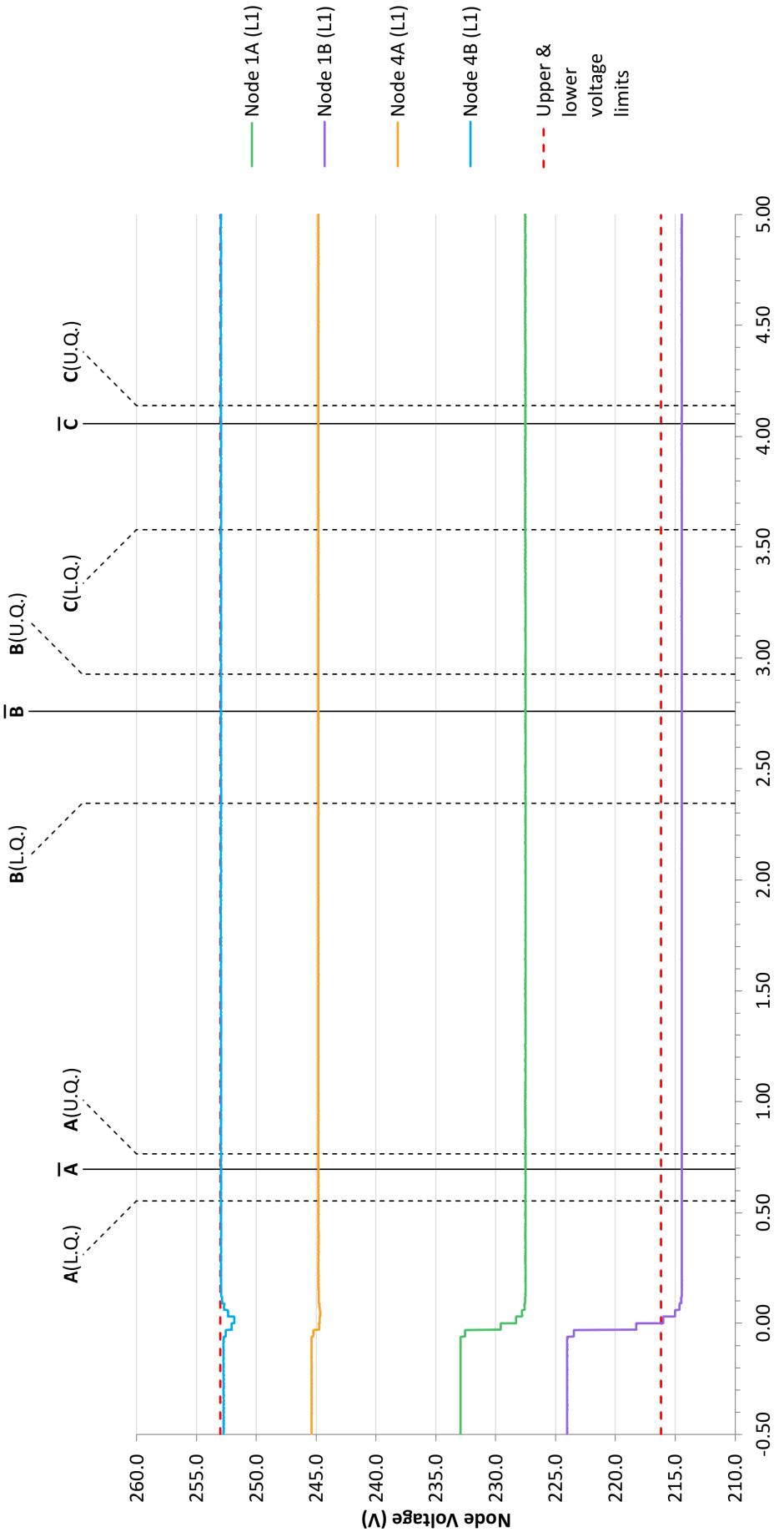

Figure 4.32: Scenario 4 voltage profiles and server events

4.7 - Discussion

Previous work incorporating real-world smart meter measurements has been subject to the limitations of data available from existing smart meters. For example, the European FP7 project IDE4L [58] demonstrated the effectiveness of distributed LV network monitoring by smart meters as a means of detecting the voltage rise at the customer connection point resulting from real power injection by a local PV installation. However, the measurements from these meters were only available with an update rate of one minute, and the data acquired was not used to inform network control. This work extends such schemes by implementing closed-loop control based on the smart meter measurements acquired. By development of a custom smart meter test bed platform, it has been possible to immediately acquire measurement data from the smart meters used, and to implement the custom voltage alarm function whereby the meters report voltage limit violations by exception in order that immediate control decisions are made. Similarly, in the LoVIA field trial [119], the one-minute average measurements received by the control algorithm were a constraint of the hardware used, with the further limitation that it was not possible to take these measurement directly at the customers point of common coupling (PCC). This work has addressed these limitations by demonstrating that real-time monitoring by smart meters at critical points in a distribution network, and connected via end-to-end communication links with a substation controller, may be effectively used to inform control of an OLTC in order to rapidly address voltage limit violations. This work further addresses the limitations of hardware-in-the-loop investigations such as [117], by demonstrating that a control system may be applied to a LV network incorporating an OLTC within an RTDS simulation, enhanced by the additional insight of the effect of real-world non-deterministic communications channels.

The maximum and minimum base demand figures used in the distribution network simulation used in this study are based on Electricity Association (EA) figures for after-diversity maximum demand (ADMD) and minimum demand of UK residential customers (0.16 kVA and 1.3 kVA respectively) [57]. These are the current figures used to estimate domestic demand for the purpose of planning. The nominal electrical vehicle charging load of 3.5 kVA per customer is based on the typical maximum single-phase domestic charging point rating of 16 A [82], with a 10 % penetration reflective of plug-in electric vehicles as a current proportion of UK car registrations [11]. The 50 % penetration of 1.1 kVA PV generation sources reflects the 40–50 % PV penetration thresholds at which voltage violations occurred in the study of [57], the generic LV network presented in which forms the basis for the simplified network simulated in this work. This is supported by the findings of [58], in which the high PV penetration

area exhibited PV generation of up to approximately 40 % of peak demand, without exhibiting voltage issues caused by power injection.

The aggregated load and source blocks employed within the simulated distribution network in this study are both a useful simplification of the system being examined, and a necessary compromise to accommodate the finite computational capacity of the RTDS unit. Though it is possible that such aggregated block might conceal localised behaviour in a real network, for example local reverse power flow and consequent voltage limit violations, which would otherwise go undetected, they are sufficient to represent the feeders examined in this study, with smart meter measurements taken at the nodes of these blocks, and passive cable sections between. The study might be extended to examine the application of the control system developed to a real-world distribution network, or section thereof. In this case, it would likely be necessary either to increase to which an aggregated representation is used in some areas of the network in order to add detail to other areas, or to augment the computational capacity of the RTDS unit.

The experimental results presented in this chapter were acquired in a time window of approximately 3.5 hours. Network latency, typically evaluated by round-trip time (RTT) impacts both throughput and response time in TCP/IP communications. Factors which strongly contribute to temporal variability in GPRS RTT include mobility (handover from one network cell to another), voice call pre-emption (priority allocation of data time-slots to voice traffic), self-congestion (delay caused by a GPRS terminal device sustaining multiple concurrent TCP connections), network congestion (high levels of traffic from other GPRS terminal devices) and radio conditions (for example RF interference, necessitating data retransmission) [224]. Of these, the factors of mobility, voice call pre-emption and self-congestion are not applicable to smart meters, and the factor of radio conditions is assumed to have no strong correlation with time-of-day or day-of-week in the UHF band, for a given location. Network traffic and congestion is strongly linked to time-of-day, though weekend variations in network load do not significantly affect latency [225]. However, only a weak correlation exists between RTT distribution and network traffic load, as illustrated by the empirical Complementary Cumulative Distribution Function (CCDF) of RTT for GPRS in four 6 h period, shown in Figure 4.33 [226]. As such, experimental results taken within a time window of less than 24-hours are presented as representative of continuous operation at the test site.

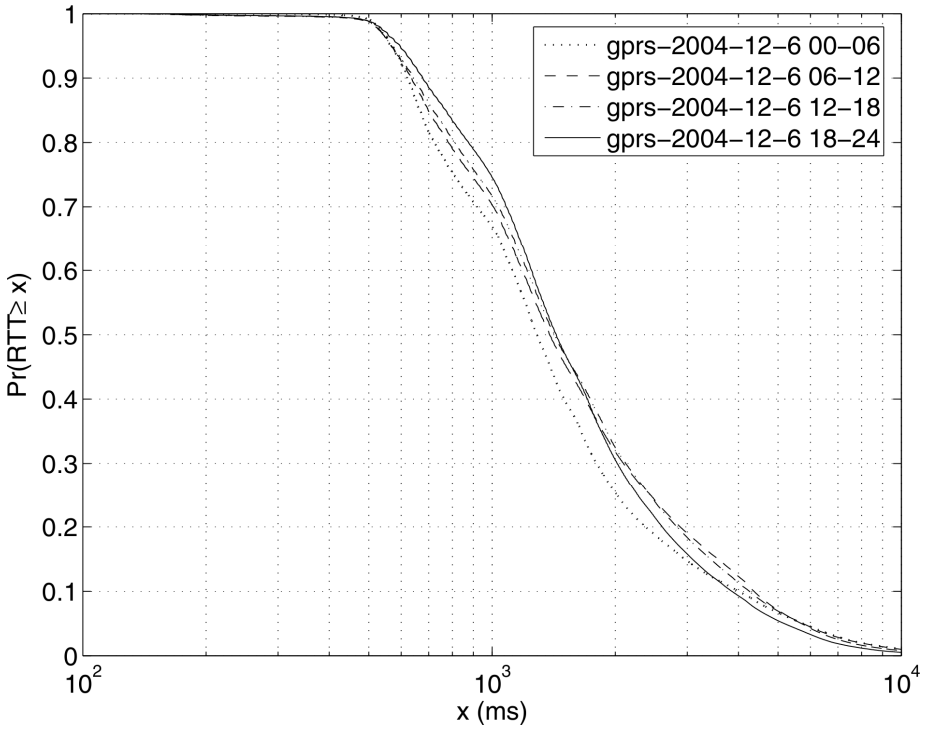

Figure 4.33: Empirical CCDF of RTT for GPRS in four different 6h periods [226]

The control system implemented in this work does not incorporate a mechanism for limiting the frequency of tap-change operations, nor for considering multiple prospective tap-change operations in making control decisions. Whilst the issue of a high frequency of tap-change operations is largely negated by the assumption that a deployed implementation of a system such as this would incorporate OLTCs with electronic commutation [95]–[100], the work presented might be extended by the inclusion of a means to limit tap-change frequency. Furthermore, the control algorithm might be augmented as described in [118], in order to anticipate the requirement for multiple tap change operations. Rather than assessing the effect of each tap-change operation in isolation, this would allow the algorithm to predict the effect of multiple successive tap changes and either perform these as a block operation, avoiding the communications and processing delay associated with multiple independent operations, or to elect not to perform any operation if the algorithm deemed that such an action would create a voltage limit violation issue elsewhere in the network.

The issue of voltage limit violation as a result of heavy, imbalanced loading was shown to be resolved by the action of the control system in this work. However, whilst the degree of voltage imbalance was reduced as an additional effect of this action, the use of a conventional coupled OLTC, in which tap changes are applied to all phases simultaneously, limits the scope for resolution of phase imbalance by means of the OLTC alone. The control algorithm implemented might be extended to permit control

of a decoupled OLTC, as presented in [101] and [102], capable of changing the tap position of each phase independently.

Whilst, in this study, it was shown that three of the four voltage violation issue scenarios demonstrated were adequately resolved by means of OLTC control alone, the control algorithm implemented might be extended to resolve local voltage violations which the controller was not able to resolve without causing further issues, for example in scenario 4. In [139], the use of local battery energy storage, in conjunction with a smart meter and OLTC, was demonstrated to be effective as a means of local voltage regulation in a simulated network. The study of [139] did not consider multiple concurrent voltage violation issues in a network, nor distributed voltage measurements by multiple smart meters, as have been examined in this work. However, the system presented in this chapter might be extended by the inclusion of energy storage as a further means of voltage control in this way, with the algorithm adapted to optimise the multiple objectives of voltage regulation, loss minimisation and longevity of the energy storage medium. This would increase the scope for the system presented to address local voltage issues in the context of the complete distribution network. Similarly, though the low X/R ratio of LV network may limit the scope for voltage regulation by means of reactive power control [123], simple local reactive control schemes have been shown to be of value in mitigating the voltage rise effect of LV-connected PV inverters [124], [125]. The system presented in this chapter might be further extended to address local voltage issues in the presence of high penetrations of PV generation by augmenting such local control schemes with an element of centralised control, in order to optimise the voltage conditions across the network collectively, whilst considering the real-world limitations of communications between distributed devices.

4.8 - Conclusion

Implementation of real-time voltage control within an LV network using the smart meter test rig has been demonstrated. By means of a voltage alarm firmware component, added to the smart meter firmware system, and a voltage control process, added to the server software, voltages at metered points in the simulated distribution network which violate preset limits are detected, and an evaluation process initiated to determine if remedial action should be taken. In the case that it is determined that remedial action should be taken, by means of a change OLTC position, this is automatically executed. The average period between the voltage at a metered point violating preset limits, and the voltages at all metered points being restored to within prescribed values, in the cases that action was deemed appropriate, was 2.66 s. In the

case that the voltage controller implemented determined that a change in tap changer position could not be performed, or would result in further voltage limit violations, it was demonstrated that no remedial action was attempted.

5 - Smart meter and AMI security

5.1 - Introduction

Analysis of the cyber security vulnerabilities of a commercially deployed smart electricity meter, and of the connection of that meter to the head-end infrastructure of the meter operator, is described. Two attack methodologies are presented, informed by this analysis, and demonstrated to permit unauthorised electronic access to the meter. Finally, recommendations are made of measures to mitigate the vulnerabilities identified and exploited.

The meter and infrastructure examined are the property of a smart meter installer and operator in the UK. This research was conducted on behalf of the meter operating company, and is presented herein on the condition of anonymity. Therefore, details which might identify the operating company or meter have been redacted, where necessary. The meter evaluated is the default choice for single-phase, domestic installations by the operating company, and typical of single-phase, domestic meters being deployed within the UK, at the time of writing. It is compliant with the first version of the UK *Smart Metering Equipment Technical Specifications* (SMETS 1) [219], published by the former Department of Energy & Climate Change.

Subsequent sections are structured as follows:

- Section 5.2 examines the technical information regarding the meter under examination available in the public domain, and the hardware elements of the device which represent vulnerabilities and hence the basis of potential attack vectors. It also describes preliminary testing of the local, optical interface of the meter, and the selection of attack methodologies.
- Section 5.3 describes the toolkit developed to permit the exfiltration of data in transit between the metrological and computational core of the meter and the attached wide area network modem, and to communicate with the local, optical interface of the meter.
- Section 5.4 Describes the processing and analysis of data captured using this tool kit, in order to expose vulnerabilities, and to extract security credentials and configuration information contained within it. It also describes the exploitation of a

vulnerability whereby extracted security credentials were used to demonstrate unauthorised access to the meter by means of the local, optical port.

- Section 5.5 provides an analysis of the implications of the vulnerabilities exposed and attacks demonstrated.
- Section 5.6 provides recommendations of revisions to the hardware and firmware of the meter, and to the protocols used for communication with the head-end of the meter operator, which may mitigate the vulnerabilities identified. These recommendations are made with reference to existing and established security protocols.
- Section 5.7 summarises the research undertaken.

5.2 - Vulnerability analysis

5.2.1 - Prior information

An Internet search for freely available literature was undertaken using the Google search engine, in order to determine what technical documentation regarding the meter under examination was in the public domain. Documents produced by the manufacturer, but distributed by third parties, were found describing:

- Hardware: This included mechanical dimensions and mounting details of the meter, images showing the form and location of a tamper detection micro-switch designed to detect removal of the terminal cover, a description of the RS-232 and power interface to connect a GSM/GPRS WAN modem, and specification of the optical port as being FLAG (IEC 62056-21) and ANSI Type 2 (ANSI C12.18) compliant. It also included a description of the hardware user interface buttons and display.
- Firmware: This included a list of the registers within the meter used for measurement, configuration and control, access to the bootloader, and direct access to the non-volatile memory of the meter. It also included the protocol and command structure for register read and write access via the modem interface and the optical port.
- Software: This included usage information for the proprietary management software, produced by the meter manufacturer for use by meter operators.

5.2.2 - Analysis of hardware

The physical architecture of the meter under test can be considered in two, distinct sections, as illustrated in Figure 5.1. The first of these sections is a sealed enclosure containing the metrological and computational core of the device. This enclosure is not designed to be accessed during the normal course of installation, configuration or use. The external interfaces for human interaction provided by the sealed section of the meter are two momentary push button switches, two visible indicator LEDs, and an LCD display. These interfaces, as described in the manufacturer's documentation, permit the local observation of:

- Metrology readings, such as accumulated energy, and instantaneous power.
- The current status of the attached WAN modem, if present, the optical interface, the internal clock of the meter, and alarms warning of errors such as failure of the internal battery.
- The serial number and Meter Point Administration Number (MPAN)

The sealed section of the meter also includes an optical communication port which the manufacturer specifies as compliant to the FLAG (IEC 62056-21) [227] and ANSI Type 2 (ANSI C12.18) [228] protocols. This port, as described in the meter manufacturer's documentation, permits a command line session to be established with the meter.

The second, serviceable section of the meter is intended to be accessed for the purposes of installation and maintenance. Brass receptacles for the termination of meter tails and an ANSI/TIA-1096-A 8P8C modular jack, for the connection of a WAN modem, emerge from the sealed section of the meter into this serviceable section. The WAN modem installed is manufactured by a third party. Documentation free available on the Internet from the manufacturer of this device specifies that the communications interface provided on the 8P8C jack is RS-232 compliant. The WAN modem also derives power from the meter through this connector, and hence is active only when the meter is energised. The serviceable enclosure of the meter is contained by a moulded plastic cover which is designed to be readily removable in the course of installation and maintenance operations. It is secured with a single screw, protected by a tamper evident tag, and carries a moulded protrusion which, when the cover is installed, activates a micro-switch. Removal of the cover results in the release of the micro-switch and, as such, is used as a means of detecting unauthorised physical access. The response of the meter in the case of this tamper detection device being triggered is specified in the manufacturer's documentation as being to log the event, but not to

take further action, for example supply disconnection, by default. The design of the cover of the serviceable enclosure is also such that the tamper detection mechanism may be readily, mechanically defeated, for example by use of a shim to maintain pressure on the micro-switch when the cover is removed. The tamper evident seal may also be replaced with readily available crimping tools and seal components, leaving little physical evidence for forensic examination.

By exploitation of the mechanical vulnerabilities described above, an attacker may access the link between the metrological and computational core of the meter and the WAN modem. In addition, an attacker has unrestricted access to the optical port. These attack vectors, along with an outline of the physical architecture of the meter, are illustrated in Figure 5.1.

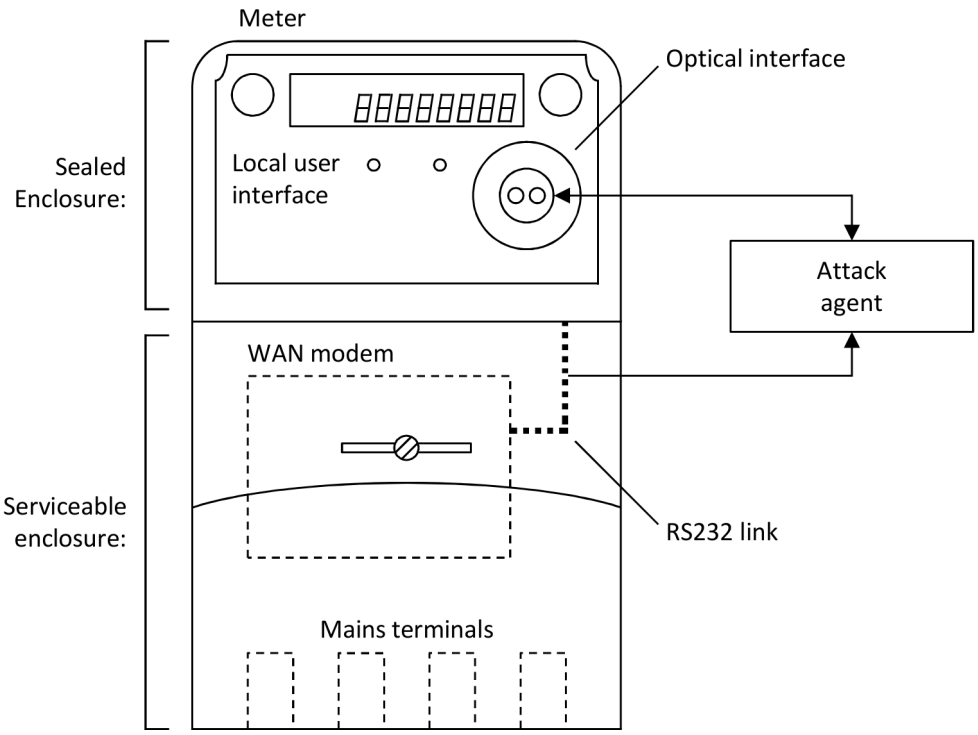

Figure 5.1: Meter and attack vectors

5.2.3 - Testing of optical interface

In order to establish whether the optical port of the meter is enabled and, this being the case, establish the parameters of the communications protocol, communication was attempted with the optical port at each of the range of different data rates stated as supported by the manufacturer. At each data rate, a null message with the framing characters <STX> and <ETX> (<0x02> and <0x03>) but without any frame content, as defined by the manufacturer's documentation, was transmitted to the optical port. At

the configured data rate, this should generate an acknowledgment of the form `<STX><ACK><ETX>` (`<0x02><0x06><0x03>`).

The hardware used for this test was an x86-64 laptop computer running the 64-bit edition of Debian GNU/Linux and a USB terminated optical read head. This contains a USB to UART bridge and an infrared receiver/transmitter pair for bidirectional communication with the optical interface of a meter.

Upon connection to the laptop computer, the USB to UART bridge within the read head is recognised as a serial device, and serial device reference to it is created in the `/dev` directory of the operating system. The device file was configured using the `stty` command. The command string used is shown below.

```
stty 300 cs8 -cstopb -parenb -F /dev/ttyUSB0
```

In this command, `300` specifies a rate of 300 b/s, `cs8` specifies 8 data bits, `-cstopb` specifies 1 stop bit, `-parenb` specifies no parity check and the `-F` argument specifies the serial device to be configured. Using this initial configuration, data was redirected from the input data file, containing the raw hexadecimal message string, to the USB interface of the optical head using the `echo` utility. The Linux `cat` utility was used to monitor for a response from the serial device.

It was found that at a data rate of 9600 b/s, an acknowledgment of the expected form was received.

5.2.4 - Choice of attack methodologies

Informed by the vulnerability analysis, the following attack strategies were chosen for analysis:

- Eavesdropping of bi-directional data from the RS-232 link between the meter and the WAN modem, in order to extract security credentials and information which might be used to impersonate either the meter or the head-end of the meter operating company.
- Establishment of a command line session with the optical port of the meter, using extracted security credentials, in a manner which permits unauthorised access to the internal system of the meter.

5.3 - Attack toolkit

5.3.1 - Architecture

The attack toolkit consists of hardware and software components which permit the exfiltration of data transferred between the meter and the WAN modem, and communication with the optical port of the meter. The logical architecture of the attack toolkit is illustrated in Figure 5.2.

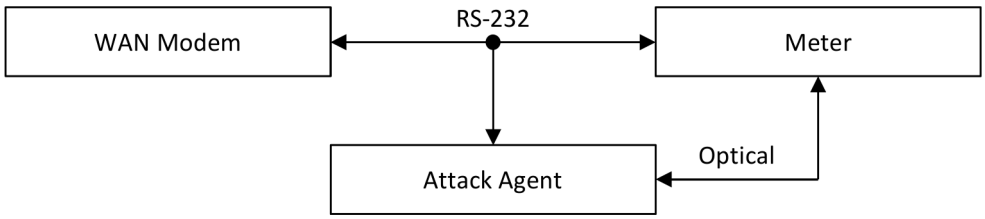

Figure 5.2: Attack toolkit architecture

5.3.2 - Hardware

For the purpose of eavesdropping on data exchanged between the meter and WAN modem, a dual RS-232/USB bridge was used. This supports two bidirectional RS-232 interfaces and, hence, the input channel of each of the interfaces was used to capture data on both the transmit and receive lines of the RS-232 connection under examination. A USB terminated optical interface head was used for communication with the optical port of the meter. The serial devices of both the RS-232/USB bridge and the optical read head were configured with a baud rate of 9600, 8 data bits, no parity check and one stop bit. The attack toolkit hardware is illustrated in Figure 5.3.

The tamper evident seal of the serviceable enclosure cover was cut in order to permit access, and the tamper detection micro-switch allowed to trigger upon removal of the cover. The link cable between the WAN modem and the meter was removed and replaced by the attack toolkit hardware.

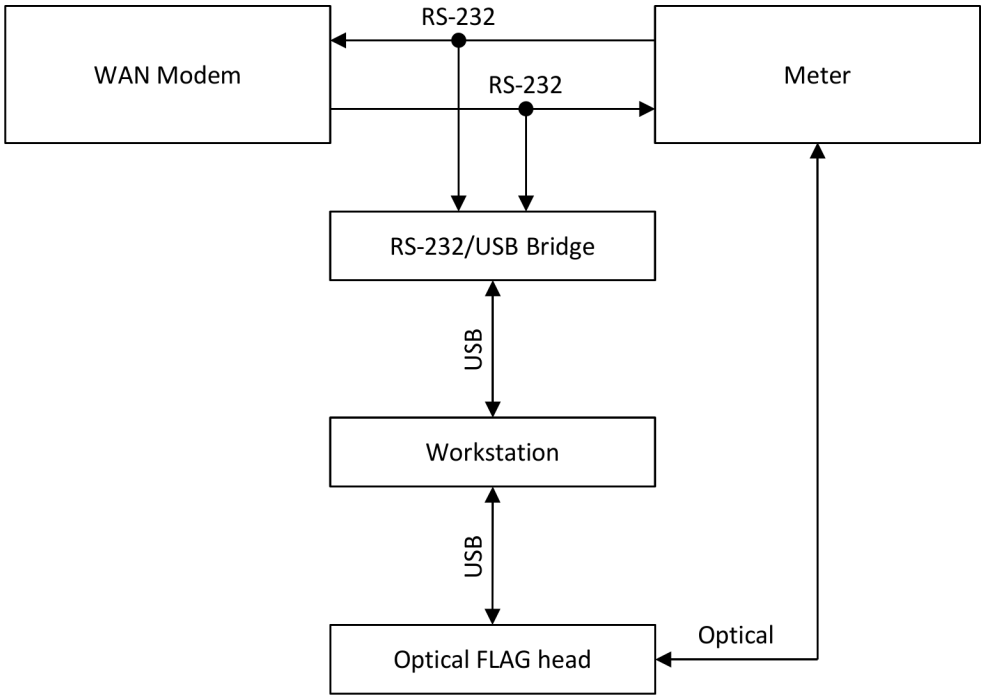

Figure 5.3: Attack toolkit hardware

5.3.3 - Base operating system and software

The workstation used was an x86-64 laptop computer running the 64-bit edition of Debian GNU/Linux. The Linux kernel of this distribution natively supported the integrated USB/serial bridge devices used in the dual RS-232/USB bridge, and the optical FLAG head. In this way, each of the RS-232 data channels and the optical interface appeared as serial devices in `/dev` of the workstation's filesystem.

5.4 - Attack procedure

5.4.1 - Attack 1

The meter and modem were energised from a fully de-energised state, and allowed to run for a period of ten minutes. During this time, the data exchanged between the meter and modem was captured by establishing pipes within the Linux operating system of the workstation to redirect data from the each of the two serial devices, capturing data flowing from the modem to the meter, and vice versa, to files. During the energised period, a connection was established between the meter and the head-end server of the meter operating company, herein referred to as the 'operator', indicated by the front panel interface of the meter.

The Linux `hexdump` utility was used to view the binary, captured data in order that it could be analysed. The utility represents each byte in the input as a two-digit, hexadecimal number.

Immediately after energisation, commands from the Hayes AT Command Set, in a human-readable format, were used by the meter to initialise the modem, as per the meter manufacturer's documentation. Two commands used by the meter to configure the modem with parameters specific to this application were as follows:

```
AT+CGDCONT=1,"IP","## -- REDACTED -- ##"
ATD*99***1#
```

The first, `AT+CGDCONT`, is used to define a packet datagram protocol (PDP) context. This is a data structure which is used to specify configuration information about a GPRS session before it is initiated. In this case, the command defined the PDP variant to be used as IPv4, and the access point to connect to as the URL of the meter operator. The second, ATD, is used to initiate a GRPS session, in this case of type IP, and using PDP context 1, defined previously. Following the successful establishment of a GPRS session, data exchanged between the meter and operator passes transparently through the modem until the escape sequence `+++` is transmitted by the meter, causing the modem to return to accepting Hayes AT commands from the meter.

From the manufacturer's documentation, it was known that the point-to-point protocol (PPP), a variant of high-level data link control (HDLC), was being used to encapsulate the data being exchanged between the meter and the operator. The Linux `hexdump` utility was used to view this binary data in order that it could be analysed. The utility represents each byte in the input as a two-digit, hexadecimal number. An example of the raw data, in this case the first PPP frame captured following transmission by the meter operator, and demarcated by `0x7e` bytes, is shown in Figure 5.4.

```
7e ff 7d 23 c0 21 7d 21 7d 21 7d 20 7d 36 7d 21 7d 24 7d 25 dc 7d 22
7d 26 7d 20 7d 20 7d 20 7d 20 7d 27 7d 22 7d 28 7d 22 7d 23 7d 24 c0
23 26 b4 7e
```

Figure 5.4: Raw PPP frame in hexadecimal

A script was written in Python to remove the escape sequences employed by PPP. These appear as the byte `0x7d`, followed by the result of a bitwise XOR operation on the original byte and `0x20`. The original byte is recovered by repeating the XOR operation on the escaped byte and `0x20`. The raw frame presented in Figure 5.4 is shown with the escape sequences removed in Figure 5.5.

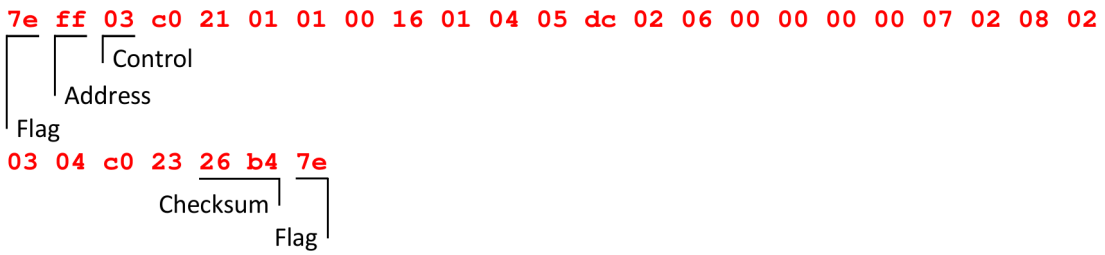

Figure 5.5: PPP frame with escape sequences removed

Since PPP is a variant of HDLC for communications between exactly two peers, and does not use frame numbering, the address and control fields are redundant and may be disregarded. For the purposes of further analysis, these fields, and the flag bytes indicating the start and end of a frame, are omitted.

The first exchange of data between the operator and meter following the establishment of a GPRS connection was a negotiation of the parameters for further PPP communication. This was performed by means of the link control protocol (LCP), contained within PPP packets, as shown in Figure 5.6. The operator first transmitted a configuration request to the meter specifying a maximum frame size of 1500 bytes, the use of no escape characters, the use of protocol and address/control field compression, and the use of the password authentication protocol (PAP). The response of the meter was a rejection of this configuration, specifying the maximum frame size option as the reason for rejection. The operator then repeated the original request with the maximum frame size option omitted. This was accepted by the meter with an Acknowledge response. The meter subsequently transmitted a configuration request to the operator specifying the use of protocol and address/control field compression, and the escaping of <XON> and <XOFF> characters for the purpose of software flow control. This was accepted by the operator with an Acknowledge response.

Following configuration of the PPP connection, the password authentication protocol was used to authenticate the meter to the operator. This is shown in Figure 5.7. The protocol requires the username and password credentials to be transmitted in plain text. In this instance, the name of the meter operator was used as both the username and password. The authentication was successful, with the operator returning an Acknowledge response and the message ‘Welcome!’.

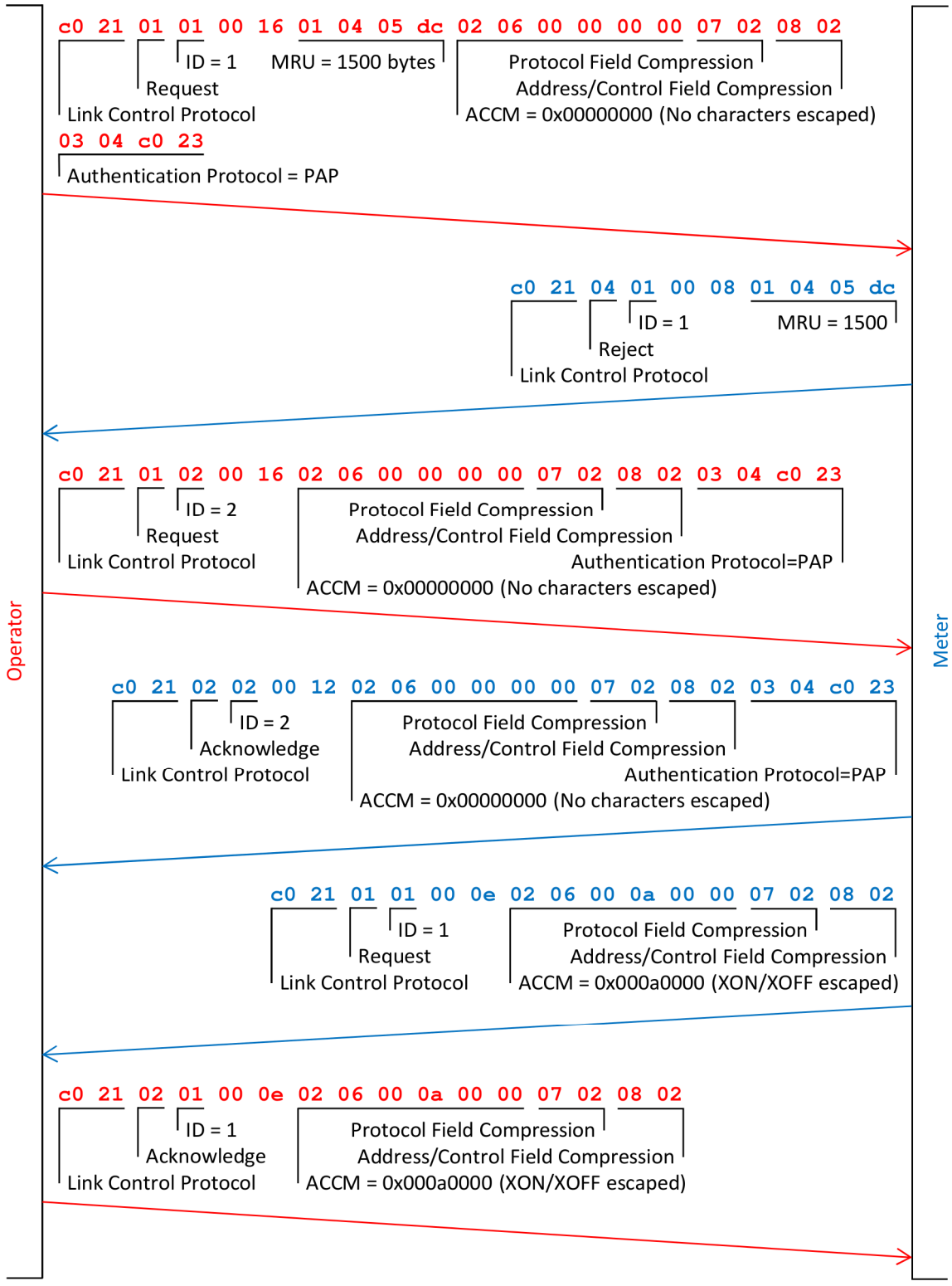

Figure 5.6: LCP negotiation

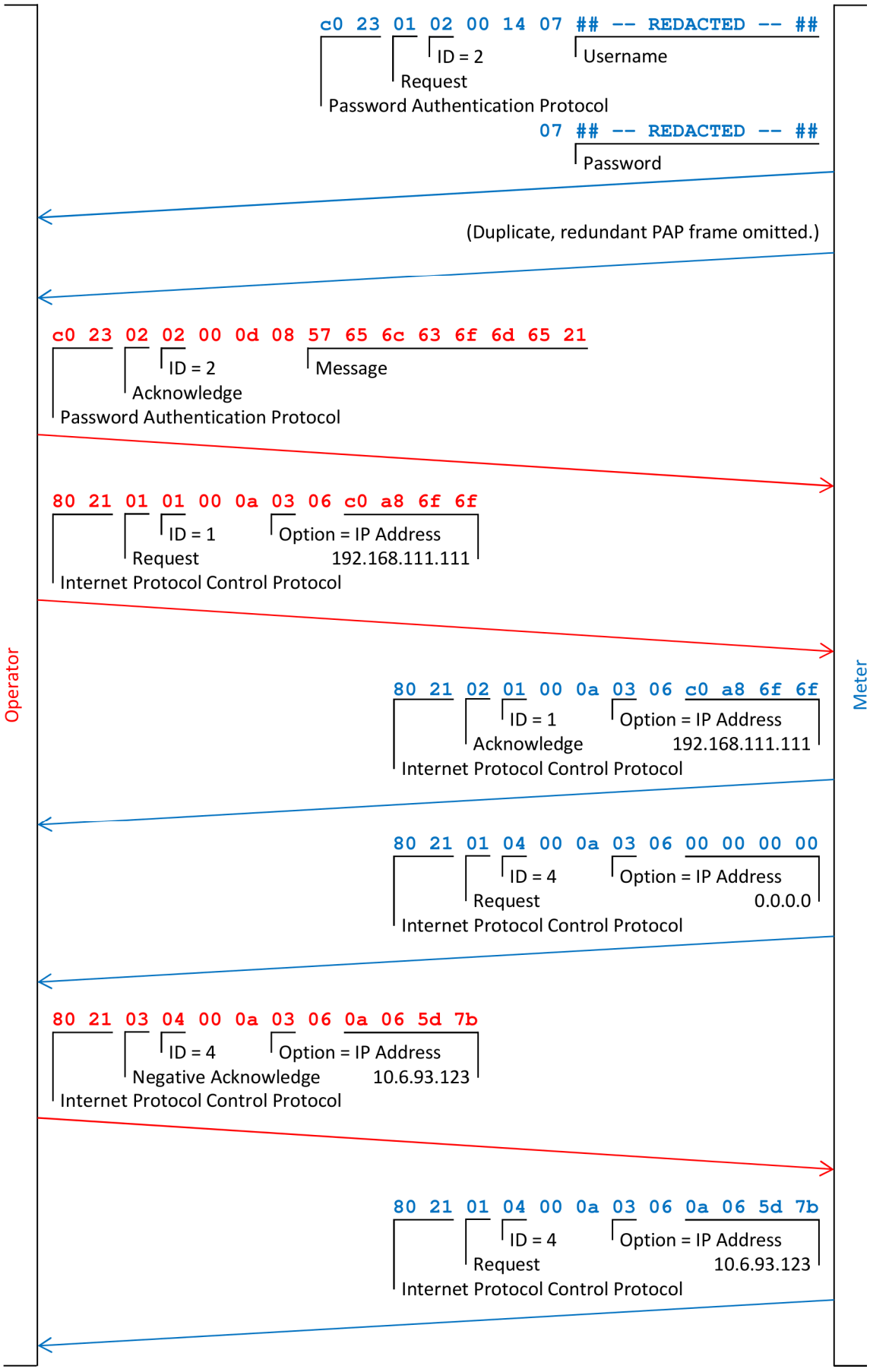

Figure 5.7: PAP authentication and IPCP configuration (continued in Figure 5.8)

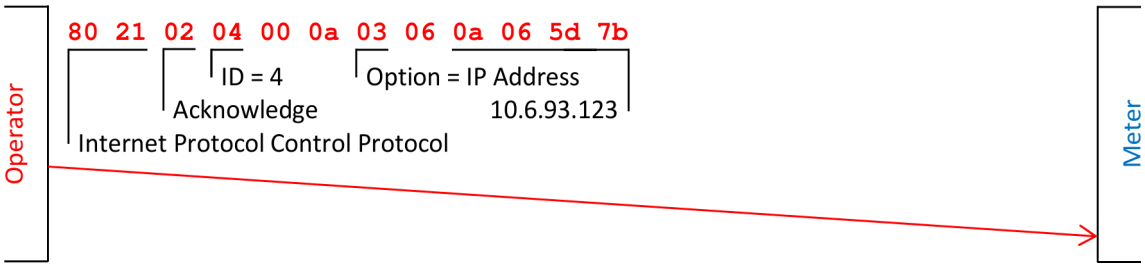

Figure 5.8: IPCP configuration (continued from Figure 5.7)

Following successful authentication, the internet protocol control protocol (IPCP) was used to negotiate the assignment of IP addresses to both the operator and meter in order that IP communications could be used for further data exchange. This is shown in Figure 5.7. The operator first transmitted a request to the meter to use the IP address 192.168.111.111, which was accepted by the meter with an Acknowledge response. The meter then requested the assignment of an address by the operator. This was done by requesting the invalid IP address 0.0.0.0, which caused the operator to respond with a Negative Acknowledge, and a suggested IP address of 10.6.93.123 for the meter. The meter then issued another request, this time using the suggested address. This was accepted by the operator with an Acknowledge response, as shown in Figure 5.8. Following configuration of the IP parameters using IPCP, data was exchanged between the operator and meter using encapsulated within UDP packets, which are in turn encapsulated by PPP. An example of the encapsulation, in this case the first UDP packet captured following transmission by the meter operator, is shown in Figure 5.9.

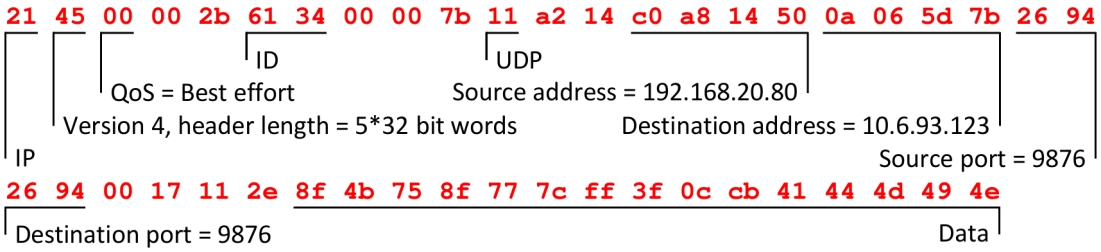

Figure 5.9: UDP frame

The UDP header information includes the source address, which may not be the originating device as a result of network address translation (NAT), the destination address, and the source and destination ports. For the purposes of further analysis, the UDP header information is omitted.

A proprietary protocol for connecting to the meter for the purpose of command line communication is described by the meter manufacturer. The first attempt by the operator to logon to the meter in this manner is shown in Figure 5.10.

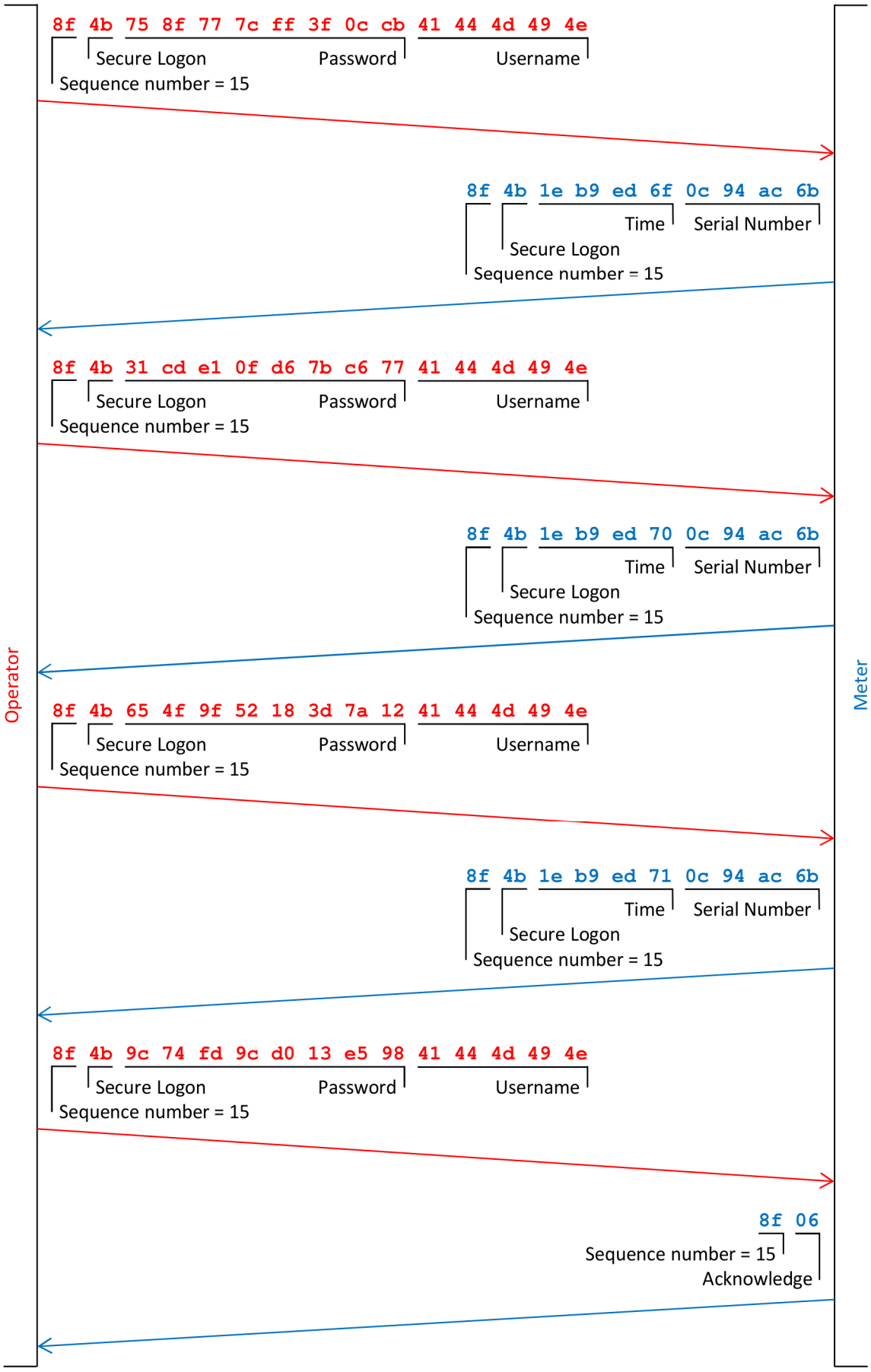

Figure 5.10: Logon attempts to meter by the operator

As defined by the manufacturer's command line protocol, command line exchanges are grouped by means of a sequence number between 0 and 15 conveyed by the second four bits of the sequence number byte, of which the first four bits are always '1'. Secure logon to the meter comprises the transmission of a 'K' character, or the byte `0x4b`, followed by an eight-byte encrypted password, and finally the username in plain text. In the first transmission by the operator in Figure 5.10, the username is seen to be 'ADMIN'. However, the logon attempt was unsuccessful, with the meter returning a time and serial number, as per the manufacturer's specification. The last four bytes of the returned string are equal to the serial number of the meter, 211 070 059, expressed as a 32-bit unsigned integer in little endian format. The preceding four bytes are the current time and date, in the same binary format, expressed as the number of seconds since the start of the year 1996. In this first case, the time retuned is equal to 515 501 423 in denary, or a date and time of 10:50:25 on 2nd May 2012. It is noted that the subsequent two logon attempts made by the operator to the meter were also unsuccessful, with the time field of the meter responses incrementing by one after each attempt. The fourth attempt by the operator to logon to the meter was successful, with the response of the meter an Acknowledge byte.

Although the encryption scheme used by the manufacturer to protect the password is not described in the documentation found, it was inferred that it uses the time as an element in the encryption. The implication of this is that a given password will be valid only during the second in which it is generated. On this basis, multiple attempts may be required before synchronisation of the times used by both meter and operator to generate the password with sufficient accuracy is achieved, and the latency of the complete transmission path between the two peers is sufficiently low for the password to still be valid on arrival.

Following the successful logon attempt, the operator requested the values of two registers, which were returned by the meter, as shown in Figure 5.11. Subsequent exchanges were not analysed until the operator requested a logoff from the meter with the transmission of an 'X' character, to which the meter responded with an Acknowledge byte.

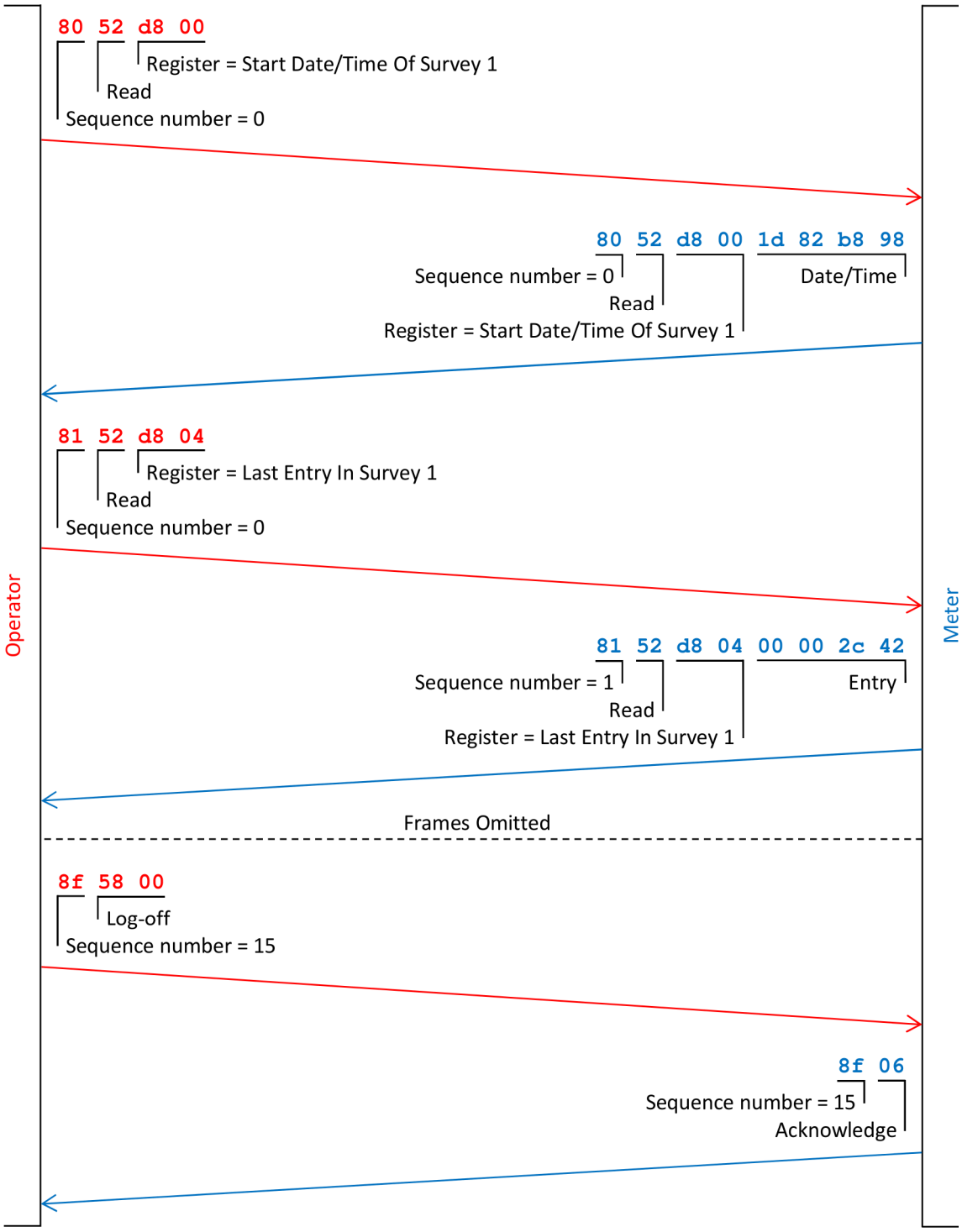

Figure 5.11: Logon and data access of meter by the operator

As a result of the eavesdropping of communication between the meter and modem, and meter and meter operator, the following information was extracted:

- GPRS configuration including operator access point name.
- LCP configuration.
- PAP username and password.
- IPCP configuration, including IP addresses and ports used.
- Username for command line logon to the meter.
- Nature of encrypted password as time-dependent.

5.4.2 - Attack 2

In Section 5.2.3, the optical port of the meter was found to be enabled for command line communications, and is specified in the manufacturer's documentation as supporting the same command line instruction set as is used for communication with the meter operator, via the WAN modem. Therefore, it was hypothesised that a replay attack could be effected against the meter, whereby an encrypted password used by the operator to login to the meter via the WAN modem might be used again to log in to the meter through the optical interface. In this way, decryption of the password would not be necessary for the attack. Furthermore, the username was already known due to being transmitted in plain text. Since the password was determined to be time-dependent, and subject to change every second, manual analysis of the data stream to extract the password was not possible whilst retaining the required 'freshness' of the password. Accordingly, a Python script was written to extract the password from a captured secure logon attempt to the meter by the operator. The Python script first removes the escape sequences employed by PPP from each raw frame, an example of which is shown in Figure 5.12, and recovers the original bytes.

```
7e 21 45 00 00 2b 64 5c 00 00 7b 7d 31 9e ec c0 a8 14 50 0a 06 5d 7b
26 94 26 94 00 17 ba 86 8f 4b 9c 74 fd 9c d0 7d 33 e5 98 41 44 4d 49
4e f4 48 7e
```

Figure 5.12: Raw PPP frame

The script then strips away the encapsulation of PPP and the successive protocol layers within: IPv4 and UDP, as shown in Figure 5.13.

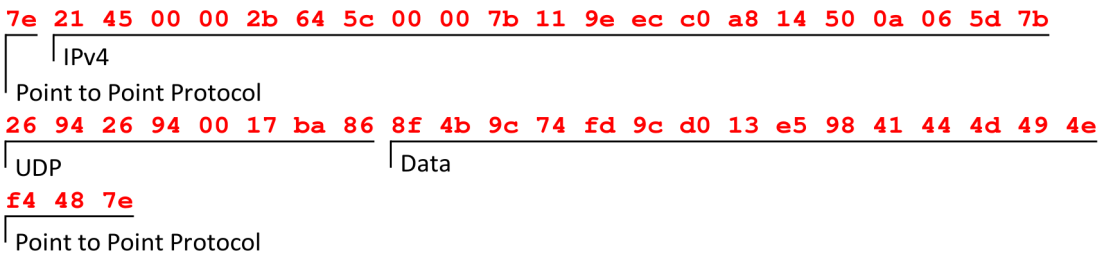

Figure 5.13: Escaped PPP frame

The command line string contained within the frame is then analysed. In the case of this example, the string was found to contain a secure logon attempt. The credentials from this are shown in Figure 5.14.

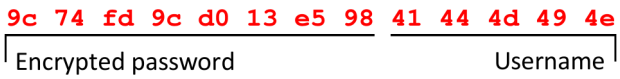

Figure 5.14: Credentials from data field of UDP packet

The framing required for communication with the optical interface of the meter is then added to the secure logon string consisting of a 'K' character, or the byte `0x4b`, followed by the encrypted password and username. The `<STX>` flag is appended to the start of the string, and a null termination character to the end. Next, the XMODEM variant of the CRC16-CCITT XMODEM checksum of the frame is calculated, and appended to the end of the frame. Finally, the `<ETX>` frame terminating flag is appended to the end of the frame, as shown in Figure 5.15.

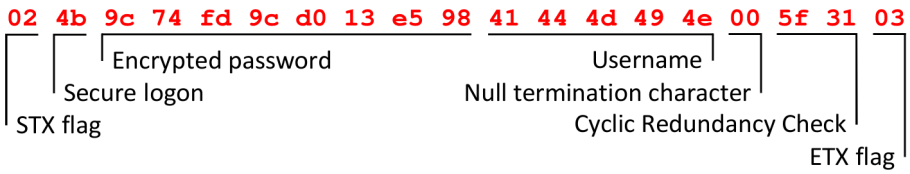

Figure 5.15: Constructed frame for optical port

The meter and modem were energised from a fully de-energised state. During the energised period, the meter and the head-end server of the metering provider established a connection, indicated by the front panel interface of the meter. Upon reception of the secure logon attempt by the meter from the operator, the Python script successfully parsed the frame, extracted the credentials, formed a frame of the type required for communication with the optical port, and transmitted it to this port via the optical head of the attack toolkit. The meter returned an Acknowledge byte via the optical port, indicating that the connection attempt was successful.

5.5 - Attack results analysis

5.5.1 - Introduction

The results of the attacks described in Section 5.4 are considered in the context of the CIA triad model of information security, as defined in ISO/IEC 27002:2013 [229], namely:

- Confidentiality: Ensuring that information is accessible only to those authorised to have access.
- Integrity: Safeguarding the accuracy and completeness of information and processing methods.
- Availability: Ensuring that authorised users have access to information and associated assets when required.

These tenets are widely employed in the field of information security, and are considered a simple test of security performance, whereby if any of the three are not fulfilled then the security of the system under test may be considered compromised.

5.5.2 - Attack 1

The data exchanged between the meter and the WAN modem comprises both the readings acquired by the meter in the course of monitoring a customer's supply, and the operational data exchanged for purposes including mutual authentication, configuration, and management of the meter by the meter operator. Since the attack required physical proximity to the meter, it would likely not be effected without the complicity of the customer. Accordingly, the exfiltration of user data, such as energy consumption in a given time period, by means of the attack, is not a primary confidentiality concern. Rather, the issue of confidentiality in this case concerns the operational data exchanged between the meter and the WAN modem, in particular the configuration data and authentication credentials. The data used at all stages of the configuration of the WAN modem by the meter, and the connection and authentication to the operator by the meter, via the modem, was exchanged in plain text. As such all the information which would be required to impersonate the meter from the perspective of the operator, at the stages of authentication and configuration examined, was obtained. Such an attack would permit energy consumption to be inaccurately reported, or falsely attributed, for the purpose of energy theft. In the case

that measurements from smart meters are used to inform distribution network control decisions, such impersonation would also permit false data injection, which may lead to necessary network control action not being taken, or unnecessary control action being taken. Furthermore, an agent impersonating a meter would be able to establish a connection to the operator through which an attack on the operator's systems might be effected.

Since the RS-232 link between the meter and WAN modem was eavesdropped rather than redirected, neither the integrity nor the availability of the data conveyed across it were compromised. However, since the data exfiltrated was sufficient to fully impersonate the meter at the stages of authentication and configuration examined, a further attack whereby the meter was impersonated would negate any assurance of data integrity or availability.

5.5.3 - Attack 2

As in the case of Attack 1, in which the confidentiality of data exchanged between the meter and the WAN modem was compromised, an authenticated terminal connection to the meter permits access to the registers within the device used to store customer energy consumption information. However, as in the case of Attack 1, this attack is unlikely to be effected without the complicity of the consumer. Rather, in addition to directly modifying the records of energy consumption for the purpose of inaccurately reporting, or falsely attributing energy consumption, access to the internal registers of the meter might allow a malicious agent to falsify readings by modifying the variables on which the calculated demand depends. For example, modification of the stored value of a current transformer ratio might allow a reduction in metered current, and hence billed consumption, to be effected. Whilst, under such circumstances, compromise of the availability of data to the meter operator does not yield an immediate benefit, compromise of the integrity of data supplied to the operator for the purpose of billing constitutes a clear motive for an attack.

More critically, the attack exposes data specific to the meter operator, which is stored in the meter, to compromise. This might include encryption keys or authentication credentials used for access to, and control of, the meter by the operator, and may expose multiple meters to attack if common keys or authentication credentials are used. Compromise of multiple meters in this way would negate any assurance of data integrity or availability, and constitutes a critical vulnerability in the case that measurements from smart meters are used to inform distribution network control

decisions, or if such meters incorporate a remote supply disconnection facility, with the associated threat of malicious denial of energy

5.6 - Recommendations

The attacks described in Section 5.4 required some physical intrusion into the enclosure of the meter, albeit only into the serviceable, terminal section. This included breaking the tamper evident seal, although this is easily restored. It would be necessary to circumvent the tamper detection micro-switch, if it was required that no evidence of the attack was to be recorded by the meter. The attacks also required disconnection of the lead connecting the WAN modem, contained within the serviceable section, to the meter, in order that the attack hardware could be connected in its place. No mechanism exists in the meter examined to detect such infiltration. However, the addition of presence detection signal lines on the interface would significantly inhibit such an attack by detecting if the electrical link between WAN modem and meter was lost. Indeed, presence detection signals are included in the UK Data Communications Company *Intimate Communications Hub Interface Specification* [230], for the purpose of mutual detection of the presence of a smart electricity meter and communications hub, responsible for WAN communications.

Of the data exfiltrated in the eavesdropping attack described in Section 5.4.1, the security credentials exchanged as plain text using the password authentication protocol (PAP) are the most significant. The use of the meter operating company's own name as both username and password for the process is poor security practice. Furthermore, the credentials could be protected by employing the, alternative, challenge handshake authentication protocol (CHAP). Under this protocol, the peer wishing to perform authentication, in this case the meter operator, transmits a randomly generated 'challenge' string to the peer to be authenticated, in this case the meter. The peer to be authenticated combines the 'challenge' string with a pre-shared secret using a one-way hashing function, such as the secure hash algorithm (SHA), and returns the result to the authenticating peer. The authenticating peer compares the returned result with its own calculation of the hashing function and, if they match, acknowledges the authentication. Since each result is valid only for one authentication attempt, the process is immune to replay attacks. The challenge authentication protocol provides further security by periodically reissuing the authentication challenge in order that the link is maintained. The protocol is, however, still vulnerable to man-in-the-middle attacks.

The replay attack described in Section 5.4.2 could be prevented by prohibiting a secure connection from being established on one interface using the same credentials previously used on another interface, or by preventing a secure connection from being established on one interface within one second of one being established on another. This would ensure that an encrypted password captured during the establishment of a secure connection on one interface would have expired before a secure connection could be established on another interface, and hence could not be reused.

In addition to security compromises made with the level of physical access to the meter assumed for the attacks demonstrated in Section 5.4, known vulnerabilities of second-generation (2G) cellular technology security, such as the demonstrated weakness of the A5/1 stream cipher, evidence the value of effective end-to-end security between meters of this type and meter operators. Such security should include both reliable authentication and encryption. A solution which would enable the existing command line protocol employed between the meter and operator to be used, following establishment of a secure link, is mutually authenticated transport layer security (TLS). Under such a scheme, both the meter and operator possess certificates which enable them to prove their identity during the establishment of a secure link. The validity of the certificates is verified by means of a trusted, third party certificate authority. In practice, the third-party certificate authority may be used to verify the identity of a server which is a local peer of that which the operator wishes to be linked to a given meter. In this way, the third-party certificate authority generates an intermediate certificate which is used to verify the identity of the local peer, and this local server then acts the certificate authority for the purpose of establishing a secure link. An illustration of the establishment process for a TLS link is shown in Figure 5.16.

Upon receipt of a request from a meter to establish a TLS connection, the meter operator presents its digital certificate, along with the public key of an asymmetric key pair, generated for the session, to the meter. The meter verifies the validity of the operator's certificate and, finding it to be valid, presents its own digital certificate to the operator, along with a secret, symmetric encryption key, generated for the session, and encrypted with the public key supplied by the operator. The operator verifies the validity of the meter's certificate and, finding it to be valid, decrypts the secret, symmetric key supplied by the meter, using the private key of the asymmetric key pair which it generated earlier in the link establishment process.

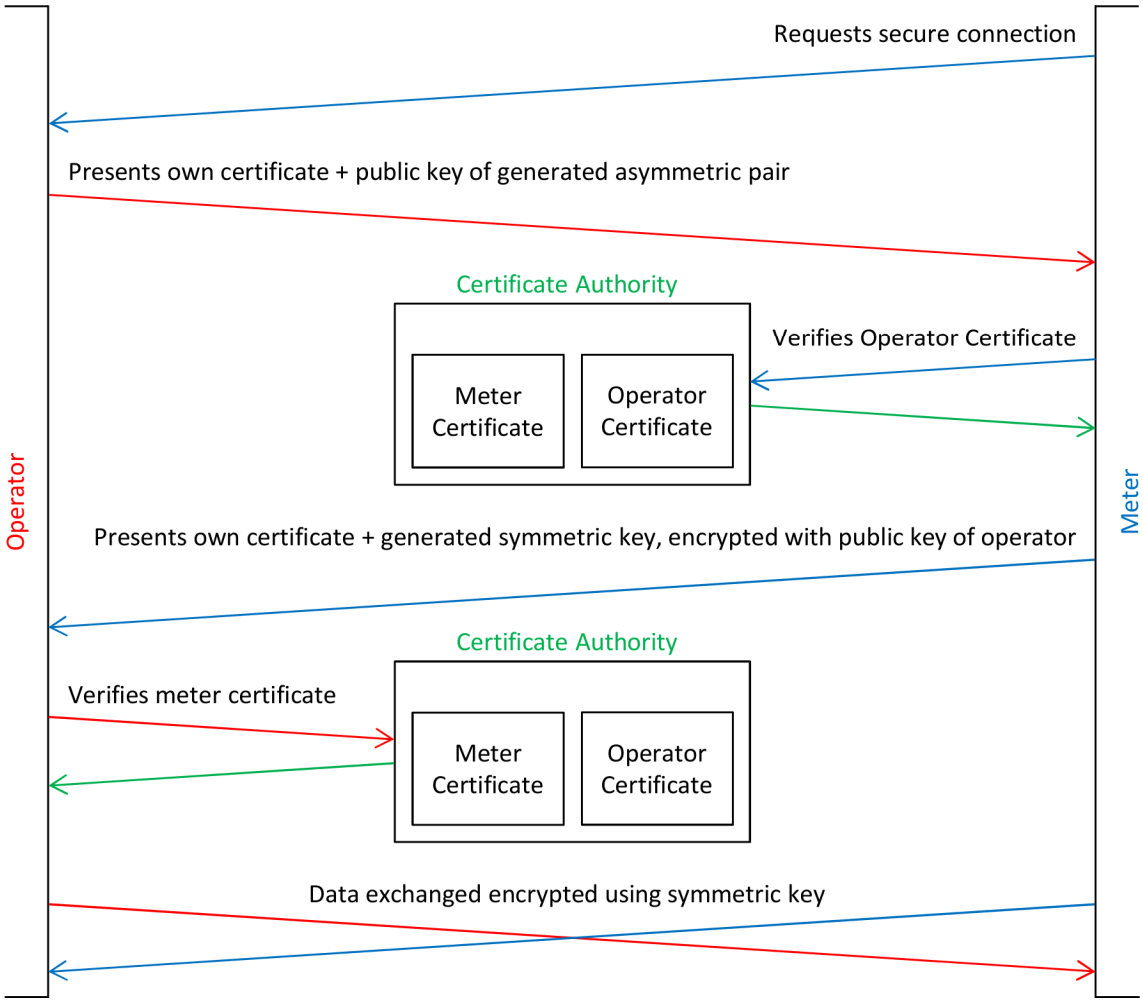

Figure 5.16: TLS link establishment process

The current UK *Smart Metering Equipment Technical Specifications* (Version 1.58) [34] specifies that smart electricity meters should be capable of supporting the following cryptographic algorithms:

- Elliptic Curve DSA
- Elliptic Curve DH
- SHA-256

Furthermore, the document specifies that the electricity meter 'shall be capable of generating Public-Private Key Pairs to support the Cryptographic Algorithms' and 'shall be capable of securely storing Security Credentials from Certificates including for use in the Cryptographic Algorithms'. A meter conforming to the current UK *Smart Metering Equipment Technical Specifications* would, therefore, be capable of supporting the security recommendations made in this section.

5.7 - Conclusion

A smart electricity meter widely deployed in the UK as part of the smart meter roll-out programme has been analysed for potential vulnerabilities, and two attack methodologies chosen. Hardware and software tools have been developed in order to effect these attacks, and the results analysed in order to determine the degree to which the security of the smart meter has been compromised, and the potential consequences of this compromise.

The first of these attacks demonstrated the acquisition of all the information required to impersonate the meter from the perspective of the operator. With this information, it would be possible to pose as a different customer in order to falsely attribute energy consumption, or to inaccurately report energy consumption, for the purpose of energy theft. If measurements from the meters of this operator were used to inform network control decisions, impersonation of this or other meters would allow false data to be injected, disrupting network control and potentially resulting in denial of energy if this disruption led to a loss of supply. Furthermore, the ability to establish a connection with the head-end system of the operator, posing as a trusted entity, exposes the operator's systems to the threat of further penetration and compromise.

The second of these attacks demonstrated local logon to the meter, posing as the operator, using intercepted and processed credentials. Connection in this way exposes data stored within the meter which is not intended to be accessed or modified by those other than the meter operator. In addition to the modification of the latest energy consumption data, for the purpose of inaccurate reporting and energy theft, it might also permit permanent modification of firmware registers used to derive consumption figures, in order to inaccurately report energy consumption in the future. A critical further concern is the exposure of encryption keys or authentication credentials which, if common to other meters of this operator, may allow access to those devices, posing as the operator. In this way, a widespread denial-of-energy attack may be effected in which supply disconnection of a large number of meters, by means of their remote disconnection facility, is directed by a malicious agent. It might also be possible to effect the widespread disruption of supply, by cyclically operating the remote disconnection device of a large number of meters in order to generate rapidly fluctuating load conditions on the distribution network.

Finally, recommendations have been made as to how the security of such a meter might be improved, including by the employment of established protocols which would

satisfy both the requirement for robust and secure mutual authentication of a smart meter and operator, and for encrypted communication between them.

6 - Conclusions and further work

6.1 - Conclusions

The research objectives presented in Section 1.2.1 have been fulfilled. Conclusions of the research conducted on the subjects of distribution network control, and smart meter and AMI security, as well as further research contributions and pertinent, future research avenues, are presented in the following sections.

6.1.1 - Distribution network control

Climate change and the unsustainable consumption of fossil fuels have seen a global policy shift towards low-carbon technologies. However, the adoption of high levels of renewable generation represents a significant change in the requirements for power distribution. In contrast to the historical approach of centralised generation, distributed renewable generation, in particular, necessitates considerably more advanced distribution network control. This is exacerbated by the additional demands of other low-carbon technologies, for example electrified transport. Smart metering on low voltage networks offers the facility for monitoring the very periphery of the distribution network. This visibility supports an advanced level of control, which in turn increases the penetration of renewable generation which may be accommodated.

In this work, a low voltage distribution network hosting a high penetration of solar PV generation, and electric vehicle charging, was considered. The distribution transformer supplying the network was equipped with an OLTC. This network was simulated on an RTDS, with the facility to provide real-time measurements of the voltage at critical points within the network as analogue output signals, and to receive SCADA commands to control the OLTC as input signals. A hardware smart meter test bed platform was developed, capable of acquiring electrical measurements and communicating these over a WAN in real-time. Four of these devices were used to monitor critical points in the simulated distribution network, by means of the analogue output signals of the RTDS. The hardware and software infrastructure required for WAN communication with multiple smart meters, and for SCADA communication, was also implemented.

A controller was developed to direct the operation of the OLTC, via SCADA, informed by measurements from the smart meters. This was based on a simple voting

algorithm, under which action was taken in response to a voltage measurement taken by one or more of the smart meters which violated preset limits, if doing so was not expected to cause a new voltage limit violation elsewhere in the network, or to exacerbate one which already existed. The operation of the controller was demonstrated in scenarios of high solar PV generation, high EV charging demand, imbalance resulting from uneven distribution of generation and demand across phases, and conflicting generation and demand conditions in adjacent feeders. In the cases of high generation, high demand, and imbalance, the controller was shown to respond to voltage limit violations by directing OLTC operation in order to rapidly restore the voltage at all monitored points to within limits, and without causing further voltage limit violations. In the case of the conflicting generation and demand conditions, the controller was shown to determine that any OLTC operation would result in further voltage limit violations, and so no further action was taken.

Existing work has shown that conventional AVC schemes may be effective in the presence of a limited penetration of DG power injection and EV charging demand. However, control in the presence of a high penetration of DG and EV charging requires visibility of LV networks beyond the secondary substation. Such visibility is made possible with the deployment of smart meters, but the response speed and flexibility of commercial meters for network monitoring, as a role secondary to their primary function of energy consumption reporting, has limited their use in published schemes. With the development of custom smart meter test beds, as part of a wider closed-loop smart meter test rig, this work has addressed this limitation. The rig further addresses the issue of placement of voltage monitoring in real-world trials, by permitting the smart meters to be deployed on a real-time distribution network simulation, in the locations most useful for a particular scenario. The evaluation of the automatic voltage controller developed in this work, accounting for the real-world communications and processing delays inherent in a real-world system, is therefore a valuable contribution to understanding in the field. The necessary simplification of the simulated distribution network and limited number of meters have been recognised as potential limitations of the system demonstrated. However, the fidelity of the power system simulated, and the number of smart meter test beds, have been sufficient for the purposes of the study undertaken.

With the widespread deployment of AMI, and the evolution of OLTC-equipped distribution transformers, including those employing solid-state commutation or power electronic conversion, the test rig and voltage controller developed in this work represents valuable tools in the development of distribution network control to accommodate high penetrations of low-carbon technologies.

6.1.2 - Smart meter and AMI security

The adoption of AMI inevitably incurs cyber security vulnerabilities which did not exist in the case of meters with no facility for remote communication. The magnitude of the threat which these constitute is significantly increased by the inclusion of a remote supply disconnection facility within smart meters. Although authoritative guidance is available on the issue of AMI security, this is not necessarily heeded by manufacturers. Approval schemes, such as the National Cyber Security Centre's (NCSC) CPA scheme, seek to address this. However, vulnerabilities have been demonstrated in existing AMI deployments, and the communication technologies typically used in them.

In this work, a cyber security vulnerability of a commercially deployed smart meter was examined. A hardware tool was constructed to permit the capture of data exchanged between the processor of the smart meter, and the modem used for WAN communication. The smart meter was configured in a standard form for domestic and light commercial metering, and data was captured in the course of communication between the smart meter and the head-end of the meter operator for the principal purpose of energy consumption recording.

The data captured was analysed, and the frames of common communication protocols were extracted. It was established that a weak system for authentication of the smart meter to the head-end of the operator was employed. As such, the authentication credentials were extracted. Data made publicly available by the manufacturer of the smart meter on the Internet provided information on the format of the credentials used for authentication of the head-end operator to the smart meter, as well as authentication in the case of communication with the local, optical port of the smart meter.

By intercepting data including credentials during the connection and authentication phases between the smart meter and the head-end of the operator, all the information required to impersonate a smart meter from the perspective of the meter operator was acquired. This would permit energy theft by impersonation of another meter, and the false reporting or attribution of consumption data. It might also permit disruption of network control by false data injection, or more extensive penetration of the head-end system of the operator by posing as a trusted entity.

A software tool was developed which extracted the credentials used for authentication of the head-end operator to the smart meter, conveyed over the WAN interface, reformatted these credentials according to the protocol used for communication with

the local, optical port of the smart meter, and issued them to this interface by means of an optical probe. It was demonstrated that, by means of this technique, local access was gained to the internal system of the smart meter, using the credentials of the meter operating company. This access exposes the possibility for the compromise of registers within the meter used in the process of consumption recording and reporting, for the purpose of energy theft, or encryption keys and authentication credentials which facilitate access to other smart meters and wider smart metering infrastructure.

Recommendations have been made in order to address the vulnerabilities of a specific smart meter exposed in this work, addressing weaknesses in both the firmware and protocols employed by the device. However, the attacks described serve to demonstrate not only vulnerabilities within a specific AMI deployment, but also highlight the importance of applying the rigorous security practices employed in existing, security-critical infrastructure, such as that for smart payment cards, in AMI schemes.

6.1.3 - Further achievements of research

A demonstration rig illustrating smart meter control in response to real-time electricity pricing for the purpose of DSM, and based on four of the smart meter test beds, was presented to HRH The Princess Royal, and the former president of the Royal Academy of Engineering, Sir John Parker FREng, at the 2012 ‘Engineering a better society’ event of the Royal Academy of Engineering. The smart meter test beds and test rig used in this research were also presented to both UK and international academic partners, and to industrial parties, including manufacturers and DNOs.

A period of secondment was taken with a commercial smart meter operator in the UK during the course of this research. At the time of this appointment, the operator was both installing smart meters and providing the head-end infrastructure to manage them. In addition to providing consultancy on cyber security provision, penetration testing of the infrastructure supplied by the operator was conducted. This formed the basis for Chapter 5 of this work. A report on cyber security considerations for smart meter design, including responses to the first iteration of DECC's UK *Smart Metering Equipment Technical Specifications*, was produced for DECC's Security Technical Experts working group.

6.2 - Further work

Pertinent, future research avenues, further to this work, are presented in the following sections.

6.2.1 - Distribution network control

Mechanisms to effect voltage control may be examined to augment, or supplant control solely by means of an OLTC. Such mechanisms include DSM providing the facility for the control of demand, generation curtailment, reactive power flow control by PV inverters, and energy storage.

Realistic time-series profiles may be applied to generation sources and loads in order to investigate the requirements for the frequency of control operations, as well as their response time in order to provide satisfactory voltage regulation. This might include changes to the granularity of power system simulation, with scope for both greater aggregation and more detailed representation in different areas of the simulated network as required.

The implications for communication capacity and performance, particularly in the case of a high penetration of smart metering, may be examined. In particular, optimisation of the facility for network monitoring against the requirements of communications performance and cost may be considered, with the rig permitting assessment of the communications impact of congestion arising from a greater number of concurrent smart meter connections.

Further, ancillary functions of smart metering, for example phase identification and outage management, including fault location, may be investigated.

6.2.2 - Smart meter and AMI security

The scope for the application of established security practice from related, security-critical infrastructure, such as that for smart payment cards, to AMI schemes, may be examined. This pertains to hardware, firmware and software design, and to communication protocols.

The use of dedicated cryptographic hardware in smart meters, and the scope for adoption of design practices and techniques employed in such hardware, for example for the purpose of tamper detection and prevention, may be investigated.

Analysis of the degree to which smart meters and smart metering infrastructure constitute an element of critical national infrastructure might be conducted. This is particularly critical if smart meters are equipped with a remote supply disconnection facility.

References

[1] U.S. Energy Information Administration (EIA), "International Energy Outlook 2019," 2019. [Online]. Available: https://www.eia.gov/outlooks/ieo/pdf/ieo2019.pdf.

[2] European Commission, "Energy roadmap 2050," 2012. [Online]. Available: https://ec.europa.eu/energy/sites/ener/files/documents/2012_energy_roadmap_2050_en_0.pdf.

[3] "Directive 2009/28/EC of the European Parliament and of the Council of 23 April 2009 on the promotion of the use of energy from renewable sources and amending and subsequently repealing Directives 2001/77/EC and 2003/30/EC," *Off. J. Eur. Union*, 2009.

[4] Department of Energy & Climate Change, "National Renewable Energy Action Plan for the United Kingdom," 2010. [Online]. Available: https://assets.publishing.service.gov.uk/government/uploads/system/uploads/attachment_data/file/47871/25-nat-ren-energy-action-plan.pdf.

[5] Department for Business Energy & Industrial Strategy, "UK Energy Statistics, 2019 & Q4 2019," 2020. [Online]. Available: https://assets.publishing.service.gov.uk/government/uploads/system/uploads/attachment_data/file/877047/Press_Notice_March_2020.pdf.

[6] Department for Business Energy & Industrial Strategy, "Energy Trends March 2020," 2020. [Online]. Available: https://assets.publishing.service.gov.uk/government/uploads/system/uploads/attachment_data/file/875381/Energy_Trends_March_2020.pdf.

[7] Department for Business Energy & Industrial Strategy, "Solar photovoltaics deployment," 2020. [Online]. Available: https://www.gov.uk/government/statistics/solar-photovoltaics-deployment. [Accessed: 13-Jun-2020].

[8] *Energy Act 2008*. 2008.

[9] International Energy Agency, "Global EV Outlook 2020," 2020.

[10] Department for Transport, "Licensed cars by propulsion or fuel type: Great Britain and United Kingdom," 2020.

[11] Society of Motor Manufacturers and Traders, "SMMT UK new car and LCV registrations outlook to 2021–January 2020," 2020.

[12] Tesla, "Supercharger," 2018. [Online]. Available: https://www.tesla.com/en_GB/supercharger. [Accessed: 01-Jun-2020].

[13] J. Ekanayake, N. Jenkins, K. Liyanage, J. Wu, and A. Yokoyama, *Smart Grid:*

Technology and Applications. John Wiley & Sons, 2012.

[14] Institution of Engineering and Technology, "What is a Smart Grid?," 2013. [Online]. Available: https://www.theiet.org/factfiles/energy/smart-grids-page.cfm.

[15] CLP Power Hong Kong, "Smart Grid," 2016. [Online]. Available: https://www.clp.com.hk/en/about-clp/power-transmission-and-distribution/smart-grid. [Accessed: 28-May-2018].

[16] *American Recovery and Reinvestment Act of 2009*. 2009.

[17] International Energy Agency, "Technology Roadmap Smart Grids," 2011. [Online]. Available: https://www.iea.org/publications/freepublications/publication/smartgrids_roadmap.pdf.

[18] European Commission, "Smart grid projects outlook 2017," 2017. [Online]. Available: http://publications.jrc.ec.europa.eu/repository/bitstream/JRC106796/sgp_outlook_2017-online.pdf.

[19] Pöyry, "An Independent Evaluation of the LCNF," 2016. [Online]. Available: http://www.poyry.co.uk/sites/www.poyry.co.uk/files/media/related_material/evaluation_of_the_lcnf_0.pdf.

[20] H. Farhangi, "The path of the smart grid," *IEEE Power Energy Mag.*, vol. 8, no. 1, pp. 18–28, Jan. 2010.

[21] Edison Electric Institute, "Smart Meters and Smart Meter Systems: A Metering Industry Perspective," 2011. [Online]. Available: https://aeic.org/wp-content/uploads/2013/07/smartmetersfinal032511.pdf.

[22] V. C. Gungor, D. Sahin, T. Kocak, S. Ergut, C. Buccella, C. Cecati, and G. P. Hancke, "A Survey on Smart Grid Potential Applications and Communication Requirements," *IEEE Trans. Ind. Informatics*, vol. 9, no. 1, pp. 28–42, Feb. 2013.

[23] Navigant Research, "Market Data: Smart Meters," 2016. [Online]. Available: https://www.navigantresearch.com/research/market-data-smart-meters.

[24] "Directive 2009/72/EC of the European Parliament and of the Council of 13 July 2009 concerning common rules for the internal market in electricity and repealing Directive 2003/54/EC," *Off. J. Eur. Union*, 2009.

[25] Department for Business Energy & Industrial Strategy, "Smart Meter Statistics in Great Britain: Quarterly Report to end December 2019," 2020. [Online]. Available: https://assets.publishing.service.gov.uk/government/uploads/system/uploads/attachment_data/file/872155/2019_Q4_Smart_Meters_Statistics_Report.pdf.

[26] A. Hansen, J. Staggs, and S. Shenoi, "Security analysis of an advanced metering infrastructure," *Int. J. Crit. Infrastruct. Prot.*, vol. 18, pp. 3–19, 2017.

[27] C. J. Foreman and D. Gurugubelli, "Identifying the Cyber Attack Surface of the Advanced Metering Infrastructure," *Electr. J.*, vol. 28, no. 1, pp. 94–103, Jan. 2015.

[28] R. Anderson and S. Fuloria, "Who Controls the off Switch?," in *2010 First IEEE International Conference on Smart Grid Communications*, 2010, pp. 96–101.

[29] National Institute of Standards and Technology, "Guidelines for Smart Grid Cybersecurity," 2014. [Online]. Available: https://nvlpubs.nist.gov/nistpubs/ir/2014/NIST.IR.7628r1.pdf.

[30] National Institute of Standards and Technology, "Security Requirements for Cryptographic Modules (FIPS PUB 140-2)," 2006. [Online]. Available: https://nvlpubs.nist.gov/nistpubs/FIPS/NIST.FIPS.200.pdf.

[31] "2012/148/EU: Commission Recommendation of 9 March 2012 on preparations for the roll-out of smart metering systems," *Off. J. Eur. Union*, 2012.

[32] European Commission, "Smart Grids Task Force," 2009. [Online]. Available: https://ec.europa.eu/energy/en/topics/markets-and-consumers/smart-grids-and-meters/smart-grids-task-force.

[33] European Network and Information Security Agency, "Proposal for a list of security measures for smart grids," 2013. [Online]. Available: https://ec.europa.eu/energy/sites/ener/files/documents/20140409_enisa.pdf.

[34] Department of Energy and Climate Change, "Smart Metering Equipment Technical Specifications Version 1.58," 2014. [Online]. Available: https://assets.publishing.service.gov.uk/government/uploads/system/uploads/attachment_data/file/381535/SMIP_E2E_SMETS2.pdf.

[35] Communications-Electronics Security Group, "CPA Security Characteristic Electricity Smart Metering Equipment Version 1.2," 2016. [Online]. Available: https://www.ncsc.gov.uk/content/files/protected_files/document_files/SMLT-SC-0002 ESME v1-2.pdf.

[36] N. Lawson, "Reverse-engineering a smart meter," *rdist*, 2010. [Online]. Available: https://rdist.root.org/2010/02/15/reverse-engineering-a-smart-meter. [Accessed: 16-May-2018].

[37] K. Jackson Higgins, "Smart Meter Hack Shuts Off The Lights," *DARKReading*, 2014. [Online]. Available: https://www.darkreading.com/perimeter/smart-meter-hack-shuts-off-the-lights/d/d-id/1316242.

[38] A. Garcia Illera and J. Vazquez Vidal, "Lights Off! The Darkness of the Smart Meters," *Black Hat Europe 2014*, 2014. [Online]. Available: https://www.youtube.com/watch?v=Z_y_vjYtAWM.

[39] *The Electricity Safety, Quality and Continuity Regulations 2002*. 2002.

[40] E. Lakervi and E. J. Holmes, *Electricity Distribution Network Design*. Institution of Engineering and Technology, 2003.

[41] T. Haggis, "Network Design Manual," *E.ON Central Networks*, no. December. pp. 1–194, 2006.

[42] F. A. Viawan, A. Sannino, and J. Daalder, "Voltage control with on-load tap changers in medium voltage feeders in presence of distributed generation," *Electr. Power Syst. Res.*, vol. 77, no. 10, pp. 1314–1322, 2007.

[43] Y. Liu, J. Bebic, B. Kroposki, J. De Bedout, and W. Ren, "Distribution system voltage performance analysis for high-penetration PV," in *2008 IEEE Energy 2030 Conference, ENERGY 2008*, 2008.

[44] E. J. Coster, J. M. a Myrzik, B. Kruimer, and W. L. Kling, "Integration Issues of Distributed Generation in Distribution Grids," *Proc. IEEE*, vol. 99, no. 1, pp. 28–39, 2011.

[45] P. Trichakis, P. Taylor, P. F. Lyons, and R. Hair, "Predicting the technical impacts of high levels of small-scale embedded generators on low-voltage networks," *IET Renew. Power Gener.*, vol. 2, no. 4, pp. 249–262, 2008.

[46] N. Jenkins, J. B. Ekanayake, and G. Strbac, *Distributed generation*. The Institution of Engineering and Technology, 2010.

[47] T. Ackermann and V. Knyazkin, "Interaction between distributed generation and the distribution network: operation aspects," *IEEE/PES Transm. Distrib. Conf. Exhib.*, vol. 2, no. 40, pp. 12–15, 2002.

[48] M. Thomson and D. G. Infield, "Impact of widespread photovoltaics generation on distribution systems," *IET Renew. Power Gener.*, vol. 1, no. 1, p. 33, 2007.

[49] M. Mcgranaghan, T. Ortmeyer, D. Crudele, T. Key, J. Smith, and P. Barker, "Renewable Systems Interconnection Study: Advanced Grid Planning and Operations," 2008. [Online]. Available: https://www1.eere.energy.gov/solar/pdfs/advanced_grid_planning_operations.pdf.

[50] E. Demirok, D. Sera, R. Teodorescu, P. Rodriguez, and U. Borup, "Clustered PV inverters in LV networks: An overview of impacts and comparison of voltage control strategies," in *2009 IEEE Electrical Power and Energy Conference, EPEC 2009*, 2009.

[51] T. Stetz, F. Marten, and M. Braun, "Improved low voltage grid-integration of photovoltaic systems in Germany," *IEEE Trans. Sustain. Energy*, vol. 4, no. 2, pp. 534–542, 2013.

[52] S. Conti, S. Raiti, and G. Tina, "Small-scale embedded generation effect on voltage profile: an analytical method," *IEE Proc. - Gener. Transm. Distrib.*, vol. 150, no. 1, p. 78, 2003.

[53] S. Conti, S. Raiti, G. Tina, and U. Vagliasindi, "Distributed Generation in LV distribution networks: Voltage and thermal constraints," in *2003 IEEE Bologna PowerTech - Conference Proceedings*, 2003, vol. 2, pp. 413–418.

[54] Energy Network Association, “Engineering Recommendation G83 Issue 2,” vol. 2, no. 2, 2012.

[55] International Electrotechnical Commission, “IEC 61727:2004 Photovoltaic (PV) systems — characteristics of the utility interface.” 2004.

[56] R. A. Shayani and M. A. G. De Oliveira, “Photovoltaic generation penetration limits in radial distribution systems,” *IEEE Trans. Power Syst.*, vol. 26, no. 3, pp. 1625–1631, 2011.

[57] S. Ingram, S. Probert, and K. Jackson, “The impact of small scale embedded generation on the operating parameters of distribution networks,” 2003. [Online]. Available: http://webarchive.nationalarchives.gov.uk/20100919182407/http://www.ensg.gov.uk/assets/22_01_2004_phase1b_report_v10b_web_site_final.pdf.

[58] A. Barbato, A. Dedè, D. Della Giustina, G. Massa, A. Angioni, G. Lipari, F. Ponci, and S. Repo, “Lessons learnt from real-time monitoring of the low voltage distribution network,” *Sustain. Energy, Grids Networks*, Jun. 2017.

[59] British Standards Institution, “BS EN 50160:2010+A1:2015 Voltage characteristics of electricity supplied by public electricity networks.” 2010.

[60] Electricity North West Ltd, “Low Voltage Network Solutions Closedown Report,” 2014. [Online]. Available: https://www.ofgem.gov.uk/system/files/docs/2017/04/lvns_closedown_report.pdf.

[61] A. Navarro-Espinosa, D. Randles, and L. F. Ochoa, “Deliverable 3.6 ‘What-if Scenario Impact Studies based on real LV networks,’” 2014. [Online]. Available: https://www.enwl.co.uk/globalassets/innovation/lvns/lvns-closedown/uom-appendices/university-of-manchester-appendix-i-lvns.pdf.

[62] Department of Energy and Climate Change, “Weekly Solar PV Installation and Capacity based on Registration Date,” 2012. [Online]. Available: https://www.gov.uk/government/statistical-data-sets/weekly-solar-pv-installation-and-capacity-based-on-registration-date.

[63] Mott McDonald, “System Integration Of Additional Micro-generation (SIAM),” 2004. [Online]. Available: http://webarchive.nationalarchives.gov.uk/+/http://www.dti.gov.uk/renewables/publications/pdfs/dgcg00028rep.pdf.

[64] P. Trichakis, P. C. Taylor, L. M. Cipcigan, P. F. Lyons, R. Hair, and T. Ma, “An Investigation of Voltage Unbalance in Low Voltage Distribution Networks with High Levels of SSEG,” in *Universities Power Engineering Conference, 2006. UPEC ’06. Proceedings of the 41st International*, 2006, vol. 1, pp. 182–186.

[65] F. Shahnia, R. Majumder, A. Ghosh, G. Ledwich, and F. Zare, “Sensitivity analysis of voltage imbalance in distribution networks with rooftop PVs,” in *IEEE PES*

General Meeting, PES 2010, 2010.

[66] Y. Li and P. A. Crossley, "Voltage balancing in low-voltage radial feeders using Scott transformers," *IET Gener. Transm. Distrib.*, vol. 8, no. 8, pp. 1489–1498, 2014.

[67] K. Ma, F. Li, and R. Aggarwal, "Quantification of Additional Reinforcement Cost Driven by Voltage Constraint under Three-Phase Imbalance," *IEEE Trans. Power Syst.*, vol. 31, no. 6, pp. 5126–5134, 2016.

[68] N. C. Woolley and J. V. Milanović, "Statistical estimation of the source and level of voltage unbalance in distribution networks," *IEEE Trans. Power Deliv.*, vol. 27, no. 3, pp. 1450–1460, 2012.

[69] A. Von Jouanne and B. Banerjee, "Assessment of voltage unbalance," *IEEE Trans. Power Deliv.*, vol. 16, no. 4, pp. 782–790, 2001.

[70] A. Rodriguez-Calvo, R. Cossent, and P. Frías, "Integration of PV and EVs in unbalanced residential LV networks and implications for the smart grid and advanced metering infrastructure deployment," *Int. J. Electr. Power Energy Syst.*, vol. 91, pp. 121–134, 2017.

[71] The Electricity Council, "Engineering Recommendation P29. Planning limits for voltage unbalance in the United Kingdom." 1990.

[72] P. Pillay and M. Manyage, "Definitions of voltage unbalance," *IEEE Power Eng. Rev.*, 2001.

[73] IEEE, *IEEE Standard Test Procedure for Polyphase Induction Motors and Generators*. 2017.

[74] L. K. Kumpulainen and K. T. Kauhaniemi, "Analysis of the impact of distributed generation on automatic reclosing," in *IEEE PES Power Systems Conference and Exposition, 2004.*, 2004, pp. 1152–1157.

[75] J. Morren and S. W. H. D. Haan, "Impact of distributed generation units with power electronic converters on distribution network protection," in *Developments in Power System Protection, 2008. DPSP 2008. IET 9th International Conference on*, 2008, pp. 664–669.

[76] K. Kauhaniemi and L. Kumpulainen, "Impact of distributed generation on the protection of distribution networks," in *2004 Eighth IEE International Conference on Developments in Power System Protection*, 2004, vol. 1, pp. 315-318 Vol.1.

[77] P. P. Barker and R. W. De Mello, "Determining the impact of distributed generation on power systems. I. Radial distribution systems," *Power Eng. Soc. Summer Meet. 2000. IEEE*, vol. 3, no. c, pp. 1645–1656 vol. 3, 2000.

[78] Institute of Electrical and Electronics Engineers, "IEEE Standard for Interconnection and Interoperability of Distributed Energy Resources with Associated Electric Power Systems Interfaces," *IEEE Std 1547-2018 (Revision of IEEE Std 1547-2003)*. pp. 1–138, Apr-2018.

[79] N. Hadjsaid, J. F. Canard, and F. Dumas, “Dispersed generation impact on distribution networks,” *IEEE Comput. Appl. Power*, vol. 12, no. 2, pp. 22–28, Apr. 1999.

[80] S. M. Brahma and A. A. Girgis, “Development of Adaptive Protection Scheme for Distribution Systems With High Penetration of Distributed Generation,” *IEEE Trans. Power Deliv.*, vol. 19, no. 1, pp. 56–63, 2004.

[81] Alstom Grid, “Network Protection & Automation Guide.” 2011.

[82] International Electrotechnical Commission, “IEC 62196-1:2014 Plugs, socket-outlets, vehicle connectors and vehicle inlets - Conductive charging of electric vehicles - Part 1: General requirements.” 2014.

[83] EPRI, “Environmental assessment of plug-in hybrid electric vehicles. Volume 1: Nationwide Greenhouse Gas Emissions.,” 2007. [Online]. Available: https://www.energy.gov/sites/prod/files/oeprod/DocumentsandMedia/EPRI-NRDC_PHEV_GHG_report.pdf.

[84] S. Slater, M. Dolman, P. Taylor, P. Trichakis, and J. Shine, “Strategies for the uptake of electric vehicles and associated infrastructure implications,” 2009. [Online]. Available: http://www.element-energy.co.uk/wordpress/wp-content/uploads/2012/05/EV_infrastructure_report_for_CCC_2009_final.pdf.

[85] S. Borlase, *Smart Grids: Infrastructure, Technology, and Solutions*. CRC Press, 2012.

[86] R. Tonkoski, L. A. C. Lopes, and T. H. M. El-Fouly, “Coordinated active power curtailment of grid connected PV inverters for overvoltage prevention,” *IEEE Trans. Sustain. Energy*, vol. 2, no. 2, pp. 139–147, 2011.

[87] M. Manbachi, H. Farhangi, A. Palizban, and S. Arzanpour, “Smart grid adaptive volt-VAR optimization: Challenges for sustainable future grids,” *Sustain. Cities Soc.*, vol. 28, pp. 242–255, 2017.

[88] M. Manbachi, M. Nasri, B. Shahabi, H. Farhangi, A. Palizban, S. Arzanpour, M. Moallem, and D. C. Lee, “Real-Time Adaptive VVO/CVR Topology Using Multi-Agent System and IEC 61850-Based Communication Protocol,” *IEEE Trans. Sustain. Energy*, vol. 5, no. 2, pp. 587–597, Apr. 2014.

[89] C. Bucher, G. Andersson, and L. Küng, “INCREASING THE PV HOSTING CAPACITY OF DISTRIBUTION POWER GRIDS – A COMPARISON OF SEVEN METHODS,” 2013.

[90] S. Koch, F. Ferrucci, A. Ulbig, and M. Koller, “Time-series simulations and assessment of smart grid planning options of distribution grids,” in *23rd International Conference on Electricity Distribution*, 2015, no. June, pp. 15–18.

[91] N. Markushevich, “The benefits and challenges of the Integrated Volt/Var Optimization in the smart grid environment,” in *2011 IEEE Power and Energy Society General Meeting*, 2011, pp. 1–8.

[92] C. Reese, C. Buchhagen, and L. Hofmann, “Voltage range as control input for

OLTC-equipped distribution transformers," in *Proceedings of the IEEE Power Engineering Society Transmission and Distribution Conference*, 2012.

[93] C. Long and L. F. Ochoa, "Voltage control of PV-rich LV networks: OLTC-fitted transformer and capacitor banks," *IEEE Trans. Power Syst.*, vol. 31, no. 5, pp. 4016–4025, 2016.

[94] T. Stetz, K. Diwold, M. Kraiczy, D. Geibel, S. Schmidt, and M. Braun, "Techno-economic assessment of voltage control strategies in low voltage grids," *IEEE Trans. Smart Grid*, vol. 5, no. 4, pp. 2125–2132, 2014.

[95] C. Kӧrner, M. Hennig, R. Schmid, and K. Handt, "Gaining experience with a regulated distribution transformer in a smart grid environment," in *CIRED 2012 Workshop: Integration of Renewables into the Distribution Grid*, 2012, pp. 161–161.

[96] R. Echavarría, A. Claudio, and M. Cotorogea, "Analysis, design, and implementation of a fast on-load tap changing regulator," *IEEE Trans. Power Electron.*, vol. 22, no. 2, pp. 527–534, 2007.

[97] J. O. Quevedo, J. C. Giacomini, R. C. Beltrame, F. E. Cazakevicius, C. Rech, L. Schuch, T. B. Marchesan, M. de Campos, P. S. Sausen, and J. R. Kinas, "Smart distribution transformer applied to Smart Grids," *2013 Brazilian Power Electron. Conf.*, pp. 1046–1053, 2013.

[98] P. Bauer and S. W. H. de Haan, "Electronic tap changer for 500 kVA/10 kV distribution transformers: design, experimental results and impact in distribution networks," in *Conference Record of 1998 IEEE Industry Applications Conference. Thirty-Third IAS Annual Meeting (Cat. No.98CH36242)*, 1998, vol. 2, pp. 1530–1537 vol.2.

[99] X. She, A. Q. Huang, and R. Burgos, "Review of solid-state transformer technologies and their application in power distribution systems," *IEEE J. Emerg. Sel. Top. Power Electron.*, vol. 1, no. 3, pp. 186–198, 2013.

[100] R. Pena-Alzola, G. Gohil, L. Mathe, M. Liserre, and F. Blaabjerg, "Review of modular power converters solutions for smart transformer in distribution system," in *2013 IEEE Energy Conversion Congress and Exposition, ECCE 2013*, 2013, pp. 380–387.

[101] M. M. Rahman, A. Arefi, G. M. Shafiullah, and S. Hettiwatte, "A new approach to voltage management in unbalanced low voltage networks using demand response and OLTC considering consumer preference," *Int. J. Electr. Power Energy Syst.*, 2018.

[102] J. Hu, M. Marinelli, M. Coppo, A. Zecchino, and H. W. Bindner, "Coordinated voltage control of a decoupled three-phase on-load tap changer transformer and photovoltaic inverters for managing unbalanced networks," *Electr. Power Syst. Res.*, 2016.

[103] S. Weckx, C. Gonzalez, T. De Rybel, and J. Driesen, "LS-SVM-based on-load tap changer control for distribution networks with rooftop PV's," in *2013 4th IEEE/PES Innovative Smart Grid Technologies Europe, ISGT Europe 2013*, 2013.

[104] A. Uchida, S. Watanabe, and S. Iwamoto, "A voltage control strategy for distribution networks with dispersed generations," in *2007 IEEE Power Engineering Society General Meeting, PES*, 2007.

[105] Y. P. Agalgaonkar, B. C. Pal, and R. A. Jabr, "Distribution voltage control considering the impact of PV generation on tap changers and autonomous regulators," *IEEE Trans. Power Syst.*, vol. 29, no. 1, pp. 182–192, 2014.

[106] C. Gao and M. A. Redfern, "Automatic compensation voltage control strategy for on-load tap changer transformers with distributed generations," in *APAP 2011 - Proceedings: 2011 International Conference on Advanced Power System Automation and Protection*, 2011, vol. 1, pp. 737–741.

[107] M. Thomson, "Automatic voltage-control relays and embedded generation," *Power Eng. J.*, vol. 14, no. 3, pp. 93–99, 2000.

[108] M. Fila, G. Taylor, P. Lang, J. Hiscock, and M. Irving, "Modelling and analysis of the enhanced TAPP scheme for distribution networks," in *16th Power Systems Computation Conference, PSCC 2008.*, 2008.

[109] J. Hiscock, N. Hiscock, and A. Kennedy, "Advanced Voltage Control for Networks with Distributed Generation," in *19th International Conference on Electricity Distribution*, 2007.

[110] J. Barr and R. Majumder, "Integration of Distributed Generation in the Volt/VAR Management System for Active Distribution Networks," *IEEE Trans. Smart Grid*, vol. 6, no. 2, pp. 576–586, Mar. 2015.

[111] D. Geibel, T. Degner, A. Seibel, T. Bülo, C. Tschendel, M. Pfalzgraf, K. Boldt, P. Müller, F. Sutter, and T. Hug, "Active, intelligent low voltage networks – Concept, realisation and field test results," in *22nd International Conference and Exhibition on Electricity Distribution (CIRED 2013)*, 2013, pp. 1–4.

[112] B. Blažič, T. Pfajfar, and I. Papič, "Voltage control in networks with distributed generation — A case study," in *2009 IEEE PES/IAS Conference on Sustainable Alternative Energy (SAE)*, 2009, pp. 1–6.

[113] R. Schwalbe, H. Brunner, M. Stifter, A. Abart, E. Traxler, M. Radauer, and W. Niederhuemer, "DG-demonet smart LV grid - increasing hosting capacity of LV grids by extended planning and voltage control," in *2015 International Symposium on Smart Electric Distribution Systems and Technologies (EDST)*, 2015, pp. 63–69.

[114] R. Schwalbe, A. Einfalt, M. Heidl, A. Abart, M. Radauer, and H. Brunner, "DG-DemoNet Smart LV Grid - Robust Control Architecture to increase DG Hosting Capacity," in *23rd International Conference on Electricity Distribution (CIRED*

2015), 2015.

[115] F. Kupzog, R. Schwalbe, W. Prüggler, B. Bletterie, S. Kadam, A. Abart, and M. Radauer, "Maximising low voltage grid hosting capacity for PV and electric mobility by distributed voltage control," *e i Elektrotechnik und Informationstechnik*, vol. 131, no. 6, pp. 188–192, Sep. 2014.

[116] A. Einfalt, F. Zeilinger, R. Schwalbe, B. Bletterie, and S. Kadam, "Controlling active low voltage distribution grids with minimum efforts on costs and engineering," in *IECON Proceedings (Industrial Electronics Conference)*, 2013, pp. 7456–7461.

[117] H. Y. Li and H. Leite, "Increasing distributed generation using automatic voltage reference setting technique," in *IEEE Power and Energy Society 2008 General Meeting: Conversion and Delivery of Electrical Energy in the 21st Century, PES*, 2008.

[118] A. Kulmala, A. Mutanen, A. Koto, S. Repo, and P. Järventausta, "RTDS verification of a coordinated voltage control implementation for distribution networks with distributed generation," in *2010 IEEE PES Innovative Smart Grid Technologies Conference Europe (ISGT Europe)*, 2010, pp. 1–8.

[119] Electricity North West Ltd, "Low Voltage Integrated Automation (LoVIA) Closedown Report," 2015. [Online]. Available: https://www.enwl.co.uk/globalassets/innovation/lovia/lovia-closedown/lovia-closedown-report.pdf.

[120] R. Tonkoski and L. A. C. Lopes, "Voltage Regulation in Radial Distribution Feeders with High Penetration of Photovoltaic," in *2008 IEEE Energy 2030 Conference*, 2008, pp. 1–7.

[121] A. G. Madureira and J. A. Peças Lopes, "Coordinated voltage support in distribution networks with distributed generation and microgrids," *IET Renew. Power Gener.*, vol. 3, no. 4, p. 439, 2009.

[122] A. Madureira, J. P. Lopes, A. Carrapatoso, and N. Silva, "The new role of substations in distribution network management," in *CIRED 2009 - 20th International Conference and Exhibition on Electricity Distribution - Part 1*, 2009, pp. 1–4.

[123] G. Mokhtari, A. Ghosh, G. Nourbakhsh, and G. Ledwich, "Smart robust resources control in lv network to deal with voltage rise issue," *IEEE Trans. Sustain. Energy*, vol. 4, no. 4, pp. 1043–1050, 2013.

[124] S. Weckx and J. Driesen, "Optimal Local Reactive Power Control by PV Inverters," *IEEE Trans. Sustain. Energy*, vol. 7, no. 4, pp. 1624–1633, 2016.

[125] VDE e.V., "VDE-AR-N 4105:2011-08 Power generation systems connected to the low-voltage distribution network." 2011.

[126] K. Tanaka, M. Oshiro, S. Toma, A. Yona, T. Senjyu, T. Funabashi, and C.-H. Kim,

"Decentralised control of voltage in distribution systems by distributed generators," *IET Gener. Transm. Distrib.*, vol. 4, no. 11, p. 1251, 2010.

[127] T. Sansawatt, L. F. Ochoa, and G. P. Harrison, "Integrating distributed generation using decentralised voltage regulation," in *IEEE PES General Meeting, PES 2010*, 2010.

[128] R. Caldon, M. Coppo, and R. Turri, "Distributed voltage control strategy for LV networks with inverter-interfaced generators," *Electr. Power Syst. Res.*, vol. 107, pp. 85–92, 2014.

[129] P. M. S. Carvalho, P. F. Correia, and L. a F. Ferreira, "Distributed Reactive Power Generation Control for Voltage Rise Mitigation in Distribution Networks," *IEEE Trans. Power Syst.*, vol. 23, no. 2, pp. 766–772, 2008.

[130] C. a. Hill, M. C. Such, D. Chen, J. Gonzalez, and W. M. Grady, "Battery Energy Storage for Enabling Integration of Distributed Solar Power Generation," *IEEE Trans. Smart Grid*, vol. 3, no. 2, pp. 850–857, 2012.

[131] L. Wang, D. H. Liang, A. F. Crossland, P. C. Taylor, D. Jones, and N. S. Wade, "Coordination of Multiple Energy Storage Units in a Low-Voltage Distribution Network," *IEEE Trans. Smart Grid*, vol. 6, no. 6, pp. 2906–2918, 2015.

[132] N. S. Wade, P. C. Taylor, P. D. Lang, and P. R. Jones, "Evaluating the benefits of an electrical energy storage system in a future smart grid," *Energy Policy*, vol. 38, no. 11, pp. 7180–7188, Nov. 2010.

[133] M. A. Kashem and G. Ledwich, "Energy requirement for distributed energy resources with battery energy storage for voltage support in three-phase distribution lines," *Electr. Power Syst. Res.*, vol. 77, no. 1, pp. 10–23, Jan. 2007.

[134] M. J. E. Alam, K. M. Muttaqi, and D. Sutanto, "Distributed energy storage for mitigation of voltage-rise impact caused by rooftoptoptop solar PV," in *IEEE Power and Energy Society General Meeting*, 2012.

[135] T. Verschueren, K. Mets, B. Meersman, M. Strobbe, C. Develder, and L. Vandevelde, "Assessment and mitigation of voltage violations by solar panels in a residential distribution grid," in *2011 IEEE International Conference on Smart Grid Communications, SmartGridComm 2011*, 2011, pp. 540–545.

[136] Y. Ueda, K. Kurokawa, and T. Tanabe, "Study on the over voltage problem and battery operation for grid-connected residential PV systems," *22nd Eur. Photovolt. Sol. Energy Conf.*, no. September, pp. 3094–3097, 2007.

[137] S. Ali, N. Pearsall, and G. Putrus, "Using Electric Vehicles To Mitigate Imbalance Requirements Associated With High Penetration Level Of Grid-Connected Photovoltaic Systems," in *22nd International Conference on Electricity Distribution (CIRED 2013)*, 2013.

[138] F. Marra, G. Y. Yang, C. Traeholt, E. Larsen, J. Ostergaard, B. Blazic, and W. Deprez, "EV charging facilities and their application in LV feeders with

photovoltaics," *IEEE Trans. Smart Grid*, vol. 4, no. 3, pp. 1533–1540, 2013.

[139] X. Liu, A. Aichhorn, L. Liu, and H. Li, "Coordinated control of distributed energy storage system with tap changer transformers for voltage rise mitigation under high photovoltaic penetration," *IEEE Trans. Smart Grid*, vol. 3, no. 2, pp. 897–906, 2012.

[140] X. Gao, F. Sossan, K. Christakou, M. Paolone, and M. Liserre, "Concurrent Voltage Control and Dispatch of Active Distribution Networks by Means of Smart Transformer and Storage," *IEEE Trans. Ind. Electron.*, vol. 65, no. 8, pp. 6657–6666, 2018.

[141] J. Fonseca, M. I. Verdelho, and R. Prata, "Impact for the DSO of integrating storage systems in a low-voltage grid with distributed energy resources," *CIRED - Open Access Proc. J.*, vol. 2017, no. 1, pp. 1795–1799, 2017.

[142] K. H. Chua, Y. S. Lim, P. Taylor, S. Morris, and J. Wong, "Energy storage system for mitigating voltage unbalance on low-voltage networks with photovoltaic systems," *IEEE Trans. Power Deliv.*, vol. 27, no. 4, pp. 1783–1790, 2012.

[143] S. Repo, D. Della Giustina, G. Ravera, L. Cremaschini, S. Zanini, J. M. Selga, and P. Järventausta, "Use case analysis of real-time low voltage network management," in *2011 2nd IEEE PES International Conference and Exhibition on Innovative Smart Grid Technologies*, 2011, pp. 1–8.

[144] Y. Kabalci, "A survey on smart metering and smart grid communication," *Renew. Sustain. Energy Rev.*, vol. 57, pp. 302–318, May 2016.

[145] K. N. Malamaki and C. S. Demoulias, "A decentralized voltage regulation method in low-voltage feeders with PV systems and domestic loads," in *International Conference on Power Engineering, Energy and Electrical Drives*, 2013, pp. 461–467.

[146] T. L. Lee, S. S. Yang, and S. H. Hu, "Design of decentralized voltage control for PV inverters to mitigate voltage rise in distribution power system without communication," in *2014 International Power Electronics Conference, IPEC-Hiroshima - ECCE Asia 2014*, 2014, pp. 2606–2609.

[147] I. Roytelman and V. Ganesan, "Coordinated local and centralized control in distribution management systems," *IEEE Trans. Power Deliv.*, vol. 15, no. 2, pp. 718–724, 2000.

[148] M. Fila, D. Reid, G. A. Taylor, P. Lang, and M. R. Irving, "Coordinated voltage control for active network management of distributed generation," in *2009 IEEE Power Energy Society General Meeting*, 2009, pp. 1–8.

[149] J. Tuominen, S. Repo, and A. Kulmala, "Comparison of the low voltage distribution network voltage control schemes," in *IEEE PES Innovative Smart Grid Technologies, Europe*, 2014, pp. 1–6.

[150] H. Fakham, F. Colas, and X. Guillaud, "Real-time simulation of multi-agent

system for decentralized voltage regulation in distribution network," in *IEEE Power and Energy Society General Meeting*, 2011.

[151] A. Vaccaro, G. Velotto, and A. F. Zobaa, "A decentralized and cooperative architecture for optimal voltage regulation in smart grids," *IEEE Trans. Ind. Electron.*, vol. 58, no. 10, pp. 4593–4602, 2011.

[152] M. E. Baran and I. M. El-Markabi, "A multiagent-based dispatching scheme for distributed generators for voltage support on distribution feeders," *IEEE Trans. Power Syst.*, vol. 22, no. 1, pp. 52–59, 2007.

[153] R. Bottura, A. Borghetti, F. Napolitano, and C. A. Nucci, "ICT-power co-simulation platform for the analysis of communication-based volt/var optimization in distribution feeders," in *ISGT 2014*, 2014, pp. 1–5.

[154] S. Lu, S. Repo, D. Della Giustina, F. A. C. Figuerola, A. Lof, and M. Pikkarainen, "Real-Time Low Voltage Network Monitoring - ICT Architecture and Field Test Experience," *IEEE Trans. Smart Grid*, vol. 6, no. 4, pp. 2002–2012, 2015.

[155] "OPERA: Open PLC European Research Alliance," 2018. [Online]. Available: http://www.ist-opera.org.

[156] S. Repo, S. Lu, T. Pöhö, D. Della Giustina, G. Ravera, J. M. Selga, and F. A. C. Figuerola, "Active distribution network concept for distributed management of low voltage network," in *2013 4th IEEE/PES Innovative Smart Grid Technologies Europe, ISGT Europe 2013*, 2013.

[157] S. S. S. R. Depuru, L. Wang, and V. Devabhaktuni, "Support vector machine based data classification for detection of electricity theft," in *2011 IEEE/PES Power Systems Conference and Exposition, PSCE 2011*, 2011.

[158] A. J. Dick, "Theft of electricity-how UK electricity companies detect and deter," in *European Convention on Security and Detection, 1995.*, 1995, pp. 90–95.

[159] M. Anas, N. Javaid, A. Mahmood, S. M. Raza, U. Qasim, and Z. A. Khan, "Minimizing electricity theft using smart meters in AMI," in *Proceedings - 2012 7th International Conference on P2P, Parallel, Grid, Cloud and Internet Computing, 3PGCIC 2012*, 2012, pp. 176–182.

[160] ActionFraud, "Millions paid to electricity scammers," 2011. [Online]. Available: https://www.actionfraud.police.uk/millions-paid-to-electricity-scammers-mar11.

[161] Crimestoppers, "Energy theft costs us all." [Online]. Available: https://www.stayenergysafe.co.uk/stories/energy-theft-costs-us-all. [Accessed: 16-May-2018].

[162] M. Streeter and S. Boggan, "IRA team who planned terror blitz on capital given 35 years," *The Independent*, 1997.

[163] "Australian jailed for bomb plots," *BBC*, 2006. [Online]. Available: http://news.bbc.co.uk/1/hi/world/asia-pacific/5277010.stm.

[164] Electricity Information Sharing and Analysis Center (E-ISAC), "Analysis of the

cyber attack on the Ukrainian power grid," 2016. [Online]. Available: https://ics.sans.org/media/E-ISAC_SANS_Ukraine_DUC_5.pdf.

[165] V3, "Ukraine power grid attacks continue but BlackEnergy malware ruled out." [Online]. Available: https://www.v3.co.uk/v3-uk/news/2440469/ukraine-investigating-suspected-russian-cyber-attack-on-power-grid. [Accessed: 16-May-2018].

[166] T. E. Griffith, "Strategic Attack of National Electrical Systems," Maxwell Air Force Base, Alabama, 1994.

[167] U.S.-China Economic And Security Review Commission, "Report to Congress," 2008. [Online]. Available: https://www.uscc.gov/sites/default/files/annual_reports/2008-Report-to-Congress-_0.pdf.

[168] S. Gorman, "Electricity Grid in U.S. Penetrated By Spies," *The Wall Street Journal*, 08-Apr-2009.

[169] R. Anderson and S. Fuloria, "Smart meter security: a survey," *Univ. Cambridge Comput. Lab. United Kingdom*, 2011.

[170] N. Falliere, L. O. Murchu, and E. Chien, "W32.Stuxnet Dossier," *White Pap. Symantec Corp., Secur. Response*, vol. 5, no. 6, p. 29, 2011.

[171] W. D. Jones, "Declarations of cyberwar," *IEEE Spectrum*, vol. 49, no. 8. p. 18, 2012.

[172] Cabinet Office, "National Risk Register of Civil Emergencies," 2017. [Online]. Available: https://assets.publishing.service.gov.uk/government/uploads/system/uploads/attachment_data/file/644968/UK_National_Risk_Register_2017.pdf.

[173] Cambridgeshire & Peterborough Resilience Forum, "Community Risk Register Supporting Document Version 3.3." 2006.

[174] South Yorkshire Local Resilience Forum, "Risk Management and Planning Group Community Risk Register." 2013.

[175] R. Rashed Mohassel, A. Fung, F. Mohammadi, and K. Raahemifar, "A survey on Advanced Metering Infrastructure," *Int. J. Electr. Power Energy Syst.*, vol. 63, pp. 473–484, 2014.

[176] E. Bou-Harb, C. Fachkha, M. Pourzandi, M. Debbabi, and C. Assi, "Communication security for smart grid distribution networks," *IEEE Commun. Mag.*, vol. 51, no. 1, pp. 42–49, 2013.

[177] D. Abbasinezhad-Mood and M. Nikooghadam, "An Ultra-Lightweight and Secure Scheme for Communications of Smart Meters and Neighborhood Gateways by Utilization of an ARM Cortex-M Microcontroller," *IEEE Transactions on Smart Grid*, 2017.

[178] Y. Mo, T. H. J. Kim, K. Brancik, D. Dickinson, H. Lee, A. Perrig, and B. Sinopoli,

"Cyber–Physical Security of a Smart Grid Infrastructure," *Proc. IEEE*, vol. 100, no. 1, pp. 195–209, Jan. 2012.

[179] A. Boustani, A. Maiti, S. Y. Jazi, M. Jadliwala, and V. Namboodiri, "Seer Grid: Privacy and Utility Implications of Two-Level Load Prediction in Smart Grids," *IEEE Trans. Parallel Distrib. Syst.*, vol. 28, no. 2, pp. 546–557, 2017.

[180] G. W. Hart, "Nonintrusive Appliance Load Monitoring," *Proc. IEEE*, vol. 80, no. 12, pp. 1870–1891, 1992.

[181] D. Carluccio and S. Brinkhaus, "Smart Hacking For Privacy (Abstract)," *28th Chaos Communication Congress*, 2011. [Online]. Available: https://events.ccc.de/congress/2011/Fahrplan/events/4754.en.html.

[182] D. Carluccio and S. Brinkhaus, "Smart Hacking for Privacy (Presentation)," *28th Chaos Communication Congress*, 2011. [Online]. Available: http://mirror.fem-net.de/CCC/28C3/mp4-h264-HQ/28c3-4754-en-smart_hacking_for_privacy_h264.mp4.

[183] R. Anderson, *Security engineering: A Guide to Building Dependable Distributed Systems*. John Wiley & Sons, 2008.

[184] S. H. Weingart, "Physical Security Devices for Computer Subsystems: A Survey of Attacks and Defenses," in *Cryptographic Hardware and Embedded Systems — CHES 2000*, 2000, pp. 302–317.

[185] Y. Xiao, *Security and privacy in smart grids*. CRC Press, 2013.

[186] P. Jafary, S. Repo, and H. Koivisto, "Secure communication of smart metering data in the smart grid secondary substation," in *Proceedings of the 2015 IEEE Innovative Smart Grid Technologies - Asia, ISGT ASIA 2015*, 2016.

[187] C. J. Bandim, J. E. R. Alves, A. V Pinto, F. C. Souza, M. R. B. Loureiro, C. A. Magalhaes, and F. Galvez-Durand, "Identification of energy theft and tampered meters using a central observer meter: a mathematical approach," in *2003 IEEE PES Transmission and Distribution Conference and Exposition (IEEE Cat. No.03CH37495)*, 2003, vol. 1, pp. 163-168 Vol.1.

[188] M. Wei and W. Wang, "Data-centric threats and their impacts to real-time communications in smart grid," *Comput. Networks*, vol. 104, pp. 174–188, 2016.

[189] J. Kim and L. Tong, "On topology attack of a smart grid: Undetectable attacks and countermeasures," *IEEE J. Sel. Areas Commun.*, vol. 31, no. 7, pp. 1294–1305, 2013.

[190] P. Y. Chen, S. Yang, J. A. McCann, J. Lin, and X. Yang, "Detection of false data injection attacks in smart-grid systems," *IEEE Commun. Mag.*, vol. 53, no. 2, pp. 206–213, 2015.

[191] D. Kundur, X. Feng, S. Mashayekh, S. Liu, T. Zourntos, and K. L. Butler-Purry, "Towards modelling the impact of cyber attacks on a smart grid," *Int. J. Secur.*

Networks, vol. 6, no. 1, pp. 2–13, 2011.

[192] Y. Yuan, Z. Li, and K. Ren, "Modeling Load Redistribution Attacks in Power Systems," *IEEE Trans. Smart Grid*, vol. 2, no. 2, pp. 382–390, Jun. 2011.

[193] R. Deng, G. Xiao, R. Lu, H. Liang, and A. V. Vasilakos, "False data injection on state estimation in power systems-attacks, impacts, and defense: A survey," *IEEE Trans. Ind. Informatics*, vol. 13, no. 2, pp. 411–423, 2017.

[194] T. M. Overman, R. W. Sackman, T. L. Davis, and B. S. Cohen, "High-Assurance Smart Grid: A Three-Part Model for Smart Grid Control Systems," *Proc. IEEE*, vol. 99, no. 6, pp. 1046–1062, Jun. 2011.

[195] M. Carpenter, T. Goodspeed, B. Singletary, E. Skoudis, and J. Wright, "Advanced metering infrastructure attack methodology," *InGuardians white Pap.*, 2009.

[196] A. R. Metke and R. L. Ekl, "Security technology for smart grid networks," *IEEE Trans. Smart Grid*, vol. 1, no. 1, pp. 99–107, 2010.

[197] H. Khurana, M. Hadley, N. Lu, and D. A. Frincke, "Smart-grid security issues," *IEEE Secur. Priv.*, vol. 8, no. 1, pp. 81–85, 2010.

[198] F. M. Cleveland, "Cyber security issues for Advanced Metering Infrasttructure (AMI)," *2008 IEEE Power Energy Soc. Gen. Meet. - Convers. Deliv. Electr. Energy 21st Century*, pp. 1–5, 2008.

[199] C. H. Gebotys, *Security in Embedded Devices*. Springer US, 2010.

[200] Y. J. Kim, V. Kolesnikov, and M. Thottan, "Resilient end-to-end message protection for large-scale cyber-physical system communications," in *2012 IEEE 3rd International Conference on Smart Grid Communications, SmartGridComm 2012*, 2012, pp. 193–198.

[201] S. Uludag, K. S. Lui, W. Ren, and K. Nahrstedt, "Secure and scalable data collection with time minimization in the smart grid," *IEEE Trans. Smart Grid*, vol. 7, no. 1, pp. 43–54, 2016.

[202] *The Meters (Certification) Regulations 1998*. 1998.

[203] Y. Yan, Y. Qian, and H. Sharif, "A secure and reliable in-network collaborative communication scheme for advanced metering infrastructure in smart grid," in *2011 IEEE Wireless Communications and Networking Conference, WCNC 2011*, 2011, pp. 909–914.

[204] G. N. Ericsson, "Cyber Security and Power System Communication - Essential Parts of a Smart Grid Infrastructure," *Power Deliv. IEEE Trans.*, vol. 25, no. 3, pp. 1501–1507, 2010.

[205] A. Marcoci, S. Raffaelli, J. M. Galan, E. Cagno, E. Cagno, G. J. L. Micheli, G. Mauri, and R. Urban, "The Meter-ON project: How to support the deployment of advanced metering infrastructures in Europe?," in *22nd International Conference and Exhibition on Electricity Distribution (CIRED 2013)*, 2013, pp. 1–4.

[206] S. Baker, S. Waterman, and G. Ivanov, "In the Crossfire: Critical Infrastructure in

the Age of Cyber War," 2010.

[207] The Commission for Energy Regulation, "Electricity Smart Metering Technology Trials Findings Report," 2011. [Online]. Available: https://www.ucd.ie/t4cms/Electricity Smart Metering Technology Trials Findings Report.pdf.

[208] R. Anderson and M. Kuhn, "Low cost attacks on tamper resistant devices," in *International Workshop on Security Protocols*, 1997, pp. 125–136.

[209] M. Nabeel, X. Ding, S. H. Seo, and E. Bertino, "Scalable end-to-end security for advanced metering infrastructures," *Inf. Syst.*, vol. 53, pp. 213–223, 2015.

[210] K. Shuaib, Z. Trabelsi, M. Abed-Hafez, A. Gaouda, and M. Alahmad, "Resiliency of Smart Power Meters to Common Security Attacks," *Procedia Comput. Sci.*, vol. 52, pp. 145–152, Jan. 2015.

[211] P. Yi, T. Zhu, Q. Zhang, Y. Wu, and J. Li, "A denial of service attack in advanced metering infrastructure network," in *2014 IEEE International Conference on Communications, ICC 2014*, 2014, pp. 1029–1034.

[212] M. Davis, "SmartGrid Device Security," in *Black Hat USA 2009*, 2009.

[213] N. Uto, B. A. P. Botelho, and R. De Simone Cividanes, "A Fast Attack against a Smart Meter Authentication Protocol," in *3rd International Conference on Informatics, Environment, Energy and Applications*, 2014.

[214] H. Dantas, Z. Erkin, C. Doerr, R. Hallie, and G. van der Bij, "eFuzz: A Fuzzer for DLMS/COSEM Electricity Meters," in *Proceedings of the 2nd Workshop on Smart Energy Grid Security*, 2014, pp. 31–38.

[215] V. C. Güngör, D. Sahin, T. Kocak, S. Ergüt, C. Buccella, C. Cecati, and G. P. Hancke, "Smart grid technologies: Communication technologies and standards," *IEEE Trans. Ind. Informatics*, vol. 7, no. 4, pp. 529–539, 2011.

[216] L. Šastný, L. Franek, and P. Fiedler, "Wireless communications in smart metering," *IFAC Proc. Vol.*, vol. 46, no. 28, pp. 330–335, 2013.

[217] J. Wright, R. Speers, and R. Melgares, "KillerBee," 2009. [Online]. Available: https://github.com/riverloopsec/killerbee.

[218] S. McIntyre, "termineter," 2012. [Online]. Available: https://github.com/securestate/termineter.

[219] Department of Energy and Climate Change, "Smart Metering Equipment Technical Specifications Version 1.1," 2014. [Online]. Available: https://assets.publishing.service.gov.uk/government/uploads/system/uploads/attachment_data/file/299395/smets.pdf.

[220] Analog Devices, "Single-Phase Multifunction Metering IC with di/dt Sensor Interface," 2011. [Online]. Available: http://www.analog.com/media/en/technical-documentation/data-sheets/ADE7753.pdf.

[221] H. Leite, “Modelling and real-time testing of an automatic local voltage controller to increase the amount of distributed generation,” University of Manchester, 2004.

[222] G. Ordnance Survey, “OS MasterMap Topography Layer [GML geospatial data],” *EDINA Digimap Ordnance Survey Service*. [Online]. Available: http://edina.ac.uk/digimap. [Accessed: 05-Sep-2014].

[223] Microsoft, “Aerial View, Cardiff,” *Bing Maps*. [Online]. Available: https://www.bing.com/maps/aerial. [Accessed: 05-Sep-2014].

[224] P. Benko, G. Malicsko, and A. Veres, “A large-scale, passive analysis of end-to-end TCP performance over GPRS,” in *Proceedings - IEEE INFOCOM*, 2004.

[225] B. Pfitzinger, T. Baumann, A. Emde, D. Macos, and T. Jestädt, “Network-wide Measurement of TCP RTT in 2G Networks,” in *HICSS*, 2018.

[226] F. Vacirca, F. Ricciato, and R. Pilz, “Large-scale RTT measurements from an operational UMTS/GPRS network,” in *Proceedings - First International Conference on Wireless Internet, WICON 2005*, 2005.

[227] International Electrotechnical Commission, “IEC 62056-21:2002 Electricity metering – Data exchange for meter reading, tariff and load control – Part 21: Direct local data exchange.” 2002.

[228] American National Standards Institute, “Protocol Specification for ANSI Type 2 Optical Port,” 2006.

[229] International Organization for Standardization and International Electrotechnical Commission, “ISO/IEC 27002:2013 Information technology -- Security techniques -- Code of practice for information security controls.” 2013.

[230] Data Communications Company, “Intimate Communications Hub Interface Specification Version 1.0,” 2014. [Online]. Available: https://www.smartdcc.co.uk/media/145112/intimate_communications_hub_interface_specifications_dcc_1.0_clean.pdf.

This page intentionally left blank

‘Strive for perfection in everything. Take the best that exists and make it better. If it doesn't exist, create it. Accept nothing nearly right or good enough.’

- Sir Frederick Henry Royce

‘The only thing greater than the power of the mind is the courage of the heart.’

- John Forbes Nash Jr